universität wien

DISSERTATION

Titel der Dissertation

Mathematical models of spatially varying selection in subdivided populations

Verfasser

Mag. Ludwig Geroldinger

angestrebter akademischer Grad

Doktor der Naturwissenschaften (Dr.rer.nat)

Wien, November 2014

Studienkennzahl lt. Studienblatt:	A 791 405
Studienrichtung lt. Studienblatt:	Mathematik
Betreuer:	ao. Univ.-Prof. tit. Univ.-Prof. Dr. Reinhard Bürger

Acknowledgments

Foremost, I would like to thank my advisor, Professor Reinhard Bürger, for his support, his patience, his guidance, as well as for all the liberty he gave me.

Having done my doctoral studies within the framework of the Doctoral Program *Vienna Graduate School of Population Genetics*, I am grateful to all who were involved in creating such a stimulating program, in particular to the Speaker Professor Christian Schlötterer and to the Deputy Speaker Professor Joachim Hermisson. I would like to thank all members of the Doctoral Program and all members of the Biomathematics Group at the Faculty of Mathematics for providing a stimulating scientific environment. In particular, I would like to mention Simon Aeschbacher, Johanna Bertl, Andrea Betancourt, Josef Hofbauer, Christian Huber, Agnes Rettelbach, Derek Setter, Linlin Su, and Claus Vogl. The coordinator of the Doctoral Program, Julia Hosp, had an open ear for all administrative problems.

During my doctoral studies I visited Professor Frédéric Guillaume at the ETH Zürich for several months. I am grateful to him for his hospitality and his support during my stay.

Finally, I would like to express my deep gratitude to my parents and my wife who always believed in me and supported me.

Summary

In this thesis, I present my research in the area of theoretical population genetics that I have carried out during my doctoral studies at the University of Vienna. The thesis is structured into two chapters, and each corresponds to one publication (the corresponding data are given at the very end of this thesis).

Both chapters are connected by the overarching question of my research, i.e., what is the potential of migration-selection balance to maintain quantitative genetic variation, local adaptation, and differentiation? To address this question, the evolution of a phenotypic trait (determined by two loci) that is under spatially varying selection in a subdivided population is investigated.

In the first chapter, *A two-locus model of spatially varying stabilizing or directional selection on a quantitative trait*, the influence of the genetic architecture (locus effects and linkage) on the maintenance of genetic variation, local adaptation, and differentiation is studied by employing a two-deme model. Special focus is put on the determination of critical migration rates below which variability can be maintained.

In the second chapter, *Clines in quantitative traits: The role of migration patterns and selection scenarios*, the interaction of selection and migration between multiple demes is explored. Different spatial structures and selection scenarios are compared in their capability to maintain clines. The influence of isolation by distance and spatial heterogeneity in selection on the shape of clines in the phenotypic mean, the genetic variance, and linkage disequilibrium is elaborated.

The motivation for this theoretical work has its roots in evolutionary biology. The subsequent introduction outlines the basic biological questions, it summarizes the main results of the thesis and gives an outlook to further research.

Ludwig Geroldinger

Vienna, November 2014

Zusammenfassung

In dieser Dissertation stelle ich meine Forschungsergebnisse aus der theoretischen Populationsgenetik vor, welche ich im Rahmen meines Doktoratsstudiums an der Universität Wien erarbeitet habe. Die Arbeit ist in zwei Kapitel unterteilt, welche unabhängigen Publikationen entsprechen (der Status der Publikationen ist am Ende der Arbeit angeführt).

Beide Kapitel beschäftigen sich mit folgender Fragestellung: Wie viel genetische Varianz, lokale Adaptation und Differenzierung lässt sich durch die Interaktion der evolutionären Kräfte Migration, Selektion und Rekombination erhalten? Um auf diese Frage einzugehen wird die Evolution eines phänotypischen Merkmals (welches durch zwei Loci bestimmt ist) unter räumlich variierender Selektion in einer strukturierten Population untersucht.

Im ersten Kapitel wird ein Modell mit zwei Inseln behandelt. Der Einfluss genetischer Architektur auf den Erhalt genetischer Varianz, lokaler Adaptation und Differenzierung wird analysiert. Ein Hauptziel ist die Berechnung der kritischen Migrationsrate, unter welcher alle Genotypen koexistieren können.

Im zweiten Kapitel wird die Interaktion von Selektion und Migration zwischen mehreren Inseln untersucht. Verschiedene Migrationsstrukturen und Selektionsszenarien werden verglichen, und zwar in Bezug auf ihr Potential ein Merkmalsgefälle (cline) zu erhalten. Des Weiteren wird der Einfluss der Migrationsverteilung und räumlich variierender Selektion auf die Form des Merkmalsgefälles im phänotypischen Mittelwert, der genetischen Varianz und „Linkage Disequilibrium“ ermittelt.

Die Fragestellungen, welche die vorliegende Arbeit motiviert haben, stammen aus der Evolutionsbiologie. In der Einleitung werden diese biologischen Fragestellungen erläutert. Außerdem werden Resultate und Methoden kurz zusammengefasst.

Ludwig Geroldinger

Wien, November 2014

Contents

Acknowledgments i

Summary ii

Zusammenfassung iii

Introduction 1

Chapter I: A two-locus model of spatially varying stabilizing or directional selection on a quantitative trait 8

1 Introduction 9

2 The model 12

3 No migration 17

4 Weak migration 20

5 Strong migration 21

6 Equilibrium configurations and bifurcation patterns for the haploid model 22

7 Results for the diploid model 49

8 Applications 54

9 Discussion 70

A Appendix 76

B Appendix 84

Chapter II: Clines in quantitative traits: The role of migration patterns and selection scenarios 85

1 Introduction 86

2 Model 88

3 Limiting Cases 91

4 Two demes 95

5 Island and stepping-stone models 101

6 Clines in the mean phenotype, genetic variance, and LD 112

7 Comparison with other multilocus models 117

8 Discussion 122

A Appendix 128

B Appendix 141

Bibliography 160

Curriculum Vitae 167

List of Publications 169

Introduction

Population genetics is concerned with the study of the genetic composition of populations. The most important evolutionary processes that determine this composition are natural selection, mutation, recombination, migration, and random genetic drift. Whereas each evolutionary force separately has been studied in detail, the interaction of these forces can be incredibly complex and is far from being well understood. The huge number of possible evolutionary scenarios and the complex interaction of factors determining evolution make mathematical modeling a useful tool. In contrast to other fields in biology, mathematical thinking was part of population genetics since its very beginning. In the third decade of the twentieth century R.A. Fisher, J.B.S. Haldane, and S. Wright laid the theoretical foundations of modern population genetics. Whereas their pioneering work established a consensus on which evolutionary factors potentially influence evolution, the relative importance of the various factors is subject to ongoing investigation and debate.

One main aim in population genetics is to understand the generation and maintenance of genetic variation which provides the potential for local adaptation and speciation. Since many, if not most, populations are spatially structured and selection will be spatially heterogenous, the interaction of migration and selection is an important determinant of genetic variation. In a heterogenous environment, specialist genotypes (selectively favored in a certain region of the environment) or generalist genotypes (high average fitness in the environment) can prevail.

Most phenotypic traits are under natural selection. If the selected trait is determined by a single locus, the interplay of migration and selection has been investigated in detail. However, usually traits are determined by multiple loci with a potentially complex genetic architecture. In this case, the interaction of gene flow with selection and the influence of the genetic architecture on genetic variation is not so well understood. A series of questions arises immediately if selection acts on multiple loci. What is the effect of linkage between the loci for the maintenance of variation? What are the consequences of epistasis and the distribution of locus effects on the genetic variability that can be maintained? How do gene flow and linkage affect the probabilistic association of alleles between the selected loci?

To shed new light on these questions, we assume the following setting. An additive quantitative trait, determined by two diallelic loci, is under quadratic selection toward a phenotypic optimum. For panmictic populations the considered model goes back to Wright (1935), who assumed that two unlinked loci of equal effect control the character and that the double heterozygote is at the fitness optimum. Several authors extended Wright's pioneering work to

different genetic architectures and multiple loci (Barton 1986; Gavrilets and Hastings 1993; Bürger and Gimelfarb 1999; Willensdorfer and Bürger 2003). However, all previous analyses were restrained to panmictic populations. In order to improve our understanding of how migration and selection shape quantitative genetic variation we extend the model to a spatially structured population where selection acts toward a spatially varying optimum. The population is subdivided into multiple demes connected by genotype-independent migration. Diploid individuals breed within demes and mate randomly. Throughout, the models are deterministic and both recurrent mutation and random genetic drift are ignored.

Methods

We describe the change in the genetic composition of the population by systems of ordinary differential or difference equations. Our analyses of these continuous or discrete dynamical systems is based on mathematical methods such as perturbation theory, bifurcation theory, local stability analysis, and the establishment of Lyapunov functions.

A central tool for the analyses of the models was the perturbation theory developed by Bürger (2009a,b). It provided the analytical techniques to determine the number and stability of equilibria for the special cases of weak and of strong migration. Guided by these results, we analyzed the parameter range of intermediate migration, i.e., when migration and selection are of similar strength.

To obtain a complete classification of the bifurcations in which stable equilibria are involved, we complemented the analytical investigations by numerical analyses. In Chapter I, the numerical calculation of fixed points of systems of ordinary differential equations aided the analysis of the model. In Chapter II, iterations of discrete dynamical systems were performed to determine stable equilibria in the parameter range where analytical results could not be obtained. In order to extend some of our results to models with a continuous spatial domain (instead of discrete demes), we determined the stationary solutions of partial differential equations numerically.

We study properties of the phenotypic mean, the genetic variance, or linkage disequilibrium at stable equilibria. The investigation of equilibrium configurations laid the foundation for this intent. If equilibria are simultaneously stable (hence convergence to equilibria depends on initial conditions), mean, variance, and linkage disequilibrium may exhibit different properties at different equilibria. We gave conditions under which this is the case.

Outline

In this PhD thesis, we studied when and how much genetic variability is maintained in a quantitative trait. If migration is weak, usually higher levels of genetic variability are maintained within subpopulations than without migration. With strong migration genetic variability will be depleted to panmictic levels because of the homogenizing effect of migration. We explored the dependence of genetic variability on the migration rates in detail and investigated the full range of migration.

In Chapter I, we investigated a two-deme model in continuous time. We obtained the equilibrium configurations and bifurcation patterns as a function of the migration rate and determined how these patterns depend on linkage, the rate of locus effects, and the degree of divergent selection.

The characterization of the possible bifurcation patterns in the range of intermediate migration was relatively simple if linkage is loose. Then, the equilibrium configurations of weak migration extend to intermediate migration. However, if linkage is tight and the two selected loci have unequal effects, a variety of bifurcation events occur in the range of intermediate migration. We determined conditions when and how often equilibria enter or leave the state space. The numerical analysis suggested that all possible bifurcations were given by saddle-node, transcritical, or pitchfork bifurcations and that no complicated dynamical behavior or Hopf bifurcations do occur.

Among our main goals was the determination of the migration rates below which genetic variation, local adaptation, and differentiation can be maintained. We found that with sufficiently strong diversifying selection, tight linkage and unequal locus effects tend to promote the maintenance of polymorphism. This complements the work of Yeaman and Whitlock (2011) on the evolution of genetic architectures in subdivided populations. Their results provided support that concentrated architectures (tightly linked loci of unequal effects) tend to evolve in subdivided populations if there is diversifying selection.

Further, we elaborated the dependence of the genetic variance, linkage disequilibrium, and various measures of local adaptation and differentiation (e.g., Q_{ST} and F_{ST}) on linkage, the rate of locus effects, and the degree of divergent selection. Whereas the detailed dependence of these quantities on the underlying parameters is highly intricate, a series of interesting patterns arises: If migration is sufficiently weak (so that both loci are kept polymorphic) and selection is strongly divergent, recombination usually increases the genetic variance at the trait. Thus, recombination tends to affect critical migration rates and the genetic variance

in opposite ways. Depending on the degree of divergent selection and the rate of migration, either specialist haplotypes or generalist haplotypes dominate the genetic composition of the population, wherefore linkage disequilibrium may be positive or negative. Conditions are given that lead to these evolutionary scenarios. For weak migration, different measures of differentiation may depend differently on the recombination rate and locus effects. We found that F_{ST} is sensitive to the genetic architecture, whereas Q_{ST} is not.

In Chapter II, we investigated a multi-deme model in discrete time. We analyzed the effects of spatial structure, selection, and recombination on the maintenance and shape of clines in a quantitative trait. Equilibrium configurations and bifurcations were determined for various migration patterns among n demes and different selection scenarios.

The sequences of bifurcation events exhibit less variety than in Chapter I, since we restricted the genetic architecture to loci of equal effects. The focus was on the incorporation of different spatial structures and selection scenarios into the model. The equilibrium configurations for weak migration depended on selection scenarios but not on migration patterns. Due to symmetry assumptions, the equilibrium configurations for strong migration are identical for all considered migration patterns and selection schemes. This enabled a comprehensive study of the equilibrium configurations for intermediate migration.

Migration patterns include the island and two stepping-stone models, and selection scenarios invoke a sudden or gradual spatial change in fitness. Stable polymorphic equilibria give rise to (stable) clines in the mean and the variance of the trait, and to linkage disequilibrium between the loci. We studied how migration patterns, in particular isolation by distance, and selection scenarios affect existence, uniqueness and properties of these clines.

Critical migration rates below which clines exist increase with isolation by distance. If the environment changes gradually, clines exist only for lower migration rates than in a step environment. In most cases, the cline in the phenotypic mean matches the local optimum closer in the stepping-stone models than in the island model. Thus, stepping-stone models facilitate local adaptation. Whereas in the stepping-stone models the cline in genetic variance is bimodal or maximized in the center of the habitat, it depends only weakly on space in the island model.

Linkage disequilibrium is induced both by stabilizing selection and migration. Stabilizing selection induces negative linkage disequilibrium, whereas the combined action of migration and directional selection causes positive linkage disequilibrium. In a gradually changing environment, some demes are under stabilizing selection, whereas other demes are under

directional selection and linkage disequilibrium may be diminished. We quantified this phenomenon. The role of linkage disequilibrium for the shape of the cline in genetic variance is ambiguous. Positive linkage disequilibrium inflates the genetic variance, whereas negative linkage disequilibrium reduces it.

Our results further delineate the parameter range in which initial conditions determine the evolutionary outcome or a unique equilibrium is asymptotically stable. We found that initial conditions are essential if migration rates are very low and the environment changes gradually.

Finally, we compared our results with previous studies that modeled dispersal by diffusion in continuous space. Although, we assumed rather strong selection, whereas diffusion models are based on the assumption of weak evolutionary forces, the models show excellent concordance.

Overall, our results from Chapters I and II demonstrate that migration-selection balance has the potential to maintain high levels of genetic variation if selection is diversifying and migration rates are in an appropriate range. Critical migration rates below which migration aids quantitative genetic variation depend strongly on the genetic architecture and population structure. In contrast to classical results from one-locus theory, they often exceed the selection strength.

Outlook

During my doctoral studies a third project was initiated in cooperation with Frédéric Guillaume. In this project we consider multiple neutral loci, linked to two selected loci determining a trait. We include random genetic drift by assuming a finite population and recurrent mutations at the neutral loci. The influence of the selected loci on differentiation in allele frequencies at the neutral loci shall be investigated. To this end, we incorporate the concept of the effective migration rate which was introduced by Barton and Bengston (1986) and is reviewed in Kobayashi et al. (2008).

Divergent selection reduces gene flow at linked neutral sites to an effective migration rate which decreases with tighter linkage to selected loci. Therefore, gene flow is inhomogeneous along the genome and minimized nearby selected sites. This causes inhomogeneous patterns of differentiation, where differentiation is maximized near selected loci, whereas the remainder of the genome is homogenized by migration. Previous authors have used the metaphor of 'genomic islands of differentiation' (GIDs) to describe this phenomenon (e.g. Feder and Nosil

2010).

It is well established that reduced gene flow can establish GIDs (Via 2009; Feder et al. 2012; Yeaman 2013). However, the relative importance of this mechanism is subject to ongoing investigation, since inhomogeneous patterns of differentiation may also be generated by other mechanisms (e.g. recent selective sweeps in isolated subpopulations). Recently, Cruickshank and Hahn (2014) proposed that the comparison of different measures of genetic differentiation may reveal the underlying factors generating the GID.

The arguments of Cruickshank and Hahn (2014) are based on the fact that different measures of genetic differentiation depend differently on diversity. On the one hand side there are relative measures of differentiation that depend on within-population heterozygosity (such as F_{ST}), on the other hand there are absolute measures of differentiation (such as the number of nucleotide differences) that do not depend on within-population heterozygosity. We intend to compare the properties of these wide-spread measures in genomic regions of high and low gene flow. How do they depend on the migration rate, the mutation rate, the population size, and the number of alleles at the neutral loci? What is the influence of the number of loci on the variance of these measures? Which patterns of differentiation suggest the inference of reduced gene flow over alternative models?

Since casting the described situation into a stochastic framework is difficult in general, we use the following simplified analytical approach: Considering only three loci - two selected and one neutral locus - we derive the effective migration rate at the neutral locus and substitute the migration rate for the effective migration rate in well-known results from neutral theory (e.g. Fu et al. 2003; Kermany et al. 2008; Dewar et al. 2011). This method reveals the effect of linkage on the allele frequency distribution at the neutral locus which provides the foundation for investigating the role of linkage on various measures of differentiation. Complementing this analytical approach, we perform individual based simulations with *Nemo* (Guillaume and Rougemont 2006).

The work presented in this thesis may be a guideline to further investigations, which we briefly discuss in the following paragraphs.

Throughout this thesis we assumed that the trait under selection is determined by two loci. Studies including multiple selected loci often assume a normal phenotypic distribution or are predominantly numerical (Tufto 2000; Yeaman and Guillaume 2009; Huisman and Tufto 2012). Since migration induces deviations from normality (skew), the incorporation of higher moments will be necessary to describe the phenotypic distribution of a trait accurately.

Following the approach of Bürger (2000, Chapter V), one may derive the dependence of the local phenotypic mean on genetic skew and migration.

In Chapter II of the thesis we briefly investigated diffusion models in continuous space. The number and stability of equilibria in these models are unknown and analytical progress has yet to be made. Whereas the methods used for the analysis of models in continuous and discrete space are different, the results are often similar. Our results on populations subdivided into discrete niches may shape the intuition for further research on models assuming continuous space.

Chapter I

A two-locus model of spatially varying stabilizing or directional selection on a quantitative trait[1]

Abstract

The consequences of spatially varying, stabilizing or directional selection on a quantitative trait in a subdivided population are studied. A deterministic two-locus two-deme model is employed to explore the effects of migration, the degree of divergent selection, and the genetic architecture, i.e., the recombination rate and ratio of locus effects, on the maintenance of genetic variation. The possible equilibrium configurations are determined as functions of the migration rate. They depend crucially on the strength of divergent selection and the genetic architecture. The maximum migration rates are investigated below which a stable fully polymorphic equilibrium or a stable single-locus polymorphism can exist. Under stabilizing selection, but with different optima in the demes, strong recombination may facilitate the maintenance of polymorphism. However usually, and in particular with directional selection in opposite direction, the critical migration rates are maximized by a concentrated genetic architecture, i.e., by a major locus and a tightly linked minor one. Thus, complementing previous work on the evolution of genetic architectures in subdivided populations subject to diversifying selection, it is shown that concentrated architectures may aid the maintenance of polymorphism. Conditions are obtained when this is the case. Finally, the dependence of the phenotypic variance, linkage disequilibrium, and various measures of local adaptation and differentiation on the parameters is elaborated.

Key words: Migration, Recombination, Geographical structure, Genetic variation, Differentiation, Genetic architecture

[1]Geroldinger L. and Bürger R., 2014. A two-locus model of spatially varying stabilizing or directional selection on a quantitative trait, Theoretical Population Biology 94, 10-41

1 Introduction

Gene flow in a geographically structured population may have opposing effects on its genetic composition. Whereas weak migration usually augments subpopulations with genetic variation, strong migration may swamp the total population with the genotype that has the highest average fitness across all environments. The theory of migration and selection at a single locus is rather well developed and reviewed in Karlin (1982), Nagylaki and Lou (2008), and Bürger (2014). The theory treating selection on multiple loci is much less complete (Bürger 2014). Key issues that need to be addressed in a multilocus context include the following. What are the consequences of linkage between the selected loci for the maintenance of variation? What is the influence of epistasis and of the distribution of locus effects on the genetic variability that can be maintained? Pioneering work on the role of recombination in migration-selection models is due to Bazykin (1973), Li and Nei (1974), Christiansen and Feldman (1975), Slatkin (1975), and Barton (1983).

Here, we consider an additive quantitative trait under stabilizing selection in a population subdivided into two demes. Our main goal is to elucidate the capacity of migration to maintain genetic variation. For a two-locus model, we study how this capacity depends on the genetic architecture of the trait (linkage and relative magnitude of locus effects) and on the strength of divergent selection induced by different positions of the trait optima.

For panmictic populations the investigation of the maintenance of genetic variation in quantitative traits under stabilizing selection goes back to Wright (1935), who concluded that no genetic variation can be maintained. His analysis assumed a quadratic fitness function and two unlinked additive loci of equal effect, such that the double heterozygote is at the fitness optimum. Subsequently, it was shown that both loci can be maintained polymorphic if their effects are sufficiently different and fitness decays other than quadratically, e.g., linearly or exponentially (Gale and Kearsey 1968, Nagylaki 1989b) or like a Gaussian (Willensdorfer and Bürger 2003), or if the loci are sufficiently tightly linked and their effects are different (Gavrilets and Hastings 1993). Barton (1986) extended Wright's model by admitting an arbitrary number of unlinked equivalent loci and an arbitrary position of the optimum. Nevertheless, at most one locus can be maintained polymorphic. Bürger and Gimelfarb (1999) showed that, for randomly chosen recombination rates and locus effects, the expected equilibrium variance decreases rapidly with the number of loci contributing to the trait from its relatively high value for two loci.

Further support for the notion that stabilizing selection depletes genetic variation comes

from the extensive literature on mutation-selection balance of quantitative traits. In a nutshell, for a large subset of the region of parameters considered to be biologically most relevant, the expected genetic variance is proportional to the sum of mutation rates at all loci affecting the trait (e.g., Latter 1960, Bulmer 1972, Turelli 1984, Bürger and Hofbauer 1994). The heritability predicted from these and other models, however, is considerably lower than that observed for the majority of quantitative traits. In other regions of the parameter space, higher levels of genetic variation can be expected (e.g., Kimura 1965, Lande 1975). For extensive reviews of this topic, see Bürger (2000, Chapters VI and VII) or Barton and Keightley (2002).

Because many, if not most, natural populations are geographically structured and selection varies spatially, it seems natural to investigate the role of migration-selection balance in maintaining quantitative genetic variation. In a subdivided population, selection is usually heterogeneous and the phenotypic optimum of a trait depends on the local environment. However, the number of theoretical studies is quite limited, and most of them necessarily make several simplifying assumptions so that results are more circumstantial and no satisfactory picture has emerged yet.

Phillips (1996) and Lythgoe (1997) generalized the model of Barton (1986) to two demes. They investigated how population differentiation depends on migration by assuming that stabilizing selection is uniform, i.e., towards the same optimum in both demes, or that the mean phenotype coincides with the optimum, which is only slightly more general. Tufto (2000) and Huisman and Tufto (2012) compared multilocus models, such as that of Lythgoe (1997), to the infinitesimal model. They showed that differences between the infinitesimal model and multilocus models with a finite number of loci depend strongly on the number of loci contributing to genetic variance, but are quite insensitive to the number of alleles per locus. They found that if the initial genetic variance is sufficiently large, the infinitesimal model provides accurate approximations for the population mean and variance of the multilocus models down to a few loci. For several unlinked loci, Spichtig and Kawecki (2004) investigated a two-deme model with directional selection acting in opposite direction. They classified the possible equilibria into three types (monomorphic at all loci, polymorphic at some loci, and polymorphic at all loci) and explored numerically which type of equilibrium is approached in the long run, and how this depends on the curvature of the fitness function, the migration rate, the relative habitat sizes, and the number of loci. Since all these investigations mainly assumed unlinked loci of equal effect, the present work focuses on the role of linkage and the relative size of locus effects.

A quite different and interesting aspect of the interaction of migration and stabilizing

selection was studied in Yeaman and Whitlock (2011) by means of simulation of a multilocus model in which new mutations of variable effect occur across the genome. They found that the genetic architecture of a trait may evolve such that, after sufficiently long time, the trait is determined by one major locus and several closely linked minor loci. This is called a concentrated genetic architecture. That unequal locus effects may influence the degree of genetic differentiation significantly was found previously by Yeaman and Guillaume (2009). In their model, unequal locus effects can lead to more skewed equilibrium distributions, which in turn affects the equilibrium mean phenotypes. An approach complementary to that of Yeaman and Whitlock (2011) showing that concentrated genetic architectures can be expected to evolve in heterogeneous environments was pursued by Bürger and Akerman (2011). They determined analytically the strength of linkage required for a mutation of small effect to invade and become established if it occurs in the neighborhood of a locus that already contributes to differentiation between subpopulations. More generally, and also complementary to Spichtig and Kawecki (2004)'s work, detailed analytical studies of the maintenance of genetic variation at two linked loci under nonepistatic (linear) directional selection in opposite direction were performed by Akerman and Bürger (2014b), who assumed absence of dominance.

In the present work, we consider a trait determined by two loci which is under quadratic stabilizing selection towards potentially different optima in two demes. We admit arbitrary recombination and focus on exploring loci with unequal effects. This is the natural complementation of the models in Phillips (1996), Lythgoe (1997), Tufto (2000), Spichtig and Kawecki (2004), and Yeaman and Guillaume (2009), where linkage and unequal locus effects are more or less neglected. However, as in most of these works, we ignore new mutations and random genetic drift. Thus, we employ a deterministic model.

We assume evolution in continuous time, population regulation within each deme (soft selection), bidirectional migration of equal strength, and symmetric positions of the phenotypic optima, i.e., if P is its position in one deme, it is $-P$ in the other. The optimum P is varied and can be at any phenotypic value, thus symmetric or asymmetric stabilizing selection, as well as directional selection in each deme is studied. A haploid and a diploid version of the model is investigated.

In the haploid case much more complete results are obtained. We describe the equilibrium configurations and bifurcation patterns as the migration rate increases. It turns out that depending on the ratio of locus effects and the position of the phenotypic optimum, three scenarios of divergent selection can be distinguished: weakly, moderately, and strongly divergent selection. They differ significantly not only in the kinds of bifurcation patterns and

equilibrium configurations that occur, but also in the amount of genetic variation and in the maximum migration rates below which genetic variation can be maintained.

For weakly or moderately divergent selection, there is stabilizing selection in each deme, i.e., an intermediate phenotype has highest fitness. Under strongly divergent selection, an extreme phenotype has highest fitness in each deme. In contrast to the haploid model, in the diploid model substantial genetic variation can be maintained despite strong migration provided the two loci have sufficiently different effects and are tightly linked. We determine the critical migration rates below which one or two loci can be maintained polymorphic. They depend crucially on the genetic basis of the trait under selection. Finally, we apply the results on the equilibrium configurations to quantify genetic variance, linkage disequilibrium (LD), and various measures of local adaptation and differentiation. Of course, the maintenance of genetic variance, LD, local adaptation, and differentiation requires evolution to a stable polymorphic equilibrium.

2 The model

We study a deterministic migration-selection model in which a sexually reproducing population is subdivided into two demes, α and β, connected by genotype-independent migration. We assume that in each deme γ ($\gamma \in \Gamma = \{\alpha, \beta\}$) genotypic fitnesses are uniquely determined by the genotypic value G of a quantitative trait and write $w_\gamma(G)$. This is the case in the classical additive model of quantitative genetics in which $w_\gamma(G)$ is obtained by averaging across the independent and normally distributed environmental contributions to the phenotype (Bürger 2000, Chapter V.1). Specifically, we assume that

$$w_\gamma(G) = w_0 - s(G - P_\gamma)^2, \tag{2.1}$$

where P_γ denotes the optimum in deme γ, $s > 0$ measures the strength of selection, and w_0 is a constant. The trait is determined additively by two diallelic loci, $\mathcal{A}$ and $\mathcal{B}$. The alleles at $\mathcal{A}$ are denoted by A and a, those at $\mathcal{B}$ by B and b. The frequencies of the four gametes, AB, Ab, aB, ab, in deme γ are designated $x_{1,\gamma}$, $x_{2,\gamma}$, $x_{3,\gamma}$, $x_{4,\gamma}$, respectively. The sexes are equivalent, and there is random mating within each deme. We assume soft selection, i.e., population regulation occurs within each deme. We ignore random genetic drift and mutation and employ a continuous-time model to describe evolution. Therefore, fitnesses should be interpreted as Malthusian parameters. Recombination between the two loci occurs at rate $r \geq 0$. The rate at which individuals in deme γ are replaced by immigrants from the other deme is denoted by $m_\gamma \geq 0$.

For our analytical investigations, we always impose the following symmetry conditions:

$$m = m_\alpha = m_\beta \tag{2.2a}$$

and

$$P = P_\beta = -P_\alpha. \tag{2.2b}$$

Robustness of our results with respect to deviations from these assumptions is treated in the Discussion.

Instead of gamete frequencies it is often more convenient to work with allele frequencies and the measure $D_\gamma = x_{1,\gamma}x_{4,\gamma} - x_{2,\gamma}x_{3,\gamma}$ of linkage disequilibrium (LD) in deme γ. We write $p_\gamma = x_{1,\gamma} + x_{2,\gamma}$ and $q_\gamma = x_{1,\gamma} + x_{3,\gamma}$ for the frequencies of A and B in deme γ. Then the gamete frequencies $x_{i,\gamma}$ are calculated from p_γ, q_γ, and D_γ by

$$x_{1,\gamma} = p_\gamma q_\gamma + D_\gamma, \qquad x_{2,\gamma} = p_\gamma(1-q_\gamma) - D_\gamma, \tag{2.3a}$$

$$x_{3,\gamma} = (1-p_\gamma)q_\gamma - D_\gamma, \quad x_{4,\gamma} = (1-p_\gamma)(1-q_\gamma) + D_\gamma\,. \tag{2.3b}$$

The constraints $x_{i,\gamma} \geq 0$ and $\sum_{i=1}^4 x_{i,\gamma} = 1$ for $i \in \{1,2,3,4\}$ and $\gamma \in \Gamma$ transform into

$$0 \leq p_\gamma \leq 1, \quad 0 \leq q_\gamma \leq 1, \tag{2.4a}$$

and

$$-\min\{p_\gamma q_\gamma, (1-p_\gamma)(1-q_\gamma)\} \leq D_\gamma \leq \min\{p_\gamma(1-q_\gamma), (1-p_\gamma)q_\gamma\}\,. \tag{2.4b}$$

We note that $D_\gamma > 0$ corresponds to an excess of the haplotypes with minimum or maximum phenotype in deme γ. See Table 1 for a glossary of symbols.

2.1 The haploid model

In the haploid case, selection acts on the four gametes, i.e., the fitness of gamete (haplotype) i in deme γ is $w_{i,\gamma} = w_\gamma(G_i)$, where G_i is the genotypic value of gamete i. We assign (deme-independent) genotypic effects $-c_1$, c_1, $-c_2$, c_2 to the four alleles A, a, B, b, respectively ($c_1, c_2 > 0$). The assumption of additivity yields $-c_1 - c_2$, $-c_1 + c_2$, $c_1 - c_2$, $c_1 + c_2$ for the genotypic values of the gametes AB, Ab, aB, ab, respectively. Without loss of generality, we use a scale such that $c_1 + c_2 = 1$, i.e., the phenotypic range is $[-1, 1]$. The phenotypic optima are restricted to satisfy $0 \leq P \leq 1$. We introduce

$$\kappa = c_2/c_1, \tag{2.5}$$

the ratio of locus effects. Without loss of generality, we always assume $0 < \kappa \leq 1$, and call $\mathcal{A}$ the major locus and $\mathcal{B}$ the minor locus.

Therefore, the genotypic values of the four haplotypes AB, Ab, aB, ab are -1, $-(1-\kappa)/(1+\kappa)$, $(1-\kappa)/(1+\kappa)$, 1, and their fitnesses in deme α ($w_{i,\alpha}$) are

$$w_0 - s(1-P)^2,\ w_0 - s\Big(\frac{1-\kappa}{1+\kappa} - P\Big)^2,\ w_0 - s\Big(\frac{1-\kappa}{1+\kappa} + P\Big)^2,\ w_0 - s(1+P)^2, \tag{2.6}$$

respectively. In deme β, P needs to be substituted by $-P$.

We use the following standard differential equations to describe the evolution of gamete frequencies in deme γ:

$$\dot{x}_{i,\gamma} = \frac{d}{dt}x_{i,\gamma} = x_{i,\gamma}(w_{i,\gamma} - \bar{w}_\gamma) - \eta_i r D_\gamma + m_\gamma(x_{i,\gamma^*} - x_{i,\gamma}). \tag{2.7}$$

They can be derived straightforwardly from the corresponding discrete-time model by assuming that all evolutionary forces (selection, recombination, and migration) are weak (Bürger 2009a). In (2.7), $\bar{w}_\gamma = \sum_{i=1}^4 w_{i,\gamma}x_{i,\gamma}$ is the mean fitness in deme γ, $\eta_1 = \eta_4 = -\eta_2 = -\eta_3 = 1$, and γ^* denotes the deme different from γ. The state space is $S_4 \times S_4$, where $S_4 = \Big\{(x_1,x_2,x_3,x_4):\ x_i \geq 0 \text{ and } \sum_{i=1}^4 x_i = 1\Big\}$ is the simplex. The differential equations for the allele frequencies and linkage disequilibria are given in Appendix A.1.

By rescaling time in (2.7), the number of parameters can be reduced by one without changing the equilibrium and stability properties. Instead of (s,r,m) we use the rescaled parameters $(1,r/s,m/s)$ in Sections 6, 7, and 8.1. In Sections 8.2, 6.3, and 8.4, we use the original scaling to emphasize the influence of the selection intensity s. Unless otherwise specified, we assume $r > 0$.

2.2 The diploid model

In this case, selection acts on the 16 different combinations of two-locus haplotypes. We assign genotypic effects $-c_1/2$, $c_1/2$, $-c_2/2$, and $c_2/2$ to the four alleles A, a, B, and b, respectively. By assuming additivity within and between loci, the genotypic values of all 16 genotypes are obtained. Again, locus effects are scaled such that $c_1 + c_2 = 1$. Then the two fully homozygous genotypes AB/AB and ab/ab have the (extreme) phenotypes -1 and 1, respectively, and all four double heterozygotes have phenotype 0. The fitness of genotype ij in deme γ is $w_{ij,\gamma} = w_\gamma(G_{ij})$, where G_{ij} is its genotypic value. If we denote the marginal fitness of haplotype i by $w_{i,\gamma} = \sum_{j=1}^4 w_{ij,\gamma}x_{j,\gamma}$, equations (2.7) again describe the evolutionary dynamics of gamete frequencies.

Table 1. Glossary of symbols. We define the symbols in the main text that occur in more than one paragraph. Roman and Greek alphabets are listed separately. Uppercase letters precede lower case ones and listing is in order of appearance in the text. The references are to the position of first appearance in the text. Reference (2.1)−, refers to the text above Equation (2.1), whereas (2.1)+ refers to the text below Equation (2.1).

Symbol	Reference	Definition
$\mathcal{A}$	(2.1)+	Major locus
A	(2.1)+	First allele at locus $\mathcal{A}$
a	(2.1)+	Second allele at locus $\mathcal{A}$
$\mathcal{B}$	(2.1)+	Minor locus
B	(2.1)+	First allele at locus $\mathcal{B}$
b	(2.1)+	Second allele at locus $\mathcal{B}$
c_1	(2.5)−	Half (haploid) or total (diploid) substitution effect at $\mathcal{A}$
c_2	(2.5)−	Half (haploid) or total (diploid) substitution effect at $\mathcal{B}$
D_γ	(2.3)−	Linkage disequilibrium in deme γ
D	(8.12)−	Linkage disequilibrium in the entire population
$\mathsf{E}^{\mathcal{A}}_{1,\gamma}$, $\mathsf{E}^{\mathcal{A}}_{2,\gamma}$	(3.6)−	SLPs in deme γ for $m = 0$ in the diploid model
e	(3.1)−	Alternative fitness parameter
F_γ	(3.1)−	Internal equilibrium in deme γ for $m = 0$ in the haploid model
$\mathsf{F}_{1,\gamma}$, $\mathsf{F}_{2,\gamma}$, $\mathsf{F}_{3,\gamma}$	(3.6)−	Internal equilibria in deme γ for $m = 0$ in the diploid model
F_1, F_2	Fig. 4	Projections used in the bifurcation diagrams
F_{ST}	(8.18)	Measure of differentiation
G	(2.1)−	Genotypic value of the trait
G_i	(2.5)−	Genotypic value of gamete i
G_{ij}	(2.7)+	Genotypic value of genotype ij (diploid)
$\bar{G}_\gamma$	(8.12)	Genotypic mean in deme γ
$I_m(\mathsf{G}_\alpha, \mathsf{H}_\beta)$	Sect. 4	Weak-migration perturbation of the equilibrium $(\mathsf{G}_\alpha, \mathsf{H}_\beta)$
I_k	(6.1)−	Internal equilibria ($0 \le k \le 7$)
L_γ	(8.16)	Migration load in deme γ
$\mathsf{M}_{i,\gamma}$	(3.1)−	Equilibrium in deme γ corresponding to fixation of gamete i
m	(2.2a)	Migration rate
m_γ	(2.2)−	Immigration rate into deme γ
$m_{\mathrm{st}}(\mathsf{E})$	(6.1)−	Migration rate at which the equilibrium E gets stable
$m_{\mathrm{un}}(\mathsf{E})$	(6.1)−	Migration rate at which the equilibrium E gets unstable
$m_{\mathrm{ad}}(\mathsf{E})$	(6.1)−	Migration rate at which the equilibrium E gets admissible
$m_{\mathrm{na}}(\mathsf{E})$	(6.1)−	Migration rate at which the equilibrium E loses admissibility
$m_*^{(j)}(\mathsf{E})$	(6.1)−	Migration rate at which the state of E changes for the jth time ($j \ge 2$), where $* \in \{\mathrm{st}, \mathrm{un}, \mathrm{ad}, \mathrm{na}\}$
$m_{2,3}$	(6.5)	Critical migration rate
$\tilde{m}_{\mathrm{st}}(\mathsf{S}^{\mathcal{A}})$	(6.10)	Critical migration rate and zero of π_2^0
$m_*^{\mathsf{D}}(\mathsf{E})$	Sect. 7	Migration rate in the diploid model at which the state of E changes, where $* \in \{\mathrm{st}, \mathrm{un}, \mathrm{ad}, \mathrm{na}\}$
$m_*^{\mathsf{D},(j)}(\mathsf{E})$	Sect. 7	Migration rate in the diploid model at which the state of E changes for the jth time ($j \ge 2$), where $* \in \{\mathrm{st}, \mathrm{un}, \mathrm{ad}, \mathrm{na}\}$
$m^0_{\max}$	Sect. 8.1	Maximum migration rate below which one locus can be polymorphic
$m_{\max}$	Sect. 8.1	Maximum migration rate below which both loci can be polymorphic
P_γ	(2.1)	Phenotypic optimum in deme γ

P	(2.2b)	Phenotypic optimum
$\bar{P}$	(6.10)+	Critical value of P
$\tilde{P}$	(6.11)−	Critical value of P
p_γ	(2.3)−	Frequency of allele A in deme γ
Q_{ST}	(8.21)−	Measure of differentiation
q_γ	(2.3)−	Frequency of allele B in deme γ
R_1, R_2	(6.1)−	Fully polymorphic boundary equilibria for $r = 0$
r	(2.2)−	Recombination rate
$\tilde{r}$	(3.3b)	Critical recombination rate
r_1	Fig. 2	Critical recombination rate (diploid)
r_2	Fig. 2	Critical recombination rate (diploid)
r^*	(6.29)−	Critical recombination rate
r^{**}	(6.29)−	Critical recombination rate
$r^\dagger$	(6.39)+	Critical recombination rate
r^{D}	(7.1)−	Critical recombination rate (diploid)
$r^{\mathsf{D},*}$	(7.2)−	Critical recombination rate (diploid)
S_4	(2.7)+	Simplex
$\mathsf{S}_1^{\mathcal{A}}$, $\mathsf{S}_2^{\mathcal{A}}$	(6.1)−	SLPs with polymorphic locus $\mathcal{A}$
$\mathsf{S}_1^{\mathcal{B}}$, $\mathsf{S}_2^{\mathcal{B}}$	(6.2)−	SLPs with polymorphic locus $\mathcal{B}$
s	(2.1)	Selection intensity
t	(2.7)	Time
u	(3.1)−	Alternative fitness parameter
Var_γ	(8.1)	Genetic variance in deme γ
Var	(8.11)+	Genetic variance in the entire population
v	(3.1)−	Alternative fitness parameter
$w_\gamma(G)$	(2.1)−	Fitness of genotypic value G in deme γ
w_0	(2.1)	Constant
$w_{i,\gamma}$	(2.5)−	Fitness of gamete i in deme γ
$\bar{w}_\gamma$	(2.7)+	Mean fitness in deme γ
$w_{ij,\gamma}$	(2.7)+	Fitness of genotype ij (diploid) in deme γ
$x_{i,\gamma}$	(2.1)+	Frequency of gamete i in deme γ
α	(2.1)−	First deme
β	(2.1)−	Second deme
Γ	(2.1)−	Set of demes
γ	(2.1)−	Arbitrary deme
γ^*	(2.7)	Deme different from γ
η_i	(2.7)+	Constants
Θ	(5.3)+	LD in the strong-migration limit
κ	(2.5)	Ratio of locus effects
ξ_i	(5.1)	Spatially averaged gamete frequencies
$\nu_{i,\gamma}$	(5.2)	Measure of spatial homogeneity
π_1, π_2	(6.10)−	Factors of the characteristic polynomial of the Jacobian at $\mathsf{S}_1^{\mathcal{A}}$
π_1^0, π_2^0	(6.10)−	Value of π_1, π_2 at zero
ϕ	(6.18)	Function of κ, P, and r
ω_i	(5.3)	Spatially averaged fitnesses of gametes
$\bar{\omega}$	(5.3)	Spatially averaged mean fitness
$\hat{}$	(6.1)−	Indicates an equilibrium value

3 No migration

For panmictic populations, the models introduced above have been analyzed previously. Here, we recapitulate and summarize the pertinent results and assume $m = 0$. Because then the dynamics of the two demes are decoupled, we describe the equilibrium configuration for each deme. Equilibria in deme γ are labeled by the corresponding subscript.

3.1 The haploid model

A general haploid diallelic two-locus model was investigated by Rutschman (1994) and by Bank et al. (2012). The relations in (A.2) reduce our model to a special case of that in Bank et al. (2012) (we write u, v, e for their α, β, γ). The parameters u, v, e (A.2) always satisfy $u \geq v > 0$ and $e > 0$.

We denote the monomorphic equilibria corresponding to fixation of gamete i in deme γ by $\mathsf{M}_{i,\gamma}$. No single-locus polymorphisms (SLPs) are admissible in this model. However, a fully polymorphic (internal) equilibrium may exist. It will be denoted by F_γ. The coordinates of this equilibrium can be expressed in terms of complicated double-square roots (eqs. (S.39), (S.41), and (S.45) in Supporting Information of Bank et al. 2012). If $P = 0$, F_γ has the simple form

$$\hat{p}_\gamma = \frac{1}{2},\ \hat{q}_\gamma = \frac{1}{2},\ \hat{D}_\gamma = \frac{r}{s}\frac{(1+\kappa)^2}{16\kappa} - \sqrt{\frac{1}{16} + \left(\frac{r}{s}\frac{(1+\kappa)^2}{16\kappa}\right)^2}. \tag{3.1}$$

In general, F_γ depends on P_γ, and $\mathsf{F}_\alpha = \mathsf{F}_\beta$ if and only if $P = 0$. From Rutschman (1994) and Theorem S.2 in Bank et al. (2012), we infer easily the existence conditions and stability properties of all equilibria in a single (randomly mating) subpopulation:

Proposition 3.1. *1. The monomorphic equilibrium $\mathsf{M}_{1,\alpha}$ ($\mathsf{M}_{4,\beta}$) is globally asymptotically stable in deme α (deme β) if and only if*

$$P > \frac{1}{1+\kappa}. \tag{3.2}$$

If $P < 1/(1+\kappa)$, then $\mathsf{M}_{1,\gamma}$ and $\mathsf{M}_{4,\gamma}$ are unstable in both demes.

2. There exists at most one internal equilibrium (F_γ, $\gamma \in \Gamma$). It is unstable whenever it exists.

3. The internal equilibrium F_γ exists if and only if both $\mathsf{M}_{2,\gamma}$ and $\mathsf{M}_{3,\gamma}$ are asymptotically stable. This is the case if and only if

$$0 \leq P < \frac{\kappa}{1+\kappa} \tag{3.3a}$$

and

$$r > \tilde{r} = \frac{4s(1-\kappa)P}{1+\kappa} \tag{3.3b}$$

hold.

4. If (3.2) *and* (3.3) *are violated, i.e., if*

$$\min\left\{\frac{\kappa}{1+\kappa}, \frac{r}{4s}\frac{1+\kappa}{1-\kappa}\right\} < P < \frac{1}{1+\kappa}, \tag{3.4}$$

then $\mathsf{M}_{2,\alpha}$ *(*$\mathsf{M}_{3,\beta}$*) is globally asymptotically stable in deme* α *(deme* β*).*

If $P = 1/(1+\kappa)$, the gametes AB and Ab have identical and maximum fitness in deme α, and gametes aB and ab have identical and maximum fitness in deme β. Therefore, in each deme locus $\mathcal{A}$ goes to fixation and all trajectories converge to an edge consisting of equilibria (Theorem 10 in Rutschman 1994).

We call selection directional if the haplotype fitnesses in deme α satisfy $w_{1,\alpha} \geq w_{2,\alpha} \geq w_{3,\alpha} \geq w_{4,\alpha}$ and $w_{1,\alpha} > w_{4,\alpha}$ (hence, the haplotype fitnesses in deme β satisfy the reversed inequalities). This is the case if and only if

$$P \geq \frac{1}{1+\kappa}. \tag{3.5}$$

If (3.5) is violated, we call selection stabilizing. Then $w_{2,\alpha} \geq w_{3,\alpha} > w_{4,\alpha}$ and $w_{2,\alpha} > w_{1,\alpha}$ holds.

Note that decreasing κ increases the parameter range under which selection is stabilizing. The special case $P_\alpha = P_\beta = P = 0$ is called uniform selection.

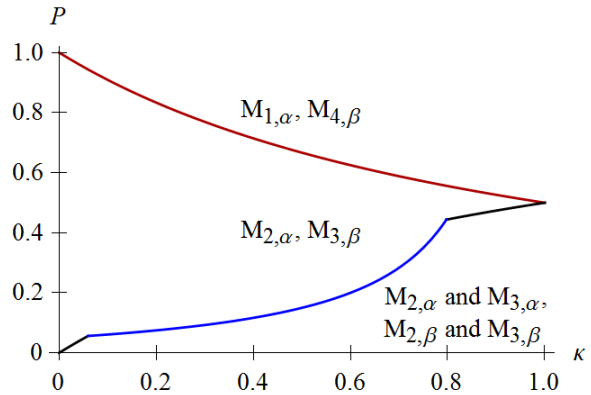

Figure 1: Regions of stability of equilibria in the haploid model for $m = 0$. Above the red line, the equilibrium $\mathsf{M}_{1,\alpha}$ ($\mathsf{M}_{4,\beta}$) is globally asymptotically stable in deme α (deme β), whereas $\mathsf{M}_{2,\alpha}$ ($\mathsf{M}_{3,\beta}$) is asymptotically stable below the red line in deme α (deme β). Below the black and the blue line, given by the left-hand side of (3.4), $\mathsf{M}_{2,\gamma}$ and $\mathsf{M}_{3,\gamma}$ are asymptotically stable in both demes. The recombination rate satisfies $r/s = 0.2$.

3.2 The diploid model

We assume $P = 0$ and review the diploid model, following Chapter VI.2 in Bürger (2000). In contrast to Section 3.1, we consider only a single deme γ. In addition to the monomorphic equilibria $\mathsf{M}_{i,\gamma}$, two other types of equilibria may be stable: (i) three internal equilibria $\mathsf{F}_{1,\gamma}$, $\mathsf{F}_{2,\gamma}$, $\mathsf{F}_{3,\gamma}$ and (ii) two SLPs $\mathsf{E}^{\mathcal{A}}_{1,\gamma}$, $\mathsf{E}^{\mathcal{A}}_{2,\gamma}$ with the major locus polymorphic. Two SLPs with the minor locus polymorphic may be admissible but are unstable.

All equilibria can be calculated explicitly. The coordinates of $\mathsf{F}_{1,\gamma}$ are obtained from (3.1) by replacing s with $s/4$. The equilibria $\mathsf{F}_{2,\gamma}$ and $\mathsf{F}_{3,\gamma}$ are called unsymmetric because their coordinates do not satisfy simple symmetry relations. They are stated in Bürger (2000, p. 205). The coordinates of the SLPs $\mathsf{E}^{\mathcal{A}}_{1,\gamma}$, $\mathsf{E}^{\mathcal{A}}_{2,\gamma}$ are given by

$$\hat{p}_\gamma = \frac{1}{2} + \kappa,\ \hat{q}_\gamma = 0,\ \hat{D}_\gamma = 0, \tag{3.6a}$$

$$\hat{p}_\gamma = \frac{1}{2} - \kappa,\ \hat{q}_\gamma = 1,\ \hat{D}_\gamma = 0, \tag{3.6b}$$

respectively. Figure 2 displays the regions of stability of the possibly asymptotically stable equilibria.

In addition to the three internal equilibria $\mathsf{F}_{1,\gamma}$, $\mathsf{F}_{2,\gamma}$, $\mathsf{F}_{3,\gamma}$, which may be asymptotically stable for small recombination rates, there is a large parameter range at which $\mathsf{E}^{\mathcal{A}}_{1,\gamma}$ and $\mathsf{E}^{\mathcal{A}}_{2,\gamma}$ are asymptotically stable. Therefore, in contrast to the haploid model, high levels of variability can be maintained without gene flow.

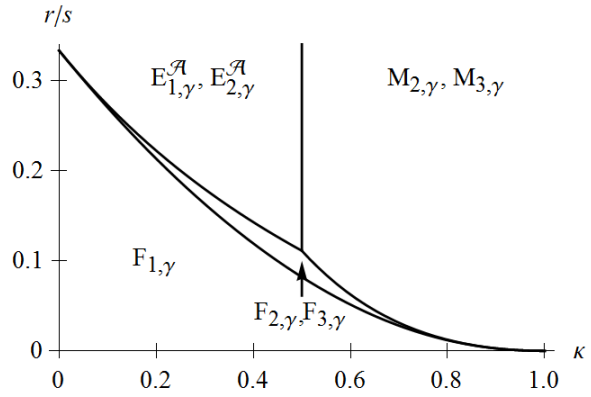

Figure 2: Regions of stability of equilibria in the diploid model for $P = 0$ and $m = 0$. The thresholds above which and below which $\mathsf{F}_{2,\gamma}$ and $\mathsf{F}_{3,\gamma}$ are stable are given by $\frac{r_1}{s} = \frac{1}{3}\frac{-1-\kappa^2+2\sqrt{1-\kappa^2+\kappa^4}}{(1+\kappa)^2}$ and $\frac{r_2}{s} = \min\left[\left(\frac{1-\kappa}{1+\kappa}\right)^2, \frac{1}{3}\frac{1-\kappa}{1+\kappa}\right]$, respectively.

We call selection directional if $w_\alpha(G)$ is decreasing in G. Then $w_\beta(G)$ is increasing in G.

Simple calculations show that this is the case if and only if

$$P \geq \frac{2+\kappa}{2(1+\kappa)}. \tag{3.7}$$

If (3.7) is violated, we call selection stabilizing.

4 Weak migration

Following Karlin and McGregor (1972a,b), regular perturbation methods can be used to infer the existence, stability, and coordinates of equilibria under weak migration from a corresponding model without migration.

If $m = 0$, the dynamics (2.7) on $S_4 \times S_4$ is simply the Euclidean product of the respective single-deme dynamics. Therefore, every equilibrium is of the form $(\mathsf{G}_\alpha, \mathsf{H}_\beta)$, where G_α and H_β are admissible equilibria in deme α and β, respectively. (For simplicity, we identify equilibria with their coordinates in the respective deme.) Hence, if $m = 0$, (2.7) may have up to 25 equilibria in the haploid case. In the diploid model we may have up to 121 equilibria already if $P = 0$. If H_β has the same coordinates as G_α, we denote the equilibrium $(\mathsf{G}_\alpha, \mathsf{H}_\beta) = (\mathsf{G}_\alpha, \mathsf{G}_\beta)$ by G. In particular, the monomorphic equilibria in the full system on $S_4 \times S_4$ are denoted by $\mathsf{M}_i = (\mathsf{M}_{i,\alpha}, \mathsf{M}_{i,\beta})$ $(i = 1, 2, 3, 4)$. They exist for every $m \geq 0$.

In Karlin and McGregor (1972b), the following was proved for sufficiently small $m > 0$. Suppose that in the absence of migration every equilibrium is hyperbolic (i.e., its Jacobian matrix has no eigenvalues with vanishing real part). Then (i) in the neighborhood of each asymptotically stable equilibrium for $m = 0$, there exists exactly one equilibrium for $m > 0$ and it is asymptotically stable; (ii) in the neighborhood of each unstable internal equilibrium for $m = 0$, there exists exactly one equilibrium for $m > 0$ and it is unstable; (iii) in the neighborhood of each unstable boundary equilibrium for $m = 0$, there exists at most one equilibrium for $m > 0$, and if it exists, it is unstable. If we denote the perturbation of $(\mathsf{G}_\alpha, \mathsf{H}_\beta)$ by $I_m(\mathsf{G}_\alpha, \mathsf{H}_\beta)$, then $I_m(\mathsf{G}_\alpha, \mathsf{H}_\beta) \to (\mathsf{G}_\alpha, \mathsf{H}_\beta)$ as $m \to 0$. If $\mathsf{G}_\alpha = \mathsf{H}_\beta$, we have $I_m(\mathsf{G}_\alpha, \mathsf{H}_\beta) = (\mathsf{G}_\alpha, \mathsf{H}_\beta)$ for $m \geq 0$. These statements hold independently of the ploidy level of the model.

If, in the haploid model, (3.2) or (3.4) applies, these conclusions can be strengthened because in the absence of migration, generically, every trajectory converges to an equilibrium point (Proposition 3.1). Therefore, a result by Akin (1993, p. 244) implies that for sufficiently small m, every trajectory of the full dynamics (2.7) converges to an equilibrium (cf. Bürger 2009a, Section 5). In particular, if an equilibrium is globally asymptotically stable if $m = 0$, its perturbation is globally asymptotically stable if m is sufficiently small.

Therefore, the stability properties of all equilibria in the haploid model can be inferred from Proposition 3.1 if migration is sufficiently weak. These inferences require several case distinctions and are deferred to Section 6. If $P = 1/(1+\kappa)$, a case not covered by Proposition 3.1, the dynamics is degenerate if $m = 0$ because there exists a manifold of equilibria. Hence, perturbation methods can not be used to infer the equilibrium structure for small m.

We set $\mathsf{I}_1 = I_m(\mathsf{F})$, where $\mathsf{F} = (\mathsf{F}_\alpha, \mathsf{F}_\beta)$. If $P = 0$, our symmetry assumptions (2.2) imply $\mathsf{F}_\alpha = \mathsf{F}_\beta$. Therefore, the coordinates of I_1 are independent of m and $\mathsf{I}_1 = \mathsf{F}$ exists for every $m > 0$ provided it exists for $m = 0$.

5 Strong migration

If migration is sufficiently strong relative to selection and recombination, the population will become approximately panmictic after a short initial phase. For general multilocus models, this intuition was rendered precise in Section 4.2 of Bürger (2009a). Following the arguments there, we introduce the spatially averaged gamete frequencies

$$\xi_i = \frac{1}{2}(x_{i,\alpha} + x_{i,\beta}), \tag{5.1}$$

and define

$$\nu_{i,\gamma} = x_{i,\gamma} - \xi_i \tag{5.2}$$

as a measure of spatial homogeneity. The averaging is performed with respect to the normalized left eigenvector of the leading eigenvalue 1 of the migration matrix, which, by (2.2a), is $(1/2, 1/2)$. Analogously, we introduce averaged fitnesses of gametes and of the entire population,

$$\omega_i = \frac{1}{2}(w_{i,\alpha} + w_{i,\beta}), \quad \bar{\omega} = \frac{1}{2}(\bar{w}_\alpha + \bar{w}_\beta), \tag{5.3}$$

and note that in the diploid model $\omega_i = \omega_i(\xi_1, \xi_2, \xi_3, \xi_4)$ is the averaged marginal fitness of gamete i. Linkage disequilibrium in the averaged gamete frequencies is denoted by $\Theta = \xi_1\xi_4 - \xi_2\xi_3$.

Now we assume that recombination and selection are both weak and rescale s and r according to

$$s = \sigma\epsilon \text{ and } r = \rho\epsilon, \tag{5.4}$$

where σ and ρ are constants and $\epsilon \to 0$. Then the dynamics (2.7) converges to its so-called strong-migration limit,

$$\frac{d\xi_i}{dt} = \xi_i(\omega_i - \bar{\omega}) - \rho\eta_i\Theta \tag{5.5a}$$

and

$$\nu_{i,\gamma} = 0 \tag{5.5b}$$

for every $\gamma \in \Gamma$ and every $i \in \{1, 2, 3, 4\}$, in which all inter-deme variation is lost. The dynamics (5.5a), which lives on the simplex S_4, describes evolution in a panmictic population subject to stabilizing selection with $s = \sigma$, $\rho = r$, and optimum $P = 0$.

If the population is haploid, Proposition 3.1 yields that M_2 and M_3 are asymptotically stable equilibria of (5.5) and no other equilibrium of (5.5) is stable. The internal equilibrium F exists (with $\mathsf{F}_\alpha = \mathsf{F}_\beta$ given by (3.1)) and is unstable. In fact, M_2 and M_3 attract all trajectories starting in $\xi_2 > \xi_3$ and $\xi_2 < \xi_3$, respectively (as follows from the proof of Theorem 9 in Rutschman 1994).

The perturbation theory developed in Bürger (2009a,b) admits extension of these results to the full dynamics (2.7). Indeed, Proposition 4.10 in Bürger (2009a) implies the following:

Proposition 5.1. *Suppose m is sufficiently large. Then all trajectories of* (2.7)*, or* (A.3)*, converge to a forward-invariant manifold close to that given by* (5.5b)*. The monomorphic equilibria M_2 and M_3 are the only asymptotically stable equilibria of* (2.7)*, and an unstable internal equilibrium exists with coordinates close to F (not shown). It satisfies the symmetry relations*

$$\hat{p}_\beta = 1 - \hat{p}_\alpha,\ \hat{q}_\beta = 1 - \hat{q}_\alpha,\ \hat{D}_\beta = \hat{D}_\alpha. \tag{5.6}$$

Generically, every trajectory converges to an equilibrium.

The last statement follows from a result in Akin (1993, p. 224) because in our model, generically, (5.5a) has only finitely many equilibria, all of which are hyperbolic, and no other chain-recurrent points exist.

If $r = 0$, then in the strong-migration limit every point satisfying $\xi_1 = \xi_4 = 0$ is an equilibrium. Therefore, Proposition 5.1 does not apply and the perturbation is singular.

In the diploid strong-migration limit, all equilibrium configurations depicted in Figure 2 occur. Thus, in sharp contrast to the haploid case, full polymorphism may be maintained. Again, for sufficiently strong migration, the equilibria of the full dynamics (2.7) are perturbations of the equilibria of the strong-migration limit.

6 Equilibrium configurations and bifurcation patterns for the haploid model

We describe the equilibrium configurations and the bifurcation patterns as functions of the migration rate. Because the model is far too complex to obtain analytical results for the admis-

sibility and stability conditions of all equilibria, we complement the analytical investigations by numerical analyses to obtain an apparently complete classification of the bifurcations in which stable equilibria are involved. If analytical methods failed, coordinates and stability of equilibria were computed numerically from (2.7) with *Mathematica* (Wolfram Research, Inc. 2010). We note that the system (2.7) is six-dimensional. The occurring bifurcations are classified according to their properties on the center manifold. An introduction to center manifold theory can be found in Kuznetsov (1998).

We start with a description of the boundary equilibria and some of their properties (Section 6.1). They are also of relevance for inferring admissibility conditions of internal, i.e., fully polymorphic, equilibria. By investigating when the real part of an eigenvalue of a boundary equilibrium passes through zero, we obtain critical migration rates at which certain internal equilibria leave or enter the state space by a transcritical bifurcation with a boundary equilibrium. Such critical migration rates may provide admissibility conditions for internal equilibria. They are worked out in Section 6.2. There, also the internal equilibria are derived that are stable for weak migration, and a general existence result for an internal equilibrium is proved. To describe the possible equilibrium configurations and the bifurcation patterns, we distinguish three cases (labeled I, II, and III): weakly, moderately, and strongly divergent selection. The first two partition stabilizing selection, the latter is equivalent to directional selection. The treatment of these three cases constitutes Sections 6.3, 6.4, and 6.5. Figure 3 visualizes the main results of this section, the dependence of the bifurcation patterns on the parameters P, κ, and r.

We write $m_{\mathrm{st}}(\mathsf{E})$ or $m_{\mathrm{un}}(\mathsf{E})$ to designate critical migration rates at which the equilibrium E becomes stable or unstable, respectively, as m increases above this value. Analogously, we write $m_{\mathrm{ad}}(\mathsf{E})$ or $m_{\mathrm{na}}(\mathsf{E})$ to designate critical migration rates at which E gains or loses admissibility, respectively. If an equilibrium becomes, for instance, stable at more than one value of m, we write (unless noted otherwise) $m_{\mathrm{st}}^{(j)}(\mathsf{E})$ for the jth such event ($j \geq 2$). For an equilibrium E, we denote the coordinates in deme γ by E_γ, i.e., $\mathsf{E} = (\mathsf{E}_\alpha, \mathsf{E}_\beta)$. If $m > 0$, we denote internal equilibria by I_k, where k labels different equilibria. The coordinates of I_k in deme γ are denoted by $\mathsf{I}_{k,\gamma} = (\hat{p}_{k,\gamma}, \hat{q}_{k,\gamma}, \hat{D}_{k,\gamma})$, where a hat, $\hat{}$, signifies an equilibrium. In several cases, we will define such equilibria by weak-migration perturbations, i.e., by $\mathsf{I}_k = I_m(\mathsf{G}_\alpha, \mathsf{H}_\beta)$. Then we use the notation I_k for the whole range of values m in which 'this' equilibrium is admissible.

To simplify the presentation and reduce the number of parameters, we scale the selection strength such that $s = 1$. Therefore, the recombination rate r and the migration m used

below correspond to r/s and m/s, respectively (Section 2).

6.1 Boundary equilibria and their stability

If $r > 0$ and $m > 0$, the only boundary equilibria that can be stable are the monomorphic equilibria M_2 or M_3, and the two SLPs, $\mathsf{S}_1^{\mathcal{A}}$ or $\mathsf{S}_2^{\mathcal{A}}$, defined below. If $r = 0$, two equilibria may be stable at which all alleles but only two gametes are present. They are denoted by R_1 and R_2 and lie on the boundary of the state space.

6.1.1 Monomorphic equilibria

Among the four monomorphic equilibria, only M_2 and M_3 can be stable if $m > 0$. Our symmetry assumptions (2.2) suggest that either both are stable or both are unstable. A linear stability analysis reveals that this is indeed the case. In particular, M_2 and M_3 are asymptotically stable if $m > m_{\mathrm{st}}(\mathsf{M}_{2,3})$, where

$$m_{\mathrm{st}}(\mathsf{M}_{2,3}) = m_{\mathrm{st}}(\mathsf{M}_2) = m_{\mathrm{st}}(\mathsf{M}_3) = \max\left\{\frac{8P^2}{r}\left(\frac{1-\kappa}{1+\kappa}\right)^2 - \frac{r}{2}, \frac{2}{\kappa}\left(P^2 - \frac{\kappa^2}{(1+\kappa)^2}\right)\right\}. \quad (6.1)$$

If $m < m_{\mathrm{st}}(\mathsf{M}_{2,3})$, they are unstable. Therefore, the equilibria M_2 and M_3 are asymptotically stable for every $m \geq 0$ if $m_{\mathrm{st}}(\mathsf{M}_{2,3}) < 0$, which is the case if and only if (3.3) holds. Thus, the stability properties of the monomorphic equilibria predicted by the strong-migration limit (Proposition 5.1) apply if $m > m_{\mathrm{st}}(\mathsf{M}_{2,3})$.

6.1.2 Single-locus polymorphisms

All single-locus polymorphisms (SLPs) can be obtained explicitly from (A.3) by setting $D_\alpha = D_\beta = 0$ and, for instance, $q_\alpha = q_\beta = 0$, and solving the remaining equations. It follows that at most four SLPs can exist. We denote them by $\mathsf{S}_1^{\mathcal{A}}$, $\mathsf{S}_2^{\mathcal{A}}$, $\mathsf{S}_1^{\mathcal{B}}$, and $\mathsf{S}_2^{\mathcal{B}}$, where the superscript $\mathcal{A}$ or $\mathcal{B}$ indicates the polymorphic locus. The coordinates of $\mathsf{S}_1^{\mathcal{A}}$ are

$$\hat{p}_{1,\alpha}^{\mathcal{A}} = \frac{1}{2} - \frac{m}{4}\frac{(1+\kappa)^2}{P(1+\kappa)+\kappa} + \sqrt{\frac{1}{4} + \left(\frac{m}{4}\right)^2 \frac{(1+\kappa)^4}{P^2(1+\kappa)^2 - \kappa^2}}, \quad (6.2a)$$

$$\hat{p}_{1,\beta}^{\mathcal{A}} = \frac{1}{2} + \frac{m}{4}\frac{(1+\kappa)^2}{P(1+\kappa)-\kappa} - \sqrt{\frac{1}{4} + \left(\frac{m}{4}\right)^2 \frac{(1+\kappa)^4}{P^2(1+\kappa)^2 - \kappa^2}}, \quad (6.2b)$$

$$\hat{q}_{1,\alpha}^{\mathcal{A}} = \hat{q}_{1,\beta}^{\mathcal{A}} = 0,\ \hat{D}_{1,\alpha}^{\mathcal{A}} = \hat{D}_{1,\beta}^{\mathcal{A}} = 0, \quad (6.2c)$$

and those of $\mathsf{S}_2^{\mathcal{A}}$ are

$$\hat{p}_{2,\alpha}^{\mathcal{A}} = 1 - \hat{p}_{1,\alpha}^{\mathcal{A}}, \quad \hat{p}_{2,\beta}^{\mathcal{A}} = 1 - \hat{p}_{1,\beta}^{\mathcal{A}}, \quad (6.2d)$$

$$\hat{q}^{\mathcal{A}}_{2,\alpha} = \hat{q}^{\mathcal{A}}_{2,\beta} = 1,\ \hat{D}^{\mathcal{A}}_{2,\alpha} = \hat{D}^{\mathcal{A}}_{2,\beta} = 0. \tag{6.2e}$$

The equilibria $\mathsf{S}^{\mathcal{A}}_1$ and $\mathsf{S}^{\mathcal{A}}_2$ are admissible if and only if $m \leq m_{\rm na}(\mathsf{S}^{\mathcal{A}})$, where

$$m_{\rm na}(\mathsf{S}^{\mathcal{A}}) = \frac{2}{\kappa}\left(P^2 - \frac{\kappa^2}{(1+\kappa)^2}\right). \tag{6.3}$$

Therefore, $m_{\rm na}(\mathsf{S}^{\mathcal{A}}) > 0$ if and only if

$$P > \frac{\kappa}{1+\kappa}. \tag{6.4}$$

Within their marginal one-locus systems, $\hat{q}_\alpha = \hat{q}_\beta = 0$ or $\hat{q}_\alpha = \hat{q}_\beta = 1$, the equilibria $\mathsf{S}^{\mathcal{A}}_1$ or $\mathsf{S}^{\mathcal{A}}_2$ are stable whenever they are admissible. The stability conditions of $\mathsf{S}^{\mathcal{A}}_1$ and $\mathsf{S}^{\mathcal{A}}_2$ in the full system can not be derived in general (but see below).

Using (6.3) and setting

$$m_{2,3} = \frac{8P^2}{r}\left(\frac{1-\kappa}{1+\kappa}\right)^2 - \frac{r}{2}, \tag{6.5}$$

we can rewrite (6.1) as

$$m_{\rm st}(\mathsf{M}_{2,3}) = \max\{m_{2,3}, m_{\rm na}(\mathsf{S}^{\mathcal{A}})\}. \tag{6.6}$$

The critical recombination rate

$$r_{2,3} = \frac{2}{\kappa}\left(\frac{\kappa^2}{(1+\kappa)^2} - P^2\right) + \frac{2}{\kappa}\sqrt{\left(\frac{\kappa^2}{(1+\kappa)^2} - P^2\right)^2 + 4P^2\kappa^2\left(\frac{1-\kappa}{1+\kappa}\right)^2} \tag{6.7}$$

has the following properties:

$$m_{2,3} < m_{\rm na}(\mathsf{S}^{\mathcal{A}}) \text{ if and only if } r > r_{2,3}, \tag{6.8a}$$

$$0 \leq r_{2,3} \leq 1, \tag{6.8b}$$

$$\tilde{r} < r_{2,3} \text{ if and only if } 0 < P < \frac{\kappa}{1+\kappa}, \tag{6.8c}$$

where $\tilde{r}$ was defined in (3.3b). We note that (6.8a) holds independently of the sign of $m_{2,3}$. In addition, $r_{2,3} = 1$ if and only if $P = 0$ and $\kappa = 1$, $r_{2,3} = 0$ if and only if $P \geq 1/2$ and $\kappa = 1$, and $r_{2,3} \to 0$ as $\kappa \to 0$.

We refrain from presenting the coordinates of the two other possible SLPs. For small m, they satisfy $\mathsf{S}^{\mathcal{B}}_1 = I_m(\mathsf{M}_{3,\alpha}, \mathsf{M}_{4,\beta})$ and $\mathsf{S}^{\mathcal{B}}_2 = I_m(\mathsf{M}_{1,\alpha}, \mathsf{M}_{2,\beta})$, whence they are unstable. They are admissible if and only if $P > 1/(1+\kappa)$ and

$$m < m_{\rm na}(\mathsf{S}^{\mathcal{B}}) = 2\kappa\left(P^2 - \frac{1}{(1+\kappa)^2}\right), \tag{6.9}$$

i.e., only if there is directional selection. Apparently, they are always unstable. They will play no role in our further analysis.

6.1.3 Stability of $\mathsf{S}_1^{\mathcal{A}}$ and $\mathsf{S}_2^{\mathcal{A}}$

We assume $P \neq 1/(1+\kappa)$. Because $\mathsf{S}_1^{\mathcal{A}} = I_m(\mathsf{M}_{2,\alpha}, \mathsf{M}_{4,\beta})$ and $\mathsf{S}_2^{\mathcal{A}} = I_m(\mathsf{M}_{1,\alpha}, \mathsf{M}_{3,\beta})$, we infer from Section 4 and Proposition 3.1 that $\mathsf{S}_1^{\mathcal{A}}$ and $\mathsf{S}_2^{\mathcal{A}}$ are unstable if m is sufficiently small. However, they can be asymptotically stable for intermediate values of m. The symmetry properties of the model imply that the stability properties of these two equilibria are the same.

The characteristic polynomial (in y) of the Jacobian at $\mathsf{S}_1^{\mathcal{A}}$ factorizes into two very complicated functions, π_1 and π_2, where the zeros of $\pi_1 = \pi_1(y, \kappa, P, m)$ yield the eigenvalues describing stability within the one-locus system on the boundary, and the zeros of $\pi_2 = \pi_2(y, \kappa, P, r, m)$ yield the eigenvalues describing stability transversal to the boundary. (The functions π_1 and π_2 can be calculated easily using a formula-manipulation program such as *Mathematica*.) The eigenvalues resulting from π_1 are negative if and only if $\mathsf{S}_1^{\mathcal{A}}$ is admissible, i.e., if $m < m_{\mathrm{na}}(\mathsf{S}^{\mathcal{A}})$.

In general, neither the eigenvalues resulting from π_2 nor their signs (of the real part) can be determined analytically. However, conditions can be extracted when and how often eigenvalues pass through zero as a function of m. This helps to determine possible bifurcations. Let $\pi_2^0(\kappa, P, r, m) = \pi_2(0, \kappa, P, r, m)$; see equations (A.4) in Appendix A.2. Then $\mathsf{S}_1^{\mathcal{A}}$ is not hyperbolic if and only if $\pi_2^0 = 0$. Of interest is only the range $0 \leq m \leq m_{\mathrm{na}}(\mathsf{S}^{\mathcal{A}})$ because otherwise $\mathsf{S}_1^{\mathcal{A}}$ and $\mathsf{S}_2^{\mathcal{A}}$ are not admissible. Simple calculations show that $\pi_2^0(\kappa, P, r, 0) > 0$ holds for all admissible parameter combinations and $\pi_2^0(\kappa, P, r, m_{\mathrm{na}}(\mathsf{S}^{\mathcal{A}})) > 0$ holds if and only if $r < r_{2,3}$ (see Appendix A.2). Therefore, $\pi_2^0(m)$, i.e., π_2^0 considered as a function of m, has an odd number of zeros between 0 and $m_{\mathrm{na}}(\mathsf{S}^{\mathcal{A}})$ if $r > r_{2,3}$ and no or an even number otherwise. In addition, from the structure of $\pi_2^0(m)$ we infer immediately that, for given κ, P and r, $\pi_2^0(m)$ can not have more then five zeros. Because

$$\tilde{m}_{\mathrm{st}}(\mathsf{S}^{\mathcal{A}}) = \frac{2\sqrt{[P^2(1+\kappa)^2 - \kappa^2][P^2(1+\kappa)^2 - 1]}}{(1+\kappa)^2} \tag{6.10}$$

and $-\tilde{m}_{\mathrm{st}}(\mathsf{S}^{\mathcal{A}})$ are two zeros, there are at most three additional ones. We note that $0 < \tilde{m}_{\mathrm{st}}(\mathsf{S}^{\mathcal{A}}) \leq m_{\mathrm{na}}(\mathsf{S}^{\mathcal{A}})$ if and only if $P > 1/(1+\kappa)$.

We define $\bar{P} = \bar{P}(\kappa)$ such that for every r, $\pi_2^0(m)$ has at most one zero in $(0, m_{\mathrm{na}}(\mathsf{S}^{\mathcal{A}}))$ if $P < \bar{P}$, and more than one otherwise. Then $\kappa/(1+\kappa) < \bar{P} < 1/(1+\kappa)$. (The first inequality follows because $\mathsf{S}_1^{\mathcal{A}}$ is not admissible if $P < \kappa/(1+\kappa)$; the second follows from the fact that $\tilde{m}_{\mathrm{st}}(\mathsf{S}^{\mathcal{A}})$ is a zero of π_2^0 and the number of zeros is even if $r < r_{2,3}$.)

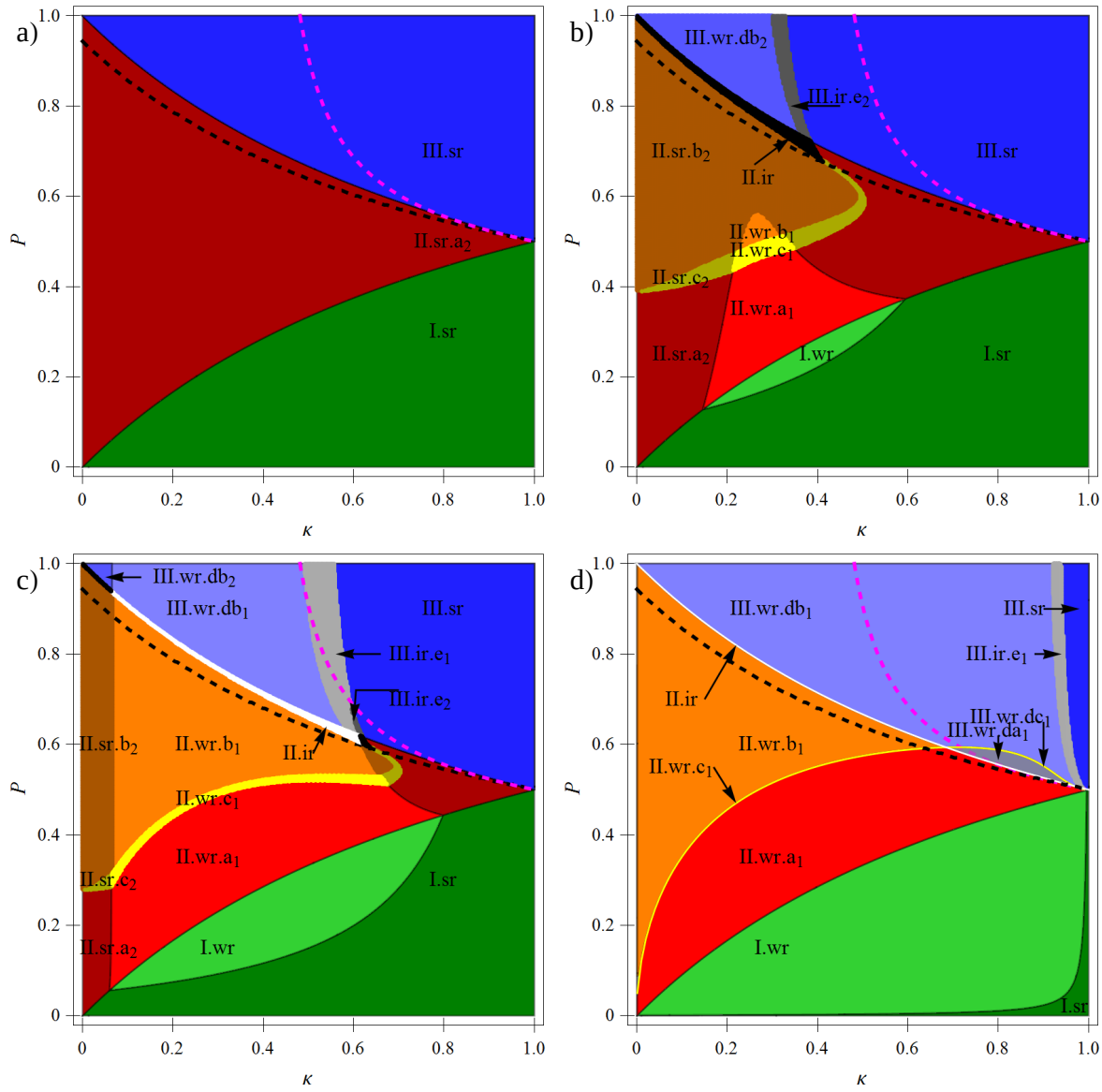

Figure 3: Bifurcation patterns and their parameter regions. The regions I, II, and III refer to the cases of weakly, moderately, and strongly divergent selection, respectively. The subcases denoted by sr, wr, and ir refer to strong, weak, and intermediate recombination, respectively. Dark shades in the colors indicate strong recombination, whereas bright shades indicate weak recombination. Intermediate recombination corresponds to the colors white or black or gray (black and dark gray indicates $r > r_{2,3}$, whereas white and bright gray indicates $r < r_{2,3}$; see text). The black dashed and pink dashed lines display $\bar{P}$ and $\tilde{P}$, respectively (Section 6.1.3). The letters a_i, b_i, c_i, d_i, and e_i refer to the bifurcation patterns occurring in region II and III, as explained in the text. The panels a, b, c, and d are for the recombination rates $r = 2$, $r = 0.38$, $r = 0.2$, and $r = 0.005$, respectively. The white and yellow colored parameter regions in panel d are even smaller than indicated.

The function $\bar{P}(\kappa)$ is displayed as a dashed black line in Figure 3. Thus, for stabilizing selection the parameter region is very small in which more than one bifurcation of a pair of internal equilibria with the pair of SLPs can occur.

In addition, we define $\tilde{P} = \tilde{P}(\kappa)$ such that, for every $r > r_{2,3}$, $\pi_2^0(m)$ has one zero in $(0, m_{\rm na}(\mathsf{S}^{\mathcal{A}}))$ if $P > \tilde{P}$, and at least two otherwise. We find (Appendix A.2) that the value $\tilde{P}$ can be determined from the condition

$$\frac{\partial \pi_2^0/\partial m \mid_{m=m_{\rm na}(\mathsf{S}^{\mathcal{A}})}}{\partial \pi_2^0/\partial r \mid_{r=r_{2,3}}} = 0 \tag{6.11}$$

which, after rearrangement, yields a polynomial equation of degree three in P^2 and eight in κ (Appendix A.2). This condition means that the turning point ($dr/dm = 0$) of the blue curve in Figures 8b,c or Figure A1 has the coordinates $r = r_{2,3}$ and $m = m_{\rm na}(\mathsf{S}^{\mathcal{A}}) = m_{2,3}$, where we recall from Section 6.1.2 that $m_{\rm na}(\mathsf{S}^{\mathcal{A}}) = m_{2,3}$ if and only if $r = r_{2,3}$. The function $\tilde{P}(\kappa)$ decreases and assumes the value 1 at $\kappa \approx 0.481$. In addition, $\tilde{P} > 1/(1+\kappa)$ if and only if $\kappa < 0.8009$ (then $\tilde{P} > 0.55543$). The function $\tilde{P}(\kappa)$ is displayed as a dashed magenta line in Figure 3.

6.1.4 No recombination

If $r = 0$, two boundary equilibria exist and may be stable at which all alleles, but only two haplotypes are present. At R_1, these are the specialist haplotypes AB and ab. The coordinates of R_1 are given by

$$\hat{p}_\alpha = \hat{q}_\alpha = \frac{1}{2} - \frac{m}{4P} + \sqrt{\frac{1}{4} + \left(\frac{m}{4P}\right)^2}, \tag{6.12a}$$

$$\hat{p}_\beta = \hat{q}_\beta = 1 - \hat{p}_\alpha, \tag{6.12b}$$

$$\hat{D}_\alpha = \hat{D}_\beta = \hat{p}_\alpha(1 - \hat{p}_\alpha). \tag{6.12c}$$

At the other equilibrium, denoted R_2, only the generalist haplotypes Ab and aB are present. It is given by

$$\hat{p}_\alpha = 1 - \hat{q}_\alpha = \frac{1}{2} - \frac{m}{4P}\frac{1+\kappa}{1-\kappa} + \sqrt{\frac{1}{4} + \left(\frac{m}{4P}\frac{1+\kappa}{1-\kappa}\right)^2}, \tag{6.13a}$$

$$\hat{p}_\beta = 1 - \hat{q}_\beta = 1 - \hat{p}_\alpha, \tag{6.13b}$$

$$\hat{D}_\alpha = \hat{D}_\beta = -\hat{p}_\alpha(1 - \hat{p}_\alpha). \tag{6.13c}$$

Both, R_1 and R_2 are always admissible if $\kappa < 1$ and satisfy $1/2 < \hat{p}_\alpha < 1$. For both equilibria, $\hat{p}_\alpha$ is of the form $1/2 - y + \sqrt{1/4 + y^2}$. In the limit $y \to \infty$, this becomes $1/2 +$

$1/(8y) + O(y^{-2})$. Hence, R_1 and R_2 exist and are well defined in limiting cases such as $P \to 0$ or $\kappa \to 1$.

In general, the stability conditions for R_1 and R_2 can not be derived. If selection is stabilizing, numerical work shows that R_2 is stable for every $m > 0$. Under directional selection, one eigenvalue of the Jacobian at R_1 and one of the Jacobian at R_2 passes through zero at $m = \tilde{m}_{\mathrm{st}}(\mathsf{S}^{\mathcal{A}})$. Numerical work shows that R_1 is stable if $m < \tilde{m}_{\mathrm{st}}(\mathsf{S}^{\mathcal{A}})$, whereas R_2 is stable if $m > \tilde{m}_{\mathrm{st}}(\mathsf{S}^{\mathcal{A}})$.

6.2 Internal equilibria

In general, neither the number nor the stability properties or coordinates of internal equilibria can be determined analytically. For sufficiently strong migration, there is always precisely one internal equilibrium, and it is unstable (Proposition 5.1). For weak migration, we calculate in Sections 6.2.1 and 6.2.2 the approximate coordinates of the internal equilibria that can be stable. In Section 6.2.3, conditions of admissibility of pairs of internal equilibria that leave or enter the state space by transcritical bifurcations with the pair M_2, M_3 are presented. First, we prove the following general result.

Proposition 6.1. *1. The haploid dynamics* (A.3) *has always at least one internal equilibrium that satisfies the symmetry relations* (5.6).

2. Equilibria that do not satisfy (5.6) *occur in pairs and satisfy the following relation:*

$$\tilde{p}_\gamma = 1 - \hat{p}_{\gamma^*}, \quad \tilde{q}_\gamma = 1 - \hat{q}_{\gamma^*}, \quad \tilde{D}_\gamma = \hat{D}_{\gamma^*}. \tag{6.14}$$

Both equilibria have the same stability properties.

The proof of the first part is based on an index theorem by Hofbauer (1990, Theorem 2), which we briefly recapitulate for convenience: Every dissipative semiflow on $\mathbb{R}^n_+$ admits at least one saturated fixed point. Moreover, if all saturated fixed points are regular, the sum of their indices equals $+1$.

Proof. 1. We start by noting that the manifold $\mathcal{M}$ given by the symmetry relations (5.6) is invariant under the dynamics (A.3). The selection and recombination dynamics on $\mathcal{M}$ is the same as in the haploid panmictic model, and the migration terms are $m(1-2p_1), m(1-2q_1), m(1-2p_1)(1-2q_1)$.

To apply Hofbauer's theorem, we first note that the haploid panmictic model with the above migration term satisfies the assumptions. The argument is analogous to that in Remark S.2 of Bank et al. (2012). Here the state space is $S_4 \times S_4$, and it is attracting in $\mathbb{R}^8_+$. The

index of an equilibrium in $\mathbb{R}^8_+$ is $(-1)^l$, where l is the number of eigenvalues with negative real part. An internal equilibrium is always saturated. If it is asymptotically stable, it has index 1. Because the manifold $\mathcal{M}$ contains no boundary equilibria, Hofbauer's theorem implies the existence of an internal equilibrium on $\mathcal{M}$ with index 1.

2. This observation follows immediately from the symmetry properties of the model, and also directly from the differential equations (A.3). □

6.2.1 Stabilizing selection and weak migration

We recall that selection is stabilizing in each deme if (3.5) is violated. Hence, we assume $P < 1/(1+\kappa)$.

Using the notation introduced in Section 4, we define $\mathsf{I}_2 = I_m(\mathsf{M}_{2,\alpha}, \mathsf{M}_{3,\beta})$ and $\mathsf{I}_3 = I_m(\mathsf{M}_{3,\alpha}, \mathsf{M}_{2,\beta})$ as the weak-migration perturbations of the indicated boundary equilibria at $m = 0$. Their coordinates are derived by straightforward perturbation methods and satisfy the symmetry relations (5.6). Numerical results suggest that I_2 and I_3 satisfy (5.6) whenever they are admissible. For I_2 we obtain

$$\hat{p}_{2,\alpha} = 1 - \frac{m(1+\kappa)}{4} \frac{r(1+\kappa)^2 + 4[\kappa + P(1+\kappa)]}{[\kappa + P(1+\kappa)][r(1+\kappa) + 4P(1-\kappa)]} + O(m^2), \tag{6.15a}$$

$$\hat{q}_{2,\alpha} = \frac{m(1+\kappa)}{4\kappa} \frac{r(1+\kappa)^2 + 4\kappa[1 - P(1+\kappa)]}{[1 - P(1+\kappa)][r(1+\kappa) + 4P(1-\kappa)]} + O(m^2), \tag{6.15b}$$

$$\hat{D}_{2,\alpha} = -\frac{m(1+\kappa)}{r(1+\kappa) + 4P(1-\kappa)} + O(m^2). \tag{6.15c}$$

Because $\mathsf{M}_{2,\alpha}$ and $\mathsf{M}_{3,\beta}$ are asymptotically stable if selection is stabilizing and $m = 0$ (Proposition 3.1), we infer from Section 4 that I_2 is admissible and asymptotically stable whenever selection is stabilizing and migration is sufficiently weak. If (3.4) holds, then I_2 is the unique internal equilibrium and globally asymptotically stable. We note that I_2 converges to R_2 if $r \to 0$.

The coordinates of I_3 are given by

$$\hat{p}_{3,\alpha} = \frac{m(1+\kappa)}{4} \frac{r(1+\kappa)^2 + 4[\kappa - P(1+\kappa)]}{[\kappa - P(1+\kappa)][r(1+\kappa) - 4P(1-\kappa)]} + O(m^2), \tag{6.16a}$$

$$\hat{q}_{3,\alpha} = 1 - \frac{m(1+\kappa)}{4\kappa} \frac{r(1+\kappa)^2 + 4\kappa[1 + P(1+\kappa)]}{[1 + P(1+\kappa)][r(1+\kappa) - 4P(1-\kappa)]} + O(m^2), \tag{6.16b}$$

$$\hat{D}_{3,\alpha} = -\frac{m(1+\kappa)}{r(1+\kappa) - 4P(1-\kappa)} + O(m^2). \tag{6.16c}$$

From Proposition 3.1 and Section 4, we conclude that I_3 is admissible and asymptotically stable if (3.3) holds and m is sufficiently small.

It is easy to prove directly from (A.3) that under stabilizing selection there are no internal equilibria satisfying the symmetry relation (5.6) and $D_\gamma = 0$. Therefore, I_2 and I_3 exhibit negative LD whenever they are admissible. We also point out that the above approximations assume that m is sufficiently small for given κ, P, and r. Hence, performing certain limits, for instance $P \to 1/(1+\kappa)$ in (6.15), or $P \to \kappa/(1+\kappa)$ or $r \to 0$ in (6.16), may not be admissible.

6.2.2 Directional selection and weak migration

If $P > 1/(1+\kappa)$, so that selection is directional (3.5), we conclude from Proposition 3.1 and Section 4 that, for small m, the internal equilibrium $\mathsf{I}_0 = I_m(\mathsf{M}_{1,\alpha}, \mathsf{M}_{4,\beta})$ is globally asymptotically stable. Therefore, no other internal equilibrium exists.

For small m, the coordinates of I_0 are given by (5.6) and

$$\hat{p}_{0,\alpha} = 1 - \frac{m}{4P}\left(1 - \frac{r}{r+4P}\,\frac{\kappa[1+P(1+\kappa)]}{\kappa - P(1+\kappa)}\right) + O(m^2), \tag{6.17a}$$

$$\hat{q}_{0,\alpha} = 1 - \frac{m}{4P}\left(1 - \frac{r}{r+4P}\,\frac{\kappa + P(1+\kappa)}{\kappa[1-P(1+\kappa)]}\right) + O(m^2), \tag{6.17b}$$

$$\hat{D}_{0,\alpha} = \frac{m}{r+4P} + O(m^2). \tag{6.17c}$$

We note that I_0 converges to R_1 if $r \to 0$.

If $P = 1/(1+\kappa)$ and $r > 0$, the approximation (6.17) does not apply because, as mentioned in Section 3.1, the dynamics is degenerate if $m = 0$. If migration is weak, singular perturbation shows that an internal equilibrium (also denoted by I_0) exists. It enters the state space through $p_\alpha = 1 - p_\beta = 1$, $q_\alpha = 1 - q_\beta = (1+\kappa)/(1+\kappa+\sqrt{1-\kappa^2})$, $D_\alpha = D_\beta = 0$. Numerical work suggests that it is unstable and that the two SLPs $\mathsf{S}_1^{\mathcal{A}}$ and $\mathsf{S}_2^{\mathcal{A}}$ are asymptotically stable if $\kappa < 1$, whereas M_2 and M_3 are asymptotically stable if $\kappa = 1$.

6.2.3 Other internal equilibria

Here, we present necessary and sufficient conditions when pairs of internal equilibria enter or leave the state space through M_2 and M_3. The proof is given in Appendix A.3. We recall from (6.8c) that $\tilde{r} < r_{2,3}$ if and only if $0 < P < \kappa/(1+\kappa)$.

Proposition 6.2. *1. A pair of internal equilibria, denoted I_4 and I_5, enters the state space by a bifurcation with the pair M_2 and M_3 if and only if $m = m_{2,3}$ and*

$$r < \min\{r_{2,3}, \tilde{r}\} \text{ and } \phi > 0, \tag{6.18}$$

where ϕ is a function of κ, P, and r which is given in (A.14). *If $m > m_{2,3}$, this pair of internal equilibria is unstable and the monomorphic equilibria are asymptotically stable.*

2. A pair of equilibria, denoted I_6 *and* I_7*, leaves the state space by bifurcations with the pair* M_2 *and* M_3 *if and only if* $m = m_{2,3}$ *and*

$$r < \min\{r_{2,3}, \tilde{r}\} \text{ and } \phi < 0. \tag{6.19}$$

This pair of internal equilibria is stable if $m < m_{2,3}$ *and the monomorphic equilibria are asymptotically stable if* $m > m_{2,3}$*.*

Remark 6.3. We list some necessary or sufficient conditions for (6.18) or (6.19). Proofs are given in Appendix A.3.

(a) If $P < \sqrt{\kappa}/(1+\kappa)$, then (6.18) is satisfied if and only if $r < \min\{r_{2,3}, \tilde{r}\}$ holds.

(b) The following condition is necessary for (6.18) to hold:

$$P \le \frac{\sqrt{3\kappa}}{\sqrt{2}(1+\kappa)} \text{ and } r < \frac{1}{2}. \tag{6.20}$$

(c) If $P > 1/(1+\kappa)$, then $\kappa > 2/3$ and $r \lessapprox 0.01838$ are necessary for (6.18) to hold, where 0.01838 has been determined numerically.

(d) The following is a necessary condition for (6.19) to hold:

$$P \ge \frac{\sqrt{\kappa}}{1+\kappa} \text{ and } r \lessapprox 0.3915\,, \tag{6.21}$$

where 0.3915 has been determined numerically.

(e) Let

$$\frac{1}{1+\kappa} < P < \frac{\sqrt{3\kappa}}{\sqrt{2}(1+\kappa)} \tag{6.22}$$

(whence $\kappa > 2/3$). Then for every P and κ there is a critical value $r_c < r_{2,3}$ such that (6.18) holds if $r < r_c$, and (6.19) holds if $r_c < r < r_{2,3}$.

(f) In the region

$$\frac{\sqrt{\kappa}}{1+\kappa} < P < \min\left\{\frac{1}{1+\kappa}, \frac{\sqrt{3\kappa}}{\sqrt{2}(1+\kappa)}\right\} \tag{6.23}$$

a pair of equilibria can enter or leave the state space through the pair M_2 and M_3. More precisely, if $\phi(r_{2,3}) > 0$, then (6.18) holds for every $r < r_{2,3}$. If $\phi(r_{2,3}) < 0$, then there is a critical value r_{cc} such that (6.18) holds if $r < r_{cc}$, and (6.19) holds if $r_{cc} < r < r_{2,3}$.

In the following we distinguish three scenarios: weakly, moderately, and strongly divergent selection. Weakly or moderately divergent selection occurs if in each deme the trait is under stabilizing selection and the optimum P satisfies (3.3) or (3.4), respectively. Divergent selection is strong, if the trait is under directional selection in each deme, i.e., $P \ge 1/(1+\kappa)$ holds.

6.3 Weakly divergent selection

We assume (3.3a), i.e., $0 \le P < \kappa/(1+\kappa)$. In terms of allelic effects this means $0 \le P < c_2$, i.e., P is displaced from the central position by at most one half of a substitution effect at the minor locus. Therefore, the fitness optima in the two demes are similar and selection is weakly divergent. From (6.4) and (6.9), we conclude that none of the SLPs is admissible. In each of the bifurcation patterns listed in this or the following sections, the equilibrium configuration of the strong-migration limit (Proposition 5.1) applies above the highest indicated bifurcation point, i.e., one internal unstable equilibrium exists and M_2 and M_3 are asymptotically stable and attract (almost) all trajectories. For stabilizing selection, except when $P = 0$, this internal equilibrium is given by I_2 and $\mathsf{I}_2 \to \mathsf{F}$ as $m \to \infty$. If $P = 0$, the internal equilibrium under strong migration is I_1.

The inequality (3.3a) defines region I in Figure 3 and elsewhere. We need to distinguish between strong recombination (Case I.sr) and weak recombination (Case I.wr).

Case I.sr. Let $r > \tilde{r}$. From (3.3) we infer that $r > \tilde{r}$ holds for every $r > 1/2$. In addition, we note that $\tilde{r} = 1/2$ if $\kappa = 1/3$ and $P = 1/4$, and $\tilde{r} \to 0$ as $\kappa \to 1$ or $P \to 0$.

In Section 6.1.1, it was shown that the monomorphic equilibria M_2 and M_3 are asymptotically stable for every $m \ge 0$. From Section 6.2.1, we conclude that for sufficiently weak migration the internal equilibria I_2 and I_3 are asymptotically stable. In addition, for sufficiently weak migration, Proposition 3.1 and Section 4 imply that no other equilibrium can be stable and $\mathsf{I}_1 = I_m(\mathsf{F})$ is internal (and unstable).

There remain ten, potentially internal but unstable, equilibria that are obtained by perturbation of unstable boundary equilibria (if $m = 0$). For them it needs to be checked if they are admissible if $m > 0$. The equilibria $I_m(\mathsf{M}_{1,\alpha}, \mathsf{M}_{4,\beta})$ and $I_m(\mathsf{M}_{4,\alpha}, \mathsf{M}_{1,\beta})$ as well as the four equilibria $I_m(\mathsf{M}_{i,\alpha}, \mathsf{F}_\beta)$, $I_m(\mathsf{F}_\alpha, \mathsf{M}_{i,\beta})$, where $i, j \in \{1, 4\}$ and $i \ne j$, are not admissible if $m > 0$. The equilibria $I_m(\mathsf{M}_{2,\alpha}, \mathsf{F}_\beta)$, $I_m(\mathsf{M}_{3,\alpha}, \mathsf{F}_\beta)$, $I_m(\mathsf{F}_\alpha, \mathsf{M}_{2,\beta})$, and $I_m(\mathsf{F}_\alpha, \mathsf{M}_{3,\beta})$ are admissible if $m > 0$ because they are externally stable if $m = 0$.

As m increases, three bifurcations occur that reduce the number of equilibria and, eventually, yield the equilibrium configuration of the strong-migration limit (Proposition 5.1). In the following, we describe these bifurcations. They were obtained by numerical work in combination with plausibility considerations and inferences from the weak-migration and the strong-migration limit. Figure 4 displays them.

Because a non-generic bifurcation pattern occurs if $\kappa = 1$ or $P = 0$, we first treat the generic case.

Pattern I.sr. If $\kappa < 1$ and $P \neq 0$, two alternative sequences of bifurcation events may occur as m increases from zero. In each case, first there is a subcritical pitchfork bifurcation in which the stable equilibrium I_3 collides with the two unstable equilibria $I_m(\mathsf{M}_{3,\alpha}, \mathsf{F}_\beta)$ and $I_m(\mathsf{F}_\alpha, \mathsf{M}_{2,\beta})$. The equilibrium I_3 loses its stability but persists, and $I_m(\mathsf{M}_{3,\alpha}, \mathsf{F}_\beta)$ and $I_m(\mathsf{F}_\alpha, \mathsf{M}_{2,\beta})$ are annihilated. The value at which this occurs is denoted by $m_{\mathrm{un}}(\mathsf{I}_3)$. As m increases above $m_{\mathrm{un}}(\mathsf{I}_3)$, the next two bifurcations can occur in both orders.

If κ is not close to one, the next bifurcation is a saddle-node (or fold) bifurcation in which the unstable equilibria I_1 and I_3 annihilate each other. This occurs at a value of m denoted by $m_{\mathrm{na}}(\mathsf{I}_3) = m_{\mathrm{na}}(\mathsf{I}_1)$. As m increases further, a subcritical pitchfork bifurcation occurs at a value denoted $m_{\mathrm{un}}(\mathsf{I}_2)$, in which the stable equilibrium I_2 collides with the two unstable equilibria $I_m(\mathsf{M}_{2,\alpha}, \mathsf{F}_\beta)$ and $I_m(\mathsf{F}_\alpha, \mathsf{M}_{3,\beta})$, loses its stability, and the unstable equilibria are annihilated. Thus, we have the following sequence of bifurcation points

$$0 < m_{\mathrm{un}}(\mathsf{I}_3) < m_{\mathrm{na}}(\mathsf{I}_3) = m_{\mathrm{na}}(\mathsf{I}_1) < m_{\mathrm{un}}(\mathsf{I}_2); \tag{6.24a}$$

see Figure 4a. If κ is close to one, the order of the second and third bifurcation is reversed, i.e., we have

$$0 < m_{\mathrm{un}}(\mathsf{I}_3) < m_{\mathrm{un}}(\mathsf{I}_2) < m_{\mathrm{na}}(\mathsf{I}_1) = m_{\mathrm{na}}(\mathsf{I}_3). \tag{6.24b}$$

Pattern I.sr.0. In the special cases $\kappa = 1$ or $P = 0$, the pitchfork bifurcations in which I_2 and I_3 lose their stability occur at the same migration rate, i.e., $m_{\mathrm{un}}(\mathsf{I}_2) = m_{\mathrm{un}}(\mathsf{I}_3)$. At the value $m_{\mathrm{na}}(\mathsf{I}_2) = m_{\mathrm{na}}(\mathsf{I}_3)$, a third subcritical pitchfork bifurcation occurs in which the three unstable internal equilibria I_1, I_2, and I_3 collide, I_2 and I_3 are annihilated, and I_1 remains admissible and unstable (Figure 4b). Thus, the sequence of bifurcation points is

$$0 < m_{\mathrm{un}}(\mathsf{I}_3) = m_{\mathrm{un}}(\mathsf{I}_2) < m_{\mathrm{na}}(\mathsf{I}_2) = m_{\mathrm{na}}(\mathsf{I}_3). \tag{6.25}$$

The equilibria I_2 and I_3, as well as $m_{\mathrm{un}}(\mathsf{I}_2) = m_{\mathrm{un}}(\mathsf{I}_3)$ and $m_{\mathrm{na}}(\mathsf{I}_2) = m_{\mathrm{na}}(\mathsf{I}_3)$ can be given explicitly if $\kappa = 1$ or $P = 0$. The case $P = 0$ and $\kappa \leq 1$ can be inferred from the case $P = 0$ and $\kappa = 1$ (Appendix A.4).

Case I.wr. Let $r < \tilde{r}$. This is equivalent to

$$\frac{r}{4}\frac{1+\kappa}{1-\kappa} < P < \frac{\kappa}{1+\kappa}. \tag{6.26}$$

Then $m_{\mathrm{st}}(\mathsf{M}_{2,3}) = m_{2,3} > 0$ and M_2 and M_3 are unstable if $0 < m < m_{2,3}$; see (6.1), (6.5), (6.6).

Pattern I.wr. If m is small, I_2 is globally asymptotically stable (Section 6.2.1). From Proposition 6.2.1, (6.8c) and Remark 6.3 (a), we infer that two internal equilibria, I_4 and I_5, enter the state space simultaneously at $m_{\mathrm{ad}}(\mathsf{I}_{4,5}) = m_{2,3}$ by transcritical bifurcations with M_2 and M_3, respectively. If m is slightly larger than $m_{2,3}$, I_4 and I_5 are unstable, and M_2 and M_3 are asymptotically stable. Also I_2 is asymptotically stable.

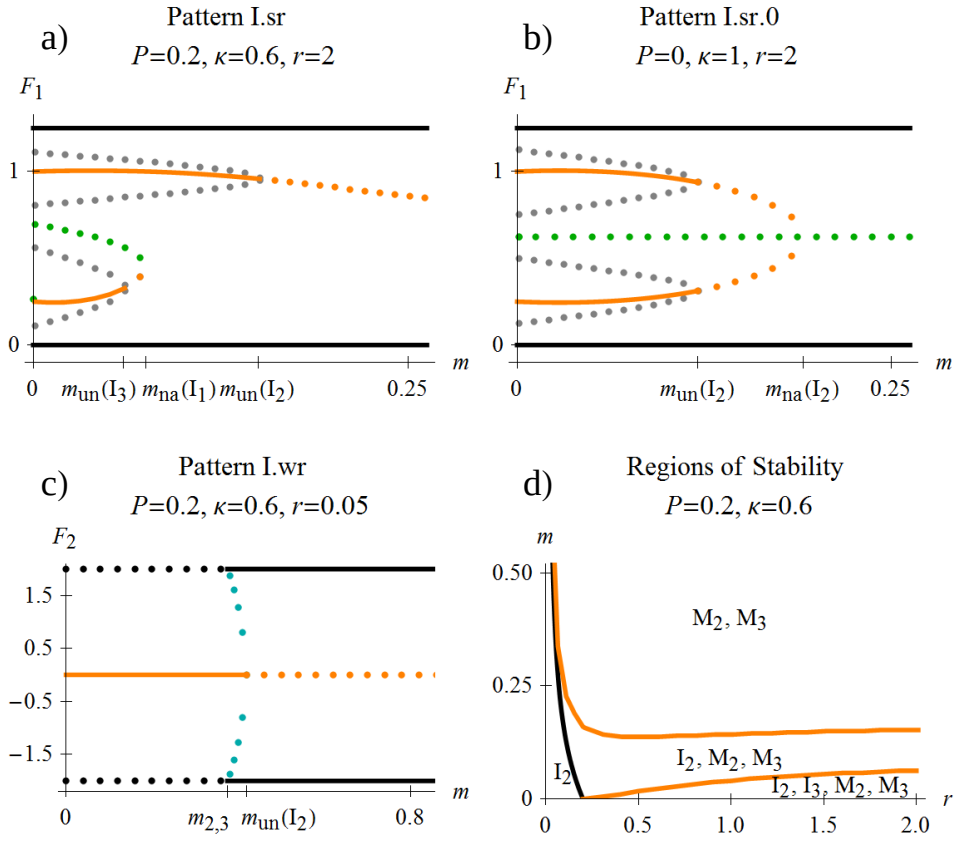

Figure 4: Bifurcation patterns and regions of stability for weakly divergent selection. Panels a, b, and c show bifurcation patterns as functions of m. The bifurcation pattern given by sequence (6.24b) is omitted. Except for panel b, only bifurcation patterns are displayed that occur for an open set of parameters, i.e., degenerate cases are omitted. To generate unambiguous two-dimensional projections of the six-dimensional coordinates, we use the functions F_1 and F_2 (see Appendix A.5). The solid and dotted lines represent stable and unstable equilibria, respectively. Gray lines show $I_m(\mathsf{M}_{2,\alpha}, \mathsf{F}_\beta)$, $I_m(\mathsf{F}_\alpha, \mathsf{M}_{2,\beta})$, $I_m(\mathsf{M}_{3,\alpha}, \mathsf{F}_\beta)$, and $I_m(\mathsf{F}_\alpha, \mathsf{M}_{3,\beta})$. Black lines show the monomorphic states M_2 and M_3. The green line in panels a and b shows I_1, given by (A.29) if $\kappa = 1$. Orange lines show I_2 and I_3. Cyan dotted lines display I_4 and I_5. Panel d displays the regions of stability of equilibria as functions of r. In each region the stable equilibria are indicated.

As m increases further, at a critical value $m_{\mathrm{na}}(\mathsf{I}_{4,5}) = m_{\mathrm{un}}(\mathsf{I}_2)$, I_4 and I_5 collide with

the stable internal equilibrium I_2 by a subcritical pitchfork bifurcation, whence I_2 becomes unstable and I_4 and I_5 are annihilated. Thus, we have the following sequence of bifurcation points:

$$0 < m_{2,3} < m_{\mathrm{un}}(\mathsf{I}_2); \tag{6.27}$$

see Figure 4c. (If a critical m indicating a change of stability of an equilibrium coincides with a critical m indicating a change of admissibility, here $m_{\mathrm{na}}(\mathsf{I}_{4,5}) = m_{\mathrm{un}}(\mathsf{I}_2)$, we only write the critical m indicating the stability change in the sequence of bifurcation points.)

Because for weakly divergent selection, M_2 and M_3 are the only boundary equilibria that admit zero as an eigenvalue, Proposition 6.2 and Remark 6.3 imply that no other bifurcation with boundary equilibria can occur. Figure 4d displays the critical migration rates that delineate the regions of stability of equilibria as functions of the recombination rate for a representative choice of P and κ.

6.4 Moderately divergent selection

We assume

$$\frac{\kappa}{1+\kappa} < P < \frac{1}{1+\kappa}. \tag{6.28}$$

In terms of allelic effects on the trait this means $c_2 < P < c_1$. Selection is stabilizing and the fitness optima in the two demes differ to a moderate extent. The inequalities (6.28) define region II in Figure 3 and elsewhere. This is the most complicated case in which the largest number of bifurcation patterns occurs. However, only four occur in a large parameter range. In general, the boundaries of the regions in which precisely one type of pattern occurs are given by complicated sets of polynomial equations in r, κ, and P. Only in some cases can we describe them analytically by simple functions.

We recall from Section 6.1 that the only SLPs that can be admissible are $\mathsf{S}_1^{\mathcal{A}}$ and $\mathsf{S}_2^{\mathcal{A}}$. They are admissible if and only if $m < m_{\mathrm{na}}(\mathsf{S}^{\mathcal{A}})$, where $m_{\mathrm{na}}(\mathsf{S}^{\mathcal{A}}) > 0$ by (6.3). For sufficiently small m, I_2 is globally asymptotically stable and no other internal equilibrium exists (Section 6.2.1). In fact, I_2 appears to be the unique internal equilibrium satisfying the symmetry relation (5.6) for arbitrary m (cf. Proposition 6.1).

In addition, pairs of internal equilibria (I_4 and I_5, or I_6 and I_7) satisfying (6.14) occur. They may emerge and disappear by one of the following bifurcation patterns, where I_j stands for I_2 or I_0 if selection is stabilizing or directional, respectively. (The case of directional selection will be needed in Section 6.5.)

a. The unstable equilibria I_4 and I_5 enter the state space at a critical value $m_{\mathrm{ad}}(\mathsf{I}_{4,5}) = m_{2,3}$ or $m_{\mathrm{ad}}(\mathsf{I}_{4,5}) = m_{\mathrm{st}}(\mathsf{S}^{\mathcal{A}})$ by transcritical bifurcations with M_2 and M_3 (type a_1, Figure 5d) or $\mathsf{S}_1^{\mathcal{A}}$ and $\mathsf{S}_2^{\mathcal{A}}$ (type a_2, Figure 5a), respectively. They get annihilated at $m_{\mathrm{na}}(\mathsf{I}_{4,5}) = m_{\mathrm{un}}(\mathsf{I}_j)$ by a subcritical pitchfork bifurcation with I_j.

b. The asymptotically stable equilibria I_6 and I_7 emerge at $m_{\mathrm{st}}(\mathsf{I}_{6,7}) = m_{\mathrm{un}}(\mathsf{I}_j)$ by a supercritical pitchfork bifurcation with I_j. The pair I_6 and I_7 leaves the state space at $m_{\mathrm{na}}(\mathsf{I}_{6,7}) = m_{2,3}$ or $m_{\mathrm{na}}(\mathsf{I}_{6,7}) = m_{\mathrm{st}}(\mathsf{S}^{\mathcal{A}})$ by transcritical bifurcations with M_2 and M_3 (type b_1, Figure 5e) or $\mathsf{S}_1^{\mathcal{A}}$ and $\mathsf{S}_2^{\mathcal{A}}$ (type b_2, Figure 5b), respectively.

c. In two simultaneous saddle-node bifurcations at $m_{\mathrm{ad}}(\mathsf{I}_{4,5}) = m_{\mathrm{st}}(\mathsf{I}_{6,7})$, the internal equilibria I_4 (unstable) and I_6 (stable), as well as I_5 and I_7 are generated. The pair I_4 and I_5 is annihilated at $m_{\mathrm{na}}(\mathsf{I}_{4,5}) = m_{\mathrm{un}}(\mathsf{I}_j)$ in a subcritical pitchfork bifurcation with I_j. The pair I_6 and I_7 leaves the state space at $m_{\mathrm{na}}(\mathsf{I}_{6,7}) = m_{2,3}$ through M_2 and M_3 (type c_1, Figure 5f) or at $m_{\mathrm{na}}(\mathsf{I}_{6,7}) = m_{\mathrm{st}}(\mathsf{S}^{\mathcal{A}})$ through $\mathsf{S}_1^{\mathcal{A}}$ and $\mathsf{S}_2^{\mathcal{A}}$ (type c_2, Figure 5c).

d. The asymptotically stable equilibria I_6 and I_7 enter the state space at $m_{\mathrm{st}}(\mathsf{I}_{6,7}) = m_{\mathrm{un}}(\mathsf{S}^{\mathcal{A}})$ by transcritical bifurcations with $\mathsf{S}_1^{\mathcal{A}}$ and $\mathsf{S}_2^{\mathcal{A}}$, respectively. They get annihilated at $m_{\mathrm{na}}(\mathsf{I}_{6,7}) = m_{\mathrm{st}}(\mathsf{I}_j)$ by a subcritical pitchfork bifurcation with I_j (Figures 7e,f).

e. The asymptotically stable equilibria I_6 and I_7 enter the state space at $m_{\mathrm{st}}(\mathsf{I}_{6,7}) = m_{\mathrm{un}}(\mathsf{S}^{\mathcal{A}})$ by transcritical bifurcations with $\mathsf{S}_1^{\mathcal{A}}$ and $\mathsf{S}_2^{\mathcal{A}}$, respectively. They leave the state space either at $m_{\mathrm{na}}(\mathsf{I}_{6,7}) = m_{2,3}$ by transcritical bifurcations with M_2 and M_3 (type e_1, Figure 7c), or at $m_{\mathrm{na}}(\mathsf{I}_{6,7}) = m_{\mathrm{st}}^{(2)}(\mathsf{S}^{\mathcal{A}})$ by transcritical bifurcations with $\mathsf{S}_1^{\mathcal{A}}$ and $\mathsf{S}_2^{\mathcal{A}}$ (type e_2, Figure 7d). In the last bifurcation, the boundary equilibria become stable.

In the cases a, b, and c, the pair of boundary equilibria becomes asymptotically stable at the transcritical bifurcation, whereas it loses stability in case d and (at the first bifurcation) in case e. In cases a and c, I_j loses its stability at the bifurcation with I_4 and I_5; in case b, I_j loses stability at the bifurcation with I_6 and I_7; in case d, I_j gains stability at the bifurcation with I_6 and I_7.

From Section 6.1.3 we recall the definitions of $\bar{P} = \bar{P}(\kappa)$ and $\tilde{P} = \tilde{P}(\kappa)$. Thus, if $P < \bar{P}$ or $P > \tilde{P}$, there is at most one value m at which the SLPs are not hyperbolic (when admissible). Hence, there is at most one value of m at which a bifurcation of type a, b, c, or d can occur. Case d does not occur if $P < \bar{P}$. If $\bar{P} < P < \min\{\tilde{P}, 1/(1+\kappa)\}$, up to three such bifurcations

can occur. As shown by Figure 3, this region is very small. In addition, if $r < r_{2,3}$, then the number of critical values m is zero or two; otherwise, it is one or three.

We shall distinguish three main cases, strong recombination (denoted II.sr), and weak recombination (II.wr), and intermediate recombination (II.ir). To this end, we define, for given κ and P, r^* and r^{**} such that the function $\pi_2^0(m)$ has two or three zeros m with $0 < m < m_{\mathrm{na}}(\mathsf{S}^{\mathcal{A}})$ if $r^{**} < r < r^*$, no zero if $r < r^{**}$, and one zero if $r > r^*$. We recall that a pair of internal equilibria can leave or enter the state space through the pair of SLPs only if $\pi_2^0(m) = 0$ (Section 6.1.3). In Figure 6c and Figure A1b, r^{**} and r^* are the left and right turning point of the blue curve, respectively. From our discussion of the properties of π_2^0 in Section 6.1.3, we conclude (provided $P < 1/(1+\kappa)$)

$$r^* = r_{2,3} \quad \text{if } P \le \bar{P} \text{ or } P > \tilde{P}, \tag{6.29a}$$

$$r^* > r_{2,3} \quad \text{if } \bar{P} < P < \tilde{P}, \tag{6.29b}$$

$$r^{**} = r_{2,3} \quad \text{if } P \le \bar{P}, \tag{6.30a}$$

$$r^{**} > r_{2,3} \quad \text{if } P > \bar{P} \text{ and } \pi_2^0(\kappa, r) \neq 0 \text{ for all } r < r_{2,3}, \tag{6.30b}$$

$$r^{**} < r_{2,3} \quad \text{if } P > \bar{P} \text{ otherwise.} \tag{6.30c}$$

We note that $r^{**} \to 0$ and $m_{\mathrm{st}}(\mathsf{S}^{\mathcal{A}}) \to 0$ as $P \to 1/(1+\kappa)$. In addition, numerical evaluation of the defining equations suggest that $r^* < 1$ holds always. Mostly, r^* is very close to $r_{2,3}$.

We recall from Proposition 6.2 and Sections 6.1 that if $r > r_{2,3}$, then (i) no internal equilibria leave or enter the state space through M_2 and M_3, and (ii) M_2 and M_3 become stable at $m = m_{\mathrm{na}}(\mathsf{S}^{\mathcal{A}})$ by exchange-of-stability bifurcations with the SLPs $\mathsf{S}_1^{\mathcal{A}}$ and $\mathsf{S}_2^{\mathcal{A}}$, respectively, which lose their admissibility at $m_{\mathrm{na}}(\mathsf{S}^{\mathcal{A}})$.

In the following, we describe all bifurcation patterns on $0 \le m < \infty$ that we identified for moderately divergent selection (Case II). We conjecture that, except for nongeneric cases, these are all possible patterns.

Case II.sr. Let $r > r^*$. Then transcritical bifurcations of internal equilibria can occur only with the SLPs $\mathsf{S}_1^{\mathcal{A}}$ and $\mathsf{S}_2^{\mathcal{A}}$. By (6.8a), we have $m_{\mathrm{st}}(\mathsf{M}_{2,3}) = m_{\mathrm{na}}(\mathsf{S}^{\mathcal{A}})$. In Figure 3, Case II.sr is indicated by dark shades of red, orange, or yellow.

Pattern II.sr.a$_2$. Here, bifurcation type a_2 occurs. The bifurcations in which the SLPs $\mathsf{S}_1^{\mathcal{A}}$ and $\mathsf{S}_2^{\mathcal{A}}$ leave the state space through the monomorphic equilibria M_2 and M_3 can occur below or above the pitchfork bifurcation of I_4, I_5, and I_2. If r is sufficiently close to r^*, the

sequence of bifurcation points is

$$0 < m_{\mathrm{st}}(\mathsf{S}^{\mathcal{A}}) < m_{\mathrm{st}}(\mathsf{M}_{2,3}) < m_{\mathrm{un}}(\mathsf{I}_2); \tag{6.31a}$$

see Figure 5a. For large values of r, also the following sequence occurs:

$$0 < m_{\mathrm{st}}(\mathsf{S}^{\mathcal{A}}) < m_{\mathrm{un}}(\mathsf{I}_2) < m_{\mathrm{st}}(\mathsf{M}_{2,3}). \tag{6.31b}$$

It is not represented in Figure 5. In Figure 3, the corresponding parameter region (including each of the sequences) is shown in dark red.

Pattern II.sr.b$_2$. Here, bifurcation type b_2 occurs, which is uniquely represented by the sequence of bifurcation points

$$0 < m_{\mathrm{st}}(\mathsf{I}_{6,7}) < m_{\mathrm{st}}(\mathsf{S}^{\mathcal{A}}) < m_{\mathrm{st}}(\mathsf{M}_{2,3}); \tag{6.32}$$

see Figure 5b. In Figure 3, the corresponding parameter region is shown in dark orange. (If a critical m indicating the loss of stability of an equilibrium coincides with a critical m indicating the gain of stability, here $m_{\mathrm{un}}(\mathsf{I}_2) = m_{\mathrm{st}}(\mathsf{I}_{6,7})$, we only write the critical m indicating the gain of stability in the sequence of bifurcation points.)

Pattern II.sr.c$_2$. Here, bifurcation type c_2 occurs. The following three sequences of bifurcation points are realized:

$$0 < m_{\mathrm{st}}(\mathsf{I}_{6,7}) < m_{\mathrm{st}}(\mathsf{S}^{\mathcal{A}}) < m_{\mathrm{st}}(\mathsf{M}_{2,3}) < m_{\mathrm{un}}(\mathsf{I}_2), \tag{6.33a}$$

$$0 < m_{\mathrm{st}}(\mathsf{I}_{6,7}) < m_{\mathrm{st}}(\mathsf{S}^{\mathcal{A}}) < m_{\mathrm{un}}(\mathsf{I}_2) < m_{\mathrm{st}}(\mathsf{M}_{2,3}), \tag{6.33b}$$

$$0 < m_{\mathrm{st}}(\mathsf{I}_{6,7}) < m_{\mathrm{un}}(\mathsf{I}_2) < m_{\mathrm{st}}(\mathsf{S}^{\mathcal{A}}) < m_{\mathrm{st}}(\mathsf{M}_{2,3}); \tag{6.33c}$$

see Figure 5c for the first possibility. In Figure 3, the corresponding parameter region (including each of the sequences) is shown in dark yellow.

Case II.wr. Let $r \leq \min\{r_{2,3}, r^{**}\}$. By (6.8a), we have $m_{\mathrm{st}}(\mathsf{M}_{2,3}) = m_{2,3}$. The SLPs $\mathsf{S}_1^{\mathcal{A}}$ and $\mathsf{S}_2^{\mathcal{A}}$ are admissible if $m < m_{\mathrm{na}}(\mathsf{S}^{\mathcal{A}})$ and unstable. If $m_{\mathrm{na}}(\mathsf{S}^{\mathcal{A}}) < m < m_{2,3}$, M_2 and M_3 are unstable and up to five internal equilibria may be admissible. Internal equilibria can enter or leave the state space only through M_2 and M_3 at the critical value $m_{2,3}$. In Figure 3, Case II.wr is indicated by bright shades of red, orange, or yellow.

Pattern II.wr.a$_1$. Here, bifurcation type a_1 occurs, which is uniquely represented by the sequence of bifurcation points

$$0 < m_{\mathrm{na}}(\mathsf{S}^{\mathcal{A}}) < m_{2,3} < m_{\mathrm{un}}(\mathsf{I}_2); \tag{6.34}$$

see Figure 5d. In Figure 3, the corresponding region is bright red.

Pattern II.wr.b$_1$. Here, bifurcation type b_1 occurs. The bifurcation in which the SLPs $\mathsf{S}_1^{\mathcal{A}}$ and $\mathsf{S}_2^{\mathcal{A}}$ leave the state space through the monomorphic equilibria M_2 and M_3 can occur below or above the pitchfork bifurcation of I_2, I_6, and I_7. Therefore, the following sequences of bifurcation points occur:

$$0 < m_{\mathrm{na}}(\mathsf{S}^{\mathcal{A}}) < m_{\mathrm{st}}(\mathsf{I}_{6,7}) < m_{2,3} \tag{6.35a}$$

(Figure 5e) or

$$0 < m_{\mathrm{st}}(\mathsf{I}_{6,7}) < m_{\mathrm{na}}(\mathsf{S}^{\mathcal{A}}) < m_{2,3}. \tag{6.35b}$$

The second sequence occurs only in a tiny parameter range. In Figure 3, the corresponding region, which includes both bifurcation sequences, is bright orange.

Pattern II.wr.c$_1$. Here, bifurcation type c_1 occurs. The bifurcations may occur in the following orders:

$$0 < m_{\mathrm{na}}(\mathsf{S}^{\mathcal{A}}) < m_{\mathrm{st}}(\mathsf{I}_{6,7}) < m_{2,3} < m_{\mathrm{un}}(\mathsf{I}_2), \tag{6.36a}$$

$$0 < m_{\mathrm{na}}(\mathsf{S}^{\mathcal{A}}) < m_{\mathrm{st}}(\mathsf{I}_{6,7}) < m_{\mathrm{un}}(\mathsf{I}_2) < m_{2,3}, \tag{6.36b}$$

$$0 < m_{\mathrm{st}}(\mathsf{I}_{6,7}) < m_{\mathrm{na}}(\mathsf{S}^{\mathcal{A}}) < m_{2,3} < m_{\mathrm{un}}(\mathsf{I}_2), \tag{6.36c}$$

$$0 < m_{\mathrm{st}}(\mathsf{I}_{6,7}) < m_{\mathrm{na}}(\mathsf{S}^{\mathcal{A}}) < m_{\mathrm{un}}(\mathsf{I}_2) < m_{2,3}, \tag{6.36d}$$

$$0 < m_{\mathrm{st}}(\mathsf{I}_{6,7}) < m_{\mathrm{un}}(\mathsf{I}_2) < m_{\mathrm{na}}(\mathsf{S}^{\mathcal{A}}) < m_{2,3}. \tag{6.36e}$$

Figure 5f displays the bifurcation pattern represented by the first sequence. In Figure 3, the corresponding region, which includes all possible bifurcation sequences, is bright yellow.

Case II.ir. Let $\min\{r_{2,3}, r^{**}\} < r < r^*$. This case of intermediate recombination and moderately divergent selection is by far the most complicated. It is restricted to the small transitory region $\bar{P} < P < 1/(1+\kappa)$ and is indicated by white ($r < r_{2,3}$) and black ($r > r_{2,3}$) in Figure 3. In this region, pairs of internal equilibria can leave or enter the state space through $\mathsf{S}_1^{\mathcal{A}}$ and $\mathsf{S}_2^{\mathcal{A}}$ for up to three values of m.

As in all cases treated above, for sufficiently small m, the equilibrium configuration described at the beginning of Section 6.4 applies. If more than one bifurcation of type a, b, c, d, or e occurs, we simply indicate this by a sequence of the letters a, b, c, d, e with proper subscripts.

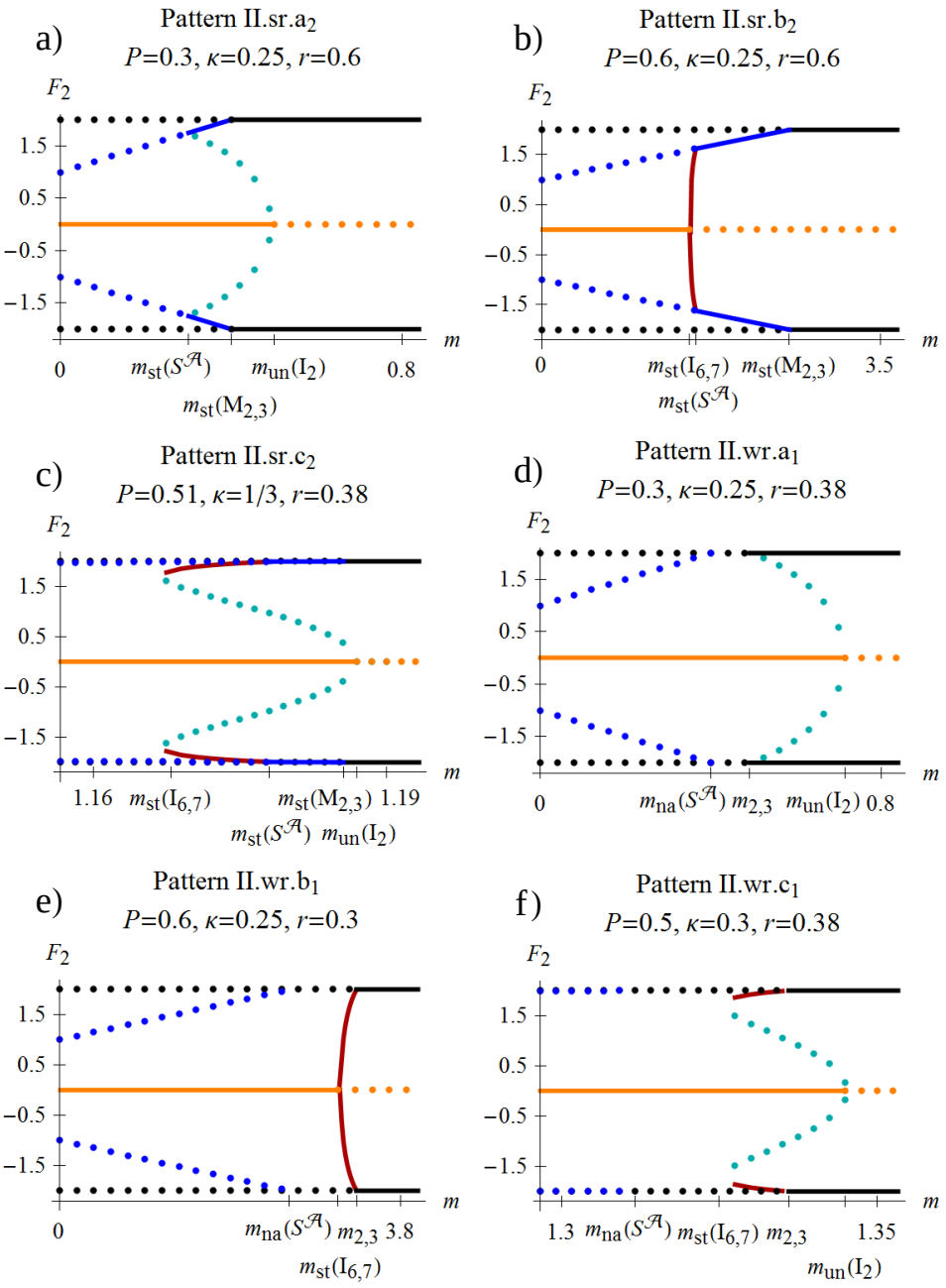

Figure 5: Bifurcation patterns for moderately divergent selection. The transformation F_2 and the colors are as in Figure 4; for I_6 and I_7, red is used; for $\mathsf{S}_1^{\mathcal{A}}$ and $\mathsf{S}_2^{\mathcal{A}}$, blue is used. The reader may note the different scales for m. In particular, in panels c and f only a small interval of m is shown for better visibility.

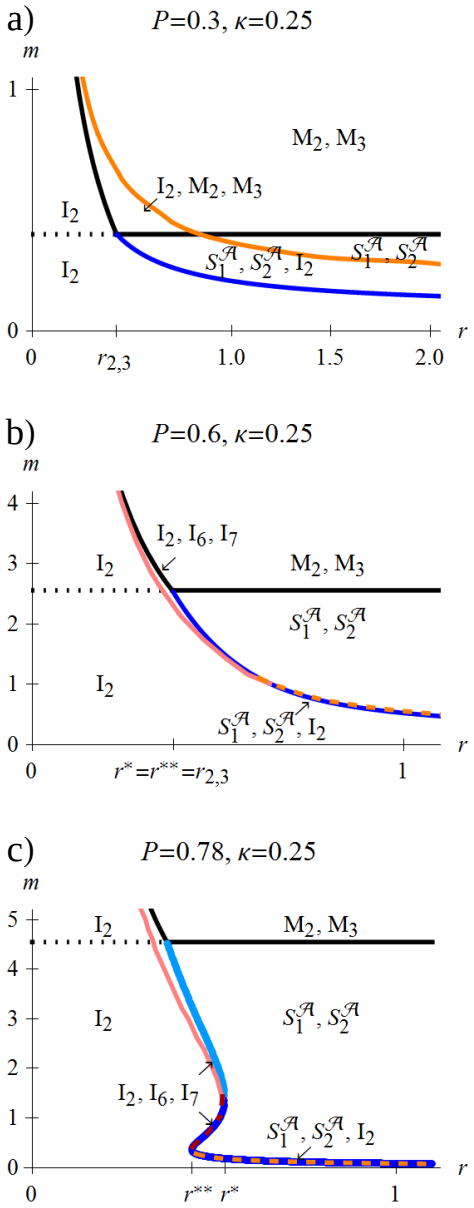

Figure 6: Regions of stability for moderately divergent selection. In each region the stable equilibria are indicated. The blue lines (dark and bright) display the zeros of π_2^0. In panels a and b, the dark blue line shows $m_{\rm st}(\mathsf{S}^{\mathcal{A}})$. In panel c, the decreasing dark blue line displays $m_{\rm st}(\mathsf{S}^{\mathcal{A}})$, and if $r^{**} < r < r^*$, the increasing dark blue line shows $m_{\rm un}(\mathsf{S}^{\mathcal{A}})$. The bright blue line displays $m_{\rm st}^{(2)}(\mathsf{S}^{\mathcal{A}})$. Orange lines represent $m_{\rm un}(\mathsf{I}_2)$ and the red line represents $m_{\rm na}(\mathsf{I}_{6,7})$. For reasons of visibility the orange lines are dashed in panels b and c and the red line is dashed in panel c. At the pink lines the equilibria I_6 and I_7 get stable. Black solid lines represent $m_{\rm st}(\mathsf{M}_{2,3})$ (6.1), whereas black dotted lines represent $m_{\rm na}(\mathsf{S}^{\mathcal{A}})$ (6.3). In panel a, Pattern II.wr.a$_1$ occurs if $r < r_{2,3}$, Pattern II.sr.a$_2$ (6.31a) occurs between $r_{2,3} < r \lessapprox 0.84$ and Pattern II.sr.a$_2$ (6.31b) occurs if $0.84 \lessapprox r$. In panel b, Pattern II.wr.b$_1$ occurs if $r < r_{2,3}$, Pattern II.sr.b$_2$ occurs between $r_{2,3} < r \lessapprox 0.62$, Pattern II.sr.c$_2$ occurs in a small neighborhood of $r \approx 0.62$ and Pattern II.sr.a$_2$ occurs if $0.62 \lessapprox r$. In panel c, Pattern II.wr.b$_1$ occurs if $0 < r < r_{2,3}$, Case II.ir occurs if $r_{2,3} < r < r^*$, and Pattern II.sr.a$_2$ (6.31b) occurs if $r^* < r$.

(i) If $r_{2,3} < r < r^{**}$, bifurcation Pattern II.sr.b_2 occurs.

(ii) If $r^{**} < r < r_{2,3}$, four different bifurcation patterns can occur. Pattern II.ir.a_2e_1 results from Pattern III.ir.e_1 below (Figure 7c) by substituting a bifurcation of type a_2 for the jump bifurcation at $\tilde{m}_{\rm st}(\mathsf{S}^{\mathcal{A}})$. The Patterns II.ir.$a_2db_1$, II.ir.$a_2da_1$, and II.ir.$a_2dc_1$ result from Patterns III.wr.db_1, III.wr.da_1, and III.wr.dc_1 (Figures 7e,g,h), respectively, by the same substitution. The two latter bifurcation patterns occur in a very tiny range of parameters.

(iii) If $\max\{r_{2,3}, r^{**}\} < r < r^{*}$, the internal equilibria always leave or enter the state space through the SLPs. The bifurcation Patterns II.ir.a_2e_2 and II.ir.a_2db_2 can occur and result from perturbation of Pattern III.ir.e_2 and Pattern III.wr.db_2, respectively (Figures 7d,f).

For the Pattern II.ir.a_2db_2, we present the sequence of bifurcation points explicitly:

$$0 < m_{\rm st}(\mathsf{S}^{\mathcal{A}}) < m_{\rm un}(\mathsf{I}_2) < m_{\rm st}(\mathsf{I}_{6,7}) < m_{\rm st}(\mathsf{I}_2) < m^{(2)}_{\rm st}(\mathsf{I}_{6,7}) < m^{(2)}_{\rm st}(\mathsf{S}^{\mathcal{A}}) < m_{\rm st}(\mathsf{M}_{2,3}), \quad (6.37)$$

where the superscript $^{(2)}$ indicates the second occasion at which an equilibrium (or a pair) becomes stable or unstable.

Figure 6 displays regions of stability of the possibly stable equilibria in dependence on the recombination rate for $\kappa = 0.25$ and various values P. From these figures, the bifurcation patterns described in the main text can be inferred by moving up along a vertical line that corresponds to a given recombination rate.

6.5 Directional selection

We assume directional selection, i.e., $P \geq 1/(1+\kappa)$; cf. (3.5). Hence, selection is strongly divergent. In Figure 3, this is region III.

We recall from Section 6.2.2 that, for small m and if $P > 1/(1+\kappa)$, the internal equilibrium I_0 is globally asymptotically stable. Therefore, no other internal equilibrium exists. Section 6.1.2 informs us that the SLPs $\mathsf{S}_1^{\mathcal{A}}$ and $\mathsf{S}_2^{\mathcal{A}}$ are admissible if $m < m_{\rm na}(\mathsf{S}^{\mathcal{A}})$, and $\mathsf{S}_1^{\mathcal{B}}$ and $\mathsf{S}_2^{\mathcal{B}}$ are admissible if $m < m_{\rm na}(\mathsf{S}^{\mathcal{B}})$, where $m_{\rm na}(\mathsf{S}^{\mathcal{A}}) \geq m_{\rm na}(\mathsf{S}^{\mathcal{B}}) > 0$ and equality holds if and only if $\kappa = 1$. Apparently, the SLPs $\mathsf{S}_1^{\mathcal{B}}$ and $\mathsf{S}_2^{\mathcal{B}}$ are always unstable. Under directional selection, the first bifurcation occurs always at $\tilde{m}_{\rm st}(\mathsf{S}^{\mathcal{A}}) > 0$, see (6.10), where $\mathsf{S}_1^{\mathcal{A}}$ and $\mathsf{S}_2^{\mathcal{A}}$ become asymptotically stable and I_0 loses its stability, i.e.,

$$m_{\rm un}(\mathsf{I}_0) = \tilde{m}_{\rm st}(\mathsf{S}^{\mathcal{A}}). \quad (6.38)$$

If $m = \tilde{m}_{\rm st}(\mathsf{S}^{\mathcal{A}})$, there is a manifold of equilibria containing I_0, M_2 and M_3 if $\kappa = 1$, and I_0, $\mathsf{S}_1^{\mathcal{A}}$ and $\mathsf{S}_2^{\mathcal{A}}$ if $\kappa < 1$. In the first case ($\kappa = 1$), it can be calculated explicitly (Appendix A.2). If $\kappa = 1$, $\mathsf{S}_1^{\mathcal{A}}$ and $\mathsf{S}_2^{\mathcal{A}}$ are never stable because $\tilde{m}_{\rm st}(\mathsf{S}^{\mathcal{A}}) = m_{\rm na}(\mathsf{S}^{\mathcal{A}}) = m_{\rm st}(\mathsf{M}_{2,3})$.

If $P = 1/(1+\kappa)$, then $\tilde{m}_{\rm st}(\mathsf{S}^{\mathcal{A}}) = 0$. We recall from Section 6.2.2 that, for small m the internal equilibrium I_0 is unstable. The SLPs $\mathsf{S}_1^{\mathcal{A}}$ and $\mathsf{S}_2^{\mathcal{A}}$ are asymptotically stable if $\kappa < 1$, whereas M_2 and M_3 are asymptotically stable if $\kappa = 1$. The sequence of bifurcation patterns for $P = 1/(1+\kappa)$ is obtained from the patterns for $P > 1/(1+\kappa)$ by omitting the bifurcation at $m = \tilde{m}_{\rm st}(\mathsf{S}^{\mathcal{A}})$. In the following we assume $P > 1/(1+\kappa)$.

Interestingly, the equilibrium I_0 exhibits positive LD if and only if $m < \tilde{m}_{\rm st}(\mathsf{S}^{\mathcal{A}})$. This follows from continuity of D_γ because $D_\gamma > 0$ if m is small, $D_\gamma = 0$ if and only if $m = \tilde{m}_{\rm st}(\mathsf{S}^{\mathcal{A}})$, and $D_\gamma < 0$ if m is slightly greater than $\tilde{m}_{\rm st}(\mathsf{S}^{\mathcal{A}})$. In fact, it is easy to show from (A.3) that $\tilde{m}_{\rm st}(\mathsf{S}^{\mathcal{A}})$ is the only value for which an internal equilibrium satisfying (5.6) is in linkage equilibrium.

The bifurcation patterns that occur above $\tilde{m}_{\rm st}(\mathsf{S}^{\mathcal{A}})$ depend crucially on the recombination rate. We recall the definition of $\tilde{P}$ from Section 6.1.3 and that of r^* from Section 6.4. Then, in analogy to (6.29), we have

$$r^* = r_{2,3} \quad \text{if } P \geq \tilde{P}, \tag{6.39a}$$

$$r^* > r_{2,3} \quad \text{if } P < \tilde{P}, \tag{6.39b}$$

and r^* indicates the turning point of the blue curve in Figure 8b and Figure A1. For given P and κ, we define $r^\dagger$ as the maximum value r for which I_0 can become stable when it exhibits negative LD. The value $r^\dagger$ is visualized by the turning point of the red curve in Figures 8b,c. It can be greater or less than $r_{2,3}$.

We call recombination strong if

$$r > r^*, \tag{6.40}$$

weak if

$$r < r^\dagger, \tag{6.41}$$

and intermediate if $r^\dagger < r < r^*$. In each of the following cases, $\mathsf{I}_0 \to \mathsf{F}$ as $m \to \infty$.

Case III.sr. We assume $r > r^*$. In Figure 3, this region is dark blue.

Pattern III.sr. As the migration rate increases from $m_{\rm un}(\mathsf{I}_0) = \tilde{m}_{\rm st}(\mathsf{S}^{\mathcal{A}})$ to $m_{\rm st}(\mathsf{M}_{2,3}) = m_{\rm na}(\mathsf{S}^{\mathcal{A}})$, the two SLPs $\mathsf{S}_1^{\mathcal{A}}$ and $\mathsf{S}_2^{\mathcal{A}}$ leave the simplex by transcritical bifurcations with M_2 and M_3, respectively. The sequence of bifurcation points is simply

$$0 < \tilde{m}_{\rm st}(\mathsf{S}^{\mathcal{A}}) \leq m_{\rm st}(\mathsf{M}_{2,3}), \tag{6.42}$$

where $\tilde{m}_{\rm st}(\mathsf{S}^{\mathcal{A}}) = m_{\rm na}(\mathsf{S}^{\mathcal{A}})$ holds only if $\kappa = 1$. Thus, if $\kappa = 1$, I_0 loses its stability when the (unstable) SLPs hit the monomorphic equilibria. The corresponding bifurcation patterns are displayed in Figures 7a and 7b. The pattern displayed in Figure 7b occurs generically whenever r is sufficiently large.

Case III.ir. We assume $r^\dagger < r < r^*$. In Figure 3, this region is gray. As m increases above $m_{\rm un}(\mathsf{I}_0) = \tilde{m}_{\rm st}(\mathsf{S}^{\mathcal{A}})$, either bifurcations of type e_1 or e_2 occur. Thus we have the following two patterns:

Pattern III.ir.e$_1$. Type e_1 occurs and the sequence of bifurcation points is

$$0 < \tilde{m}_{\rm st}(\mathsf{S}^{\mathcal{A}}) < m_{\rm st}(\mathsf{I}_{6,7}) < m_{\rm na}(\mathsf{S}^{\mathcal{A}}) < m_{2,3}; \tag{6.43}$$

see Figure 7c.

Pattern III.ir.e$_2$. Type e_2 occurs and the sequence of bifurcation points is

$$0 < \tilde{m}_{\rm st}(\mathsf{S}^{\mathcal{A}}) < m_{\rm st}(\mathsf{I}_{6,7}) < m_{\rm st}(\mathsf{S}^{\mathcal{A}}) < m_{\rm st}(\mathsf{M}_{2,3}), \tag{6.44}$$

where $m_{\rm st}(\mathsf{M}_{2,3}) = m_{\rm na}(\mathsf{S}^{\mathcal{A}})$; see Figure 7d. We note that Pattern III.ir.e_2 occurs only if $r^* > r_{2,3}$.

Case III.wr. We assume $r < r^\dagger$. In Figure 3, this region is light blue. If $m < \tilde{m}_{\rm st}(\mathsf{S}^{\mathcal{A}})$, $\mathsf{I}_0 \to \mathsf{R}_1$ as $r \to 0$, whereas if $m > \tilde{m}_{\rm st}(\mathsf{S}^{\mathcal{A}})$, $\mathsf{I}_0 \to \mathsf{R}_2$ as $r \to 0$. Therefore, the coordinates of the internal equilibrium I_0 can be obtained approximately for small r by perturbing R_1 or R_2. However, they are complicated and we do not present them.

If recombination is weak, then, except in the small region $1/(1+\kappa) < P < \sqrt{3\kappa}/[\sqrt{2}(1+\kappa)]$ (see Remark 6.3f), only the following two bifurcation patterns can occur.

Pattern III.wr.db$_1$. Here, type d occurs first, then type b_1. However, the transcritical bifurcations of the unstable equilibria $\mathsf{S}_1^{\mathcal{A}}$ and $\mathsf{S}_2^{\mathcal{A}}$ with M_2 and M_3 can occur at different instances. Therefore, we have the following possible sequences of bifurcation points:

$$0 < \tilde{m}_{\rm st}(\mathsf{S}^{\mathcal{A}}) < m_{\rm st}(\mathsf{I}_{6,7}) < m_{\rm st}(\mathsf{I}_0) < m_{\rm na}(\mathsf{S}^{\mathcal{A}}) < m_{\rm st}^{(2)}(\mathsf{I}_{6,7}) < m_{2,3} \tag{6.45}$$

(Figure 7e), or

$$0 < \tilde{m}_{\rm st}(\mathsf{S}^{\mathcal{A}}) < m_{\rm st}(\mathsf{I}_{6,7}) < m_{\rm st}(\mathsf{I}_0) < m_{\rm st}^{(2)}(\mathsf{I}_{6,7}) < m_{\rm na}(\mathsf{S}^{\mathcal{A}}) < m_{2,3}. \tag{6.46}$$

Pattern III.wr.db$_2$. Here, type d occurs first, then type b_2. Therefore, the sequence of bifurcation points is

$$0 < \tilde{m}_{\rm st}(\mathsf{S}^{\mathcal{A}}) < m_{\rm st}(\mathsf{I}_{6,7}) < m_{\rm st}(\mathsf{I}_0) < m_{\rm st}^{(2)}(\mathsf{I}_{6,7}) < m_{\rm st}^{(2)}(\mathsf{S}^{\mathcal{A}}) < m_{\rm st}(\mathsf{M}_{2,3}), \tag{6.47}$$

where $m_{\rm st}(\mathsf{M}_{2,3}) = m_{\rm na}(\mathsf{S}^{\mathcal{A}})$; see Figure 7f. Pattern III.wr.db$_2$ occurs only if $r^* > r_{2,3}$.

The following two bifurcation patterns occur only in a small parameter region. Very tight linkage is a necessary condition for them to occur. The corresponding regions in Figure 3 occur only in panel d.

Pattern III.wr.da$_1$. Here, type d occurs first, then type a$_1$. Therefore, the sequence of bifurcation points is

$$0 < \tilde{m}_{\rm st}(\mathsf{S}^{\mathcal{A}}) < m_{\rm st}(\mathsf{I}_{6,7}) < m_{\rm st}(\mathsf{I}_0) < m_{\rm na}(\mathsf{S}^{\mathcal{A}}) < m_{2,3} < m^{(2)}_{\rm un}(\mathsf{I}_0); \tag{6.48}$$

see Figure 7g. The equilibrium configuration of the strong-migration limit applies if $m > m^{(2)}_{\rm un}(\mathsf{I}_0)$.

Pattern III.wr.dc$_1$. Here, type d occurs first, then type c$_1$. The bifurcations in this pattern may occur in two different orders. The sequence of bifurcation points is either given by

$$0 < \tilde{m}_{\rm st}(\mathsf{S}^{\mathcal{A}}) < m_{\rm st}(\mathsf{I}_{6,7}) < m_{\rm st}(\mathsf{I}_0) < m_{\rm na}(\mathsf{S}^{\mathcal{A}}) < m^{(2)}_{\rm st}(\mathsf{I}_{6,7}) < m_{2,3} < m^{(2)}_{\rm un}(\mathsf{I}_0) \tag{6.49a}$$

(Figure 7h) or by

$$0 < \tilde{m}_{\rm st}(\mathsf{S}^{\mathcal{A}}) < m_{\rm st}(\mathsf{I}_{6,7}) < m_{\rm st}(\mathsf{I}_0) < m_{\rm na}(\mathsf{S}^{\mathcal{A}}) < m^{(2)}_{\rm st}(\mathsf{I}_{6,7}) < m^{(2)}_{\rm un}(\mathsf{I}_0) < m_{2,3}. \tag{6.49b}$$

The last four bifurcation events in (6.49a) and (6.49b) correspond to the bifurcation sequences (6.36a) and (6.36b), respectively, of Pattern II.wr.c$_1$.

A remarkable feature of the bifurcation diagrams occurring for moderate or weak recombination is that there is an interval of intermediate migration rates in which a pair of SLPs is stable, but no internal equilibrium, whereas for somewhat lower or higher migration rates one or two internal equilibria are stable. The bifurcation patterns in Case III.wr are reminiscent of bifurcation patterns found in a two-locus model of intraspecific competition for a continuum of resources (Bürger 2002).

Figure 8 displays regions of stability of the possibly stable equilibria in dependence on different parameters for $P = 1$. If $P = 1$, all bifurcation patterns except III.wr.da$_1$ and III.wr.c$_1$ can occur. For strong recombination (Case III.sr), Figure 8a shows the regions of stability of the three possible types of stable equilibria as functions of κ and m. Figures 8b and 8c show the regions of stability of the potentially stable equilibria as functions of r and m for two values of κ. As in Figure 6, the bifurcation patterns described in the main text can be inferred by moving up along a vertical line that corresponds to a given recombination rate. Among others, Figure 8 visualizes our definitions of weak ($r < r^{\dagger}$), intermediate, and

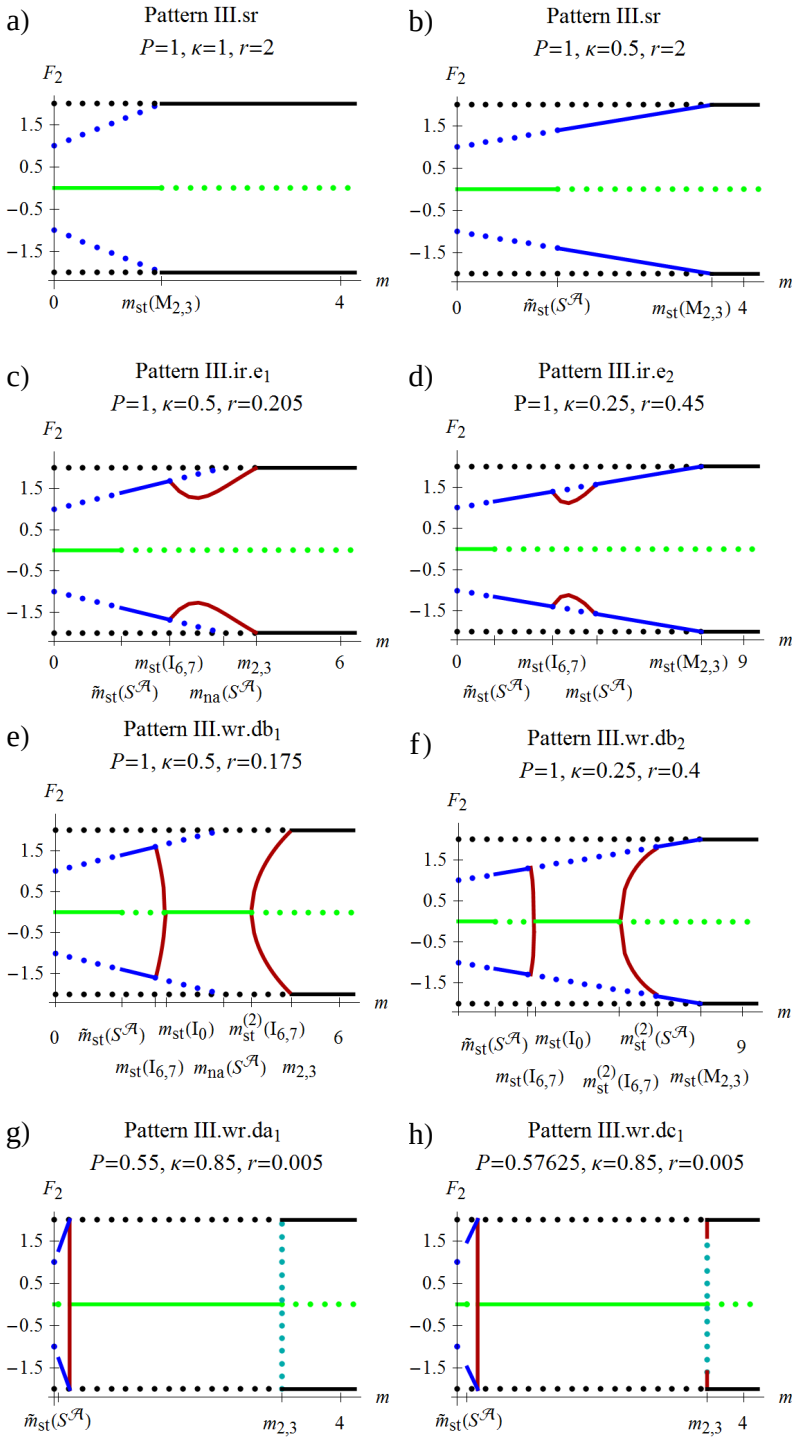

Figure 7: Bifurcation patterns as functions of m with directional selection. The case of strong recombination is displayed in panels a and b. The case of intermediate recombination is displayed in panels c and d. The case of weak recombination is displayed in panels e, f, g, and h. The transformation F_2 and the colors are as in Figure 4; for I_0, bright green is used.

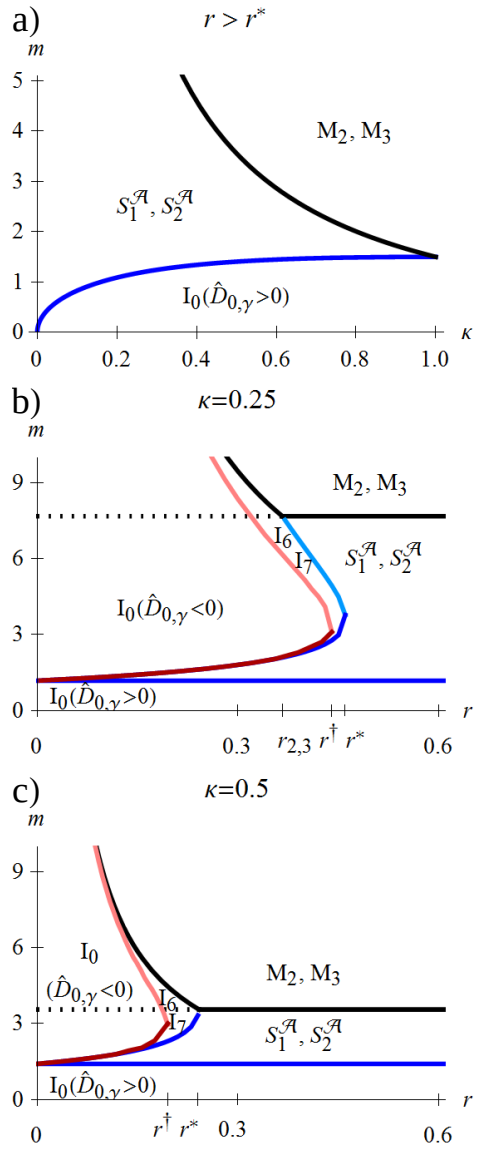

Figure 8: Regions of stability for directional selection. Panel a displays the critical migration rates $\tilde{m}_{\rm st}(\mathsf{S}^{\mathcal{A}})$ (blue) and $m_{\rm st}(\mathsf{M}_{2,3})$ (black) at which the minor and major locus, respectively, become monomorphic if recombination is strong. Panels b and c display critical migration rates delineating different regions of equilibrium configurations in dependence of r. The blue lines (dark and bright) display the zeros of π_2^0. Below the horizontal dark blue line, representing $\tilde{m}_{\rm st}(\mathsf{S}^{\mathcal{A}})$, the equilibrium I_0 is (presumably) globally asymptotically stable and exhibits positive LD. At the curved dark blue lines, $m_{\rm st}(\mathsf{I}_{6,7}) = m_{\rm un}(\mathsf{S}^{\mathcal{A}})$, I_6 and I_7 enter the simplex through $\mathsf{S}_1^{\mathcal{A}}$ and $\mathsf{S}_2^{\mathcal{A}}$, respectively. At the curved bright blue line in panel b, $m_{\rm na}(\mathsf{I}_{6,7}) = m_{\rm st}(\mathsf{S}^{\mathcal{A}})$, I_6 and I_7 leave the simplex through $\mathsf{S}_1^{\mathcal{A}}$ and $\mathsf{S}_2^{\mathcal{A}}$, respectively. At the red lines, $m_{\rm na}(\mathsf{I}_{6,7}) = m_{\rm st}(\mathsf{I}_0)$, I_6 and I_7 collide with I_0. At the pink lines, $m_{\rm st}^{(2)}(\mathsf{I}_{6,7})$, I_6 and I_7 get stable. At the horizontal black lines (dotted if $r < r_{2,3}$, solid if $r > r_{2,3}$), which show $m_{\rm na}(\mathsf{S}^{\mathcal{A}})$, $\mathsf{S}_1^{\mathcal{A}}$ and $\mathsf{S}_2^{\mathcal{A}}$ leave the simplex. Above the solid black lines, which show $m_{\rm st}(\mathsf{M}_{2,3})$, the monomorphic states M_2 and M_3 are asymptotically stable. In panels b and c, Pattern III.sr, displayed in Figure 7b, occurs if $r > r^*$; patterns of the type described in Case III.wr occur if $r < r^\dagger$. If $r^\dagger < r < r^*$, the bifurcation pattern displayed in Figure 7d occurs in panel b and the bifurcation pattern displayed in Figure 7c occurs in panel c. In panel b, if $r_{2,3} < r < r^\dagger$, the bifurcation pattern displayed in Figure 7f occurs.

strong recombination ($r > r^*$). It also shows that for low recombination rates the bifurcation Pattern III.wr.db$_1$ is the most common one.

7 Results for the diploid model

For the diploid model, we consider only directional selection and refrain from treating stabilizing selection. If selection is stabilizing and $m = 0$, the number of different equilibrium configurations is extensive and has not been fully described analytically except for $P = 0$ (Bürger and Gimelfarb 1999; Bürger 2000, Chapter VI.2). If $P > 0$, the equilibrium configuration is quite complicated as different types of equilibria (monomorphic and one-locus polymorphic) can be simultaneously stable (Gavrilets and Hastings 1993; Bürger 2000, Chapter VI.2). We noted in Section 4 that, with migration, the diploid model can have up to 121 admissible equilibria if $P = 0$. Therefore, the general case of $P \geq 0$ seems even more intractable.

In the following we assume directional selection, i.e., (3.7). Because in the strong-migration limit the dynamics is equivalent to that of a two-locus model with the same parameters s, r, κ, and stabilizing selection towards $P = 0$ (Section 5), the equilibrium configuration of the strong-migration limit (5.5) can be inferred directly from Figure 2. Therefore, in the strong-migration limit, M_2 and M_3 are asymptotically stable if $\kappa \geq 1/2$ and $r > r_2$, whereas the SLPs $\mathsf{E}_1^{\mathcal{A}}$ and $\mathsf{E}_2^{\mathcal{A}}$ are asymptotically stable if $\kappa < 1/2$ and $r > r_2$ (for the definitions of r_1 and r_2, see Figure 2). If $r < r_1$, the internal equilibrium F_1, which corresponds to F in the haploid model, is asymptotically stable. If $r_1 < r < r_2$, the two unsymmetric equilibria F_2 and F_3 are asymptotically stable. The fact that two-locus variation can be maintained under arbitrary strong migration is fundamentally different to the haploid case. In this section we assume $s = 1$, $r > 0$, and $m > 0$.

7.1 Boundary equilibria and their stability

In the diploid model, there are the same types of possibly stable boundary equilibria as in the haploid model: (i) the monomorphic equilibria (M_2 or M_3), (ii) the SLPs ($\mathsf{S}_1^{\mathcal{A}}$ or $\mathsf{S}_2^{\mathcal{A}}$), and, if $r = 0$, (iii) the full polymorphisms (R_1 or R_2). However, the coordinates of $\mathsf{S}_1^{\mathcal{A}}$, $\mathsf{S}_2^{\mathcal{A}}$, R_1 and R_2 are lengthy solutions of cubic equations.

A linear stability analysis in the full system is only feasible for the monomorphisms. It yields that M_2 and M_3 are asymptotically stable if $1/2 < \kappa \leq 1$, $r > r^{\mathsf{D}}$, and $m > m_{\mathrm{st}}^{\mathsf{D}}(\mathsf{M}_{2,3})$,

where

$$m_{\rm st}^{\mathsf{D}}(\mathsf{M}_{2,3}) = \frac{(1-2\kappa(1-P)+2P)(1-2\kappa(1+P)-2P)}{2(1+\kappa)^2(1-2\kappa)} \tag{7.1a}$$

and

$$r^{\mathsf{D}} = \left(\frac{1-\kappa}{1+\kappa}\right)^2 - m + \sqrt{m^2 + 4P^2\left(\frac{1-\kappa}{1+\kappa}\right)^2}. \tag{7.1b}$$

We note that $r^{\mathsf{D}} \to r_2$ as $m \to \infty$.

7.2 Bifurcation patterns under directional selection

As in the haploid model, for weak migration there exists the globally attracting internal equilibrium $\mathsf{I}_0 = I_m(\mathsf{M}_{1,\alpha}, \mathsf{M}_{4,\beta})$ which satisfies (5.6). In the following, we discuss the differences that occur relative to the patterns in Case III of the haploid model.

Instead of the jump bifurcation at $m = \tilde{m}_{\rm st}(\mathsf{S}^{\mathcal{A}})$ in the haploid model, the pattern b_2 occurs, i.e., the equilibrium I_0 becomes unstable and the two stable equilibria I_6 and I_7 are established at $m_{\rm un}^{\mathsf{D}}(\mathsf{I}_0) = m_{\rm st}^{\mathsf{D}}(\mathsf{I}_{6,7})$. The equilibria I_6 and I_7 leave the state space by transcritical bifurcations with $\mathsf{S}_1^{\mathcal{A}}$ and $\mathsf{S}_2^{\mathcal{A}}$ at $m_{\rm st}^{\mathsf{D}}(\mathsf{S}^{\mathcal{A}}) = m_{\rm na}^{\mathsf{D}}(\mathsf{I}_{6,7})$.

From the strong-migration limit we infer that for sufficiently strong migration $\mathsf{S}_1^{\mathcal{A}}$ and $\mathsf{S}_2^{\mathcal{A}}$ leave the state space if $\kappa > 1/2$, but remain in the state space and converge to $\mathsf{E}_1^{\mathcal{A}}$ and $\mathsf{E}_2^{\mathcal{A}}$ if $\kappa < 1/2$. If $\kappa = 1/2$, $\mathsf{S}_1^{\mathcal{A}}$ and $\mathsf{S}_2^{\mathcal{A}}$ converge to M_2 and M_3, respectively.

In the following we distinguish between weak, intermediate, and strong recombination. We call recombination weak if $r < r_1$, strong if $r > r^{\mathsf{D},*}$, and intermediate if $r_1 < r < r^{\mathsf{D},*}$. The value $r^{\mathsf{D},*}$ is defined as the minimum recombination rate such that no equilibrium enters the state space if $m > m_{\rm st}^{\mathsf{D}}(\mathsf{S}^{\mathcal{A}})$ and $r > r^{\mathsf{D},*}$. We have $r_2 \le r^{\mathsf{D},*}$, because if $r < r_2$ and $m = m_{\rm st}^{\mathsf{D}}(\mathsf{S}^{\mathcal{A}})$ the equilibrium configuration of the strong-migration limit does not apply. Numerical work shows that $r^{\mathsf{D},*}$ is only slightly larger than r_2. (In the haploid model this recombination threshold was r^*.)

Case D.sr. We assume $r > r^{\mathsf{D},*}$.

Pattern D.sr.1. If $1/2 < \kappa \le 1$, the two SLPs $\mathsf{S}_1^{\mathcal{A}}$ and $\mathsf{S}_2^{\mathcal{A}}$ leave the state space by transcritical bifurcations with M_2 and M_3 at $m_{\rm st}^{\mathsf{D}}(\mathsf{M}_{2,3})$, respectively. If $\kappa < 1$, we obtain the following sequence of bifurcation points:

$$0 < m_{\rm st}^{\mathsf{D}}(\mathsf{I}_{6,7}) < \; m_{\rm st}^{\mathsf{D}}(\mathsf{S}^{\mathcal{A}}) < m_{\rm st}^{\mathsf{D}}(\mathsf{M}_{2,3}); \tag{7.2}$$

see Figure 9a. If $m > m_{\rm st}^{\mathsf{D}}(\mathsf{M}_{2,3})$, the equilibrium configuration of the strong-migration limit applies, i.e., M_2 and M_3 are asymptotically stable and I_0 is unstable. This case corresponds to Case III.sr.

If $\kappa = 1$, $\mathsf{S}_1^{\mathcal{A}}$ and $\mathsf{S}_2^{\mathcal{A}}$ never become stable because we have $m_{\mathrm{na}}^{\mathsf{D}}(\mathsf{I}_{6,7}) = m_{\mathrm{na}}^{\mathsf{D}}(\mathsf{S}^{\mathcal{A}}) = m_{\mathrm{st}}^{\mathsf{D}}(\mathsf{M}_{2,3})$, i.e., I_6 and I_7 loose their stability when the (unstable) SLPs hit the monomorphic equilibria.

Pattern D.sr.2. If $0 < \kappa \leq 1/2$, the two SLPs $\mathsf{S}_1^{\mathcal{A}}$ and $\mathsf{S}_2^{\mathcal{A}}$ remain in the state space as $m \to \infty$. We obtain the following sequence of bifurcation points:

$$0 < m_{\mathrm{st}}^{\mathsf{D}}(\mathsf{I}_{6,7}) < \ m_{\mathrm{st}}^{\mathsf{D}}(\mathsf{S}^{\mathcal{A}}); \tag{7.3}$$

see Figure 9b. If $m > m_{\mathrm{st}}^{\mathsf{D}}(\mathsf{S}^{\mathcal{A}})$, the equilibrium configuration of the strong-migration limit applies, i.e., two SLPs are asymptotically stable and I_0 is unstable.

Case.D.wr. We assume $r < r_1$. As m increases above $m_{\mathrm{st}}^{\mathsf{D}}(\mathsf{S}^{\mathcal{A}})$, first a bifurcation of type d occurs. The equilibria I_6 and I_7 re-enter the state space at $m_{\mathrm{un}}^{\mathsf{D}}(\mathsf{S}^{\mathcal{A}}) = m_{\mathrm{st}}^{\mathsf{D},(2)}(\mathsf{I}_{6,7})$ and collide with I_0 in a supercritical pitchfork bifurcation at $m_{\mathrm{st}}^{\mathsf{D}}(\mathsf{I}_0) = m_{\mathrm{na}}^{\mathsf{D},(2)}(\mathsf{I}_{6,7})$. The equilibrium I_0 is (presumably) globally asymptotically stable if $m > m_{\mathrm{st}}^{\mathsf{D}}(\mathsf{I}_0)$, whence the strong-migration limit applies. As $m \to \infty$, I_0 converges to F_1. We have

$$0 < m_{\mathrm{st}}^{\mathsf{D}}(\mathsf{I}_{6,7}) < \ m_{\mathrm{st}}^{\mathsf{D}}(\mathsf{S}^{\mathcal{A}}) < m_{\mathrm{st}}^{\mathsf{D},(2)}(\mathsf{I}_{6,7}) < m_{\mathrm{st}}^{\mathsf{D}}(\mathsf{I}_0). \tag{7.4}$$

From the strong-migration limit we infer that there are two possible patterns:

Pattern D.wr.1. If $1/2 < \kappa \leq 1$, $\mathsf{S}_1^{\mathcal{A}}$ and $\mathsf{S}_2^{\mathcal{A}}$ leave the state space through M_2 and M_3, respectively, and $m_{\mathrm{st}}^{\mathsf{D}}(\mathsf{I}_0) < m_{\mathrm{na}}^{\mathsf{D}}(\mathsf{S}^{\mathcal{A}})$.

Pattern D.wr.2. If $0 < \kappa \leq 1/2$, $\mathsf{S}_1^{\mathcal{A}}$ and $\mathsf{S}_2^{\mathcal{A}}$ remain in the state space (Figure 9c).

Case.D.ir. We assume $r_1 < r \leq r^{\mathsf{D},*}$. As m increases above $m_{\mathrm{st}}^{\mathsf{D}}(\mathsf{S}^{\mathcal{A}})$, as in Case.D.wr, the equilibria I_6 and I_7 re-enter the state space at $m_{\mathrm{un}}^{\mathsf{D}}(\mathsf{S}^{\mathcal{A}}) = m_{\mathrm{st}}^{\mathsf{D},(2)}(\mathsf{I}_{6,7})$. The equilibrium I_0 may become stable in a supercritical pitchfork bifurcation with I_6 and I_7 at $m_{\mathrm{st}}^{\mathsf{D}}(\mathsf{I}_0) = m_{\mathrm{na}}^{\mathsf{D},(2)}(\mathsf{I}_{6,7})$ (type d), or remain unstable for increasing migration rates. If I_0 becomes stable, I_0 loses its stability again by a supercritical pitchfork bifurcation and the two stable equilibria I_6 and I_7 are re-established at $m_{\mathrm{un}}^{\mathsf{D},(2)}(\mathsf{I}_0) = m_{\mathrm{st}}^{\mathsf{D},(3)}(\mathsf{I}_{6,7})$. In both cases, the two internal equilibria I_6 and I_7 are stable. In the following we distinguish the two cases $r_1 < r < r_2$ and $r_2 < r \leq r^{\mathsf{D},*}$, in which different equilibrium configurations apply in the strong-migration limit.

If $r_1 < r < r_2$, i.e., the two unsymmetric equilibria F_2 and F_3 are asymptotically stable in the strong-migration limit, the equilibria I_6 and I_7 converge to F_2 and F_3, respectively, as $m \to \infty$. We have either

$$0 < m_{\mathrm{st}}^{\mathsf{D}}(\mathsf{I}_{6,7}) < \ m_{\mathrm{st}}^{\mathsf{D}}(\mathsf{S}^{\mathcal{A}}) < m_{\mathrm{st}}^{\mathsf{D},(2)}(\mathsf{I}_{6,7}) \tag{7.5}$$

or

$$0 < m_{\mathrm{st}}^{\mathsf{D}}(\mathsf{I}_{6,7}) < \ m_{\mathrm{st}}^{\mathsf{D}}(\mathsf{S}^{\mathcal{A}}) < m_{\mathrm{st}}^{\mathsf{D},(2)}(\mathsf{I}_{6,7}) < m_{\mathrm{st}}^{\mathsf{D}}(\mathsf{I}_0) < m_{\mathrm{st}}^{\mathsf{D},(3)}(\mathsf{I}_{6,7}). \tag{7.6}$$

If $m > m_{\mathrm{st}}^{\mathsf{D},(i)}(\mathsf{I}_{6,7})$ ($i = 2$ or $i = 3$), the equilibrium configuration of the strong-migration limit applies. As in Case.D.sr and Case.D.wr, both the sequences (7.5) and (7.6) yield two possible patterns:

Pattern D.ir.1. Sequence (7.5) applies and $\mathsf{S}_1^{\mathcal{A}}$ and $\mathsf{S}_2^{\mathcal{A}}$ leave the state space through M_2 and M_3, respectively ($1/2 < \kappa \leq 1$). We have $m_{\mathrm{st}}^{\mathsf{D},(2)}(\mathsf{I}_{6,7}) < m_{\mathrm{na}}^{\mathsf{D}}(\mathsf{S}^{\mathcal{A}})$.

Pattern D.ir.2. Sequence (7.5) applies and $\mathsf{S}_1^{\mathcal{A}}$ and $\mathsf{S}_2^{\mathcal{A}}$ remain in the state space ($0 < \kappa \leq 1/2$). The corresponding bifurcation diagram is displayed in Figure 9d.

Pattern D.ir.3. Sequence (7.6) applies and $\mathsf{S}_1^{\mathcal{A}}$ and $\mathsf{S}_2^{\mathcal{A}}$ leave the state space through M_2 and M_3, respectively ($1/2 < \kappa \leq 1$). We either have $m_{\mathrm{st}}^{\mathsf{D}}(\mathsf{I}_0) < m_{\mathrm{na}}^{\mathsf{D}}(\mathsf{S}^{\mathcal{A}}) < m_{\mathrm{st}}^{\mathsf{D},(3)}(\mathsf{I}_{6,7})$ or $m_{\mathrm{st}}^{\mathsf{D},(3)}(\mathsf{I}_{6,7}) < m_{\mathrm{na}}^{\mathsf{D}}(\mathsf{S}^{\mathcal{A}})$.

Pattern D.ir.4. Sequence (7.6) applies and $\mathsf{S}_1^{\mathcal{A}}$ and $\mathsf{S}_2^{\mathcal{A}}$ remain in the state space ($0 < \kappa \leq 1/2$). The corresponding bifurcation diagram is displayed in Figure 9e.

In the following we assume $r_2 < r \leq r^{\mathsf{D},*}$. Numerical work shows that this parameter range is small. If $1/2 < \kappa < 1$, I_6 and I_7 leave the simplex by transcritical bifurcations with M_2 and M_3, respectively. There are two possible patterns:

Pattern D.ir.5. The sequence of bifurcation points is

$$0 < m_{\mathrm{st}}^{\mathsf{D}}(\mathsf{I}_{6,7}) < \ m_{\mathrm{st}}^{\mathsf{D}}(\mathsf{S}^{\mathcal{A}}) < m_{\mathrm{st}}^{\mathsf{D},(2)}(\mathsf{I}_{6,7}) < m_{\mathrm{st}}^{\mathsf{D}}(\mathsf{M}_{2,3}). \tag{7.7}$$

Pattern D.ir.6. The sequence of bifurcation points is

$$0 < m_{\mathrm{st}}^{\mathsf{D}}(\mathsf{I}_{6,7}) < \ m_{\mathrm{st}}^{\mathsf{D}}(\mathsf{S}^{\mathcal{A}}) < m_{\mathrm{st}}^{\mathsf{D},(2)}(\mathsf{I}_{6,7}) < m_{\mathrm{st}}^{\mathsf{D}}(\mathsf{I}_0) < m_{\mathrm{st}}^{\mathsf{D},(3)}(\mathsf{I}_{6,7}) < m_{\mathrm{st}}^{\mathsf{D}}(\mathsf{M}_{2,3}). \tag{7.8}$$

These patterns correspond to Pattern III.ir.e_1 and Pattern III.wr.db_1 (Figures 7c,e) with the only difference that the jump-bifurcation is replaced by a supercritical pitchfork bifurcation. The equilibrium configuration of the strong-migration limit applies if $m > m_{\mathrm{st}}^{\mathsf{D}}(\mathsf{M}_{2,3})$. Numerical examples for these two patterns are given by $P = 1$, $\kappa = 0.75$, and $r = 0.025$ or $r = 0.021$. Analogues of Pattern III.ir.e_2 and Pattern III.wr.db_2 have not been found.

If $0 < \kappa < 1/2$, numerical work suggests that $r^{\mathsf{D},*} - r_2$ is either zero or extremely small. (In the corresponding discrete-time version of (2.7) $r_2 < r^{\mathsf{D},*}$ holds, and patterns similar to Pattern III.ir.e_2 and Pattern III.wr.db_2 were found. However, the last bifurcation event does not occur and the SLPs remain stable as $m \to \infty$.)

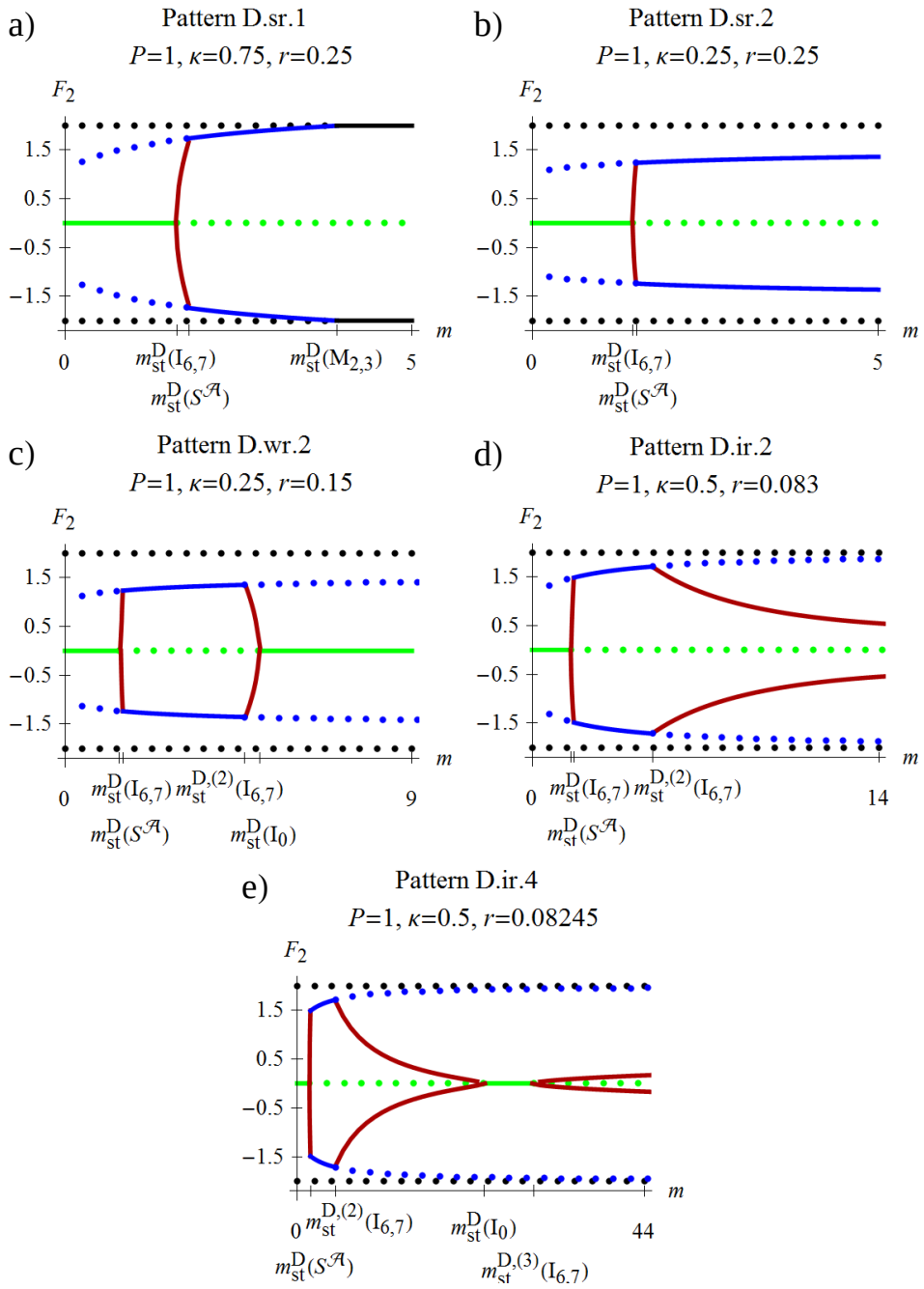

Figure 9: Bifurcation patterns as functions of m in the diploid model with directional selection. The panels display bifurcation patterns for strong, intermediate, weak recombination, as indicated. The transformation F_2 and the colors are as in Figure 7.

Finally, we note that in the diploid model we did not find analogues of Pattern III.wr.da$_1$ or Pattern III.wr.dc$_1$. These patterns occurred only for very weak recombination in the haploid model. If recombination is very weak in the diploid model, F_1 is stable in the strong-migration limit.

8 Applications

Here, we examine the roles of migration, of the degree of divergent selection, and of the genetic architecture of the trait on genetic variation, local adaptation, and differentiation in the subdivided population. In addition, we study the sign and magnitude of LD. Unless mentioned otherwise we treat the haploid model and employ the results about the equilibrium configurations and bifurcation patterns derived above.

8.1 Maximum migration rates admitting polymorphism, local adaptation, and differentiation

In Section 5, it was shown that for sufficiently large migration rates, genetic polymorphism can not be maintained. Depending on the initial conditions one of the intermediate, or generalist, haplotypes Ab or aB becomes eventually fixed. We denote the maximum migration rates below which one or both loci can be maintained polymorphic by $m^0_{\max}$ or $m_{\max}$, respectively. Clearly, $m_{\max} \leq m^0_{\max}$ holds always. We note, however, that convergence to a fully polymorphic equilibrium is not always guaranteed if $m < m_{\max}$ because boundary equilibria may be simultaneously stable with a full polymorphism, or there may be gaps in the range of values m for which a stable internal equilibrium is maintained. If $m > m^0_{\max}$, the population becomes homogeneous at equilibrium and all genetic variation, local adaptation, and differentiation is eventually lost, independently of initial conditions.

We explore how these maximum migration rates depend on P, κ, and r. Whereas P determines the strength of divergent selection on the subpopulations and, in particular, whether selection on the trait is stabilizing or directional in each deme, κ and r are the determinants of the genetic architecture of the trait. As in Section 6, we scale the parameters such that $s = 1$.

From the results in Section 6, the values of $m_{\max}$ and $m^0_{\max}$ are readily deduced for each parameter combination (Appendix A.6). However, the detailed dependence of $m_{\max}$ and $m^0_{\max}$ on the underlying parameters is highly intricate. Nevertheless, several informative and interesting features are revealed. Figure 10 visualizes the dependence of $m_{\max}$ and $m^0_{\max}$ on P and κ for strong and for weak recombination.

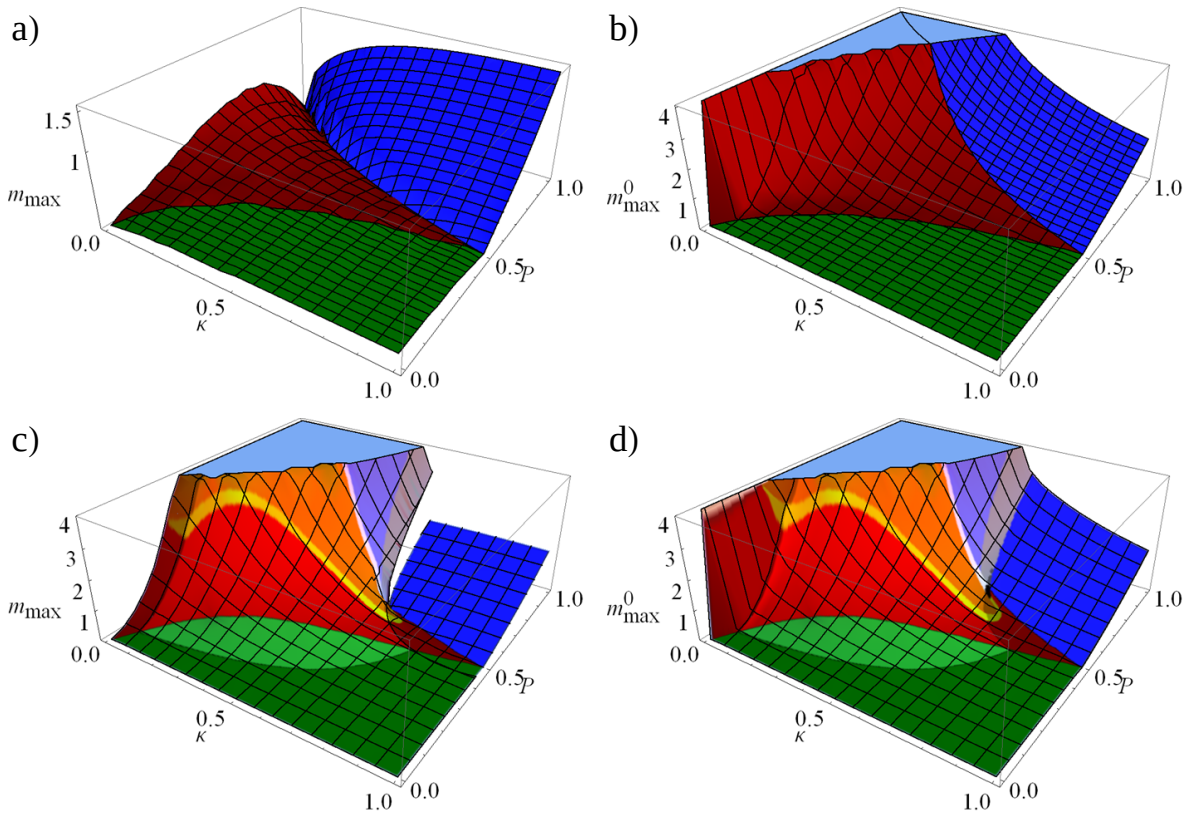

Figure 10: Maximum migration rates below which one or two loci can be maintained polymorphic. Panels a and b display $m_{\max}$ and $m^0_{\max}$, respectively, as functions of P and κ for strong recombination ($r = 2$); panels c and d display $m_{\max}$ and $m^0_{\max}$ for $r = 0.2$. Whether this is weak or not according to the classifications used in Sections 6.3 – 6.5 depends on κ and P. Since the case $\kappa = 0$ is excluded from our analysis, κ is restricted to the interval $(0.001, 1)$ in the Figure. The color code is as in Figure 3. The gap in the graph of panel c shows a discontinuity in $m_{\max}$ that is also visible in Figure 8b at $r = r^*$. (In the dark blue region $r > r^*$ holds, whereas in the gray and light blue regions $r < r^*$ holds.)

8.1.1 Weakly divergent selection

For weakly divergent selection, (A.31) and (A.33) show that $m_{\max} = m^0_{\max} = m_{\text{un}}(\mathsf{l}_2)$. The main conclusion, clearly visible from the green regions in Figure 10 and valid unless linkage is much tighter than in this figure, is that $m_{\max}$ and $m^0_{\max}$ are quite small compared to most other parameter regions. However, the dependence on the parameters P, κ, and r is complicated and nonlinear (for $\kappa = 1$ or $P = 0$ explicit analytical results are derived in Appendix A.4). For instance, $m_{\max} = m^0_{\max}$ may increase in P (if κ is small), be maximized at intermediate P, or decrease in P (if κ is large). This is best visible from the interactive version of Figure 10 (Online Supplement, Figure 1).

As a function of r, $m_{\max} = m^0_{\max}$ may be minimized at an intermediate recombination rate (see the upper orange curve in Figure 4d which assumes its minimum near $r = 0.4$). The rapid decrease of $m_{\max} = m^0_{\max}$ in Figure 4d at very small recombination rates occurs in Case I.wr and is suggested by the inequality $m_{\rm st}(\mathsf{M}_{2,3}) < m_{\rm un}(\mathsf{I}_2)$ (6.27) and the fact that $m_{\rm st}(\mathsf{M}_{2,3})$ shows this behavior. In fact, because $m_{\rm st}(\mathsf{M}_{2,3})$ increases to infinity as $r \to 0$ by (6.1), so does $m_{\max} = m^0_{\max}$. This is not visible in Figure 10 because it does not show the case of very tight linkage.

Two-locus polymorphism can be maintained for migration rates in excess of the selection strength ($m_{\max} > s = 1$) only if linkage is very tight, P is not too small, and κ is not close to 1. (Equation (3.3a) implies that $m_{\rm st}(\mathsf{M}_{2,3}) < 1$ whenever $r \gtrapprox 0.1181$.) In addition, for weakly divergent selection and strong recombination the fully polymorphic equilibria are never globally stable because the monomorphic equilibria M_2 and M_3 are always locally stable. Thus, even if $m < m_{\max} = m^0_{\max}$, ultimate maintenance of polymorphism at both loci depends on initial conditions.

8.1.2 Moderately divergent selection

A glance at the red, orange, and yellow regions in Figure 10 reveals that in this case both maximum migration rates can vary greatly in dependence on the parameters. Comparison of panels a and c shows that $m_{\max}$ depends in qualitatively different ways on P and κ if recombination is either strong or weak. For sufficiently strong recombination, only bifurcation pattern II.sr.a$_2$ applies. Then $m_{\max}$ decreases in κ and, for given κ, is maximized at intermediate values of P (Figure 10a). Thus, increasingly strong divergent selection does not necessarily facilitate the maintenance of a two-locus polymorphism.

This peculiar feature is caused by the fact that near the curve $P = 1/(1+\kappa)$, which separates the region of directional selection from that of stabilizing selection, the SLPs $\mathsf{S}_1^{\mathcal{A}}$ and $\mathsf{S}_2^{\mathcal{A}}$ are asymptotically stable for arbitrarily small $m > 0$, see (6.10), and the internal equilibrium I_0 is unstable if $r > r^*$. Therefore, $m_{\max} = 0$ if $P = 1/(1+\kappa)$ and $r > r^*$. In Figure 10a, $r > r^*$ holds for every κ, whereas in Figure 10c, $r > r^*$ holds for $\kappa \gtrapprox 0.619$. Numerical work suggests that $r^* \lessapprox 0.862$ holds always if $P = 1/(1+\kappa)$.

For weak recombination, $m_{\max} = m^0_{\max}$, which increases in P and decreases in κ for every r. From (A.31) – (A.33), we find that $m^0_{\max} \geq m_{\rm st}(\mathsf{M}_{2,3})$ and $m^0_{\max} = m_{\rm na}(\mathsf{S}^{\mathcal{A}})$ if r is sufficiently large. Numerical and analytical results indicate that, all other parameters given, $m_{\max}$ is strictly decreasing in r, and $m^0_{\max}$ either decreases in r (if r is small) or is independent of r (if r is large).

In summary, for moderately divergent selection $m_{\max}$ tends to be high if linkage is tight, P is large, but κ not too large. Whereas for migration rates well below $m_{\max}$, global convergence to a fully polymorphic equilibrium occurs, this is not necessarily the case if m is only slightly below $m_{\max}$; then it may depend on the initial conditions if a fully polymorphic equilibrium is ultimately reached. In addition, in the small parameter region of intermediate r (patterns of type II.ir), there may be gaps in the range of values m for which an internal equilibrium is stable. The migration rate $m^0_{\max}$ can be very large for every recombination rate and every P provided κ is sufficiently small. Tighter linkage, increasing strength of divergent selection, and increasing disparity of locus effects facilitate the maintenance of polymorphism at at least one locus.

8.1.3 Strongly divergent selection

Comparison of panels a and c of Figure 10 shows that for strong recombination $m_{\max}$ depends in a qualitatively different way on P and κ than for weak recombination. If recombination is strong, $m_{\max}$ increases in P and in κ. For weaker recombination (panel c), $m_{\max}$ also increases in P. However, it decreases rapidly in κ if κ is below some intermediate value (0.48 in Figure 10c), and increases slightly if κ is above this value. The reason is that above and below this intermediate value of κ, different bifurcation patterns occur, as indicated by the different colors. Finally, (A.34) and (A.35) inform us that $m_{\max}$ is strictly decreasing in r if $r < r^*$, and $m_{\max}$ is independent of r if $r > r^*$.

As Figure 8 shows, there may be gaps in the range of values m for which an internal equilibrium is stable. However, the fully polymorphic equilibrium I_0 is always (presumably, globally) stable if $m < \tilde{m}_{\rm st}(\mathsf{S}^{\mathcal{A}})$ (6.10). Hence, $m_{\max} \geq \tilde{m}_{\rm st}(\mathsf{S}^{\mathcal{A}})$.

We infer from (A.34) – (A.36) that $m^0_{\max} = m_{\rm st}(\mathsf{M}_{2,3})$ except for the two patterns III.wr.da$_1$ and III.wr.dc$_1$ (6.49a), when $m^0_{\max} \approx m_{\rm st}(\mathsf{M}_{2,3})$. Therefore, we conclude from (A.37) that $m^0_{\max}$ is increasing in P and decreasing in κ.

In summary, the parameter combinations most conducive to the maintenance of one-locus or two-locus polymorphism are contained in the region of strongly divergent selection. For strong recombination, $m_{\max}$ is maximized at $P = 1$ and $\kappa = 1$ (equal locus effects), whereas for weak recombination $m_{\max}$ is maximized if $P = 1$ and $\kappa \to 0$ (the total effect on the trait is concentrated on one locus).

8.1.4 Main conclusions

Under weakly divergent selection, the capacity to maintain polymorphism is rather limited. In general, it can be maintained only for low migration rates and only for a subset of initial conditions. For high migration rates, polymorphism can be maintained only if linkage is very tight.

Also for moderately divergent selection, two-locus polymorphism can be maintained only for relatively weak migration if recombination is strong. If recombination is weak, however, it can be maintained for migration rates much higher than the selection intensity s. In general, the potential for maintaining one or both loci polymorphic is highest under strongly divergent selection. However, even then $m_{\max}$ depends in qualitatively different ways on κ contingent on the strength of recombination.

Except for weakly divergent selection, we conclude that tight linkage of loci of unequal effects facilitates the maintenance of genetic variation considerably. Thus, genetic architectures, in which most of the total genotypic effect is concentrated on a single locus or in a cluster of tightly linked loci, seem most powerful in maintaining polymorphism in the face of strong migration.

8.2 Genetic variance

We investigate the genetic variance that is maintained at stable equilibria. Since multiple equilibria may be simultaneously stable, the variance maintained may depend strongly on initial conditions. In the formulas below, the original scaling of parameters is used, i.e., we do not set $s = 1$. A straightforward exercise yields the genetic variance in deme γ in terms of allele frequencies and linkage disequilibria:

$$\mathrm{Var}_\gamma = 4\,\frac{p_\gamma(1-p_\gamma) + \kappa^2 q_\gamma(1-q_\gamma) + 2\kappa D_\gamma}{(1+\kappa)^2}. \tag{8.1}$$

8.2.1 Stabilizing selection and weak migration

If selection in each deme is stabilizing, the internal equilibrium I_2 is asymptotically stable for sufficiently small m. Using (8.1) and (6.15), the variance at I_2 in deme γ can be approximated by

$$\mathrm{Var}_\gamma(\mathsf{I}_2) = \hat{D}_{2,\gamma}\left(4\left(\frac{1-\kappa}{1+\kappa}\right)^2 + \frac{r}{s}\frac{1-P+\kappa^2(1+P)}{(1-P-\kappa P)(P+\kappa+\kappa P)}\right) + O(m^2), \tag{8.2}$$

where

$$\hat{D}_{2,\gamma} = -\frac{m(1+\kappa)}{r(1+\kappa)+4sP(1-\kappa)} < 0 \tag{8.3}$$

is the LD. The variance is the same in both demes because of the symmetry of I_2. We note that (8.2) holds for sufficiently small m, given κ, P, r, and s. Thus, fixing m in (8.2) and taking additional limits, for instance $P \to 1/(1+\kappa)$, may not be admissible.

It is readily shown that for strong recombination, $\mathrm{Var}_\gamma(\mathsf{I}_2)$ may increase or decrease in κ and P, whereas in the limit $r \to 0$, $\mathrm{Var}_\gamma(\mathsf{I}_2)$ decreases in κ and P. Thus, no simple general patterns seem to emerge. Interestingly, $\mathrm{Var}_\gamma(\mathsf{I}_2)$ increases in r if and only if $P > (1-\kappa)/(2+2\kappa)$. Hence, for stronger divergent selection, recombination facilitates the maintenance of variation. However, we note that $P > (1-\kappa)/(2+2\kappa)$ can be satisfied also for weakly divergent selection, i.e., for $P < \kappa/(1+\kappa)$, provided $\kappa > 1/3$.

The approximation (8.2) simplifies to $m/(Ps)$ as $\kappa \to 0$ and to $2m/(s-4P^2s)$ if $\kappa = 1$. If $P = 0$, the variance at I_2 simplifies to

$$\mathrm{Var}_\gamma(\mathsf{I}_2) = \frac{m}{s}\frac{1+\kappa^2}{\kappa} + \frac{4m}{r}\left(\frac{1-\kappa}{1+\kappa}\right)^2 + O(m^2). \tag{8.4}$$

Thus, for nearly uniform selection and moderate or strong recombination, appreciable levels of genetic variance, on the order of m/s, can be maintained. Tighter linkage increases this variance and, in the limit $r \to \infty$, it approaches $m(1+\kappa^2)/(s\kappa)$, its value at linkage equilibrium. Importantly, as P increases from 0, $\mathrm{Var}_\gamma(\mathsf{I}_2)$ decreases, as is easily shown directly from (8.2). As above, (8.4) requires that m is sufficiently small compared with r and κ. Therefore, the limit $r \to 0$ needs separate treatment (Section 8.2.3).

In the special case $P = (1-\kappa)/(1+\kappa)$, when the optima in deme α and β coincide with the genotypic values of Ab and aB, respectively, we obtain the simple formulas

$$\mathrm{Var}_\gamma(\mathsf{I}_2) = \begin{cases} \frac{m}{s} + O(r) + O(m^2) & \text{if } r \text{ is small,} \\ \frac{2m}{s} + O(\frac{1}{r}) + O(m^2) & \text{if } r \text{ is large.} \end{cases} \tag{8.5}$$

For weakly divergent selection and if recombination is sufficiently strong (Case I.sr), in addition to I_2, the internal equilibrium I_3 exists and is asymptotically stable for small m. Using (6.16), the variance at I_3 in deme γ can be approximated from (8.2) by substituting $-P$ for P. We obtain that $\mathrm{Var}_\gamma(\mathsf{I}_3) \geq \mathrm{Var}_\gamma(\mathsf{I}_2)$ holds always (see also Figure 11a), and $\mathrm{Var}_\gamma(\mathsf{I}_3)$ increases in P but decreases in κ and r. Numerical work (not shown) suggests that this is true whenever I_3 is stable. Finally, the two monomorphic equilibria M_2 and M_3 are asymptotically stable for every parameter combination. Obviously, no genetic variation is maintained there. Hence, whether and how much genetic variation is maintained depends strongly on initial conditions if divergent selection is weak.

For moderately divergent selection, I_2 is the unique stable equilibrium if m is sufficiently small. For intermediate migration rates, it may be simultaneously stable with the SLPs $\mathsf{S}_1^{\mathcal{A}}$

and $\mathsf{S}_2^{\mathcal{A}}$ or the internal equilibria I_6 and I_7. The variances at $\mathsf{S}_1^{\mathcal{A}}$ and $\mathsf{S}_2^{\mathcal{A}}$ can be derived from (6.2). However, they are complicated and not shown. They satisfy the symmetry relations $\mathrm{Var}_\alpha(\mathsf{S}_1^{\mathcal{A}}) = \mathrm{Var}_\beta(\mathsf{S}_2^{\mathcal{A}})$ and $\mathrm{Var}_\alpha(\mathsf{S}_2^{\mathcal{A}}) = \mathrm{Var}_\beta(\mathsf{S}_1^{\mathcal{A}})$, are concave in m, and vanish at $m = 0$ and $m = m_{\mathrm{na}}(\mathsf{S}^{\mathcal{A}})$. In addition, $\mathrm{Var}_\alpha(\mathsf{S}_1^{\mathcal{A}}) \geq \mathrm{Var}_\alpha(\mathsf{S}_2^{\mathcal{A}})$ holds and the maxima of $\mathrm{Var}_\alpha(\mathsf{S}_1^{\mathcal{A}})$ and $\mathrm{Var}_\alpha(\mathsf{S}_2^{\mathcal{A}})$ are

$$\frac{1}{(1+\kappa)^2} \quad \text{and} \quad \frac{1}{(1+\kappa)^2}\frac{P-\kappa+\kappa P}{P+\kappa+\kappa P}, \tag{8.6}$$

respectively. They can be realized when these equilibria are stable (e.g. Figure 11c). As Figure 11 also shows, the genetic variance maintained at a SLP may be higher or lower than at a fully polymorphic equilibrium.

8.2.2 Directional selection and weak migration

If selection is directional and $P > 1/(1+\kappa)$, I_0 is the unique stable equilibrium for weak migration. From (8.1) and (6.17) we obtain

$$\mathrm{Var}_\gamma(\mathsf{I}_0) = \hat{D}_{0,\gamma}\left(4 + \frac{r}{s}\frac{1+\kappa^2-P(1+\kappa)^2}{(1-P-\kappa P)(P-\kappa+\kappa P)}\right) + O(m^2), \tag{8.7}$$

where $\hat{D}_{0,\gamma} = m/(r+4Ps) > 0$ is the LD. It is readily shown that for strong recombination, $\mathrm{Var}_\gamma(\mathsf{I}_0)$ may increase or decrease in κ and P, whereas in the limit $r \to 0$, $\mathrm{Var}_\gamma(\mathsf{I}_0)$ is independent of κ and decreases in P. In addition, it is easy to show that $\mathrm{Var}_\gamma(\mathsf{I}_0)$ increases in r if $P > 1/2$, hence, whenever $P > 1/(1+\kappa)$.

Near $P = 1$, and if all other parameters are fixed, $\mathrm{Var}_\gamma(\mathsf{I}_0)$ decreases in P, hence it is maximized for some intermediate value of P. If $P = 1$, (8.7) simplifies to

$$\mathrm{Var}_\gamma(\mathsf{I}_0) = \frac{2m}{s}\left(1 - \frac{2s}{r+4s}\right) + O(m^2), \tag{8.8}$$

which to first order in m is independent of κ and increases in r. Figure 11c indicates that the influence of κ on the genetic variance is also negligible for intermediate migration rates. For higher migration rates, $\mathrm{Var}_\gamma(\mathsf{I}_0)$ may decrease as r increases (e.g. Figure 12a).

In the limits of weak or strong recombination, (8.8) yields

$$\mathrm{Var}_\gamma(\mathsf{I}_0) = \begin{cases} \frac{m}{s} + \frac{mr}{4s^2} + O(r^2) + O(m^2) & \text{if } r \text{ is small,} \\ \frac{2m}{s} - \frac{4m}{r} + O(\frac{1}{r^2}) + O(m^2) & \text{if } r \text{ is large.} \end{cases} \tag{8.9}$$

It seems remarkable that in these limiting cases essentially the same amount of variance is maintained under strong divergent selection as in the special case leading to (8.5), in which divergent selection is weak (if $\kappa > 1/2$) or moderate (if $\kappa < 1/2$). Nevertheless, there is a

substantial difference between these cases, because under stabilizing selection, variance will be maintained only for appropriate initial conditions (i.e., sufficient initial differentiation between the subpopulations).

Since (6.17) and (8.7) assume that m is sufficiently small for given κ, P, and r, the limit $P \to 1/(1+\kappa)$ can not be performed in (8.7). If $P = 1/(1+\kappa)$ and $\kappa < 1$, the internal equilibrium I_0 is unstable. The SLPs $\mathsf{S}_1^{\mathcal{A}}$ and $\mathsf{S}_2^{\mathcal{A}}$ are asymptotically stable for weak migration (Section 6.2.2). The variances in deme α and β at $\mathsf{S}_1^{\mathcal{A}}$ are approximately $m/[s(1+\kappa)]$ and $m/[s(1-\kappa)]$, respectively. At $\mathsf{S}_2^{\mathcal{A}}$, these are the variances in deme β and α.

8.2.3 Weak recombination

Some of the approximations given above do not apply if recombination is weak. In the absence of recombination simple approximations for the variance can be obtained from Section 6.1.4. They are valid for a wide range of migration rates. Let I_j denote I_2 if selection is stabilizing and I_0 if selection is directional.

If $r = 0$ and selection is stabilizing, then R_2 is stable for every $m > 0$, whereas for directional selection R_2 is stable only if $m > \tilde{m}_{\rm st}(\mathsf{S}^{\mathcal{A}})$ (Section 6.1.4). If $m > 0$ for stabilizing selection or $m > \tilde{m}_{\rm st}(\mathsf{S}^{\mathcal{A}})$ for directional selection, and if r is sufficiently small, the equilibrium I_j can be regarded as a perturbation of R_2 (see also Section 6.2.1 and Case III.wr). Then the genetic variance at I_j is approximated by the variance at R_2 and we obtain

$$\mathrm{Var}_\gamma(\mathsf{I}_j) \approx \mathrm{Var}_\gamma(\mathsf{R}_2) = \frac{m^2}{2P^2s^2}\left(\sqrt{\left(\frac{2Ps}{m}\right)^2\left(\frac{1-\kappa}{1+\kappa}\right)^2+1}-1\right). \tag{8.10}$$

In the limit $Ps/m \to 0$, this variance converges to $(1-\kappa)^2/(1+\kappa)^2$.

If $r = 0$ and selection is directional, R_1 is stable if $m < \tilde{m}_{\rm st}(\mathsf{S}^{\mathcal{A}})$ (Section 6.1.4). If $m < \tilde{m}_{\rm st}(\mathsf{S}^{\mathcal{A}})$, selection is directional, and if r is sufficiently small, the equilibrium I_0 can be regarded as a perturbation of R_1 and we obtain the approximation

$$\mathrm{Var}_\gamma(\mathsf{I}_0) \approx \mathrm{Var}_\gamma(\mathsf{R}_1) = \frac{2}{1+\sqrt{1+4P^2s^2/m^2}}. \tag{8.11}$$

For small m, this behaves asymptotically as $m/(Ps)$, which generalizes part of (8.9).

From (8.10) and (8.11) we conclude that for directional selection and sufficiently weak recombination, the variance depends strongly on κ if $m > \tilde{m}_{\rm st}(\mathsf{S}^{\mathcal{A}})$, but is almost independent of κ if $m < \tilde{m}_{\rm st}(\mathsf{S}^{\mathcal{A}})$.

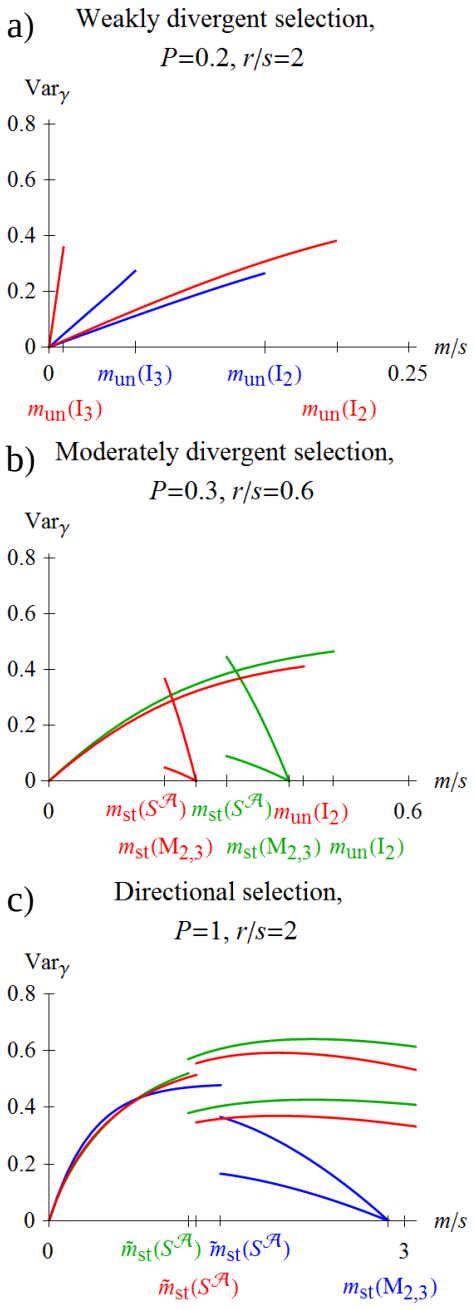

Figure 11: The genetic variance at stable polymorphic equilibria as a function of the migration rate for different values of κ (green: $\kappa = 0.25$, red: $\kappa = 0.3$, blue: $\kappa = 0.6$). Panels a and b show the variances for the bifurcation patterns I.sr (as in Figure 4a) and II.sr.a$_2$ (as in Figure 5a), i.e., for stabilizing selection. Panel c displays variances for directional selection and strong recombination (Pattern III.sr, Figure 7b). From comparison with the respective bifurcation diagrams and the indicated critical values of m, the equilibria corresponding to the different lines are easily inferred. Different lines of the same color correspond to different stable equilibria. Lines are only shown for the range of values, for which the corresponding equilibria are stable.

8.2.4 Genetic variance in the entire population

It is instructive to consider the genetic variance in the entire population. To this end, we assume that the demes are equally large and calculate Var(E) at an equilibrium E from the spatially averaged gamete frequencies ξ_i (5.1) at E. For the case of directional selection, results are displayed in Figure 12c. Comparison with Figure 12a shows that the total variance is much higher than the within-deme variances if migration is weak and (essentially) coincides with the within-deme variances above a threshold (in this case between $\tilde{m}_{\rm st}(\mathsf{S}^{\mathcal{A}})$ and $m_{\rm st}(\mathsf{I}_0)$). The reason is that for weak migration, different haplotypes and alleles dominate the two demes (because selection is divergent), whereas for sufficiently strong migration, the total population is well mixed.

8.2.5 Conclusions

The detailed dependence of the genetic variance on the underlying parameters is highly intricate. In particular, under weakly divergent selection, polymorphic equilibria coexist with monomorphic equilibria in large parts of the parameter space, hence whether variance is maintained at all strongly depends on initial conditions. Nevertheless, some patterns do emerge.

For weak migration, the equilibrium variance at fully polymorphic equilibria is always approximately proportional to m/s, however, the proportionality factor strongly depends on r, κ, and P. For nearly uniform selection, the proportionality factor may increase or decrease with P, and the variance at the simultaneously stable equilibria may depend in opposite ways on P. For strongly divergent selection, the variance decreases near $P = 1$. In this case, however, the equilibrium variance is independent of initial conditions. In addition, for stronger divergent selection, polymorphic equilibria usually can be maintained for higher migration rates than for weaker divergent selection, thus the potential for maintaining high levels of variation is increased.

The role of recombination in maintaining genetic variation is ambiguous. For small values of P and if κ is not too close to one, more variance can be maintained if the loci are tightly linked, whereas the opposite is the case for strongly divergent selection and for moderately divergent selection if $P > (1 - \kappa)/(2 + 2\kappa)$. If selection is stabilizing and recombination is weak, then the variance at the internal equilibria decreases with κ. If selection is directional and recombination is weak or $P = 1$, the variance is nearly independent of κ. If recombination is strong, the variance may increase or decrease in κ.

For moderate or strong migration, analytical results could be obtained only for $r = 0$; see (8.10) and (8.11). In general, the variance may behave in complicated ways then. For

instance, it may decay smoothly to zero as m converges to $m^0_{\max}$, or it may suddenly decrease to zero from a large value (see Figure 11b). In addition to Figure 11, three-dimensional plots of the genetic variance are presented in the Online Supplement (Figure 2).

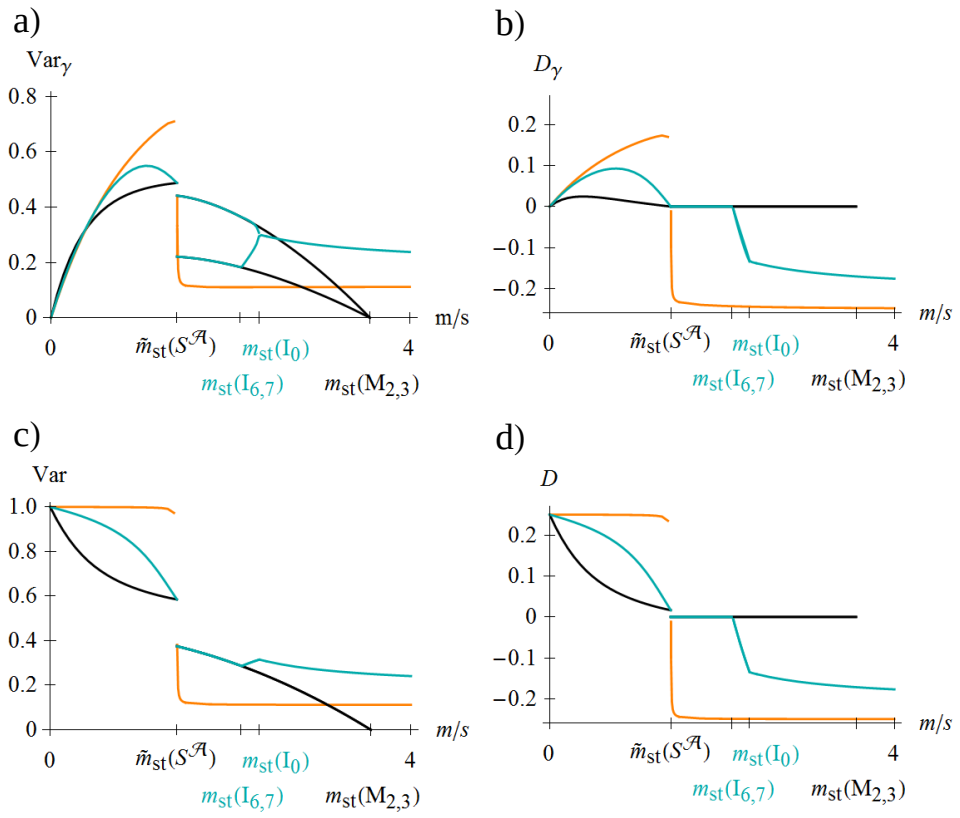

Figure 12: The genetic variance in deme γ (a), LD in deme γ (b), the genetic variance in the entire population (c), and LD in the entire population (d) are shown at the stable polymorphic equilibria as functions of the migration rate. The parameters $\kappa = 0.5$ and $P = 1$ (directional selection) are fixed. Different colors indicate different values of r (black: $r = 2$, cyan: $r = 0.175$, orange: $r = 0.001$). The bifurcation pattern corresponding to the black line is of type III.sr (as in Figure 7b), whereas the patterns corresponding to the cyan and orange lines are of type III.wr.db$_1$ (as in Figure 7e).

8.3 Linkage disequilibrium

The sign of LD determines whether the specialists AB, ab (positive) or the generalists Ab, aB (negative LD) are overrepresented in relation to the constituent allele frequencies. We investigate LD at stable fully polymorphic equilibria. In a haploid panmictic population under quadratic stabilizing selection no such equilibria exist (Section 3). In a diploid panmictic population under quadratic stabilizing selection, LD at a fully polymorphic equilibrium is

always negative (Bürger and Gimelfarb 1999; Bürger 2000, Chap. VI.2). In contrast, LD is positive at internal equilibria in a two-island model with genic directional selection in opposite direction (Li and Nei 1974; Akerman and Bürger 2014b). In the present model, depending on the parameters P, κ, and r, LD can be positive or negative.

8.3.1 Stabilizing selection

We showed in Section 6.2.1 that the equilibria I_2 and I_3 exhibit negative LD whenever they are admissible. Equations (6.15c) and (6.16c) show that for weak migration LD at I_2 increases as a function of P and decreases in κ, whereas LD at I_3 exhibits the opposite dependence. Numerical work (not shown) suggests that this is true whenever these equilibria a stable.

With moderately divergent selection, the internal equilibria I_6 and I_7 may also be stable. Numerical work suggests that LD is negative at I_6 and I_7. Therefore, we conjecture that if there is stabilizing selection in each deme, then LD is negative whenever a fully polymorphic equilibrium is stable.

8.3.2 Directional selection

In Section 6.5, it was shown that the internal equilibrium I_0 exhibits positive LD if $m < \tilde{m}_{\mathrm{st}}(\mathsf{S}^{\mathcal{A}})$ and negative LD if $m > \tilde{m}_{\mathrm{st}}(\mathsf{S}^{\mathcal{A}})$. (If $m > \tilde{m}_{\mathrm{st}}(\mathsf{S}^{\mathcal{A}})$, tight linkage is necessary for I_0 to be stable.) For small m, LD is approximated by $m/(r+4Ps)$. Numerical work suggests that $D_\gamma(\mathsf{I}_0)$ increases with κ whenever $m < \tilde{m}_{\mathrm{st}}(\mathsf{S}^{\mathcal{A}})$ and decreases with κ whenever $m > \tilde{m}_{\mathrm{st}}(\mathsf{S}^{\mathcal{A}})$ (not shown).

We conclude that under directional selection, LD is positive if migration is weak and may be negative if migration is strong (Figure 12b).

8.3.3 Stabilizing selection in the diploid model

Although we refrained from analyzing all bifurcation patterns in the diploid model with stabilizing selection, we investigated LD at possibly stable internal equilibria. Numerical work shows that in the diploid model positive LD can be maintained under stabilizing selection. A numerical example is given by $P = 0.6$, $\kappa = 0.75$, and $r/s = 2.5$, when LD is negative if $0 < m \lessapprox 0.04$ and positive if $0.04 \lessapprox m < m_{\max} \approx 0.54$. Whether LD gets positive with increasing migration rates depends on κ. For instance, if $P = 0.6$, $\kappa = 0.25$, and $r/s = 2.5$, LD is negative for $0 < m < m_{\max} \approx 0.05$. We also found parameter combinations for which LD changes its sign more than once. For instance, if $P = 0.9$, $\kappa = 0.1$, and $r/s = 0.25$, LD is negative if $0 < m \lessapprox 0.011$, positive if $0.011 \lessapprox m \lessapprox 0.87$, negative if $0.87 \lessapprox m \lessapprox 0.92$, zero if

$0.92 \lessapprox m \lessapprox 8.75$ and negative if $8.75 \lessapprox m$. The fact that LD is negative for arbitrary strong migration is inferred from the equilibrium configuration of the strong-migration limit where F_1 is asymptotically stable.

8.3.4 Linkage disequilibrium in the entire population

In analogy to the genetic variance in Section 8.2.4 we calculated the LD, D, in the entire population from the averaged gamete frequencies ξ_i. For directional selection, D is displayed in Figure 12d. Comparison with Figure 12b shows that the absolute value of D is much higher than the absolute value of D_γ if migration is weak. Above a threshold, the population is well mixed and $D = D_\alpha = D_\beta$, at least approximately.

8.4 Local adaptation and genetic differentiation

As measures for the degree of local adaptation we investigate the migration load and the deviation of the mean from the local optimum. Subsequently, we study the commonly used measures F_{ST} and Q_{ST} of differentiation. For simplicity we restrict the analysis to the case of directional selection with $P = 1$.

8.4.1 Weak migration

Deviation of the mean from the local optimum. In terms of allele frequencies the phenotypic mean in deme γ is

$$\bar{G}_\gamma = 1 - 2\frac{p_\gamma + \kappa q_\gamma}{1+\kappa}. \tag{8.12}$$

If migration is weak, the deviation of the mean at I_0 from the optimum is

$$|\bar{G}_\gamma(\mathsf{I}_0) - P_\gamma| = \frac{m}{2s}\frac{(1+\kappa)^2 r + 4\kappa s}{\kappa(r+4s)} + O(m^2). \tag{8.13}$$

In the limits of weak or strong recombination, (8.13) yields

$$|\bar{G}_\gamma(\mathsf{I}_0) - P_\gamma| = \begin{cases} \frac{m}{2s} + O(r) + O(m^2) & \text{if } r \text{ is small,} \\ \frac{m}{2s}\frac{(1+\kappa)^2}{\kappa} + O(\frac{1}{r}) + O(m^2) & \text{if } r \text{ is large.} \end{cases} \tag{8.14}$$

Therefore, strong recombination decreases local adaptation as measured by $|\bar{G}_\gamma(\mathsf{I}_0) - P_\gamma|$ by a factor of four (if $\kappa = 1$) or higher (if $\kappa < 1$).

We note that the measure $|\bar{G}_\alpha(\mathsf{I}_0) - \bar{G}_\beta(\mathsf{I}_0)|$ of differentiation is obtained from (8.13) because, if $P = 1$,

$$|\bar{G}_\alpha(\mathsf{I}_0) - \bar{G}_\beta(\mathsf{I}_0)| = 2(1 - |\bar{G}_\gamma(\mathsf{I}_0) - P_\gamma|). \tag{8.15}$$

Migration load. The migration load in deme γ is defined as $L_\gamma = w_0 - \bar{w}_\gamma$. A straightforward exercise yields

$$L_\gamma = s[(\bar{G}_\gamma - P_\gamma)^2 + \mathrm{Var}_\gamma]. \tag{8.16}$$

If migration is weak, (8.16) simplifies to $L_\gamma(\mathsf{l}_0) = s\mathrm{Var}_\gamma(\mathsf{l}_0) + O(m^2)$, and (8.8) yields

$$L_\gamma(\mathsf{l}_0) = 2m\left(1 - \frac{2s}{r+4s}\right) + O(m^2). \tag{8.17}$$

Therefore, to first order in m, $L_\gamma(\mathsf{l}_0)$ is independent of κ and increases in r. The load is approximately twice as high for loose linkage as for very tight linkage. This complements a result of Bürger and Akerman (2011), who derived a similar formula in a diploid continent-island model with genic selection. Comparison of (8.14) with (8.17) shows that for strong recombination the deviation of the mean from the local optimum is strongly influenced by the ratio of locus effects (κ), whereas the migration load is (to this order of approximation) independent of it.

Genetic differentiation measured by F_{ST}. Following Akerman and Bürger (2014b), we define a multilocus version of F_{ST} that measures the covariance of haplotype frequencies:

$$F_{\mathrm{ST}} = \frac{\sum_i \mathrm{V}(x_i)}{\sum_i \bar{x}_i(1-\bar{x}_i)}, \tag{8.18}$$

where $\bar{x}_i = (x_{i,\alpha} + x_{i,\beta})/2$ is the frequency of gamete i in the whole population and $\mathrm{V}(x_i) = (x_{i,\alpha}^2 + x_{i,\beta}^2)/2 - \bar{x}_i^2$.

For weak migration, F_{ST} at the equilibrium l_0 is

$$F_{\mathrm{ST}}(\mathsf{l}_0) = 1 - \frac{m}{r+4s}\left(4 + \frac{r}{s}\frac{(1+\kappa)^2\left(1+\kappa^2\right)}{\kappa^2}\right) + O(m^2). \tag{8.19}$$

Therefore, F_{ST} is decreasing in r and increasing in κ. In the limits of weak or strong recombination, (8.19) yields

$$F_{\mathrm{ST}}(\mathsf{l}_0) = \begin{cases} 1 - \frac{m}{s} + O(r) + O(m^2) & \text{if } r \text{ is small,} \\ 1 - \frac{m}{s}\frac{(1+\kappa)^2\left(1+\kappa^2\right)}{\kappa^2} + O(\frac{1}{r}) + O(m^2) & \text{if } r \text{ is large.} \end{cases} \tag{8.20}$$

Thus, for strong recombination F_{ST} decreases at least eight times faster (if $\kappa = 1$) with increasing migration rate than for weak recombination. This shows that if migration is weak, F_{ST} is very sensitive to the underlying genetics of the trait.

Genetic differentiation measured by $Q_{\rm ST}$. To introduce the measure $Q_{\rm ST}$ for differentiation on a quantitative character, we define the average genotypic variance within demes, $\mathrm{Var_S}$, and the genotypic variance among sub-populations, $\mathrm{Var_T}$,

$$\mathrm{Var_S} = \frac{1}{2}(\mathrm{Var}_\alpha + \mathrm{Var}_\beta), \tag{8.21}$$

$$\mathrm{Var_T} = \frac{1}{2}[(\bar{G}_\alpha - \bar{G})^2 + (\bar{G}_\beta - \bar{G})^2], \tag{8.22}$$

where $\bar{G} = (\bar{G}_\alpha + \bar{G}_\beta)/2$. Because our population is haploid, we define (Whitlock 2008)

$$Q_{\rm ST} = \frac{\mathrm{Var_T}}{\mathrm{Var_T} + \mathrm{Var_S}}. \tag{8.23}$$

If migration is weak, $Q_{\rm ST}$ at I_0 is given by

$$Q_{\rm ST}(\mathsf{I}_0) = 1 - \mathrm{Var}_\gamma(\mathsf{I}_0) + O(m^2). \tag{8.24}$$

From (8.24) and (8.8) we immediately obtain the dependency of $Q_{\rm ST}(\mathsf{I}_0)$ on r. In sharp contrast to $F_{\rm ST}(\mathsf{I}_0)$, $Q_{\rm ST}(\mathsf{I}_0)$ is (to this order of approximation) independent of κ.

8.4.2 Intermediate migration

Figure 13 illustrates the dependence of L_γ, $|\bar{G}_\gamma - P_\gamma|$, $F_{\rm ST}$, and $Q_{\rm ST}$ on the recombination and migration rate. In accordance with the approximations derived above, L_γ and $Q_{\rm ST}$ depend only weakly on r if $m < \tilde{m}_{\rm st}(\mathsf{S}^{\mathcal{A}})$, whereas the dependence of $|\bar{G}_\gamma - P_\gamma|$ and $F_{\rm ST}$ on r is amplified by κ.

For weak migration, the measures for differentiation $|\bar{G}_\alpha - \bar{G}_\beta|$, $F_{\rm ST}$, and $Q_{\rm ST}$ are non-decreasing in κ. However, numerical investigations show that for intermediate migration rates and loose linkage, differentiation decreases in κ (Online Supplement, Figures 3 and 4).

From Figure 13 some peculiar phenomena are apparent. In the parameter range where the SLPs are simultaneously stable, the load may increase or decrease with the migration rate: $L_\alpha(\mathsf{S}_1^{\mathcal{A}}) = L_\beta(\mathsf{S}_2^{\mathcal{A}})$ increases in m, but $L_\alpha(\mathsf{S}_2^{\mathcal{A}}) = L_\beta(\mathsf{S}_1^{\mathcal{A}})$ decreases in m (Figure 13a). An analogous behavior is observed for the deviations of the means from the optima (Figure 13b). Therefore, the achieved degree of local adaptation may depend strongly on initial conditions. From Figure 13c we further observe that $F_{\rm ST}$ does not necessarily decline with the migration rate if m is close to $\tilde{m}_{\rm st}(\mathsf{S}^{\mathcal{A}})$. A similar phenomenon was found by Akerman and Bürger (2014b), where $F_{\rm ST}$ could increase at a fully polymorphic equilibrium. Further, we note that for weak recombination, there is a large interval of migration rates ($\tilde{m}_{\rm st}(\mathsf{S}^{\mathcal{A}}) < m < m^0_{\rm max}$) where both loci are maintained polymorphic but $F_{\rm ST}$ and $Q_{\rm ST}$ are very low (Figures 13c,d).

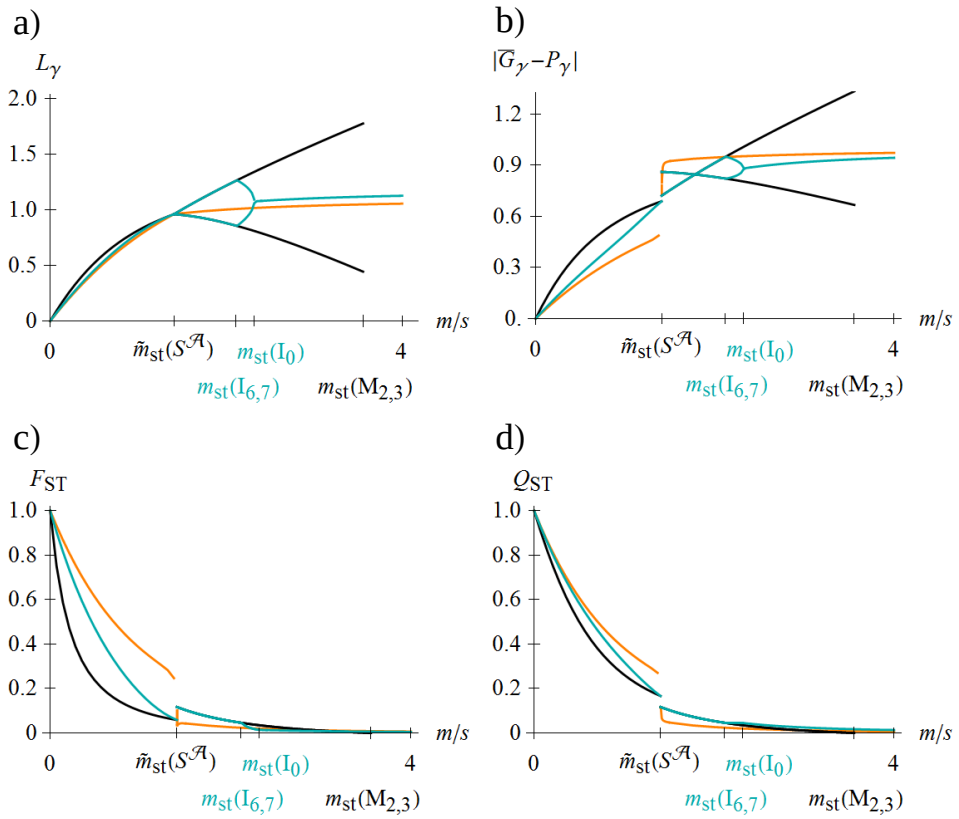

Figure 13: Local adaptation, measured by L_γ (panel a) or $|\bar{G}_\gamma - P_\gamma|$ (panel b), and differentiation, measured by F_{ST} (panel c) or Q_{ST} (panel d), at stable polymorphic equilibria as functions of the migration rate. The parameters and their corresponding bifurcation patterns are the same as in Figure 12 ($P = 1$, $\kappa = 0.5$, black: $r = 2$, cyan: $r = 0.175$, orange: $r = 0.001$).

8.4.3 Conclusions

Different measures of local adaptation and of differentiation may depend differently on r and κ, at least for weak migration. In contrast to the migration load and to Q_{ST}, the measures $|\bar{G}_\alpha - \bar{G}_\beta|$, $|\bar{G}_\gamma - P_\gamma|$, and F_{ST} are quite sensitive to the underlying genetic architecture. Loci of unequal effects amplify the effect of loose linkage in reducing local adaptation or differentiation. If $P < 1$, each measure depends in a complicated way on the underlying parameters and often also on initial conditions.

Comparison of Figures 13c and 13d suggests that $F_{ST} \leq Q_{ST}$ for directional selection in each deme. With increasing r, Q_{ST} exceeds F_{ST} more significantly. This is in accordance with inference methods based on F_{ST}/Q_{ST} contrasts, which usually conclude diversifying selection if Q_{ST} exceeds F_{ST} significantly. However, with weakly divergent selection (3.3a)

both $F_{\mathrm{ST}} < Q_{\mathrm{ST}}$ and $Q_{\mathrm{ST}} < F_{\mathrm{ST}}$ was found (results not shown). This may compromise the inference of stabilizing selection towards a common optimum if Q_{ST} is much smaller than F_{ST} (see Whitlock 2008 for discussion).

9 Discussion

Despite substantial efforts, the genetic and evolutionary factors that determine the frequently observed high heritabilities in quantitative traits are not yet well understood (Bürger 2000, Barton and Keightley 2002, Johnson and Barton 2005, Hill 2010). Although migration and heterogeneous selection are not required to maintain genetic variation and are unlikely to be ubiquitous forces in maintaining it (loc. cit.), in many populations and for some, especially ecologically relevant, traits they may be important (e.g., Felsenstein 1976, Barton 1999). The purpose of this work was to study how migration and diversifying selection on a quantitative trait interact to evolve and maintain genetic variation in a subdivided population and, along with it, local adaptation and differentiation.

We assume that the trait is determined additively by two diallelic loci. The heterogeneous environment is modeled by two demes in which, depending on the position of the optima, the trait is under quadratic stabilizing or directional selection. In contrast to previous related work (Phillips 1996, Lythgoe 1997, Spichtig and Kawecki 2004), which was mainly numerical and assumed uniform stabilizing selection and/or independent loci of equal effects, we allow for an arbitrary degree of divergent selection, i.e., difference between the two fitness optima, and an arbitrary genetic architecture, i.e., recombination rate and locus effects. Our results are predominantly analytical but complemented by numerical work.

A haploid and a diploid version of the model are introduced in Section 2. In Section 3, the relevant results on stabilizing selection in a panmictic population are summarized. The perturbation theory developed by Karlin and McGregor (1972a,b) and Bürger (2009a) allowed us to conclude that for weak migration at least one internal, i.e., fully polymorphic, equilibrium is asymptotically stable (Section 4). The above cited perturbation theory in combination with the theory for a panmictic population under stabilizing selection yields the equilibrium and stability properties for strong migration. Whereas in a haploid population, one of the two generalist haplotypes, Ab or aB, is ultimately fixed and all polymorphism is lost, in the diploid model polymorphism at one or even both loci can be maintained for appropriate genetic architectures (Section 5).

By a combination of analytical and numerical methods, we obtained a presumably com-

plete description of all equilibrium configurations and bifurcation patterns for the haploid model (Section 6). Because the diploid model is even more complex, we focused on the case of directional selection (Section 7).

In Section 6.1, the admissibility and stability conditions for the boundary equilibria are derived. Internal equilibria are treated in Section 6.2. In general, several internal equilibria may coexist. Propositions 6.1 and 6.2 contain results about existence, symmetry properties, and bifurcations with boundary equilibria. In addition, weak-migration approximations for the most important stable internal equilibria are obtained. The remainder of Section 6 is devoted to the determination of the possible equilibrium configurations and bifurcation patterns as a function of the migration rate m.

Depending on the degree of divergent selection and the ratio of locus effects, we distinguished three cases: weakly divergent selection (Case I, Section 6.3), moderately divergent selection (Case II, Section 6.4), and strongly divergent selection (Case III, Section 6.5). In the first two cases, selection in each deme is stabilizing, though increasingly asymmetric; in the third case, it is directional. According to the strength of recombination, further subcases needed to be considered. For sufficiently strong recombination, generically, only the three bifurcation patterns Pattern I.sr (Figure 4a), Pattern II.sr.a_2 (Figure 5a), and Pattern III.sr (Figure 7b) can occur. However, with tighter linkage and loci of unequal effects a multitude of different patterns was uncovered (Figure 3).

In Case I, up to seven fully polymorphic equilibria may exist if migration is weak and recombination strong (Figures 4a,b). Two of them can be simultaneously stable. In addition, the monomorphic equilibria corresponding to fixation of Ab or aB are stable. Thus, for weak migration, historical contingencies strongly influence the genetic structure. At moderate migration rates, internal equilibria are annihilated or lose there stability by subcritical pitchfork bifurcations or saddle-node bifurcations. For tight linkage, a pair of unstable internal equilibria can enter the state space, but is annihilated at a slightly larger migration rate (Figure 4c).

In Case II and Case III, up to five fully polymorphic equilibria may exist and up to three of them can be simultaneously stable (Figures 5 and 7). For weak migration, generically, there is always one globally attracting fully polymorphic equilibrium. Additionally, and also in contrast to Case I, the SLPs can be asymptotically stable. If recombination is strong, internal equilibria can enter or leave the state space only for one value of m. If recombination is intermediate or weak (Cases II.ir, III.wr, III.ir), internal equilibria can enter or leave the state space for up to three values of m. In particular, ranges of migration rates in which fully

polymorphic equilibria are stable may be interrupted by ranges in which SLPs are stable (e.g., Figures 7c,d,e,f). For sufficiently large migration rates, one of the generalist haplotypes, Ab or aB, becomes ultimately fixed.

The diploid model was studied in detail only for directional selection (Section 7). For low migration rates, the equilibrium configurations are analogous to those in the haploid model. For intermediate or large migration rates this changes (Figure 9). The most fundamental difference is that fully polymorphic equilibria are asymptotically stable for arbitrarily strong migration if the genetic architecture conforms to one of the regions in Figure 2 indicated by $\mathsf{F}_{1,\gamma}$ or $\mathsf{F}_{2,\gamma}$, $\mathsf{F}_{3,\gamma}$. This is true independently of the strength of divergent selection. As pointed out in Section 4, for stabilizing selection equilibrium configurations in the diploid model may be much more complex than in the haploid model.

Among our main goals was the determination of the maximum migration rates below which polymorphism at one or both loci can be maintained. They are denoted by $m^0_{\max}$ or $m_{\max}$, respectively, and studied in Section 8.1 by applying the results on the equilibrium configurations. These migration rates depend crucially on the strength of divergent selection and the genetic basis of the trait (Figure 10). Under weakly divergent selection, strong recombination may promote the maintenance of polymorphism. Otherwise, concentrated genetic architectures, i.e., a major locus with a tightly linked minor one, favor polymorphism and allow its maintenance for migration rates much higher than the strength s selection. Complementing the work of Yeaman and Whitlock (2011), who showed that concentrated genetic architectures evolve in subdivided populations, we found that these architectures may considerably facilitate the maintenance of polymorphism and, therefore, provide the potential for divergence even in the presence of relatively strong gene flow.

Our results on $m^0_{\max}$ also shed new light on the findings of Lythgoe (1997) and Phillips (1996), who analyzed $m^0_{\max}$ for independent loci of equal effect assuming that the phenotypic mean coincides with the optimum. The latter assumption essentially requires uniform selection across demes. The setup of Lythgoe (1997) and Phillips (1996) corresponds to that underlying our Pattern I.sr.0 (Figure 4b). Therefore, their results, as well as ours on that pattern, indicate that $m^0_{\max}$ is generally very low in relation to the strength of selection. The current work, which relaxes several of their assumptions, does not only show that $m^0_{\max}$ may be many times higher than s, but also demonstrates the importance of linkage and unequal locus effects in maintaining genetic variation.

Spichtig and Kawecki (2004) assumed two demes in which directional selection acts in opposite direction on a quantitative trait. They admitted a range of shapes for the fitness

functions, including linear and quadratic functions. For one to five unlinked equivalent loci, they evaluated numerically the migration rates $m_{\max}$ and $m^0_{\max}$. Their Figure 2 shows that $m_{\max}$ increases as their shape parameters γ declines from 2 (corresponding to quadratic selection, as in our model) to 1 (corresponding to linear selection). Spichtig and Kawecki (2004) also presented results showing that $m_{\max}$ is somewhat smaller for loci with unequal effects if $\gamma > 1$. Comparison of panels a and c of our Figure 10 at $P = 1$ shows that their finding holds only if recombination is strong relative to selection. If recombination is weak, $m_{\max}$ is massively elevated if loci have very different effects, i.e., if κ is small. Our study of these maximum migration rates unveils the sensibility of $m_{\max}$ or $m^0_{\max}$ to the underlying genetics and provides a much more complete picture.

In Section 8.2, we derived approximations for the genetic variance at stable equilibria. If migration is weak, the equilibrium variance at a fully polymorphic equilibrium is proportional to m/s. However, the proportionality factor depends in a complicated way on the genetic architecture of the trait. Whereas with directional selection the proportionality factor is independent of κ if $P = 1$, and weakly dependent on κ if P is somewhat lower, the ratio of locus effects κ has substantial influence under stabilizing selection; compare, for instance (8.4) and (8.8). Our results greatly generalize the approximations for the variance in Lythgoe (1997, eq. 7) and Phillips (1996, eq. 2) and highlight the intricate influence of the genetic architecture.

Recombination may increase or decrease the genetic variance (see e.g. (8.2) or Figure 2 in the Online Supplement). Interestingly, recombination may affect $m_{\max}$ and the genetic variance in opposite ways. For instance, under directional selection, $m_{\max}$ is a decreasing function of r (and strongly decreasing if κ is small), whereas (8.7) and (8.8) show that $\mathrm{Var}_\gamma(\mathsf{l}_0)$ increases in r if migration is weak. For moderate or high migration rates, however, the dependence of the variance on the recombination rate may be complex (Figure 12).

In Section 6.3, we examined sign and magnitude of LD. In the haploid model with stabilizing selection, we found that LD is always negative. With directional selection, LD is positive and increasing in m if migration is weak. It remains positive for intermediate migration rates, i.e., if $m < \tilde{m}_{\mathrm{st}}(\mathsf{S}^{\mathcal{A}})$. For strong migration ($\tilde{m}_{\mathrm{st}}(\mathsf{S}^{\mathcal{A}}) < m < m_{\max}$) LD is generally negative (e.g., Figure 12b). This can be explained as follows. From migration-selection models with nonepistatic diversifying selection (Li and Nei 1974, Christiansen and Feldman 1975, Bürger and Akerman 2011, Akerman and Bürger 2014b), it is known that LD is positive and unimodal if $0 < m < m_{\max}$. Stabilizing selection or, more generally, negative epistasis tends to induce negative LD (e.g. Bürger 2000). This is the dominating effect when selection in each

deme is stabilizing because then intermediate haplotypes are selectively favored and negative epistasis is strong.

If there is directional selection in each deme, epistasis is much weaker (this follows from (A.2) by observing that e/u and e/v are decreasing in P). Therefore, LD is mainly generated by migration and becomes positive as m increases from zero. (If $m = 0$, we have $D = 0$ because in the haploid model only monomorphic equilibria can be stable.) As m increases to $\tilde{m}_{\rm st}(\mathsf{S}^{\mathcal{A}})$, LD decreases to zero. If $m > \tilde{m}_{\rm st}(\mathsf{S}^{\mathcal{A}})$, LD is zero at SLPs and negative at fully polymorphic equilibria (Figure 12b). The reason is that for such high migration rates, there is already substantial mixing between the populations and spatially averaged selection is stabilizing, as in the strong-migration limit. As m reaches or increases above $m_{\max}$, LD becomes zero again (not shown in Figure 12b) because only monomorphic equilibria are stable. In the diploid model, LD is negative under stabilizing selection if migration is weak but can become positive at intermediate migration rates and negative again at high migration rates (results not shown).

In Section 8.4, we studied how the degree of local adaptation and that of differentiation depends on the parameters. For simplicity, we assumed $P = 1$, i.e., the strongest form of directional selection. As measures for local adaptation, we used the migration load, L_γ, and the deviation of the mean from the optimum, $|\bar{G}_\gamma - P_\gamma|$. Differentiation was measured by $F_{\rm ST}$ and $Q_{\rm ST}$. Each of the pair of measures showed very different sensitivity to the underlying genetic architecture. If migration is weak, L_γ (8.17) and $Q_{\rm ST}$ (8.24) exhibit rather weak dependence on κ and r, whereas $|\bar{G}_\gamma - P_\gamma|$ (8.13) and $F_{\rm ST}$ (8.19) exhibit a much stronger dependence (Figure 13). If migration is intermediate and linkage loose, all measures of differentiation decrease with κ, supporting the finding of Yeaman and Guillaume (2009) that unequal locus effects lead to more differentiation and skew.

The symmetry assumption (2.2) greatly simplified the analysis of the model and made the description of all bifurcation patterns possible. In the following we discuss the robustness of our results to small deviations from (2.2). If migration is weak, the same arguments as in Section 4 yield that at least one fully polymorphic equilibrium is always stable. If migration is strong, one can show easily that either M_2 and M_3 are simultaneously stable or one of M_2 or M_3 is globally asymptotically stable. Small deviations from (2.2) imply that stable fully polymorphic equilibria are extinguished by saddle-node bifurcations instead of pitchfork bifurcations. For instance, in Case I both I_2 and I_3 are annihilated by separate saddle-node bifurcations with an other unstable equilibrium. The pairs of equilibria, I_4 and I_5, I_6 and I_7, or $\mathsf{S}_1^{\mathcal{A}}$ and $\mathsf{S}_2^{\mathcal{A}}$ no longer gain or lose their admissibility or stability at the same migration

rate. However, if $\kappa = 1$, we still have $m_{\mathrm{st}}(\mathsf{M}_2) = m_{\mathrm{st}}(\mathsf{M}_3)$. Under directional selection the jump-bifurcation persists. Numerical work suggests that with small deviations from (2.2) the migration rates $m_{\max}$ and $m^0_{\max}$ decrease with weakly divergent selection but may increase or decrease with moderately or strongly divergent selection.

Because the present model included epistasis, the selection pressure on one locus depends on the allele frequencies at the other locus. Therefore, there is no simple way to define selection coefficients for each locus. However, one may consider the maximum fitness difference between genotypes, $S = \max_i w_i - \min_i w_i$, as an alternative measure for the strength of selection. Using (2.6) an easy calculation shows that S increases in P. If selection is stabilizing, S may increase or decrease in κ, whereas S is constant in κ if selection is directional. The ambiguous dependence of S on κ is responsible for some of the intricate dependencies of key quantities on κ if selection is stabilizing.

Overall, we may conclude that migration-selection balance has the potential to maintain high levels of genetic variation if selection is diversifying and migration rates are in an appropriate range. Although, our explicit expressions for the genetic variance maintained under weak migration share formal similarities with approximations under mutation-selection balance (i.e., variances are proportional to m/s in the first case and U/s, U the gametic mutation rate, in the second), there are substantial differences. One reason is that the variance under migration-selection balance levels off at intermediate migration rates (which may nevertheless be much higher than gametic mutation rates) and then decreases. Another reason is the different dependence on the genetic basis of the trait under selection. Finally, it is an open problem to what extent the present results can be extrapolated to traits determined by several or many loci. The work of Barton (1983), Phillips (1996), Lythgoe (1997), Spichtig and Kawecki (2004) and Bürger (2009b, 2010) suggests that this may be strongly model dependent.

Acknowledgments. We are grateful to Dr. Simon Aeschbacher and Prof. Josef Hofbauer for helpful discussions, and to Prof. Thomas Nagylaki and one anonymous reviewer for their comments. Financial support by the Austrian Science Fund (FWF) through the Vienna Graduate School of Population Genetics (Project W1225) and Project P25188 is gratefully acknowledged.

A Appendix

A.1 Relation to Bank et al. (2012)

Since we applied some of the results in Bank et al. (2012), we introduce their notation. The following parameterization of the fitnesses of the four gametes AB, Ab, aB, ab in deme α was used:

$$u + v - e,\ u,\ v,\ 0. \tag{A.1}$$

Here, e is a measure of the epistasis induced by the nonlinearity of the fitness function. (Adding the same constant to all haplotype fitnesses does not change the dynamics.) Comparison of (2.6) with (A.1) yields

$$u = \frac{4s(\kappa + (1+\kappa)P)}{(1+\kappa)^2},\ v = \frac{4\kappa s(1 + (1+\kappa)P)}{(1+\kappa)^2},\ e = \frac{8\kappa s}{(1+\kappa)^2}, \tag{A.2}$$

and $w_0 = s(1+P)^2$. The fitnesses of the four gametes in deme β are $e-u-v$, $e-u$, $e-v$, and 0. Because $e > 0$, epistasis is negative.

It is an easy exercise to show that the allele frequencies p_γ and q_γ, and the LD measures D_γ evolve according to

$$\dot{p}_\alpha = up_\alpha(1-p_\alpha) + vD_\alpha + e(1-p_\alpha)(D_\alpha + p_\alpha q_\alpha) + m_\alpha(p_\beta - p_\alpha), \tag{A.3a}$$

$$\dot{q}_\alpha = vq_\alpha(1-q_\alpha) + uD_\alpha + e(1-q_\alpha)(D_\alpha + p_\alpha q_\alpha) + m_\alpha(q_\beta - q_\alpha), \tag{A.3b}$$

$$\begin{aligned}\dot{D}_\alpha = {} & [u(1-2p_\alpha) + v(1-2q_\alpha)]\, D_\alpha + e(D_\alpha + p_\alpha q_\alpha)[D_\alpha + (1-p_\alpha)(1-q_\alpha)] \\ & - rD_\alpha + m_\alpha\left[D_\beta - D_\alpha + (p_\beta - p_\alpha)(q_\beta - q_\alpha)\right],\end{aligned} \tag{A.3c}$$

$$\dot{p}_\beta = -up_\beta(1-p_\beta) - vD_\beta + ep_\beta[D_\beta + (1-p_\beta)(1-q_\beta)] + m_\beta(p_\alpha - p_\beta), \tag{A.3d}$$

$$\dot{q}_\beta = -vq_\beta(1-q_\beta) - uD_\beta + eq_\beta[D_\beta + (1-p_\beta)(1-q_\beta)] + m_\beta(q_\alpha - q_\beta), \tag{A.3e}$$

$$\begin{aligned}\dot{D}_\beta = {} & -[u(1-2p_\beta) + v(1-2q_\beta)]\, D_\beta + e(D_\beta - p_\beta q_\beta)[D_\beta + (1-p_\beta)(1-q_\beta)] \\ & - rD_\beta + m_\beta\left[D_\alpha - D_\beta + (p_\alpha - p_\beta)(q_\alpha - q_\beta)\right].\end{aligned} \tag{A.3f}$$

The use of u, v, and e instead of s, P, and κ makes the contribution of epistasis to the dynamics immediately visible.

A.2 The functions π_1^0, π_2^0

In order to state the functions π_1^0 and π_2^0 we set

$$\pi_1^0 = \pi_{1a}^0 + K\pi_{1b}^0, \tag{A.4a}$$

$$\pi_2^0 = \pi_{2a}^0 + K\pi_{2b}^0, \tag{A.4b}$$

where

$$K = \sqrt{4s^2 + \frac{(1+\kappa)^4 m^2}{(1+\kappa)^2 P^2 - \kappa^2}}. \tag{A.4c}$$

We have

$$\pi^0_{1a} = \frac{16\kappa^2}{(1+\kappa)^9}\left(\frac{(1+\kappa)^4 m^2}{(P-\kappa+\kappa P)^2(\kappa+P+\kappa P)^2} + \frac{4s^2}{(P-\kappa+\kappa P)(\kappa+P+\kappa P)}\right), \tag{A.4d}$$

$$\pi^0_{1b} = \left(-\frac{16\kappa^2}{(1+\kappa)^6}\frac{Pm}{(P-\kappa+\kappa P)^2(\kappa+P+\kappa P)^2}\right), \tag{A.4e}$$

and

$$\begin{aligned}\pi^0_{2a} =& -64P^8 s^4(1-\kappa)(1+\kappa)^6 + \\ & 4P^6 s^2\big[r(1+\kappa)^3(2m-r) + 16sr(1+\kappa) - 16s^2(1-\kappa)(1-2\kappa^2)\big] + \\ & 4P^4 s(1+\kappa)^2\big[(mr(1+\kappa)^5(3m-r) - 32\kappa^2 r s^2(1+\kappa)) + \\ & s(1+\kappa)^3(4mr - r^2(1-2\kappa^2) - 4m^2(1-\kappa^2)) + 16\kappa^2 s^3(1-\kappa)(2-\kappa^2)\big] + \\ & P^2\big[m^2 r(1+\kappa)^7(4m-r) - 4\kappa^2 smr(1+\kappa)^5(3m-r) - \\ & 4\kappa^2 s^2(1+\kappa)^3(2mr(2+\kappa^2) - r^2(2-\kappa^2) - 4m^2(1-\kappa^2)) + 64\kappa^4 s^3 r(1+\kappa) - 64\kappa^4 s^4(1-\kappa)\big] + \\ & \kappa^2 r^2(1+\kappa)((1+\kappa)^4 m^2 - 4\kappa^2 s^2),\end{aligned} \tag{A.4f}$$

$$\begin{aligned}\pi^0_{2b} =& -2P(P-\kappa+\kappa P)(\kappa+P+\kappa P) \\ & \big[(2\kappa^2 smr(1+\kappa)^2 + (1+\kappa)^4(m^2 r + 6P^2 smr - mr^2)) + \\ & 2s(P-\kappa+\kappa P)(\kappa+P+\kappa P)(4sr + (1+\kappa)(4P^2 sr(1+\kappa) - 16P^2 s^2(1-\kappa) - r^2(1+\kappa)))\big].\end{aligned} \tag{A.4g}$$

For fixed κ and P, $\pi^0_2(\kappa, P, r, m) = 0$ defines a curve in (r, m) coordinates which separates regions with different numbers of negative eigenvalues of $\mathsf{S}_1^{\mathcal{A}}$ (or $\mathsf{S}_2^{\mathcal{A}}$). On the curve one eigenvalue is zero. If the derivative dr/dm along the curve is positive at $m = m_{\rm na}(\mathsf{S}^{\mathcal{A}}) = m_{2,3}$ (whence $r = r_{2,3}$), then $\pi^0_2(m)$ has one or three zeros if r is slightly larger than $r_{2,3}$ (Figure A1). If this derivative is negative, then $\pi^0_2(m)$ has a unique zero if $r > r_{2,3}$. It is given by $\tilde{m}_{\rm st}(\mathsf{S}^{\mathcal{A}})$ if $P \geq 1/(1+\kappa)$. These considerations yield the condition (6.11). Algebraic evaluation of this condition with *Mathematica* followed by appropriate rearrangement yields the equivalent condition

$$\kappa^6 - \kappa^4(1+\kappa)\left(3-5\kappa-6\kappa^2\right)P^2 - \kappa^2(1+\kappa)^3\left(3-3\kappa+\kappa^2+9\kappa^3\right)P^4 - (1+\kappa)^6\left(1-2\kappa-\kappa^2\right)P^6 = 0. \tag{A.5}$$

Figure A1 complements Figure 6 and Figure 8b by visualizing the curves $\pi^0_1 = 0$ and $\pi^0_2 = 0$ in the transitory region of stabilizing and directional selection.

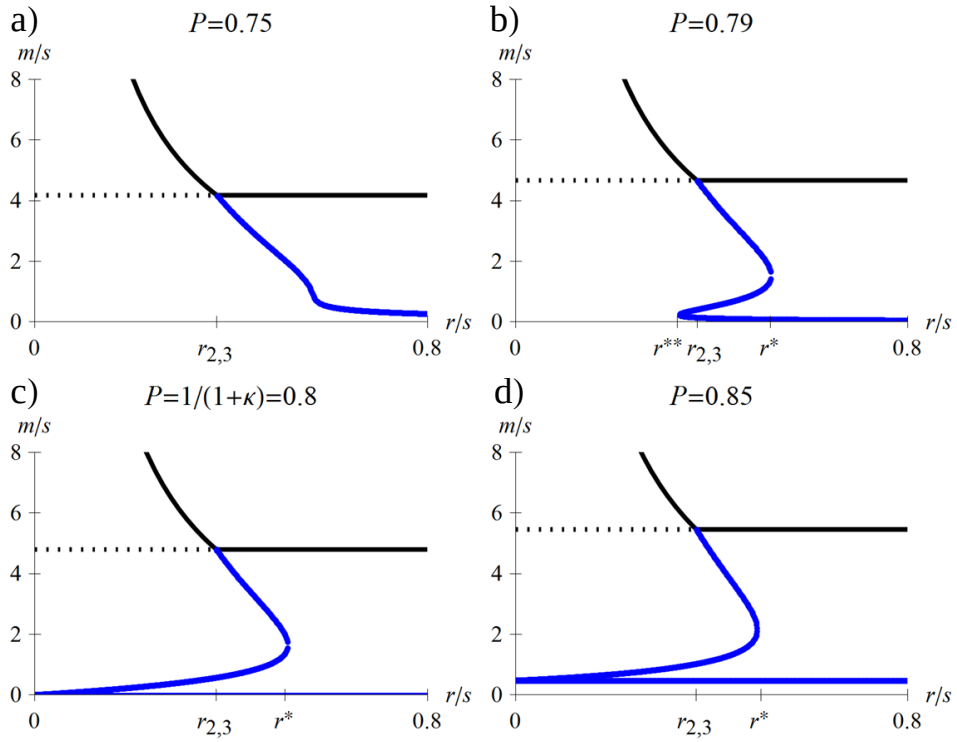

Figure A1: The Figure shows critical migration rates as a function of r for $\kappa = 0.25$ and several P. The blue lines plot the zeros of π_2^0. The solid black lines show $m_{\rm st}(\mathsf{M}_{2,3})$ as in Figure 6 and Figures 8b,c. The horizontal black lines (dotted if $r < r_{2,3}$, solid if $r > r_{2,3}$) show $m_{\rm na}(\mathsf{S}^{\mathcal{A}})$, which is a zero of π_1^0.

Equilibrium manifold at $m = \tilde{m}_{\rm st}(\mathsf{S}^{\mathcal{A}})$. The equilibrium manifold at $m = \tilde{m}_{\rm st}(\mathsf{S}^{\mathcal{A}})$ can be calculated for $\kappa = 1$. It is given by

$$\{(p_\gamma, q_\gamma, D_\gamma)_{\gamma\in\Gamma} \mid p_\alpha = 1 - q_\beta,\ \ q_\alpha = \frac{(2P+1)q_\beta}{2P + 2q_\beta - 1},\ \ p_\beta = \frac{(2P-1)(1-q_\beta)}{2P + 2q_\beta - 1},\ \ D_\alpha = D_\beta = 0\}. \tag{A.6}$$

A.3 Proofs of Proposition 6.2 and Remark 6.3

We start with a summary of relations between s, P, κ and u, v, e, as introduced in Appendix A.1. The following holds always:

$$u \geq v > 0 \text{ and } e > 0 \text{ and } 2v > e > 0, \tag{A.7}$$

$$\tilde{r} = u - v. \tag{A.8}$$

In addition we observe

$$P < \frac{\kappa}{1+\kappa} \text{ if and only if } e > u, \tag{A.9}$$

$$P > \frac{1}{1+\kappa} \text{ if and only if } v > e. \tag{A.10}$$

To calculate the perturbation (I_5 or I_7) of M_3 at $m_{2,3} + \epsilon$, we set

$$p_\gamma = \epsilon\sigma_\gamma, \quad q_\gamma = 1 - \epsilon\tau_\gamma, \quad D_\gamma = \epsilon\zeta_\gamma. \tag{A.11}$$

Because $m_{2,3} > 0$ if and only if $r < u - v$, we assume $r < u - v$ throughout, which is equivalent to assuming $r < \tilde{r}$. From series expansion of the equilibrium conditions up to order ϵ^2, we find

$$\sigma_\alpha = \frac{-(r+u-v)}{r(u-v)\phi} A_1 A_2, \qquad \tau_\alpha = \frac{r+u-v}{r(u-v)\phi} B_1 B_2, \qquad \zeta_\alpha = \frac{-(r+u-v)}{r(u-v)\phi} A_1 B_2, \tag{A.12a}$$

$$\sigma_\beta = \frac{-(r-u+v)}{r(u-v)\phi} A_1 C_1, \qquad \tau_\beta = \frac{(r-u+v)}{r(u-v)\phi} B_1 C_2, \qquad \zeta_\beta = \frac{(r-u+v)}{r(u-v)\phi} A_1 B_1, \tag{A.12b}$$

where

$$A_1 = -(u-v)^2 e + 2v(v-e)r + er^2, \tag{A.13a}$$

$$A_2 = (u-v)^2 e + 2(v^2 - 2uv + ue)r + (2v-e)r^2, \tag{A.13b}$$

$$B_1 = -(u-v)^2 e + 2u(u-e)r + er^2, \tag{A.13c}$$

$$B_2 = -(u-v)^2 e - 2(u^2 - 2uv + ve)r + (2u-e)r^2, \tag{A.13d}$$

$$C_1 = -(u-v)^2 e - 2(v^2 - 2uv + ue)r + (2v-e)r^2, \tag{A.13e}$$

$$C_2 = (u-v)^2 e + 2(u^2 - 2uv + ve)r + (2u-e)r^2, \tag{A.13f}$$

and

$$\begin{aligned}\phi = {} & (u-v)^4(-8uv + 4(u+v)e + e^2) + 7(u-v)^2 e[-2uv + (u+v)e]r \\ & + [8uv(u^2+v^2) - 4(u+v)^3 e + (3u+v)(u+3v)e^2]r^2 \\ & + [6uve - 3(u+v)e^2]r^3.\end{aligned} \tag{A.14}$$

The perturbation (A.11) of M_3 is an admissible equilibrium if it satisfies (2.4). It follows that an equilibrium enters the state space at $m_{2,3}$ if

$$\sigma_\gamma > 0 \text{ and } \tau_\gamma > 0 \text{ and } \min\{-\sigma_\gamma, -\tau_\gamma\} \le \zeta_\gamma \le 0 \text{ for } \gamma \in \Gamma, \tag{A.15}$$

and it leaves the state space if

$$\sigma_\gamma < 0 \text{ and } \tau_\gamma < 0 \text{ and } 0 \le \zeta_\gamma \le \min\{-\sigma_\gamma, -\tau_\gamma\} \text{ for } \gamma \in \Gamma. \tag{A.16}$$

To evaluate these conditions, we recall (A.7). In addition, we assume $u > v$ because we require $0 < r < u - v$.

Straightforward calculations yield that (A.15) holds if and only if $\phi > 0$ and $B_1 < 0$. However, under our assumptions, $B_1 < 0$ holds if and only if $r < r_{2,3}$. Because we (had to) assume $r < \tilde{r}$, I_4 and I_5 enter the state space through M_2 and M_3, respectively, at $m_{2,3}$ if and only if (6.18) holds.

Analogously, we find that a pair of equilibria (I_6, I_7) leaves the state space through M_2 and M_3 at $m_{2,3}$ if and only if (6.19) holds. In both cases, M_2 and M_3 are asymptotically stable for every $m > m_{2,3}$. This follows from the stability condition $m > m_{\mathrm{st}}(\mathsf{M}_{2,3})$ in Section 6.1.1 together with (6.5), (6.8a), and the requirement $r < \min\{r_{2,3}, \tilde{r}\}$.

Because, the monomorphic equilibria are asymptotically stable if $m > m_{2,3}$ (Section 6.1.1), the pair of equilibria entering the state space at $m_{2,3}$ must be unstable. Numerical work shows that the pair of equilibria leaving the state space is asymptotically stable when they exist. This finishes the proof of Proposition 6.2.

To prove Remark 6.3 we collect some important properties of ϕ, considered as a polynomial function of degree three in r. They can be easily checked with *Mathematica*:

$$\text{The coefficient of } r^3 \text{ in } \phi(r) \text{ is negative if and only if } P < \frac{\sqrt{\kappa}}{1+\kappa}, \tag{A.17}$$

$$\phi(0) < 0 \text{ if and only if } P > \frac{\sqrt{3\kappa}}{\sqrt{2}(1+\kappa)}, \tag{A.18}$$

$$\frac{d\phi}{dr}(0) < 0 \text{ if and only if } P > \frac{\sqrt{\kappa}}{1+\kappa}, \tag{A.19}$$

$$\phi(\tilde{r}) < 0 \text{ if and only if } \frac{\sqrt{\kappa}}{1+\kappa} < P < \frac{1}{1+\kappa}, \tag{A.20}$$

$$\phi(r_{2,3}) < 0 \text{ if } P > \min\left\{\frac{1}{1+\kappa}, \frac{\sqrt{3\kappa}}{\sqrt{2}(1+\kappa)}\right\} \text{ and } \kappa < 1. \tag{A.21}$$

From these properties, we can draw the following conclusions:

$$\text{If } P < \frac{\sqrt{\kappa}}{1+\kappa}, \text{ then } \phi(r) > 0 \text{ if } r \leq \tilde{r}; \tag{A.22}$$

$$\text{if } P > \frac{\sqrt{3\kappa}}{\sqrt{2}(1+\kappa)}, \text{ then } \phi(r) < 0 \text{ if } r \leq r_{2,3} \text{ and } \kappa < 1. \tag{A.23}$$

Remark 6.3a is an immediate consequence of (6.18) and (A.22).

From (A.23) and (6.18) we infer that $P \leq \sqrt{3\kappa}/[\sqrt{2}(1+\kappa)]$ is a necessary condition for a pair of equilibria to enter the state space through M_2 and M_3. In addition, $\min\{r_{2,3}, \tilde{r}\} \leq 1/2$ holds with equality if $P = 1/4$ and $\kappa = 1/3$, where we note that these values are on the curve $P = \kappa/(1+\kappa)$, which separates the regions of weakly and moderately divergent selection.

Because, also $\phi > 0$ holds in a (small) neighborhood of $P = 1/4$ and $\kappa = 1/3$ if $r < 1/2$, we have proved Remark 6.3b.

Remark 6.3c follows from numerical determination of condition (A.23).

From (A.22) and (6.19), we infer that $P \geq \sqrt{\kappa}/(1+\kappa)$ is a necessary condition for a pair of equilibria to leave the state space through M_2 and M_3. Numerical evaluation of the condition (A.22) shows that, in addition, $r \lessapprox 0.3915$ is required. If $r \approx 0.3915$, then $\phi < 0$ holds only in a tiny neighborhood of $P = 0.463$ and $\kappa = 0.276$. If $r \gtrapprox 0.3916$, (A.22) is nowhere satisfied. Therefore, Remark 6.3d holds.

Remark 6.3e follows from (A.18), (A.19), and (A.21).

If (6.23) holds, we have $\phi(0) > 0$ by (A.18), $d\phi/dr(0) < 0$ by (A.19), and $\phi(\tilde{r}) < 0$ by (A.20). Because $r_{2,3} < \tilde{r}$ holds, (A.17) implies that (6.18) holds for every $r < r_{2,3}$ provided $\phi(r_{2,3}) > 0$. The second statement (for $\phi(r_{2,3}) < 0$) follows from the same argument. Therefore, Remark 6.3f holds.

A.4 Explicit results for stabilizing selection if $\kappa = 1$ or $P = 0$

If $\kappa = 1$, then selection is stabilizing if and only if $P < 1/2$. Selection is weakly divergent and the bifurcation pattern displayed in Figure 4b applies for every $r > 0$. If $P = 0$, the same bifurcation pattern applies. First, we present the coordinates of the equilibria I_2 and I_3 and the critical values $m_{\mathrm{un}}(\mathsf{I}_2) = m_{\mathrm{un}}(\mathsf{I}_3)$ and $m_{\mathrm{na}}(\mathsf{I}_2) = m_{\mathrm{na}}(\mathsf{I}_3)$ for the special case $\kappa = 1$.

If $\kappa = 1$, I_2 and I_3 are given by

$$\hat{p}_{2,\alpha} = \hat{q}_{3,\alpha} = \frac{1}{2} + \frac{2Pm}{s\,(1-4P^2)} + \sqrt{\frac{1}{4} - \frac{m}{r} + \frac{m}{rs}\frac{2m-r}{1-4P^2} + \left(\frac{m}{s}\frac{2P}{1-4P^2}\right)^2}, \tag{A.24a}$$

$$\hat{p}_{3,\alpha} = \hat{q}_{2,\alpha} = \frac{1}{2} + \frac{2Pm}{s\,(1-4P^2)} - \sqrt{\frac{1}{4} - \frac{m}{r} + \frac{m}{rs}\frac{2m-r}{1-4P^2} + \left(\frac{m}{s}\frac{2P}{1-4P^2}\right)^2}, \tag{A.24b}$$

$$\hat{D}_{2,\alpha} = \hat{D}_{3,\beta} = \frac{m}{r}\left(-1 + \frac{m}{s}\frac{2}{1-4P^2}\right), \tag{A.24c}$$

and we have

$$m_{\mathrm{un}}(\mathsf{I}_2) = m_{\mathrm{un}}(\mathsf{I}_3) = \frac{s}{4}\left(1 - 4P^2 + \frac{r}{s} - \sqrt{\left(1 - 4P^2 + \frac{r}{s}\right)^2 - \frac{4r}{3s}(1-4P^2)}\right), \tag{A.25}$$

and

$$m_{\mathrm{na}}(\mathsf{I}_2) = m_{\mathrm{na}}(\mathsf{I}_3) = \frac{s}{4}\,\frac{1-4P^2}{2rP^2 + s(1-4P^2)}\left(r + s(1-4P^2) - \sqrt{(1-4P^2)[r^2 + s^2(1-4P^2)]}\right). \tag{A.26}$$

If $P = 0$ and $\kappa \leq 1$, the coordinates of the equilibria I_2 and I_3 and the critical values $m_{\rm un}(\mathsf{I}_2)$ and $m_{\rm na}(\mathsf{I}_2)$ can be inferred from (A.24), (A.25) and (A.26) by the substitution $s \to 4\kappa s/(1+\kappa)^2$, respectively. The reason is that if $P = 0$, AB has the same fitness as ab, and Ab has the same fitness as aB; see (2.6).

From the above results, it is straightforward to derive the dependence of $m_{\rm un}(\mathsf{I}_2)$ and $m_{\rm na}(\mathsf{I}_2)$ on the parameters. If $\kappa = 1$, (A.25) yields that $m_{\rm un}(\mathsf{I}_2)$ decreases in P and satisfies

$$0 < m_{\rm un}(\mathsf{I}_2) \leq \frac{s}{4}\left(1 + \frac{r}{s} - \sqrt{\left(1+\frac{r}{s}\right)^2 - \frac{4r}{3s}}\right) \leq \frac{s}{6}, \tag{A.27}$$

where $m_{\rm un}(\mathsf{I}_2) \to 0$ as $P \to 1/2$, and $s/6$ in the limit $r \to \infty$ if $P = 0$.

If $P = 0$, $m_{\rm un}(\mathsf{I}_2)$ is increasing in r and κ. We obtain,

$$0 < m_{\rm un}(\mathsf{I}_2) < \frac{2s\kappa}{3(1+\kappa)^2} \leq \frac{s}{6}, \tag{A.28}$$

where $m_{\rm un}(\mathsf{I}_2) \to 0$ as $r \to 0$, $2s\kappa/[3(1+\kappa)^2]$ in the limit $r \to \infty$, and $s/6$ in the limit $r \to \infty$ if $\kappa = 1$.

If $\kappa = 1$, an equilibrium with $\hat{p}_\alpha = \hat{q}_\alpha$ is admissible for $0 \leq P \leq 1$. If $0 \leq P < 1/2$ this equilibrium is unstable and is denoted by I_1. If $1/2 < P \leq 1$ this equilibrium is stable and is denoted by I_0. Under the assumption of linkage equilibrium ($\hat{D}_\alpha = \hat{D}_\beta = 0$), the allele frequencies at I_1 and I_0 are given by

$$\hat{p}_\alpha = \hat{q}_\alpha = \frac{1}{2} + \frac{P}{3} - \frac{\sqrt{s\,(12m+3s+4P^2s)}}{3s}\,\mathrm{Sin}\left[\frac{1}{3}\,\mathrm{ArcSin}\left[\frac{2Ps\left(18m-9s+4P^2s\right)}{\sqrt{s\,(12m+3s+4P^2s)^3}}\right]\right]. \tag{A.29}$$

A.5 The functions F_1 and F_2

The functions F_1 and F_2 we used in the bifurcation diagrams are given by

$$F_1(p_\alpha, p_\beta) = 2p_\alpha(1-p_\beta) - p_\alpha^2(1-2p_\beta) + \frac{p_\beta}{4}, \tag{A.30a}$$

$$F_2(p_\alpha, p_\beta, q_\alpha, q_\beta) = q_\alpha + q_\beta - (p_\alpha + p_\beta). \tag{A.30b}$$

A.6 The maximum migration rates $m_{\max}$ and $m^0_{\max}$

If selection is stabilizing, then

$$m_{\max} = \begin{cases} m_{\mathrm{un}}(\mathsf{I}_2) & \text{in Case I and in Patterns II.sr.a}_2\text{, II.sr.c}_2\text{ (6.33a), (6.33b)} \\ & \text{II.wr.a}_1\text{, II.wr.c}_1\text{ (6.36a), (6.36c),} \\ m_{2,3} & \text{in Patterns II.wr.b}_1\text{, II.wr.c}_1\text{ (6.36b), (6.36d), (6.36e),} \\ m_{\mathrm{st}}(\mathsf{S}^{\mathcal{A}}) & \text{in Patterns II.sr.b}_2\text{, II.sr.c}_2\text{ (6.33c),} \\ m^{(2)}_{\mathrm{st}}(\mathsf{S}^{\mathcal{A}}) & \text{in Case II.ir if } r_{2,3} < r < r^*, \\ m_{\mathrm{i}} & \text{in Case II.ir if } r \le r_{2,3}, \end{cases} \tag{A.31}$$

where m_{i} is given by

$$m_{\mathrm{i}} = \begin{cases} m_{2,3} & \text{in Patterns II.ir.a}_2\text{e}_1\text{, II.ir.a}_2\text{db}_1\text{, II.ir.a}_2\text{dc}_1\text{ (analogue of 6.49b),} \\ m^{(2)}_{\mathrm{un}}(\mathsf{I}_2) & \text{in Patterns II.ir.a}_2\text{da}_1\text{, II.ir.a}_2\text{dc}_1\text{ (analogue of 6.49a),} \end{cases} \tag{A.32}$$

and

$$m^0_{\max} = \begin{cases} m_{\mathrm{na}}(\mathsf{S}^{\mathcal{A}}) > m_{\max} & \text{in Patterns II.sr.a}_2\text{ (6.31b), II.sr.b}_2\text{, II.sr.c}_2\text{ (6.33b),} \\ & \text{(6.33c), and in Case II.ir if } r_{2,3} < r < r^*, \\ m_{\max} & \text{otherwise.} \end{cases} \tag{A.33}$$

If selection is directional, then

$$m_{\max} = \begin{cases} \tilde{m}_{\mathrm{st}}(\mathsf{S}^{\mathcal{A}}) & \text{if } r^* < r, \\ m^{(2)}_{\mathrm{st}}(\mathsf{S}^{\mathcal{A}}) & \text{if } r_{2,3} < r < r^*, \\ m_{\mathrm{ii}} & \text{if } r \le r_{2,3}, \end{cases} \tag{A.34}$$

where m_{ii} is given by

$$m_{\mathrm{ii}} = \begin{cases} m_{2,3} & \text{in Patterns III.ir.e}_1\text{, III.wr.db}_1\text{, III.wr.dc}_1\text{ (6.49b),} \\ m^{(2)}_{\mathrm{un}}(\mathsf{I}_0) & \text{in Patterns III.wr.da}_1\text{, III.wr.dc}_1\text{ (6.49a),} \end{cases} \tag{A.35}$$

and

$$m^0_{\max} = \begin{cases} m_{\mathrm{na}}(\mathsf{S}^{\mathcal{A}}) > m_{\max} & \text{if } r_{2,3} < r, \\ m_{\max} & \text{otherwise.} \end{cases} \tag{A.36}$$

Numerical results show that m_{i} and m_{ii} are very close to $m_{2,3}$ when they are not equal to it.

With directional selection and strong recombination ($r^* < r$), there is no two-locus polymorphism above $\tilde{m}_{\mathrm{st}}(\mathsf{S}^{\mathcal{A}})$. If $r \le r_{2,3}$, this critical value is $m_{2,3}$ in most of the patterns and close to $m_{2,3}$ otherwise.

From (6.3), (6.5), (6.6), and (6.10), the dependence of $m_{\mathrm{na}}(\mathsf{S}^{\mathcal{A}})$, $m_{2,3}$, $m_{\mathrm{st}}(\mathsf{M}_{2,3})$, and $\tilde{m}_{\mathrm{st}}(\mathsf{S}^{\mathcal{A}})$ on the parameters is easily deduced. One obtains

$$m_{\mathrm{na}}(\mathsf{S}^{\mathcal{A}}),\ m_{2,3},\ \text{and } m_{\mathrm{st}}(\mathsf{M}_{2,3}) \text{ increase in } P \text{ and decrease in } \kappa \text{ and } r; \tag{A.37a}$$

$\tilde{m}_{\mathrm{st}}(\mathsf{S}^{\mathcal{A}})$ increases in P and in κ; (A.37b)

$m_{\mathrm{na}}(\mathsf{S}^{\mathcal{A}})$ and $\tilde{m}_{\mathrm{st}}(\mathsf{S}^{\mathcal{A}})$ are independent of r. (A.37c)

Unfortunately, the remaining critical migration rates can not be calculated analytically, except for $m_{\mathrm{un}}(\mathsf{I}_2)$ if $\kappa = 1$ or $P = 0$; see (A.25). Therefore, their dependence on the parameters has been worked out by extensive numerical calculations.

B Appendix

Supplementary Figures related to this article can be found online at http://dx.doi.org/10.1016/j.tpb.2014.03.002.

Chapter II

Clines in quantitative traits: The role of migration patterns and selection scenarios[2]

Abstract

The existence, uniqueness, and shape of clines in a quantitative trait under selection toward a spatially varying optimum is studied. The focus is on deterministic diploid two-locus n-deme models subject to various migration patterns and selection scenarios. Migration patterns may exhibit isolation by distance, as in the stepping-stone model, or random dispersal, as in the island model. The phenotypic optimum may change abruptly in a single environmental step, more gradually, or not at all. Symmetry assumptions are imposed on phenotypic optima and migration rates. We study clines in the mean, variance, and linkage disequilibrium (LD). Clines result from polymorphic equilibria. The possible equilibrium configurations are determined as functions of the migration rate. Whereas for weak migration, many polymorphic equilibria may be simultaneously stable, their number decreases with increasing migration rate. Also for intermediate migration rates polymorphic equilibria are in general not unique, however, for loci of equal effects the corresponding clines in the mean, variance, and LD are unique. For sufficiently strong migration, no polymorphism is maintained. Both migration pattern and selection scenario exert strong influence on the existence and shape of clines. The results for discrete demes are compared with those from models in which space varies continuously and dispersal is modeled by diffusion. Comparisons with previous studies, which investigated clines under neutrality or under linkage equilibrium, are performed. If there is no long-distance migration, the environment does not change abruptly, and linkage is not very tight, populations are almost everywhere close to linkage equilibrium.

Key words: Heterogeneous environment; Recombination; Dispersal; Linkage disequilibrium; Population subdivision; Multilocus polymorphism

[2]Geroldinger L. and Bürger R., 2014. Clines in quantitative traits: The role of migration patterns and selection scenarios, Theoretical Population Biology, in press

1 Introduction

Strength and patterns of migration in a spatially structured population are important determinants of the degree of local adaptation and the genetic variation that can be maintained in a heterogeneous environment. If there is an environmental gradient, clines in the gene frequencies or in the mean or other characteristics of a quantitative trait may be established. Such clines have been an important topic of both empirical and theoretical research since the pioneering work of Haldane (1948). The existence and shape of clines depends on the strength and patterns of migration, the properties of spatially varying selection, and the underlying genetics. In this work we assume that genetic variation is maintained by selection and migration, and ignore mutation and random genetic drift.

For populations subdivided into discrete demes, migration is frequently modeled by an island or a stepping-stone model. The former assumes that outbreeding individuals disperse uniformly to all other demes, whereas the latter assumes that the probability of migration decreases with distance, i.e., there is isolation by distance. For populations occupying a continuous habitat, migration is usually approximated by diffusion. Diffusion models, as well as certain generalizations, are derived by assuming that large migration steps are unlikely in short time intervals and selection is weak (Nagylaki 1975, 1989a). Naturally, such models exhibit isolation by distance.

The large majority of previous theoretical investigations assumes that selection acts on a single diallelic locus. For discrete demes and numerous types of migration patterns and selection schemes, Karlin (1982) performed a comprehensive investigation on the maintenance of protected polymorphisms (corresponding to the existence of clines). Although his results show that more mixing (e.g., by a higher migration rate or by migration to more distant demes) tends to restrict the conditions for a protected polymorphism, he also gave examples where less mixing inhibits a polymorphism. We shall compare the propensity of frequently employed migration patterns in maintaining clines at two recombining loci. Reviews of the extensive literature on one-locus migration-selection models may be found in Lenormand (2002), Nagylaki and Lou (2008), and Bürger (2014).

Also for the diffusion model, as well as more general forms of dispersal in continuous space, a wealth of results about existence, uniqueness, and properties of polymorphic equilibria and clines in gene frequencies at a single locus has accumulated. This literature is reviewed by Nagylaki and Lou (2008) and Lou et al. (2013). The maintenance of a cline is facilitated by reducing the ratio of diffusion rate to selection intensity, and it is impeded if long-distance

dispersal is incorporated into the diffusion model (Nagylaki 2012, Su and Nagylaki 2014).

Due to its complexity, multilocus theory is much less developed. This holds both for models with discrete or continuous space. Most investigations make rather restrictive assumptions, such as absence of epistasis or of linkage disequilibrium (LD), or assume two demes. We relax these assumptions and, additionally, provide a comparison of multi-deme models with diffusion models. The available theory for discrete demes is reviewed in Bürger (2014). Multilocus or quantitative-genetic models with diffusion in a spatially varying environment have been studied by Slatkin (1975, 1978), Felsenstein (1977), Barton (1983, 1999), Kruuk et al. (1999), and Hu (2005).

In the present work we consider a quantitative trait that is subject to selection toward a phenotypic optimum in each location. The trait is determined by two diallelic, recombining loci. The diploid sexual population may be subdivided into a finite number n of demes or occupy a continuous domain. Mating is random in each location. The phenotypic optimum varies in space. If it is close to the middle of available phenotypes, the trait is under stabilizing selection; if it is close to or at an extreme phenotype, the trait is under directional selection. We impose selection scenarios that differ in the way the optimum changes across space. This change may be gradual, occur in several steps of moderate size, or abruptly in one big step such that there are only two different environments. Such selection scenarios have been discussed in the literature on hybrid zones (e.g., Barton 1999, Kruuk et al. 1999, Kawakami and Butlin 2012). Spatially uniform stabilizing selection is also investigated. We study the following migration patterns: (i) the island model in which migrating individuals reach every deme (island) with the same probability, (ii) stepping-stone models in which individuals migrate either only to next neighbors or to demes in the vicinity such that the probability decreases with distance, and (iii) a diffusion model for a population that inhabits a continuous bounded one-dimensional habitat.

Our main goal is to investigate how the conditions for the existence of polymorphic stationary solutions, or clines, and their properties (e.g., spatial shape) depend on the number of demes, the rate and pattern of migration, the selection scenario, and recombination. Most analysis is dedicated to models with a finite number of demes. However, an essential component will be the comparison of 12-deme models with diffusion models. To make useful comparisons between different patterns or scenarios, the equilibrium configurations and bifurcation patterns are described as functions of the migration rate. The important limiting cases of weak and of strong migration are treated in Section 3. For two demes and loci of equal effect an almost complete mathematical analysis is obtained (Section 4). It complements pre-

vious analyses assuming absence of epistasis (Akerman and Bürger 2014a,b) or selection on haploids (Geroldinger and Bürger 2014). The analysis of the two-deme case is not only an important guide to the, mainly numerical, analysis of models with a higher number of demes (Section 5), but also helps to establish analytical results for the island model.

We describe the spatial dependence of the distribution of the trait by its mean phenotype, its genetic variance, and the LD between loci. In Section 6, the properties and shapes of the corresponding clines are compared for the different migration patterns and selection scenarios. Section 7 is dedicated to the comparison of our results with those from previous multilocus analyses of neutral clines (Feldman and Christiansen 1975; Christiansen 1986) and analyses of multilocus or quantitative-genetic diffusion models, in particular those of Slatkin (1975, 1978), Felsenstein (1977), and Barton (1983, 1999). In Section 8, our main results are summarized and discussed.

2 Model

We study a deterministic migration-selection model in which a sexually reproducing, diploid population is subdivided into n demes connected by genotype-independent migration. It is assumed that the genotypic fitnesses are uniquely determined by the genotypic value G of a quantitative trait. We posit that in each deme $k \in \{1, \ldots, n\}$, fitness is given by the quadratic function

$$w_k(G) = 1 - s(G - P_k)^2, \tag{2.1}$$

where the phenotypic optimum P_k depends on k, and $s > 0$ measures the strength of selection. It is assumed that s is sufficiently small such that $w_k(G) > 0$ on the range of genotypic values (also called phenotypes). If the optimum P_k is close to the middle of the phenotypic range, the trait is under stabilizing selection in deme k; if it is close to the boundary, it is under directional selection.

The trait is determined additively by two diallelic loci, $\mathcal{A}$ and $\mathcal{B}$, which recombine at rate $r > 0$. We assign the genotypic contributions $-c_1/2$, $c_1/2$, $-c_2/2$, and $c_2/2$ to the four alleles A, a, B, and b, respectively. The genotypic values of all 16 genotypes are obtained by adding all allelic contributions. Without loss of generality, we use a scale such that $c_1 + c_2 = 1$. Then the phenotypic range is $[-1, 1]$, the two double homozygotes AB/AB and ab/ab have the (extreme) phenotypes -1 and 1, respectively, and all four double heterozygotes have phenotype 0. We restrict the phenotypic optima to this range, i.e., we assume $-1 \leq P_k \leq 1$. Finally, we

introduce the ratio of locus effects

$$\kappa = c_2/c_1. \tag{2.2}$$

Unless mentioned otherwise we assume $\kappa = 1$, i.e., $c_1 = c_2$.

The frequencies of the four gametes, AB, Ab, aB, ab, in deme k are designated $x_{1,k}$, $x_{2,k}$, $x_{3,k}$, $x_{4,k}$, respectively. The fitness of zygotes consisting of gametes i and j in deme k is $w_{ij,k} = w_k(G_{ij})$, where G_{ij} is the genotypic value. The mean fitness in deme k is given by $\overline{w}_k = \sum_{i=1}^4 w_{i,k}x_{i,k}$, where $w_{i,k} = \sum_{j=1}^4 w_{ij,k}x_{j,k}$ denotes the marginal fitness of haplotype i in deme k.

We assume equivalent sexes, random mating within demes, and that population regulation occurs within each deme (soft selection). We denote linkage disequilibrium in deme k by $D_k = x_{1,k}x_{4,k} - x_{2,k}x_{3,k}$. Then the change of gamete frequencies in deme k due to selection and recombination is

$$x_{i,k}^{(s)} = x_{i,k}\frac{w_{i,k}}{\overline{w}_k} - \eta_i r D_k^{(s)}, \tag{2.3a}$$

where $\eta_1 = \eta_4 = 1$, $\eta_2 = \eta_3 = -1$, and

$$D_k^{(s)} = \frac{w_{14,k}}{\overline{w}_k} D_k \tag{2.3b}$$

denotes LD after selection.

Let $\mathcal{M} = (m_{kl})$ denote the backward-migration matrix, i.e., m_{kl} denotes the probability that an individual in deme k immigrated from deme l. After migration random mating and reproduction occur within demes. Therefore, the frequency $x'_{i,k}$ of the ith gamete in deme k in the next generation is:

$$x'_{i,k} = \sum_{l=1}^{n} m_{kl} x_{i,l}^{(s)}. \tag{2.3c}$$

Equations (2.3) define a discrete dynamical system on the n-fold Euclidean product S_4^n of the simplex

$$S_4 = \left\{ (\xi_1, \xi_2, \xi_3, \xi_4) : \ \xi_i \geq 0 \text{ and } \sum_{i=1}^{4} \xi_i = 1 \right\}. \tag{2.4}$$

For convenience we introduce the allele frequencies $p_k = x_{1,k} + x_{2,k}$ and $q_k = x_{1,k} + x_{3,k}$ of alleles A and B in deme k. Then the gamete frequencies $x_{i,k}$ are given by the relations

$$x_{1,k} = p_k q_k + D_k, \qquad x_{2,k} = p_k(1 - q_k) - D_k, \tag{2.5a}$$

$$x_{3,k} = (1 - p_k)q_k - D_k, \quad x_{4,k} = (1 - p_k)(1 - q_k) + D_k. \tag{2.5b}$$

We shall use the notation $x_k = (x_{1,k}, x_{2,k}, x_{3,k}, x_{4,k})$. See Table 1 for a glossary of symbols.

Table 1. Glossary of symbols. We define the symbols in the main text that occur in more than one paragraph. Roman and Greek letters are listed separately. Uppercase letters precede lower case ones and listing is in order of appearance in the text. The references are to the position of first appearance in the text. Reference (2.1)−, refers to the text above Equation (2.1), whereas (2.1)+ refers to the text below Equation (2.1).

Symbol	Reference	Definition
$\mathcal{A}$	(2.1)+	First locus
A	(2.1)+	First allele at locus $\mathcal{A}$
a	(2.1)+	Second allele at locus $\mathcal{A}$
$\mathcal{B}$	(2.1)+	Second locus
B	(2.1)+	First allele at locus $\mathcal{B}$
b	(2.1)+	Second allele at locus $\mathcal{B}$
c_1	(2.1)+	Substitution effect at $\mathcal{A}$
c_2	(2.1)+	Substitution effect at $\mathcal{B}$
D_k	(2.3a)−	Linkage disequilibrium in deme k
$\mathsf{E}_k^{\mathcal{A},*}$, $\mathsf{E}_k^{\mathcal{B},*}$	(3.1)	SLPs in deme k for $m = 0$, where $* \in \{0, 1\}$
F_k	(3.1)+	Internal equilibrium in deme k for $m = 0$
G	(2.1)−	Genotypic value of the trait
$\bar{G}_k$	(5.6)+	Genotypic mean in deme k
$I_m(G)$	(3.3)+	Weak-migration perturbation of the equilibrium G
I^j	(4.2)−	Internal equilibria ($0 \le j \le 5$)
$\mathcal{I}$	(5.1)−	Migration matrix of the island model
$\mathcal{M}$	(2.3c)−	Backward-migration matrix
M_k^i	(3.1)−	Equilibrium in deme k corresponding to fixation of gamete i
m_{kl}	(2.3c)−	Probability that an individual in deme k immigrated from deme l
m	(3.2)	Migration rate
$\bar{m}$	(5.2)	Rescaled migration rate
$m_{\max}$	(4.9)−	Maximum migration rate below which a stable polymorphic equilibrium can occur
$m_{\mathrm{st}}(\mathsf{G})$	(4.1)−	Migration rate at which the equilibrium G gets stable for $n = 2$
$m_{\mathrm{un}}(\mathsf{G})$	(4.1)−	Migration rate at which the equilibrium G gets unstable for $n = 2$
$m_{\mathrm{ad}}(\mathsf{G})$	(4.1)−	Migration rate at which the equilibrium G gets admissible for $n = 2$
$m_{\mathrm{na}}(\mathsf{G})$	(4.1)−	Migration rate at which the equilibrium G loses admissibility for $n = 2$
$m_*^{\mathrm{X},\mathcal{M}}(\mathsf{G})$	(5.8)+	Migration rate at which the state of G changes, where $* \in \{\mathrm{st}, \mathrm{un}, \mathrm{ad}, \mathrm{na}\}$. X indicates the selection scenario and $\mathcal{M}$ the migration matrix
N_i	(3.1)	Partitions of the set of demes $\{1, \ldots, n\}$
n	(2.1)−	Number of demes
P_k	(2.1)	Phenotypic optimum in deme k
P	(4.1)−	Phenotypic optimum for two environments ($P = -P_1 = P_2$)
P_c	(4.5)−	Critical value of P for $n = 2$
p_k	(2.4)+	Frequency of allele A in deme k
q_k	(2.4)+	Frequency of allele B in deme k
r	(2.1)+	Recombination rate
S_4	(2.4)	Simplex

$\mathcal{S}$	(5.3)−	Migration matrix of the stepping-stone model
$\mathcal{S}_2$	(5.3)+	Migration matrix of the generalized stepping-stone model
s	(2.1)	Selection intensity
$\tilde{s}$	(5.16)−	Rescaled selection intensity
t	(7.4a)	Time
V_k	(5.6)+	Phenotypic variance in deme k
V_T	(6.2)+	Phenotypic variance in the entire population
$w_k(G)$	(2.1)	Fitness of genotypic value G in deme k
$w_{ij,k}$	(2.2)+	Fitness of genotype ij in deme k
$w_{i,k}$	(2.2)+	Fitness of gamete i in deme k
$\bar{w}_k$	(2.2)+	Mean fitness in deme k
$x_{i,k}$	(2.2)+	Frequency of gamete i in deme k
x_k	(2.5)+	Vector of gamete frequencies in deme k
y	(7.4a)	Spatial variable in a continuous domain
κ	(2.2)	Ratio of locus effects
η_i	(2.3a)	Constants
σ^2	(7.4a)	Diffusion rate in a continuous domain
$^{(s)}$	(2.3a)	Indicates haplotype (or gene) frequencies after selection and recombination
$'$	(2.3c)	Indicates haplotype (or gene) frequencies in the next generation
$\hat{}$	(3.1)+	Indicates an equilibrium value

3 Limiting Cases

We determine equilibria and their stability properties analytically for the limiting cases of no migration, weak migration, and strong migration.

3.1 No migration

For panmictic populations the model has been analyzed previously (reviewed in Bürger 2000, Chap. VI.2). We recapitulate the relevant results. Because in the absence of migration the dynamics of the demes are decoupled, we describe the equilibrium configuration for a single deme k.

Three types of equilibria may exist: (i) monomorphic equilibria, (ii) single-locus polymorphisms (SLPs), and (iii) fully polymorphic equilibria. The monomorphic equilibrium corresponding to fixation of gamete i in deme k is denoted by M_k^i. Four SLPs, corresponding to the fixation of one allele at one locus, exist. Their coordinates are

$$\mathsf{E}_k^{\mathcal{A},0}: \quad \hat{p}_k = \frac{3}{2} - 2P_k, \quad \hat{q}_k = 0, \hat{D}_k = 0, \tag{3.1a}$$

$$\mathsf{E}_k^{\mathcal{A},1}: \quad \hat{p}_k = -\frac{1}{2} - 2P_k, \hat{q}_k = 1, \hat{D}_k = 0, \tag{3.1b}$$

$$\mathsf{E}_k^{\mathcal{B},0}: \quad \hat{q}_k = \frac{3}{2} - 2P_k, \quad \hat{p}_k = 0, \hat{D}_k = 0, \tag{3.1c}$$

$$\mathsf{E}_k^{\mathcal{B},1}: \quad \hat{q}_k = -\frac{1}{2} - 2P_k,\, \hat{p}_k = 1,\, \hat{D}_k = 0, \tag{3.1d}$$

where the superscript $\mathcal{A}$ or $\mathcal{B}$ of E indicates the polymorphic locus, and the superscript 0 or 1 which allele is fixed at the other locus. The hat, $\hat{}$, signifies an equilibrium.

The equilibria $\mathsf{E}_k^{\mathcal{A},0}$ and $\mathsf{E}_k^{\mathcal{B},0}$ are admissible if and only if $1/4 < P_k < 3/4$; $\mathsf{E}_k^{\mathcal{A},1}$ and $\mathsf{E}_k^{\mathcal{B},1}$ are admissible if and only if $-3/4 < P_k < -1/4$. Stability conditions of all boundary equilibria are available for arbitrary locus effects κ (Bürger 2000). Because $\kappa = 1$, the SLPs are asymptotically stable when they are admissible. If $P_k \geq 3/4$ or $P_k \leq -3/4$, the trait is under directional selection and M_k^4 or M_k^1, respectively, is globally asymptotically stable (Appendix A.1). If $-1/4 \leq P_k \leq 1/4$, then M_k^2 and M_k^3 are simultaneously asymptotically stable. If $-3/4 < P_k < 3/4$ (and $\kappa = 1$), there exists a unique internal equilibrium F_k which is always unstable (Appendix A.1).

These considerations show that depending on the phenotypic optimum P_k, one of the following five qualitatively different equilibrium configurations occurs.

(i) If $-1 \leq P_k \leq -3/4$, M_k^1 is globally asymptotically stable.

(ii) If $-3/4 < P_k < -1/4$, $\mathsf{E}_k^{\mathcal{A},1}$ and $\mathsf{E}_k^{\mathcal{B},1}$ are simultaneously asymptotically stable and F_k is unstable.

(iii) If $-1/4 < P_k < 1/4$, M_k^2 and M_k^3 are simultaneously asymptotically stable and F_k is unstable.

(iv) If $1/4 < P_k < 3/4$, $\mathsf{E}_k^{\mathcal{A},0}$ and $\mathsf{E}_k^{\mathcal{B},0}$ are simultaneously asymptotically stable and F_k is unstable.

(v) If $3/4 \leq P_k \leq 1$, M_k^4 is globally asymptotically stable.

3.2 Weak Migration

We apply the perturbation theory developed by Karlin and McGregor (1972a,b) to infer existence and local stability of equilibria for weak migration from the model with no migration. The migration matrix $\mathcal{M}$ is supposed to satisfy

$$m_{kl} = \begin{cases} 1 - m & \text{if } k = l, \\ \gamma_{kl}\, m & \text{if } k \neq l, \end{cases} \tag{3.2}$$

where the $\gamma_{kl} \in [0, 1]$ are constants that satisfy $\sum_{l:l\neq k} \gamma_{kl} = 1$.

If $m = 0$, the dynamics (2.3) on S_4^n is given by the Euclidean product of the single-deme dynamics on S_4. Every equilibrium is of the form

$$\prod_{1\leq k\leq n} \mathsf{G}_k, \tag{3.3}$$

where G_k is an equilibrium in deme k. If all components of the equilibrium (3.3) are identical, i.e., $\mathsf{G}_k = \mathsf{G}_1$ for $1 \le k \le n$, we denote the equilibrium (3.3) by G.

If in the absence of migration every equilibrium is hyperbolic, perturbation theory shows that the following holds for sufficiently small m (Karlin and McGregor 1972b): (i) in the neighborhood of each asymptotically stable equilibrium for $m = 0$, there exists exactly one equilibrium for $m > 0$ and it is asymptotically stable; (ii) in the neighborhood of each unstable internal equilibrium for $m = 0$, there exists exactly one equilibrium for $m > 0$ and it is unstable; (iii) in the neighborhood of each unstable boundary equilibrium for $m = 0$, there exists at most one equilibrium for $m > 0$, and if it exists, it is unstable. If we denote the perturbation of $\prod_{k=1}^n \mathsf{G}_k$ by $I_m(\prod_{k=1}^n \mathsf{G}_k)$, then $I_m(\prod_{k=1}^n \mathsf{G}_k) \to \prod_{k=1}^n \mathsf{G}_k$ as $m \to 0$. The proof of Theorem 4.1 in Karlin and McGregor (1972b) shows that an equilibrium may leave the state space after perturbation only if it is transversally unstable.

The following proposition combines the results for panmictic populations summarized in Section 3.1 with the perturbation theory outlined above.

Proposition 3.1. *Assume* (2.3), *let m be sufficiently small, and define the sets*

$$N_1 = \{k \mid P_k \in [-1, -3/4)\},\ N_2 = \{k \mid P_k \in (-3/4, -1/4)\},\ N_3 = \{k \mid P_k \in (-1/4, 1/4)\},$$
$$N_4 = \{k \mid P_k \in (1/4, 3/4)\},\ N_5 = \{k \mid P_k \in (3/4, 1]\}. \tag{3.4}$$

The following asymptotically stable equilibria exist:

$$I_m\left(\prod_{k\in N_1} \mathsf{M}_k^1 \times \prod_{k\in N_2} \mathsf{G}_k \times \prod_{k\in N_3} \mathsf{H}_k \times \prod_{k\in N_4} \mathsf{J}_k \times \prod_{k\in N_5} \mathsf{M}_k^4\right), \tag{3.5a}$$

where

$$\mathsf{G}_k \in \{\mathsf{E}_k^{\mathcal{A},1}, \mathsf{E}_k^{\mathcal{B},1}\},\ \mathsf{H}_k \in \{\mathsf{M}_k^2, \mathsf{M}_k^3\},\ \mathsf{J}_k \in \{\mathsf{E}_k^{\mathcal{A},0}, \mathsf{E}_k^{\mathcal{B},0}\}. \tag{3.5b}$$

The following are unstable equilibria:

$$I_m\left(\prod_{k\in N_1} \mathsf{M}_k^1 \times \prod_{k\in N_2} \mathsf{G}_k \times \prod_{k\in N_3} \mathsf{H}_k \times \prod_{k\in N_4} \mathsf{J}_k \times \prod_{k\in N_5} \mathsf{M}_k^4\right), \tag{3.6a}$$

where

$$\mathsf{G}_k \in \{\mathsf{E}_k^{\mathcal{A},1}, \mathsf{E}_k^{\mathcal{B},1}, \mathsf{F}_k\},\ \mathsf{H}_k \in \{\mathsf{M}_k^2, \mathsf{M}_k^3, \mathsf{F}_k\},\ \mathsf{J}_k \in \{\mathsf{E}_k^{\mathcal{A},0}, \mathsf{E}_k^{\mathcal{B},0}, \mathsf{F}_k\}, \tag{3.6b}$$

and

$$\mathsf{G}_k = \mathsf{F}_k, \textit{ or } \mathsf{H}_k = \mathsf{F}_k, \textit{ or } \mathsf{J}_k = \mathsf{F}_k \textit{ for at least one } k. \tag{3.6c}$$

The proof is given in Appendix A.2.

We note that not all unstable equilibria are given by (3.6): e.g., if $N_1 \neq \emptyset$, M_2 is an unstable equilibrium for weak migration. In general, it has to be checked separately whether the perturbation of an unstable boundary equilibrium leaves the state space. Notably, Proposition 3.1 holds independently of the migration matrix $\mathcal{M}$.

Remark 3.2. The values $|P_k| = 1/4$ and $|P_k| = 3/4$ are excluded in the above Proposition, because then not every equilibrium is hyperbolic and separate treatment is needed. Numerical work suggests that Proposition 3.1 remains valid if $P_k = -3/4$ is added to N_1, $P_k = -1/4$ and $P_k = 1/4$ are added to N_3, and $P_k = 3/4$ is added to N_5.

Remark 3.3. We conjecture that almost all trajectories converge to one of the equilibria in (3.5) if m is small. If for every k either $P_k = 0$ or $|P_k| > 3/4$ holds, this conjecture follows from global perturbation theory (Bürger 2009a, Section 5; or Bürger 2014, Theorem 7.7 and Remark 7.8). The reason is that if $m = 0$ and $|P_k| > 3/4$, there is global convergence to an asymptotically stable equilibrium (Section 3.1); if $m = 0$ and $P_k = 0$, the Lyapunov function $x_{2,k}/x_{3,k}$ establishes (exponential) convergence to M_3 for every trajectory with $x_{3,k} > x_{2,k}$, and to M_2 for every trajectory with $x_{2,k} > x_{3,k}$; trajectories satisfying $x_{2,k} = x_{3,k}$ converge to F_k. In both cases the convergence patterns persist for small m.

3.3 Strong migration

With the special migration schemes of Section 5 in mind, we assume an even number n of demes and posit that selection and migration satisfy the following symmetry conditions for every $k, l \in \{0, \ldots, n/2 - 1\}$:

$$P_{\frac{n}{2}-k} = -P_{\frac{n}{2}+1+k}, \tag{3.7a}$$

$$m_{\frac{n}{2}-k,\frac{n}{2}-l} = m_{\frac{n}{2}+1+k,\frac{n}{2}+1+l}. \tag{3.7b}$$

These conditions describe a mirror symmetry between demes $(1, \ldots, n/2)$ and $(n/2+1, \ldots, n)$, such that in deme $n/2 - k$ selection acts on the haplotypes AB, Ab, aB, ab in the same way as selection in deme $n/2 + 1 + k$ on ab, aB, Ab, AB, respectively. In particular, selection on the trait occurs in opposite direction in these two sets of demes.

Proposition 3.4. *Assume* (3.7).

1. If migration is sufficiently strong, i.e., m/s and m/r are sufficiently large, then M^2 and M^3 are asymptotically stable and no other equilibrium is stable. The equilibrium $\mathsf{F} = \prod_k \mathsf{F}_k$ exists, is the unique internal equilibrium, and is unstable.

2. The critical migration rate at which M^2 *and* M^3 *become asymptotically stable, denoted* $m_{\mathrm{st}}^{\mathrm{X},\mathcal{M}}(\mathsf{M}^{2,3})$ *(Section 5.2), is independent of* r. M^2 *and* M^3 *are stable if and only if they are stable with respect to their marginal one-locus systems.*

The proof is given in Appendix A.3. There it is also shown that if $\kappa < 1$, the migration rates at which M^2 and M^3 become stable depend on r.

The analysis below will show that the equilibrium configuration of the strong-migration limit, as defined by Proposition 3.4.1, may apply only for much larger migration rates than $m_{\mathrm{st}}^{\mathrm{X},\mathcal{M}}(\mathsf{M}^{2,3})$.

4 Two demes

In this section we assume $n = 2$ and (3.7), i.e., $-P_1 = P_2 = P$ and $m_{12} = m_{21} = m$. Then the strength of divergent selection between the demes increases with increasing P. Our goal here is to describe the equilibrium configurations and bifurcation patterns as the migration rate increases.

We find the equilibria of (2.3) by using the algorithm *NSolve* of *Mathematica* (Wolfram Research, Inc. 2010) and determine their local stability properties by calculating the eigenvalues numerically. Global stability results are inferred from forward iterations of (2.3). They were performed with *Mathematica* and the following adjustments: In each deme, 1000 initial values from the interior were chosen as $(\log(y_1), \log(y_2), \log(y_3), \log(y_4))/\sum_{i=1}^4 \log(y_i)$, where the y_i are independent and uniformly distributed in $(0, 1)$. Iterations were stopped if the Euclidean distance between successive values declined below 10^{-9}. Two equilibrium values were considered as equal if their Euclidean distance (in S_4^n) was less than 0.001.

In combination with our analytical results for weak and for strong migration, we obtain a presumably complete classification of bifurcations in which the stable equilibria are involved.

For any equilibrium G, we designate by $m_{\mathrm{st}}(\mathsf{G})$ or $m_{\mathrm{un}}(\mathsf{G})$ the critical migration rate at which G becomes stable or unstable, respectively, as m increases above this value. Analogously, we write $m_{\mathrm{ad}}(\mathsf{G})$ or $m_{\mathrm{na}}(\mathsf{G})$ for the critical migration rate at which G gains or loses admissibility, respectively. These critical migration rates turn out to be unique.

Proposition 3.4 shows that in the limit of strong migration, M^2 and M^3 are simultaneously stable. A linear stability analysis of M^2 and M^3 reveals that these equilibria are stable if and only if $m > m_{\mathrm{st}}(\mathsf{M}^{2,3})$, where

$$m_{\mathrm{st}}(\mathsf{M}^{2,3}) := m_{\mathrm{st}}(\mathsf{M}^2) = m_{\mathrm{st}}(\mathsf{M}^3) = s\frac{1-16P^2}{2s\,(1-12P^2)-8} = 2s\left(P^2 - \frac{1}{16}\right) + O(s^2). \qquad (4.1)$$

We note that $m_{\rm st}(\mathsf{M}^{2,3})$ is independent of r (cf. Section 3.3) and $m_{\rm st}(\mathsf{M}^{2,3}) > 0$ if and only if $|P| > 1/4$.

From one-locus theory (Karlin and Campbell 1980, Bürger 2014) and our symmetry assumptions ($-P_1 = P_2 = P$ and $\kappa = 1$), we infer that four SLPs exist if and only if all monomorphic equilibria are unstable. Otherwise, no SLP exists. The allele frequency at an SLP is a zero of a cubic polynomial which does not have simple form. Numerical investigations suggest that the SLPs are always unstable. (They are stable within their marginal one-locus system but unstable with respect to the interior of the state space). They play no role in the further analysis.

At several instances we define internal equilibria I^j by weak-migration perturbations, e.g. $\mathsf{I}^j = I_m(\mathsf{G}_1^j, \mathsf{H}_2^j)$. Then we use the notation I^j for the whole range of parameters where this equilibrium exists. The following equilibrium plays a central role in the subsequent analysis

$$\mathsf{I}^1 = \begin{cases} I_m(\mathsf{F}_1, \mathsf{F}_2) & \text{if } P < 3/4, \\ I_m(\mathsf{M}_1^1, \mathsf{M}_2^4) & \text{if } P \geq 3/4. \end{cases} \tag{4.2}$$

Its coordinates are continuous in P since $\mathsf{F}_1 \to \mathsf{M}_1^1$ and $\mathsf{F}_2 \to \mathsf{M}_2^4$ as $P \to 3/4$ (Appendix A.1).

Because Proposition 3.1 shows that the equilibrium configuration for weak migration depends on P, we distinguish three cases according to increasing strength of divergent selection.

Case I

Let $0 \leq P < 1/4$. Then there is stabilizing selection in each deme, and divergent selection between demes is weak. According to (4.1), M^2 and M^3 are asymptotically stable for every $m \geq 0$. For sufficiently weak migration, $\mathsf{I}^2 = I_m(\mathsf{M}_1^2, \mathsf{M}_2^3)$ and $\mathsf{I}^3 = I_m(\mathsf{M}_1^3, \mathsf{M}_2^2)$ are the only internal stable equilibria (Proposition 3.1). The equilibria I^1, $I_m(\mathsf{M}_1^2, \mathsf{F}_2)$, $I_m(\mathsf{M}_1^3, \mathsf{F}_2)$, $I_m(\mathsf{F}_1, \mathsf{M}_2^2)$, and $I_m(\mathsf{F}_1, \mathsf{M}_2^3)$ are admissible and unstable if $m > 0$. As m increases, the following three bifurcations[3] occur which reduce the number of equilibria and, eventually, yield the equilibrium configuration of the strong-migration limit.

The equilibrium I^2 collides with the two unstable equilibria $I_m(\mathsf{M}_1^2, \mathsf{F}_2)$ and $I_m(\mathsf{F}_1, \mathsf{M}_2^3)$ in a subcritical pitchfork bifurcation in which I^2 loses its stability but persists, and the unstable equilibria are annihilated. Analogously, I^3 collides with the two unstable equilibria $I_m(\mathsf{M}_1^3, \mathsf{F}_2)$ and $I_m(\mathsf{F}_1, \mathsf{M}_2^2)$ in a subcritical pitchfork bifurcation. The value at which I^2 and I^3 loose their stability is denoted by $m_{\rm un}(\mathsf{I}^{2,3}) = m_{\rm un}(\mathsf{I}^2) = m_{\rm un}(\mathsf{I}^3)$. At the value $m_{\rm na}(\mathsf{I}^{2,3}) = m_{\rm na}(\mathsf{I}^2) = m_{\rm na}(\mathsf{I}^3)$, a third subcritical pitchfork bifurcation occurs in which the three unstable internal

[3]Bifurcations are classified according to their properties on the center manifold (Kuznetsov 1998).

equilibria I^1, I^2, and I^3 collide, I^2 and I^3 are annihilated, and I^1 remains admissible and unstable. In this case the sequence of bifurcation points is

$$0 < m_{\mathrm{un}}(\mathsf{I}^{2,3}) < m_{\mathrm{na}}(\mathsf{I}^{2,3}) \tag{4.3}$$

(Figure 2a). If $m > m_{\mathrm{na}}(\mathsf{I}^{2,3})$, the equilibrium configuration of the strong-migration limit applies.

For each of the equilibria I^1, I^2, and I^3, the equilibrium allele frequencies and LD in demes 1 and 2 satisfy the symmetry relation

$$\hat{p}_2 = 1 - \hat{p}_1, \;\; \hat{q}_2 = 1 - \hat{q}_1, \;\; \hat{D}_2 = \hat{D}_1. \tag{4.4}$$

Equations (A.10) and (A.11) in Appendix A.4 provide approximations for I^1, I^2, and I^3 by assuming weak evolutionary forces and linkage equilibrium.

Case II

Let $1/4 < P < 3/4$. Then there is (asymmetric) stabilizing selection in each deme, and divergent selection between demes is moderately strong. We recall from Section 3.1 that if $m = 0$, the equilibria $\mathsf{E}_1^{\mathcal{A},1}$ and $\mathsf{E}_1^{\mathcal{B},1}$ ($\mathsf{E}_2^{\mathcal{A},0}$ and $\mathsf{E}_2^{\mathcal{B},0}$) are simultaneously asymptotically stable in deme 1 (deme 2). Additionally, there is the unstable internal equilibrium F_k in each deme. If migration is weak, there are nine internal equilibria. Among them, $\mathsf{I}^2 = I_m(\mathsf{E}_1^{\mathcal{B},1}, \mathsf{E}_2^{\mathcal{B},0})$, $\mathsf{I}^3 = I_m(\mathsf{E}_1^{\mathcal{A},1}, \mathsf{E}_2^{\mathcal{A},0})$, $\mathsf{I}^4 = I_m(\mathsf{E}_1^{\mathcal{B},1}, \mathsf{E}_2^{\mathcal{A},0})$, and $\mathsf{I}^5 = I_m(\mathsf{E}_1^{\mathcal{A},1}, \mathsf{E}_2^{\mathcal{B},0})$ are asymptotically stable. The definitions of I^2 and I^3 extend those in Case I, because $\mathsf{E}_k^{\mathcal{B},1}$ and $\mathsf{E}_k^{\mathcal{A},0}$ converge to M_k^2, and $\mathsf{E}_k^{\mathcal{B},0}$ and $\mathsf{E}_k^{\mathcal{A},1}$ converge to M_k^3 as $P \to 1/4$ (Section 3.1).

As the migration rate increases, the stable equilibrium I^2 collides with the two unstable equilibria $I_m(\mathsf{E}_1^{\mathcal{B},1}, \mathsf{F}_2)$ and $I_m(\mathsf{F}_1, \mathsf{E}_2^{\mathcal{B},0})$ in a subcritical pitchfork bifurcation, i.e., I^2 becomes unstable and $I_m(\mathsf{E}_1^{\mathcal{B},1}, \mathsf{F}_2)$ and $I_m(\mathsf{F}_1, \mathsf{E}_2^{\mathcal{B},0})$ are annihilated. Analogously, I^3 collides with the two unstable equilibria $I_m(\mathsf{E}_1^{\mathcal{A},1}, \mathsf{F}_2)$ and $I_m(\mathsf{F}_1, \mathsf{E}_2^{\mathcal{A},0})$ in a subcritical pitchfork bifurcation. Both bifurcations occur at the same migration rate $m_{\mathrm{un}}(\mathsf{I}^{2,3})$. As the migration rate increases further, a third subcritical pitchfork bifurcation occurs at which the three unstable equilibria I^1, I^2 and I^3 collide, I^2 and I^3 are annihilated and I^1 remains admissible and unstable (Figures 2d,f).

For larger m we distinguish two subcases, depending on whether the two stable equilibria I^4 and I^5 do or do not collide with I^1. The equilibria I^4 and I^5 collide if and only if $P_c \leq P < 3/4$, where P_c is an increasing function of s which can not be calculated explicitly. In the

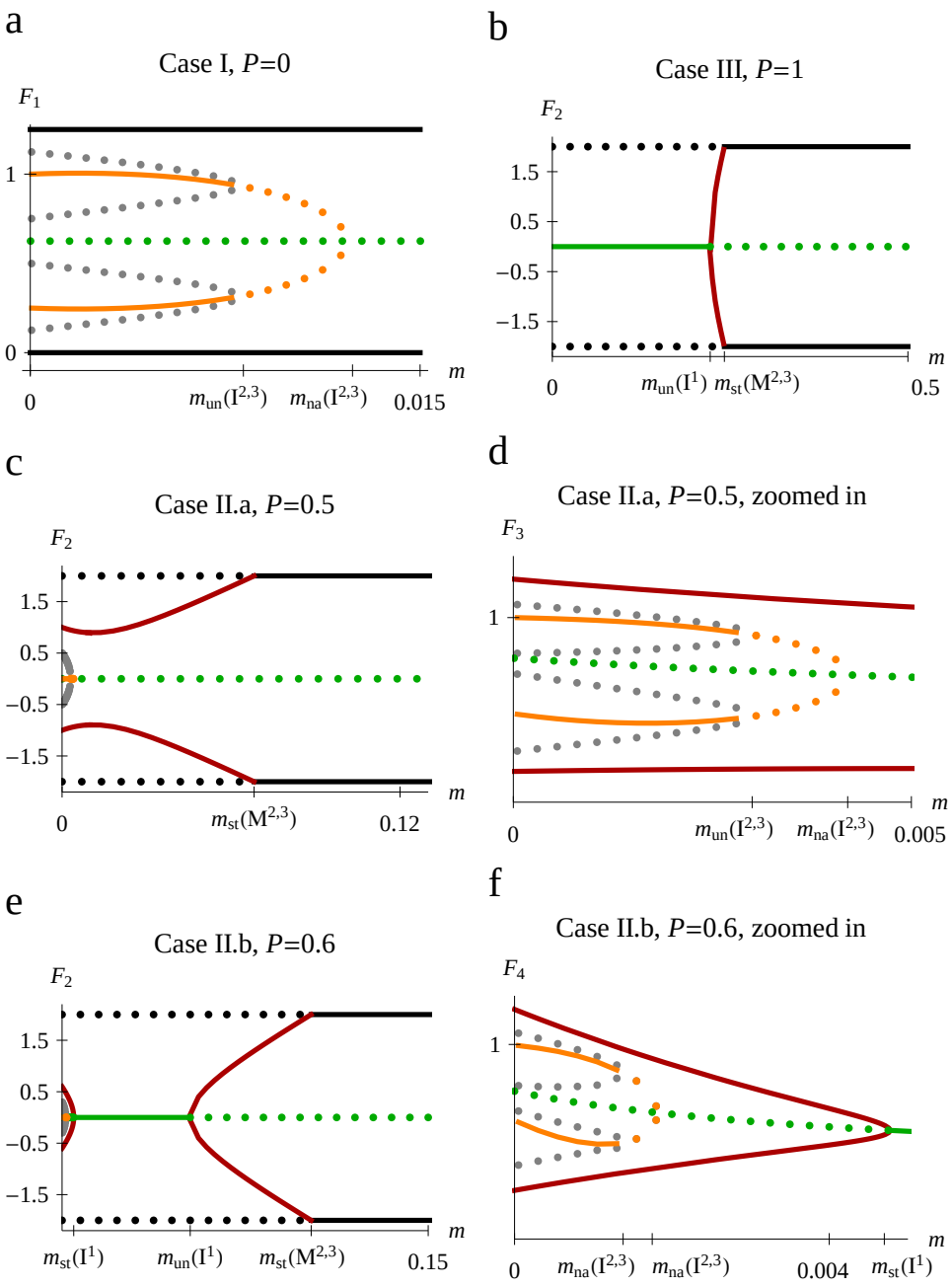

Figure 2: Bifurcation patterns for two demes. The functions F_1, F_2, F_3, and F_4 provide two-dimensional projections of the six-dimensional coordinates and are given in Appendix A.5. Solid and dotted lines represent stable and unstable equilibria, respectively. The equilibrium I^1 is displayed in green, the equilibria I^2 and I^3 are displayed in orange, and I^4 and I^5 in red. Gray dotted lines in panel a show the equilibria $I_m(\mathsf{M}_1^2, \mathsf{F}_2)$, $I_m(\mathsf{M}_1^3, \mathsf{F}_2)$, $I_m(\mathsf{F}_1, \mathsf{M}_2^2)$, and $I_m(\mathsf{F}_1, \mathsf{M}_2^3)$, whereas in the other panels gray lines show $I_m(\mathsf{E}_1^{\mathcal{A},1}, \mathsf{F}_2)$, $I_m(\mathsf{F}_1, \mathsf{E}_2^{\mathcal{B},0})$, $I_m(\mathsf{E}_1^{\mathcal{B},1}, \mathsf{F}_2)$, $I_m(\mathsf{F}_1, \mathsf{E}_2^{\mathcal{B},0})$. Panels d and f are zoomed-in versions of panels c and e, respectively. In Case II.a, the bifurcations can occur in different orders; see (4.6). The SLPs are not shown because they are always unstable and bifurcate only with the monomorphic equilibria when they leave the state space. The asymmetries in panels d and f result from the nonlinear projections F_3 and F_4, respectively. Parameters are $r = 0.5$ and $s = 0.2$.

continuous-time approximation (Appendix A.4), however, the coordinates of I^4 and I^5 can be calculated (A.13), and P_c is given by

$$P_c = \frac{\sqrt{5}}{4}. \tag{4.5}$$

Case II.a

If $1/4 < P < P_c$, the two stable equilibria I^4 and I^5 do not collide and leave the state space at the migration rate $m_{\mathrm{st}}(\mathsf{M}^{2,3})$ by transcritical bifurcations with the two boundary equilibria M^2 and M^3, respectively. The equilibrium I^1 is unstable for all migration rates. The bifurcations can occur in three different orders:

$$0 < m_{\mathrm{un}}(\mathsf{I}^{2,3}) < m_{\mathrm{na}}(\mathsf{I}^{2,3}) < m_{\mathrm{st}}(\mathsf{M}^{2,3}), \tag{4.6a}$$

$$0 < m_{\mathrm{un}}(\mathsf{I}^{2,3}) < m_{\mathrm{st}}(\mathsf{M}^{2,3}) < m_{\mathrm{na}}(\mathsf{I}^{2,3}), \tag{4.6b}$$

$$0 < m_{\mathrm{st}}(\mathsf{M}^{2,3}) < m_{\mathrm{un}}(\mathsf{I}^{2,3}) < m_{\mathrm{na}}(\mathsf{I}^{2,3}). \tag{4.6c}$$

The first order is the most common (Figure 3) and is displayed in Figures 2c,d. Above the highest indicated bifurcation point, the equilibrium configuration of the strong-migration limit applies.

Case II.b

If $P_c \leq P < 3/4$, a supercritical pitchfork bifurcation occurs at $m_{\mathrm{na}}(\mathsf{I}^{4,5}) := m_{\mathrm{na}}(\mathsf{I}^4) = m_{\mathrm{na}}(\mathsf{I}^5) = m_{\mathrm{st}}(\mathsf{I}^1)$ when the three equilibria I^4, I^5, and I^1 collide. The equilibria I^4 and I^5 annihilate each other and I^1 becomes stable. At the critical migration rate $m_{\mathrm{ad}}(\mathsf{I}^{4,5}) := m_{\mathrm{ad}}(\mathsf{I}^4) = m_{\mathrm{ad}}(\mathsf{I}^5) = m_{\mathrm{un}}(\mathsf{I}^1)$, a second supercritical pitchfork bifurcation occurs, in which I^1 becomes unstable and I^4 and I^5 are re-established. As the migration rate increases further, the stable equilibria I^4 and I^5 leave the state space at $m_{\mathrm{st}}(\mathsf{M}^{2,3})$ by transcritical bifurcations with M^2 and M^3, respectively. The sequence of bifurcation events is given by

$$0 < m_{\mathrm{un}}(\mathsf{I}^{2,3}) < m_{\mathrm{na}}(\mathsf{I}^{2,3}) < m_{\mathrm{st}}(\mathsf{I}^1) < m_{\mathrm{un}}(\mathsf{I}^1) < m_{\mathrm{st}}(\mathsf{M}^{2,3}) \tag{4.7}$$

(Figures 2e,f).

Case III

Let $P > 3/4$. Then there is directional selection in each deme, and divergent selection between demes is strong. If migration is weak, I^1 is the globally attracting internal equilibrium. At $m_{\mathrm{ad}}(\mathsf{I}^{4,5}) = m_{\mathrm{un}}(\mathsf{I}^1)$, the equilibrium I^1 becomes unstable and the two stable equilibria I^4 and

I^5 are established in a supercritical pitchfork bifurcation. As the migration rate increases, I^4 and I^5 leave the state space at $m_{\mathrm{st}}(\mathsf{M}^{2,3})$ by transcritical bifurcations with M^2 and M^3, respectively. The sequence of bifurcation events is given by

$$0 < m_{\mathrm{un}}(\mathsf{I}^1) < m_{\mathrm{st}}(\mathsf{M}^{2,3}) \tag{4.8}$$

(Figure 2b).

Remark 4.1. If $P = 1/4$, Case I applies, and if $P = 3/4$, Case III applies. Because they are degenerate (Remark 3.2), they require separate treatment.

Remark 4.2. The above results are related to our previous work (Geroldinger and Bürger 2014), where we mainly studied a haploid model and explored the influence of unequal locus effects ($\kappa < 1$) and of the recombination rate on the maximum migration rates admitting polymorphism. Case I exhibits the same bifurcation pattern as Pattern I.sr.0 in Geroldinger and Bürger (2014). Case II does not have an analogue in the haploid model. Since the SLPs are not admissible in the haploid model for $m = 0$, at most two internal equilibria can be stable, whereas in the present diploid model the four internal equilibria I^2, I^3, I^4, and I^5 may be simultaneously stable. Case III is identical to Pattern D.sr.1 with $\kappa = 1$ in Geroldinger and Bürger (2014). The equilibria I^4 and I^5 correspond to I_6 and I_7 in Geroldinger and Bürger (2014).

Remark 4.3. If $m = 0$, then $\hat{D}_k = 0$ for every stable equilibrium and every k. For weak migration, approximations of the internal equilibria show that $D(\mathsf{I}^2) < 0$ and $D(\mathsf{I}^3) < 0$ (if $0 \le P < 3/4$), $D(\mathsf{I}^4) = D(\mathsf{I}^5) = 0$ (if $1/4 < P < 3/4$), and $D(\mathsf{I}^1) > 0$ (if $P \ge 3/4$). For the continuous-time model it can be shown that $D(\mathsf{I}^4) = D(\mathsf{I}^5) = 0$ for all migration rates; see (A.13). Therefore, if migration is weak, at every stable equilibrium we have $\hat{D} \le 0$ if $P < 3/4$ (stabilizing selection) and $\hat{D} > 0$ if $P \ge 3/4$ (directional selection). Numerical work suggests that this also holds for intermediate migration rates. For the haploid model, it could be proved that in the case analogous to Case I (i.e., Pattern I.sr.0 in Geroldinger and Bürger 2014), LD at I^2 and I^3 is negative for all migration rates.

Remark 4.4. The above analysis shows that for sufficiently strong divergent selection ($P > P_c$) there is an interval of migration rates for which a unique asymptotically stable internal equilibrium (I^1) exists which, presumably, is globally attracting. This interval increases with P (Figure 3a) and includes 0 if $P \ge 3/4$. If $P < P_c$, there are always multiple simultaneously stable equilibria. For Case I, Figure 3b shows the fraction of trajectories converging to one of the stable equilibria I^2, I^3, M^2 and M^3 as a function of the migration rate.

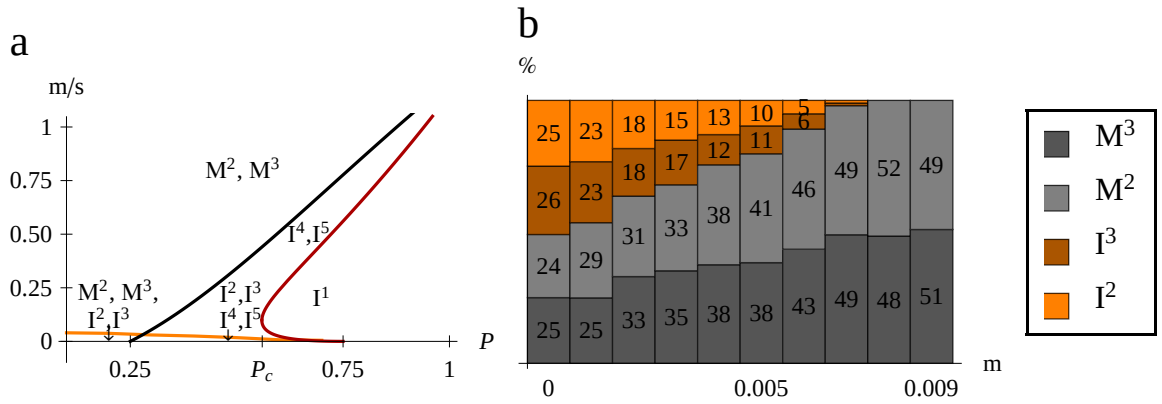

Figure 3: Panel a shows the regions of stability of the equilibria M^2, M^3, I^1, I^2 I^3, I^4 and I^5 as a function of P. The red line shows $m_{\mathrm{st}}(\mathsf{I}^1)$ and $m_{\mathrm{un}}(\mathsf{I}^1)$; the black line $m_{\mathrm{st}}(\mathsf{M}^{2,3})$ (4.1). The orange line shows $m_{\mathrm{un}}(\mathsf{I}^{2,3})$ and is obtained by numerical calculation of the bifurcation point. Panel b shows the fraction of trajectories converging to one of the four simultaneously stable equilibria if $P = 0.2$ (Case I). Initial values were chosen as described at the beginning of Section 4. In both panels, $r = 0.5$ and $s = 0.2$.

Remark 4.5. The maximum migration rate $m_{\max}$ up to which a stable polymorphic equilibrium can occur is given by

$$m_{\max} = \begin{cases} m_{\mathrm{un}}(\mathsf{I}^{2,3}) & \text{in Case I and Case II (4.6c),} \\ m_{\mathrm{st}}(\mathsf{M}^{2,3}) & \text{in Case II (4.6a), (4.6b) and Case III.} \end{cases} \tag{4.9}$$

In Figure 3a these migration rates are displayed as functions of P. Whereas $m_{\mathrm{un}}(\mathsf{I}^{2,3})$ is increasing with the recombination rate (results not shown), $m_{\mathrm{st}}(\mathsf{M}^{2,3})$ is independent of r (4.1). Therefore, the critical ratio m/s above which the equilibrium configuration of the strong-migration limit applies is independent of r if P is sufficiently large.

5 Island and stepping-stone models

In this section we investigate the influence of the migration pattern, the number of demes, and of different selection scenarios on the equilibrium configurations. In particular, we shall compare migration patterns exhibiting different degrees of mixing and different degrees of isolation by distance. Our selection scenarios include models in which there is one major step-like change in the environment, models in which the environment changes (more) gradually, and a model with uniform stabilizing selection.

5.1 Migration patterns and selection scenarios

We investigate the island model and two stepping-stone models. Whereas the former has no geographic structure, the latter exhibit isolation by distance. Two versions of the stepping-stone model will be considered. In the first, individuals migrate only to neighboring demes, whereas in the second migration to more distant demes, or islands, is admitted but occurs with decreasing probability.

The island model

The (forward and backward) migration matrix of the island model $\mathcal{I} = (m_{kl})$ is given by

$$m_{kl} = \begin{cases} 1 - m & \text{if } k = l, \\ \frac{m}{n-1} & \text{if } k \neq l. \end{cases} \tag{5.1}$$

Proposition A.1 demonstrates that in each deme the coordinates of the equilibria depend on k only through the position of the optimum P_k. This holds for every choice n, m, and s, and confirms that the island model exhibits no spatial structure. Also the following relation between an island model with an even number n of islands to the two-deme model is notable.

Remark 5.1. If $n/2$ demes have optimum $-P$ and $n/2$ demes have optimum P, then for every equilibrium in the two-deme model with migration rate m there is an equilibrium in the island model with migration rate

$$\bar{m} = 2\left(1 - \frac{1}{n}\right) m \tag{5.2}$$

(Proposition A.2). This rescaling of the migration rate is a consequence of the following argument. In the two-deme model, m denotes the probability that an individual breeds in the other deme. This coincides with the probability that an individual migrates to a deme with a different environment. In the island model, the second interpretation of m does not hold if $n \geq 4$. Instead, the probability of switching the selective environment is $mn/[2(n-1)]$. Therefore, (5.2) transforms critical migration rates at which the equilibrium structure changes for the two-deme model to analogous critical migration rates for the island model. It is useful even if $P = 0$ because spatially heterogeneous equilibria may exist in the two-deme model (e.g., I^2, I^3).

Stepping-stone models

The backward-migration matrix of the (single-step) stepping-stone model $\mathcal{S} = (m_{kl})$ is given by

$$m_{kl} = \begin{cases} 1-m & \text{if } k = l, \\ \frac{m}{2} & \text{if } |k-l| = 1,\ 1 < k < n, \\ m & \text{if } |k-l| = 1,\ k \in \{1, n\}, \\ 0 & \text{otherwise.} \end{cases} \tag{5.3}$$

In this migration pattern individuals can migrate only to neighboring demes. Alternatively, we consider a generalized stepping-stone model, where migration to more distant demes is possible but its rate decreases with distance. The matrix $\mathcal{S}_2$ of this generalized stepping-stone model is given in Appendix A.7 for $n = 6$ and $n = 12$. In all our migration patterns, m may be interpreted as the probability of outbreeding.

Obviously, the statements of Proposition A.1 and A.2 do not apply to the stepping-stone models. In the stepping-stone models an increasing number of demes increases isolation by distance. Therefore, equilibrium frequencies change gradually in space even if the environment changes sharply.

In Section 7, we will compare our results on the stepping-stone models to previous investigations using diffusion approximations in continuous time and space in an unbounded domain.

Selection scenarios

For each of the migration patterns, we consider the following selection scenarios (Figure 4):

$$\text{Scenario A} : P_k = \begin{cases} -1 & \text{if } 1 \le k \le \frac{n}{2}, \\ 1 & \text{if } \frac{n}{2} < k \le n, \end{cases} \qquad \text{where } n \in 2\mathbb{N}, \tag{5.4a}$$

$$\text{Scenario B} : P_k = \begin{cases} -1 & \text{if } 1 \le k \le \frac{n}{3}, \\ 0 & \text{if } \frac{n}{3} < k \le \frac{2n}{3}, \\ 1 & \text{if } \frac{2n}{3} < k \le n, \end{cases} \qquad \text{where } n \in 6\mathbb{N}, \tag{5.4b}$$

$$\text{Scenario C} : P_k = -1 + (k-1)\frac{2}{n-1}, \qquad \text{where } n \in 2\mathbb{N}, \tag{5.4c}$$

$$\text{Scenario D} : P_k = 0 \text{ for all } k, \qquad \text{where } n \in 2\mathbb{N}. \tag{5.4d}$$

Scenario A models a sharp change, or single step, in the phenotypic optimum from -1 to 1. In one half of the demes ($k \le n/2$) genotype AB/AB is the best adapted, whereas ab/ab is the best adapted in the other half ($k > n/2$). Scenario B assumes two steps in the phenotypic optimum, from -1 to 0 and from 0 to 1. Therefore, heterozygotes and the (repulsion) genotypes

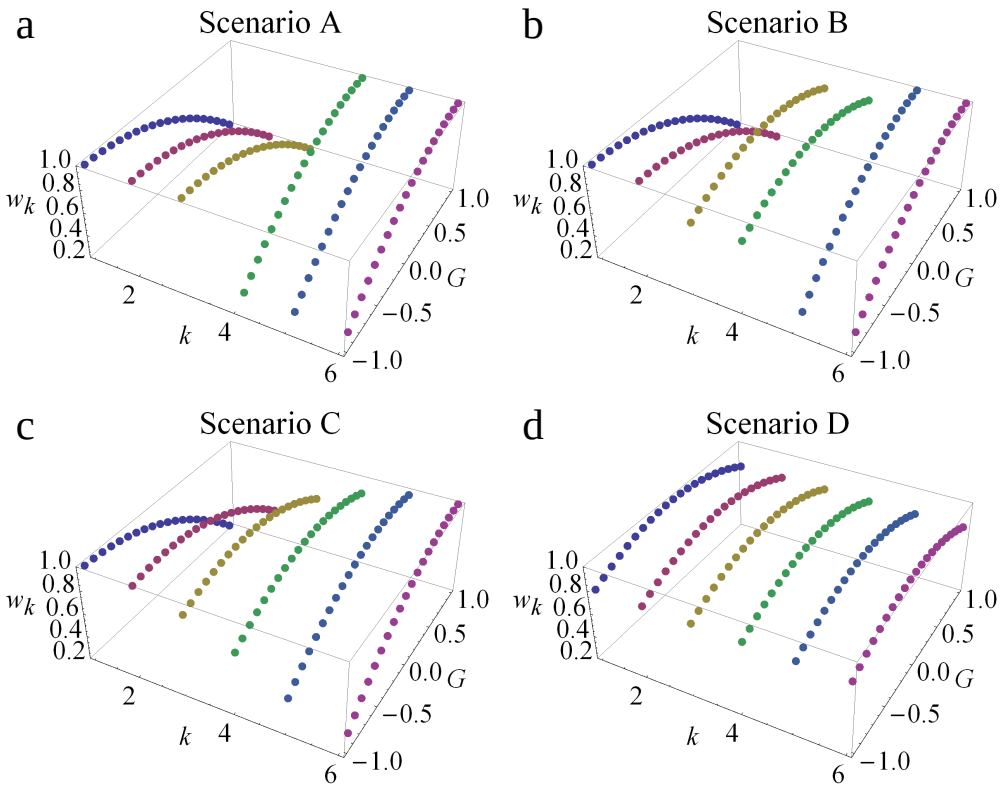

Figure 4: The selection scenarios (5.4) for $s = 0.2$ and $n = 6$.

Ab/Ab and aB/aB are selectively favored in the center of the domain. Scenario C assumes that the phenotypic optimum changes linearly in space, which ensures that each genotype is well adapted in some deme if the number of demes is large enough. In Scenario D there is uniform stabilizing selection toward $P = 0$ in all demes.

Simple calculations or a glance at Figure 4 reveal that for fixed selection intensity s, the maximum fitness difference between genotypes in each deme, $S_k = \max_{ij} w_{ij,k} - \min_{ij} w_{ij,k}$, varies among the selection scenarios.

Recalling (3.1), we note that except for Scenario C the relative sizes of the sets N_i ($1 \le i \le 5$) are independent of n. In Scenario A, we have $|N_1| = |N_5| = n/2$ and $N_2 = N_3 = N_4 = \emptyset$; in Scenario B, $|N_1| = |N_3| = |N_5| = n/3$ and $N_2 = N_4 = \emptyset$ hold; and in Scenario D, $|N_3| = n$. However, in Scenario C we have $N_1 = N_2 = N_4 = N_5 = 1$ and $N_3 = 2$ if $n = 6$, but $N_1 = N_5 = 2$, $N_2 = N_4 = 3$, and $N_3 = 2$ if $n = 12$. This fact is responsible for some peculiar dependencies of critical migration rates on n in Scenario C. To avoid this phenomenon in Scenario B, and also to keep the number of demes even, we assumed $n \in 6\mathbb{N}$.

5.2 Equilibrium configurations

We start by noting that the migration patterns (5.1), (5.3), (A.22), and the selection scenarios (5.4) satisfy (3.7). Therefore, the following proposition follows immediately from (2.3).

Proposition 5.2. *1. Equilibria that do not satisfy*

$$\hat{p}_k = 1 - \hat{p}_{n-k+1}, \quad \hat{q}_k = 1 - \hat{q}_{n-k+1}, \quad \hat{D}_k = \hat{D}_{n-k+1}. \tag{5.5}$$

occur in pairs, $(\hat{p}, \hat{q}, \hat{D})$ and $(\tilde{p}, \tilde{q}, \tilde{D})$. Each pair satisfies the relations

$$\tilde{p}_k = 1 - \hat{p}_{n-k+1}, \quad \tilde{q}_k = 1 - \hat{q}_{n-k+1}, \quad \tilde{D}_k = \hat{D}_{n-k+1}. \tag{5.6}$$

The equilibria of each pair have the same stability properties and satisfy $\hat{\bar{G}}_k = -\tilde{\bar{G}}_{n-k+1}$ and $\hat{V}_k = \tilde{V}_{n-k+1}$, where $\bar{G}_k$ and V_k denote the mean genotypic value and the genetic variance in deme k.

2. Equilibria that do not satisfy

$$\hat{p}_k = \hat{q}_k, \tag{5.7}$$

occur in pairs, $(\hat{p}, \hat{q}, \hat{D})$ and $(\tilde{p}, \tilde{q}, \tilde{D})$. Each pair satisfies the relations

$$\tilde{p}_k = \hat{q}_k, \quad \tilde{q}_k = \hat{p}_k, \quad \tilde{D}_k = \hat{D}_k. \tag{5.8}$$

The equilibria of each pair have the same stability properties, the same mean genotypic value, and the same variance.

Whereas the first statement also holds if $\kappa < 1$, the second statement requires $\kappa = 1$. Equation (5.5) generalizes (4.4). In (A.23), the equilibria I^1, I^2, I^3, I^4, and I^5 are defined for weak migration and n demes. As in the two-deme model, the equilibria I^1, I^2, and I^3 satisfy (5.5). In addition, I^1 fulfills (5.7), and I^2 and I^3 fulfill (5.8). The equilibria I^4 and I^5 satisfy (5.6) and (5.8).

The coordinates of the stable equilibria were calculated from forward iterations of (2.3) (see Section 4). Because several equilibria lie on the manifold given by the symmetry relation (5.5), their coordinates could be computed efficiently by iteration of (2.3) on this manifold. Local stability was determined by numerical evaluation of the eigenvalues of the Jacobian of (2.3).

For increasing migration rate, the number of stable equilibria decreases from its usually high value for weak migration (Proposition 3.1). The numerical computations suggest that, in close analogy to the two-deme model, the reduction of internal equilibria is always due to pitchfork bifurcations.

In this section we investigate the number of stable internal equilibria and the migration rates at which the bifurcations occur. These migration rates depend on the migration pattern, the selection scenario, the number of demes n, as well as on s and r. They are denoted by $m_*^{\mathrm{X},\mathcal{M}}(\mathsf{G})$, where $* \in \{\mathrm{ad}, \mathrm{na}, \mathrm{st}, \mathrm{un}\}$ indicates whether the equilibrium G changes admissibility or stability (as in Section 4), $\mathrm{X} \in \{\mathrm{A}, \mathrm{B}, \mathrm{C}, \mathrm{D}\}$ indicates the selection scenario, and $\mathcal{M} \in \{\mathcal{I}, \mathcal{S}, \mathcal{S}_2\}$ the migration matrix.

Numerical work suggests the following: Internal equilibria never enter the state space through the boundary, and SLPs are never stable if $m > 0$. There is at least one internal equilibrium (I^1) satisfying (5.5). Proposition 3.1 implies that for every migration pattern $\mathcal{M}$, we have $m_{\mathrm{st}}^{\mathrm{X},\mathcal{M}}(\mathsf{M}^{2,3}) > 0$ if $\mathrm{X} \in \{\mathrm{A}, \mathrm{B}, \mathrm{C}\}$ and $m_{\mathrm{st}}^{\mathrm{D},\mathcal{M}}(\mathsf{M}^{2,3}) = 0$. In Scenarios A, B, and C, the equilibrium configuration of the strong-migration limit applies if $m > m_{\mathrm{st}}^{\mathrm{X},\mathcal{M}}(\mathsf{M}^{2,3})$.

Scenario A

Proposition 3.1 implies that for weak migration there is a unique stable internal equilibrium which we denote by I^1 (A.23a). In the absence of migration every trajectory converges to M_k^1 (if $k \leq n/2$) or M_k^4 (if $k > n/2$) (Section 3.1). Therefore, I^1 is globally asymptotically stable for weak migration (Section 3.2). As the migration rate increases, the equilibrium I^1 becomes unstable and two stable equilibria I^4 and I^5 are established in a supercritical pitchfork bifurcation at $m_{\mathrm{un}}^{\mathrm{A},\mathcal{M}}(\mathsf{I}^1) = m_{\mathrm{st}}^{\mathrm{A},\mathcal{M}}(\mathsf{I}^{4,5})$. The equilibria I^4 and I^5 leave the state space through M^2 and M^3, respectively, at $m_{\mathrm{un}}^{\mathrm{A},\mathcal{M}}(\mathsf{I}^{4,5}) = m_{\mathrm{st}}^{\mathrm{A},\mathcal{M}}(\mathsf{M}^{2,3})$. Therefore, the bifurcation pattern is analogous to that of Case III in the two-deme model (Figure 2b). The critical migration rates $m_{\mathrm{un}}^{\mathrm{A},\mathcal{M}}(\mathsf{I}^1)$ and $m_{\mathrm{st}}^{\mathrm{A},\mathcal{M}}(\mathsf{M}^{2,3})$ depend on the number of demes n, the migration pattern $\mathcal{M}$, and the selection intensity s; the former depends also on r.

For the island model, the migration rates $m_{\mathrm{st}}^{\mathrm{A},\mathcal{I}}(\mathsf{M}^{2,3})$ and $m_{\mathrm{un}}^{\mathrm{A},\mathcal{I}}(\mathsf{I}^1)$ are obtained from the two-deme model by rescaling according to (5.2):

$$m_{\mathrm{st}}^{\mathrm{A},\mathcal{I}}(\mathsf{M}^{2,3}) = 2\left(1 - \frac{1}{n}\right) m_{\mathrm{st}}(\mathsf{M}^{2,3}), \tag{5.9a}$$

$$m_{\mathrm{un}}^{\mathrm{A},\mathcal{I}}(\mathsf{I}^1) = 2\left(1 - \frac{1}{n}\right) m_{\mathrm{un}}(\mathsf{I}^1), \tag{5.9b}$$

where $m_{\mathrm{st}}(\mathsf{M}^{2,3})$ and $m_{\mathrm{un}}(\mathsf{I}^1)$ are the critical migration rates from the two-deme model; see (A.14) and (4.1), respectively.

The migration rates $m_{\mathrm{un}}^{\mathrm{A},\mathcal{M}}(\mathsf{I}^1)$ and $m_{\mathrm{st}}^{\mathrm{A},\mathcal{M}}(\mathsf{M}^{2,3})$ in the stepping-stone models can not be determined analytically and are evaluated numerically in Table A.1 and Figure 5. It is important to note that for large s they may exceed $1/2$ (our maximum migration rate).

Indeed, in the stepping-stone models rather small s is required such that $m_{\mathrm{st}}^{\mathrm{A},\mathcal{M}}(\mathsf{M}^{2,3}) \leq 1/2$. Then

$$m_{\mathrm{un}}^{\mathrm{X},\mathcal{I}}(\mathsf{I}^1) \leq m_{\mathrm{un}}^{\mathrm{X},\mathcal{S}_2}(\mathsf{I}^1) \leq m_{\mathrm{un}}^{\mathrm{X},\mathcal{S}}(\mathsf{I}^1), \tag{5.10}$$

$$m_{\mathrm{st}}^{\mathrm{X},\mathcal{I}}(\mathsf{M}^{2,3}) \leq m_{\mathrm{st}}^{\mathrm{X},\mathcal{S}_2}(\mathsf{M}^{2,3}) \leq m_{\mathrm{st}}^{\mathrm{X},\mathcal{S}}(\mathsf{M}^{2,3}), \tag{5.11}$$

always seems to hold for X = A. Therefore, in the island model the equilibrium configuration of the strong-migration limit, hence a homogeneous population, is reached at lower migration rates than in the stepping-stone models. The reason is that short-range migration has a weaker homogenizing effect than distance-independent migration. For the same reason, $m_{\mathrm{un}}^{\mathrm{A},\mathcal{S}}(\mathsf{I}^1)$, $m_{\mathrm{un}}^{\mathrm{A},\mathcal{S}_2}(\mathsf{I}^1)$, $m_{\mathrm{st}}^{\mathrm{A},\mathcal{S}}(\mathsf{M}^{2,3})$, and $m_{\mathrm{st}}^{\mathrm{A},\mathcal{S}_2}(\mathsf{M}^{2,3})$ increase with the number of demes n in the stepping-stone models. Thus, both sets of inequalities support the notion that increasing isolation by distance facilitates the maintenance of genetic variation.

Scenario B

In Scenario B, in which there are three environments (5.4b), we assume $n \in 6\mathsf{N}$. The stable internal equilibria for weak migration are obtained from Proposition 3.1 and are given in (A.24). There are $2^{n/3}$ such equilibria. If $n \geq 12$, the number of stable equilibria quickly reduces to four (the number of stable equilibria if $n = 6$) as m increases from zero. These four equilibria are I^2, I^3, I^4, and I^5 (A.23).

Numerical work suggests that $m_{\mathrm{un}}^{\mathrm{B},\mathcal{M}}(\mathsf{I}^{2,3}) < m_{\mathrm{un}}^{\mathrm{B},\mathcal{M}}(\mathsf{I}^{4,5})$ holds always. Therefore, the number of stable internal equilibria is greater than or equal to four if $m < m_{\mathrm{un}}^{\mathrm{B},\mathcal{M}}(\mathsf{I}^{2,3})$. If m is slightly larger than $m_{\mathrm{un}}^{\mathrm{B},\mathcal{M}}(\mathsf{I}^{2,3})$, I^4 and I^5 are the only stable equilibria. Except for I^4 and I^5 all stable internal equilibria get annihilated by bifurcations with unstable internal equilibria.

The equilibria I^4 and I^5 may either leave the state space through M^2 and M^3, respectively, or collide with the internal unstable equilibrium I^1 (A.23a). The first case is analogous to Case II.a in the two-deme model (Figure 2c) and the second case is analogous to Case II.b in the two-deme model (Figure 2e). If I^4 and I^5 collide with I^1, the two stable equilibria I^4 and I^5 are annihilated and I^1 becomes stable. As the migration rate increases, I^1 gets unstable, and the two stable equilibria I^4 and I^5 are re-established. Finally, I^4 and I^5 leave the state space by transcritical bifurcations with M^2 and M^3, respectively, at $m_{\mathrm{st}}^{\mathrm{B},\mathcal{M}}(\mathsf{M}^{2,3})$.

In the island model, the migration rate $m_{\mathrm{st}}^{\mathrm{B},\mathcal{I}}(\mathsf{M}^{2,3})$ can be calculated using an argument analogous to that for Scenario A by invoking Proposition A.2.2.:

$$m_{\mathrm{st}}^{\mathrm{B},\mathcal{I}}(\mathsf{M}^{2,3}) = \frac{3}{2}\left(1 - \frac{1}{n}\right)\tilde{m}_{\mathrm{st}}^{\mathrm{B},\mathcal{I}}(\mathsf{M}^{2,3}), \tag{5.12a}$$

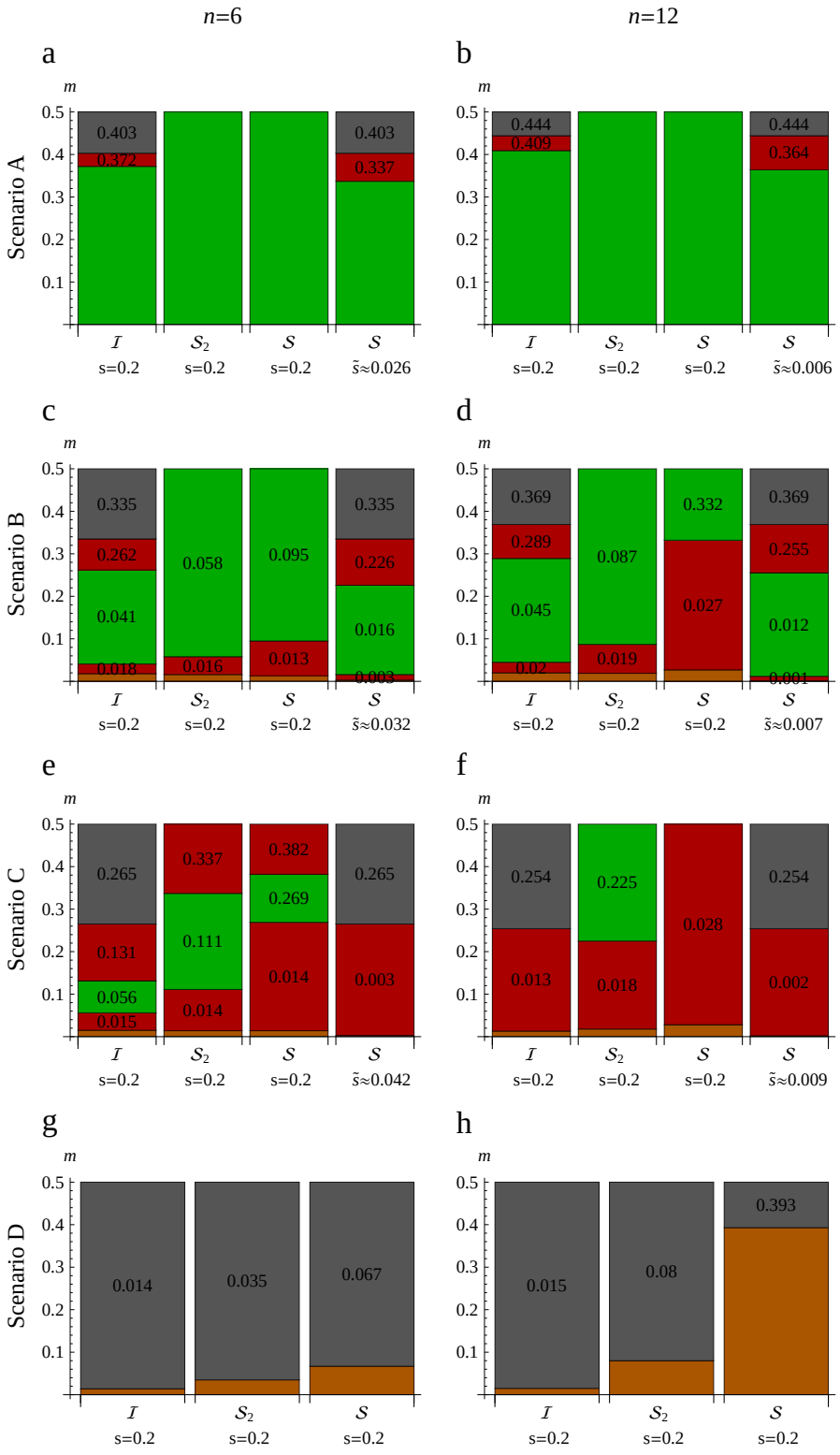

Figure 5: Intervals of the migration rate in which the equilibrium configurations of the various selection scenarios and migration patterns occur. Colors indicate the equilibrium configurations. Orange: more than two equilibria are stable ($m \leq m_{\text{un}}^{\text{X},\mathcal{M}}(\mathsf{I}^{2,3})$). Red: the two internal equilibria I^4 and I^5 are stable. Green: I^1 is globally stable ($m_{\text{st}}^{\text{X},\mathcal{M}}(\mathsf{I}^1) \leq m \leq m_{\text{un}}^{\text{X},\mathcal{M}}(\mathsf{I}^1)$). Gray: M^2 and M^3 are stable. The numbers give the critical migration rate at which the corresponding configuration emerges, provided it is non-zero. The recombination rate is $r = 0.5$.

where

$$\tilde{m}_{\rm st}^{\rm B,\mathcal{I}}(\mathsf{M}^{2,3}) = \frac{30s}{4\sqrt{304 - s(128 - 49s)} + 37s - 52} \approx 1.69s + O(s^2) \tag{5.12b}$$

is derived from a linear stability analysis in the three-island model with $P_1 = -1$, $P_2 = 0$, and $P_3 = 1$. The scaling factor of $\frac{3}{2}\left(1 - \frac{1}{n}\right)$ arises because in Scenario B the probability of switching the selective environment is $2nm/[3(n-1)]$.

Comparing the numerically evaluated critical migration rates in Table A.1 for the different migration patterns, we observe that, in addition to (5.10) and (5.11) with X = B,

$$m_{\rm st}^{\rm X,\mathcal{I}}(\mathsf{I}^1) \le m_{\rm st}^{\rm X,\mathcal{S}_2}(\mathsf{I}^1) \le m_{\rm st}^{\rm X,\mathcal{S}}(\mathsf{I}^1) \tag{5.13}$$

holds for X=B; see also Figure 5.

For the critical migration rate $m_{\rm un}^{\rm B,\mathcal{M}}(\mathsf{I}^{2,3})$, both $m_{\rm un}^{\rm B,\mathcal{I}}(\mathsf{I}^{2,3}) > m_{\rm un}^{\rm B,\mathcal{S}}(\mathsf{I}^{2,3})$ (Figure 5c, Table A.1, $n = 6$) and $m_{\rm un}^{\rm B,\mathcal{I}}(\mathsf{I}^{2,3}) < m_{\rm un}^{\rm B,\mathcal{S}}(\mathsf{I}^{2,3})$ (Figure 5d, Table A.1, $n = 12$) may hold. Therefore, in contrast to $m_{\rm un}^{\rm B,\mathcal{M}}(\mathsf{I}^1)$, $m_{\rm st}^{\rm B,\mathcal{M}}(\mathsf{M}^{2,3})$, $m_{\rm st}^{\rm B,\mathcal{M}}(\mathsf{I}^1)$ (see (5.10), (5.11), (5.13)), $m_{\rm un}^{\rm B,\mathcal{M}}(\mathsf{I}^{2,3})$ is not necessarily increasing with isolation by distance. The source of this ambiguous dependence is the following. On the one hand, strong migration homogenizes the spatial genetic differences and depletes genetic variation (this effect is determining all other critical migration rates, which are higher). On the other hand, immigrants from demes with different selective environments aid within-deme variation. The second effect becomes very weak with increasing isolation by distance because neighboring demes tend to have the same environment. It is weak if $n = 12$, but it is dominating if $n = 6$.

Scenario C

In Scenario C, the environment changes steadily (5.4c). For sufficiently weak migration the stable equilibria are given by (A.25) and their number by (A.26), which gives $2^4, 2^8$ for $n = 6$, 12, respectively. The qualitative dependence of the equilibrium configurations on m is similar to Scenario B, except that for very small m there are more equilibria. However, the bifurcation pattern corresponding to Case II.a of the two-deme model occurs much more often than that of Case II.b. Figure 5 and Table A.1 also show that in several cases, I^1 never becomes stable (eg., the green region is missing in Figures 5e,f). Finally, the inequalities (5.10), (5.11), and (5.13) hold for X = C if the corresponding migration rates are between 0 and 1/2, which is not always the case.

Figure 5f, shows that the migration pattern may affect the establishment of a globally attracting equilibrium in a non-intuitive way. Whereas the equilibrium I^1 becomes stable for $\mathcal{S}_2$, it does not for $\mathcal{I}$ or $\mathcal{S}$ (see also Figure B.1 in Appendix B, Online Supplement).

Scenario D

If there is uniform stabilizing selection toward 0, there are 2^n stable equilibria for weak migration of which 2^n-2 are internal; M^2 and M^3 are stable for every $m \geq 0$; see Proposition 5.2 and (A.27). The equilibria I^4 and I^5 do not exist and I^1 is never stable. In a series of pitchfork bifurcations, these 2^n-2 stable internal equilibria are reduced to the stable internal equilibria I^2 and I^3, which are obtained from (A.23) with $N_1 = N_2 = N_4 = N_5 = \emptyset$. Similar to Case I of the two-deme model (Figure 2a), the four equilibria M^2, M^3, I^2, and I^3 are stable up to $m_{\mathrm{un}}^{\mathrm{D},\mathcal{M}}(\mathsf{I}^{2,3})$. As in that case, the equilibrium configuration of the strong-migration limit applies if $m > m_{\mathrm{na}}^{\mathrm{D},\mathcal{M}}(\mathsf{I}^{2,3}) > m_{\mathrm{un}}^{\mathrm{D},\mathcal{M}}(\mathsf{I}^{2,3})$. Thus, in contrast to Scenarios A, B, and C, the strong-migration limit does not apply for every $m > m_{\mathrm{st}}^{\mathrm{D},\mathcal{M}}(\mathsf{M}^{2,3})$. For the island model we infer the critical migration rate above which no (stable) polymorphism is possible from the two-deme model (Remark 5.1):

$$m_{\mathrm{un}}^{\mathrm{D},\mathcal{I}}(\mathsf{I}^{2,3}) = 2\left(1-\frac{1}{n}\right) m_{\mathrm{un}}(\mathsf{I}^{2,3}), \tag{5.14}$$

where $m_{\mathrm{un}}(\mathsf{I}^{2,3})$ is the corresponding migration rate in the two-deme model. In contrast to Scenarios B and C, the influence of the different migration patterns on $m_{\mathrm{un}}^{\mathrm{D},\mathcal{M}}(\mathsf{I}^{2,3})$ is simple, i.e.,

$$m_{\mathrm{un}}^{\mathrm{D},\mathcal{I}}(\mathsf{I}^{2,3}) \leq m_{\mathrm{un}}^{\mathrm{D},\mathcal{S}_2}(\mathsf{I}^{2,3}) \leq m_{\mathrm{un}}^{\mathrm{D},\mathcal{S}}(\mathsf{I}^{2,3}) \tag{5.15}$$

holds (Figures 5g,h).

5.3 Comparison and summary

If migration is sufficiently weak, the equilibrium configuration depends on the number n of demes and the selection scenario, but is independent of the migration pattern (Proposition 3.1). For sufficiently strong migration, the equilibrium configuration of the strong-migration limit applies (Proposition 3.4). It is independent of the migration pattern, the number of demes, and the selection scenario. The equilibrium configurations in the parameter range where migration and selection are intermediate can be described with the help of the critical migration rates $m_{\mathrm{un}}^{\mathrm{X},\mathcal{M}}(\mathsf{I}^{2,3})$, $m_{\mathrm{st}}^{\mathrm{X},\mathcal{M}}(\mathsf{I}^1)$, $m_{\mathrm{un}}^{\mathrm{X},\mathcal{M}}(\mathsf{I}^1)$, and $m_{\mathrm{st}}^{\mathrm{X},\mathcal{M}}(\mathsf{M}^{2,3})$. They partition the interval $0 \leq m \leq 1/2$ in up to five parts:

(i) If $0 \leq m < m_{\mathrm{un}}^{\mathrm{X},\mathcal{M}}(\mathsf{I}^{2,3})$, more than two equilibria (internal or monomorphic) are stable;

(ii) if $m_{\mathrm{un}}^{\mathrm{X},\mathcal{M}}(\mathsf{I}^{2,3}) \leq m < m_{\mathrm{st}}^{\mathrm{X},\mathcal{M}}(\mathsf{I}^1)$, two internal equilibria (I^4, I^5) are stable;

(iii) if $m_{\mathrm{st}}^{\mathrm{X},\mathcal{M}}(\mathsf{I}^1) \leq m < m_{\mathrm{un}}^{\mathrm{X},\mathcal{M}}(\mathsf{I}^1)$, one internal equilibrium (I^1) is stable;

(iv) if $m_{\mathrm{un}}^{\mathrm{X},\mathcal{M}}(\mathsf{I}^1) \leq m < m_{\mathrm{st}}^{\mathrm{X},\mathcal{M}}(\mathsf{M}^{2,3})$, two internal equilibria (I^4, I^5) are stable;

(v) if $m_{\rm st}^{\rm X,\mathcal{M}}(\mathsf{M}^{2,3}) \le m$, the monomorphisms M^2 and M^3 are stable.

Figure 5 displays these intervals for every selection scenario and migration model. For Scenarios B and C, all five types may occur; for Scenario A only (iii), (iv), and (v) occur; for Scenario D only (i) and (v) occur.

Comparison of the first bar with the second and third in panels a – f of Figure 4 shows that in the stepping-stone models genetic variation is lost (gray regions) for higher migration rates than in the island model. Often these migration rates exceed 0.5; then there is no gray region. Clearly, this reflects the fact that gene flow has a stronger homogenizing effect in the absence of isolation by distance than in its presence. To demonstrate the ubiquity of this finding and to compare patterns $\mathcal{I}$ and $\mathcal{S}$ in more detail, we proceed as follows. Start with $\mathcal{I}$ for given n, s, r, and X. Denote by $\tilde{s} = \tilde{s}^{\rm X}(m_{\rm st}^{\rm X,\mathcal{I}}(\mathsf{M}^{2,3}))$ the selection intensity in the corresponding stepping-stone model such that $m_{\rm st}^{\rm X,\mathcal{S}}(\mathsf{M}^{2,3}) = m_{\rm st}^{\rm X,\mathcal{I}}(\mathsf{M}^{2,3})$, i.e., such that with $\mathcal{S}$ and $\tilde{s}$ the transition to the strong-migration limit occurs at the same m as with $\mathcal{I}$ and s. In particular, M^2 and M^3 get stable at the same migration rate in both migration patterns.

The fourth bar in panels a – f of Figure 5 shows the intervals in which the different equilibrium configurations occur for the stepping-stone model with selection intensity $\tilde{s}$. By definition of $\tilde{s}$, the gray regions occur above the same migration rate as for the island model (first bar). Comparison of the first and the fourth bar in panels a – f shows that in the island model with selection intensity s, the regions where I^1 is stable are larger than in the stepping-stone model with selection intensity $\tilde{s}$. This appears to reflect the greater importance of initial conditions in migration patterns involving isolation by distance.

The number of demes has two effects on the equilibrium configuration. First, for weak migration, the number of stable internal equilibria increases with the number of demes if $\mathrm{X} = \mathrm{B}, \mathrm{C}, \mathrm{D}$. Second, in the stepping-stone models the degree of isolation by distance increases with n. Therefore, critical migration rates in the stepping-stone models increase with n (Figure 6). For $\mathcal{I}$, the role of n is well understood in Scenarios A and B; see (5.9) and (5.12). However, in Scenario C, $m_{\rm st}^{\rm C,\mathcal{I}}(\mathsf{M}^{2,3})$ decreases from 0.265 for $n = 6$ to 0.254 for $n = 12$. This is due to the relative variation of the sizes of N_i (3.1) as explained below equation (5.4).

A comparison of Scenarios A, B, and C shows that the parameter range where I^1 is stable decreases from A to C, i.e.,

$$m_{\rm un}^{\rm A,\mathcal{M}}(\mathsf{I}^1) - m_{\rm st}^{\rm A,\mathcal{M}}(\mathsf{I}^1) \ge m_{\rm un}^{\rm B,\mathcal{M}}(\mathsf{I}^1) - m_{\rm st}^{\rm B,\mathcal{M}}(\mathsf{I}^1) \ge m_{\rm un}^{\rm C,\mathcal{M}}(\mathsf{I}^1) - m_{\rm st}^{\rm C,\mathcal{M}}(\mathsf{I}^1), \tag{5.16}$$

where $m_{\rm st}^{\rm A,\mathcal{M}}(\mathsf{I}^1) = 0$ (in Figure 5, compare the green stacks among panels a, c, and e, as well as among b, d, and f). Also the maximum migration rate below which polymorphism is

possible,

$$m_{\max} = \begin{cases} m_{\mathrm{st}}^{\mathrm{X},\mathcal{M}}(\mathsf{M}^{2,3}) & \text{if } \mathrm{X} = \mathrm{A}, \mathrm{B}, \mathrm{C}, \\ m_{\mathrm{un}}^{\mathrm{D},\mathcal{M}}(\mathsf{I}^{2,3}) & \text{if } \mathrm{X} = \mathrm{D}, \end{cases} \tag{5.17}$$

decreases from Scenario A to Scenario D, i.e.,

$$m_{\mathrm{un}}^{\mathrm{D},\mathcal{M}}(\mathsf{I}^{2,3}) \leq m_{\mathrm{st}}^{\mathrm{C},\mathcal{M}}(\mathsf{M}^{2,3}) \leq m_{\mathrm{st}}^{\mathrm{B},\mathcal{M}}(\mathsf{M}^{2,3}) \leq m_{\mathrm{st}}^{\mathrm{A},\mathcal{M}}(\mathsf{M}^{2,3}) \tag{5.18}$$

(Figure 5, Table A.1). In this sense, a single abrupt change in the environment is more favorable for the maintenance of genetic variation than a more gradual change.

For weak migration the number of coexisting stable internal equilibria increases from Scenario A to D. Hence, in a more gradually changing environment, initial conditions affect evolution much more than in an environment that changes abruptly.

Similar to the two-deme model (Remark 4.5), $m_{\mathrm{un}}^{\mathrm{X},\mathcal{M}}(\mathsf{I}^{2,3})$ is increasing in r if $\mathrm{X} \in \{\mathrm{B}, \mathrm{C}, \mathrm{D}\}$; see Table A.1. The reason is that LD at the equilibria I^2 and I^3 is negative in the demes under stabilizing selection (eq. (A.34), Figure 9c). Therefore, more recombination increases genetic variance because it reduces the negative LD (Bürger 2000, p. 74). The critical migration rates $m_{\mathrm{st}}^{\mathrm{X},\mathcal{M}}(\mathsf{I}^1)$ and $m_{\mathrm{un}}^{\mathrm{X},\mathcal{M}}(\mathsf{I}^1)$ may increase or decrease with r but depend only very weakly on r (Table A.1). However, $m_{\mathrm{st}}^{\mathrm{X},\mathcal{M}}(\mathsf{M}^{2,3})$ is independent of r (Proposition 3.4).

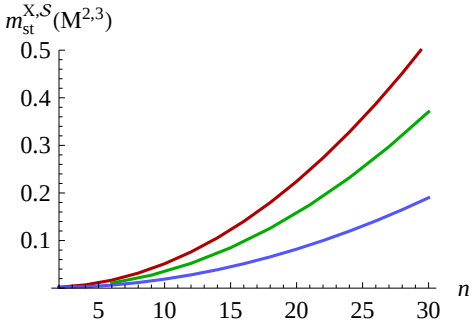

Figure 6: The migration rate $m_{\mathrm{st}}^{\mathrm{X},\mathcal{S}}(\mathsf{M}^{2,3})$ shown as a function of n for Scenario A (red), B (green), and C (blue). The selection intensity is $s = 0.001$.

6 Clines in the mean phenotype, genetic variance, and LD

Here we investigate how the migration patterns and selection scenarios determine the spatial distribution of the population across demes. In particular, we are interested in how mean phenotype, genetic variance, and LD vary in space. We focus on the range $m > m_{\mathrm{un}}^{\mathrm{X},\mathcal{M}}(\mathsf{I}^{2,3})$ and briefly treat the case of very small migration rates, when four or more equilibria may be stable simultaneously, further below. For every migration pattern and selection scenario, as

well as for representative values of s and r, we calculated the mean phenotype, the genetic variance, and the measure D of LD at equilibrium in every deme and displayed them as functions of the deme number k. This was done for a fine grid of admissible migration rates (Figures B.2, B.3, B.4, B.5, B.6, B.7 in Appendix B, Online Supplement). Figure 7 displays representative results for one migration rate.

6.1 Clines in the mean phenotype and local adaptation

The panels in the left column of Figure 7 display the clines in the mean phenotype. The degree of local adaptation in deme k is measured by $|\bar{G}_k - P_k|$. In most cases, the stepping-stone models favor local adaptation compared to the island model (Figures B.2, B.3, B.4). However, the relation

$$|\bar{G}_k - P_k|_{\mathcal{I}} \geq |\bar{G}_k - P_k|_{\mathcal{S}_2} \geq |\bar{G}_k - P_k|_{\mathcal{S}} \tag{6.1}$$

is valid in every deme only in Scenario A. In Scenario B, it is the island model that maximizes local adaptation in the demes under stabilizing selection because $|\bar{G}_k - P_k|_{\mathcal{I}} = 0$ if $n/3 < k \leq 2n/3$; cf. (A.32), (A.35). However, it leads to poor adaptation in demes under directional selection (Figure 7d). For Scenario C, counter examples to (6.1) occur in demes with stabilizing selection, e.g., if $r = 0.5$, $n = 12$, $s = 0.2$, $m = 0.02$, and $k = 6, 7$ (Figure B.4).

6.2 Genetic variance

In a step environment (Scenario A) and with stepping-stone migration ($\mathcal{S}$, $\mathcal{S}_2$), the within-deme variance is always maximized in the center of the cline (Figure 7b), and it decreases toward the boundaries. For Scenarios B and C, this does not hold: the variance may be maximized in the center or elsewhere (Figures 7e,h). The bimodal patterns occur mainly for weak single-step migration (Figures B.3, B.4). In the absence of migration, different haplotypes are fixed in demes with directional or stabilizing selection. Therefore, in Scenario B weak migration induces substantial variance in the demes adjacent to an environmental change. In Scenario C, the following arguments show that for weak migration the variance is bimodal. If $m = 0$, then $V_k > 0$ for $1/4 < |P_k| < 3/4$, and $V_k = 0$ otherwise (Section 3.1). Therefore, if migration is weak, the variance in the demes with $1/4 < |P_k| < 3/4$ is higher than in the demes in the center of the range or close to the boundary.

If in Scenarios B or C, migration rates are such that I^1 is the unique stable equilibrium, i.e., $m_{\mathrm{st}}^{\mathrm{X},\mathcal{M}}(\mathsf{I}^1) < m < m_{\mathrm{un}}^{\mathrm{X},\mathcal{M}}(\mathsf{I}^1)$ (whence migration is no longer weak), the genetic variance decreases from the center of the cline to its boundaries (Figures B.3, B.4).

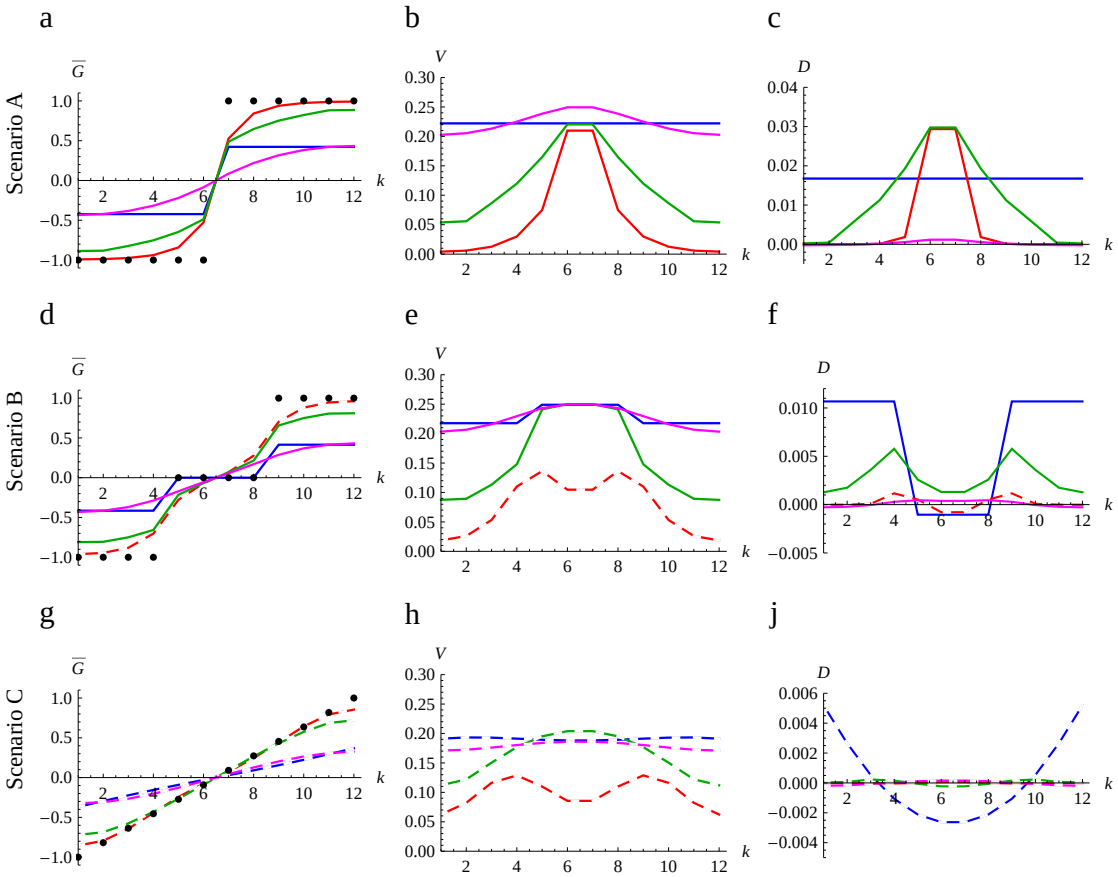

Figure 7: Clines in the mean phenotype (left), the genetic variance (middle), and LD (right) for different selection scenarios and migration patterns. Blue lines indicate the island model, red lines the stepping-stone model, and green lines the generalized stepping-stone model. Magenta lines show the stepping-stone model with $\tilde{s}$. The corresponding equilibrium configuration for each migration patterns can be inferred from Figure 5. Solid lines indicate that I^1 is the unique stable equilibrium, whereas dashed lines indicate that I^4 and I^5 are simultaneously stable (they exhibit the same mean, variance, and LD). In the left column, dots mark the positions of the optimum. The parameters are $s = 0.2$, $r = 0.5$, $m = 0.13$, and $n = 12$.

For the island model, the genetic variance is either spatially uniform (Scenario A) or weakly dependent on space (Scenarios B and C). In the latter case, it may be maximized or minimized in the center, or it may be bimodal (Figures B.3, B.4).

Although Figure 7 suggests the simple relation

$$V_{k,\mathcal{I}} \geq V_{k,\mathcal{S}_2} \geq V_{k,\mathcal{S}} \tag{6.2}$$

for the variances V_k (in deme k) maintained by the three migration patterns, it does not hold in general. Obviously, (6.2) is violated if $m_{\mathrm{st}}^{\mathrm{X},\mathcal{I}}(\mathsf{M}^{2,3}) < m < m_{\mathrm{st}}^{\mathrm{X},\mathcal{S}}(\mathsf{M}^{2,3})$, but it may also be violated if $m < m_{\mathrm{st}}^{\mathrm{X},\mathcal{I}}(\mathsf{M}^{2,3})$ (Figures B.2, B.3, B.4).

Finally we consider the genetic variance V_T in the entire population. It is calculated from the spatially averaged gamete frequencies and displayed in Figure 8 as a function of m. Whereas in Scenario A, V_T is monotone decreasing in m, weak migration may increase V_T in Scenario B and Scenario C. The variance decreases rapidly when m approaches $m_{\max}$, i.e., when the cline starts to collapse. For given m, V_T decreases from Scenario A to B to C. Further, the effect of linkage on V_T decreases from Scenario A to B to C because the absolute magnitude of LD decreases from Scenario A to B to C (Section 6.3).

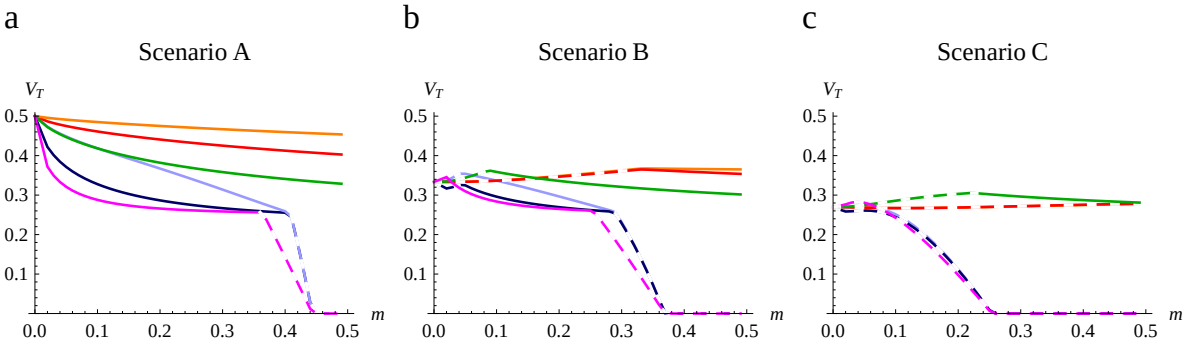

Figure 8: The genetic variance in the entire population as a function of the migration rate. The island model (blue) is shown for $r = 0.5$ (dark) and $r = 0.05$ (light). Red and orange lines show the stepping-stone model for $r = 0.5$ and $r = 0.05$, respectively. Green and magenta lines display the generalized stepping-stone model and the stepping-stone model with $\tilde{s}$, respectively ($r = 0.5$). At dashed lines, equilibria are simultaneously stable. For reasons of visibility only $V_T(\mathsf{I}^{4,5})$ is shown for $m < m_{\mathrm{un}}^{\mathrm{X},\mathcal{M}}(\mathsf{I}^{2,3}) \leq 0.028$, whereas V_T at the other stable equilibria is not displayed. Parameters are $s = 0.2$ and $n = 12$.

6.3 Linkage disequilibrium

Linkage disequilibrium depends strongly on the selection scenario, the migration pattern, and the spatial location. In Scenario A, the situation is simple. For the stepping-stone

models, D assumes its maximum in the center of the cline and decays monotonically to a very small positive or negative value at the boundaries (e.g., Figure 7c). A similar pattern was reported by Slatkin (1975), who modeled dispersal in continuous space by diffusion and assumed nonepistatic directional selection at every location. At the boundaries of the cline, LD may be negative ($D_1, D_n < 0$). This peculiar phenomenon is likely due to the fact that in the demes at the boundary, migration is unidirectional. In an infinite domain, LD will approach zero in increasingly distant demes. For the island model with weak migration, LD is positive and the same in all islands (A.28).

In Scenarios B and C, LD may be a complicated function of the distance from the center (Figures 7f,j). It tends to be positive in some demes and negative in others. In Scenario B with the stepping-stone models and weak to moderate migration (Figures 7f), LD is maximized in demes $n/3$ and $2n/3 + 1$, which are the demes under directional selection next to the environmental step. For higher migration rates, LD is usually maximized in the center of the cline (Figures B.3, B.4). In Scenario B with $\mathcal{I}$, LD assumes the same positive value in all demes under directional selection and the same positive or negative value elsewhere.

In Scenario C with stepping-stone migration, each deme is close to linkage equilibrium for a wide range of migration rates (Figure B.4). However, the island model exhibits deviations from linkage equilibrium. They are not negligible if linkage is tight (Figure B.7).

There are two general conclusions that can be drawn. (i) For every investigated migration pattern, Scenario A is the one in which the highest LD occurs (in the demes next to the environmental step), and Scenario C is the one in which the maximum (absolute) LD is the lowest. This does not mean that in Scenario C, LD is everywhere lower than in Scenario A. (ii) For weak and intermediate migration and each of the selection scenarios A, B, or C, the average absolute amount of LD is highest with $\mathcal{I}$ and lowest with $\mathcal{S}$.

In order to explain the patterns of LD in Scenario B and C, we recall from Remark 4.3 that in the two-deme model migration induces negative LD if $0 \leq P < 3/4$ (stabilizing selection) and positive LD if $P \geq 3/4$ (directional selection). Proposition A.3 and Remark A.4 partially generalize this result: In Scenario B, weak migration induces non-positive LD in the demes under stabilizing selection and non-negative LD in the demes under directional selection. If migration connects environments under stabilizing selection with environments under directional selection (as in Scenarios B and C), negative and positive LD may offset each other. It is apparent from Figure 7 that LD in Scenario C is much lower than in Scenario B which, in turn, is lower than in Scenario A. Its magnitude depends on the migration pattern, m, and the deme (Figures 7f,j and Figures B.3, B.4, B.8). The degree of isolation by distance

can have an ambiguous effect on the sign of LD. In Figure 7f ($k = 6, 7$), LD is negative for $\mathcal{S}$ and $\mathcal{I}$, but positive for $\mathcal{S}_2$.

6.4 The parameter range $0 < m < m_{\text{un}}^{\text{X},\mathcal{M}}(\mathsf{I}^{2,3})$

In this usually very small range of migration rates (Figure 5), at least four equilibria are simultaneously stable in Scenarios B, C, and D. These equilibria may exhibit different means and variances (Figure 9). The maximum variance (among stable equilibria) in the center of the habitat is of the same magnitude as for intermediate migration rates; compare Figure 7e ($m = 0.13$) with Figure 9b ($m = 0.01$). The maximum LD (among stable equilibria) in the center of the habitat may be much higher than for intermediate migration rates; compare Figure 7f ($m = 0.13$) with Figure 9c ($m = 0.01$).

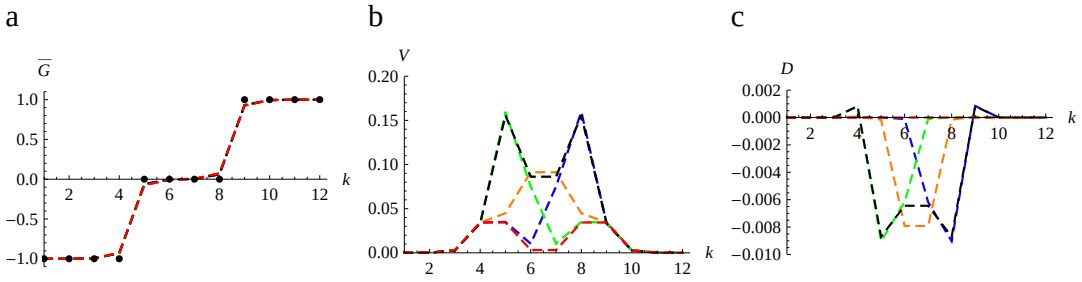

Figure 9: Clines in the mean phenotypic value (a), in the genetic variance (b), and in LD (c) at simultaneously stable equilibria in the stepping-stone model with Scenario B and $n = 12$. The parameters are $r = 0.5$, $s = 0.2$, and $m = 0.01$ which is smaller than $m_{\text{un}}^{\text{B},\mathcal{S}}(\mathsf{I}^{2,3}) \approx 0.028$. Ten equilibria (out of the 16 for weak migration) are stable. Five pairs exhibit different mean, variance and LD. Each color corresponds to a pair of simultaneously stable equilibria. The red dashed lines show I^4 and I^5 and correspond to the red lines in Figures 7d,e,f.

7 Comparison with other multilocus models

Here, we compare our results of Section 6 to previously investigated clinal multilocus models.

7.1 A neutral model

Feldman and Christiansen (1975) studied a model without selection in which two 'continents' are fixed for different genetic backgrounds and are connected by $n-2$ demes with (single-step) stepping-stone migration into which they feed their genotypes. For two neutral loci, with AB fixed in deme 1 and ab fixed in deme n, there is a unique cline which is linear in the allele frequencies and globally asymptotically stable. Linkage disequilibrium is unimodal with a

maximum value of

$$D_k \approx \frac{m}{r(n-1)^2} \tag{7.1}$$

in the center of the cline. For a generalization to multiple loci, see Christiansen (1986).

Comparing Figure 7c with the approximation $m/[r(n-1)^2] = 0.13/(0.5 * 11^2) \approx 0.0022$ shows that LD in the neutral cline is usually much lower than in Scenario A with strong selection. However, it tends to be higher than in Scenario C (Figure 7j), in which the cline in the mean is nearly linear. The variance in the center of the neutral cline is of the same order of magnitude as in the cline under migration-selection balance. At the boundaries, though, it is (fixed at) zero (compare Figure B.9 with Figures B.2, B.3, B.4).

The approximation (7.1) uses that in the model of Feldman and Christiansen (1975) allele frequencies in adjacent demes differ by $1/(n-1)$. Kruuk et al. (1999, eq. (A.4)) generalized (7.1) to

$$D_k \approx \frac{m}{r}(p_k - p_{k+1})(q_k - q_{k+1}), \tag{7.2}$$

which assumes

$$p_{k-1} - p_k = p_k - p_{k+1}, \quad q_{k-1} - q_k = q_k - q_{k+1}. \tag{7.3}$$

Figure B.10 shows the accuracy of approximation (7.2) for each of the selection scenarios A, B, or C. If (7.3) is approximately satisfied, as in Scenario C, (7.2) approximates LD well for small migration rates. In the center of the cline with Scenario A (7.3) is obviously violated and (7.2) performs poorly. For the performance of an extension of (7.2) to weak selection by Barton and Shpak (2000) see Figure B.10.

7.2 Continuous space

Several models have been set up to describe clines at multiple loci or in polygenic traits in a continuous domain. Slatkin (1975) studied the effects of linkage on the clines in allele frequency at two loci and the associated LD. He assumed a step environment on the real line, analogous to our Scenario A, and used partial differential equations of the form

$$\frac{\partial x_i}{\partial t}(y,t) = \frac{\sigma^2}{2}\frac{\partial^2 x_i}{\partial y^2}(y,t) + x_i(y,t)(w_i(y,t) - \bar{w}(y,t)) - r\eta_i D(y,t), \tag{7.4a}$$

where σ^2 is the diffusion rate, $x_i(y,t)$ and $w_i(y,t)$ are the frequency and marginal fitness, respectively, of gamete i at position y at time t, $\bar{w}(y,t)$ is the mean fitness, and $D(y,t)$ denotes LD (Appendix A.11). These equations can be deduced as an approximation to the discrete-time model (2.3) with stepping-stone migration among a large number of demes in the same way as in Nagylaki (1975, 1989a), and need to be complemented by appropriate boundary

conditions (usually, zero-flux conditions). Then σ^2 is the (scaled) variance in dispersal distance. By assuming absence of epistasis, dominance, and LD, the cline in allele frequencies, i.e., the non-trivial equilibrium solution, can be calculated explicitly (Slatkin 1975). However, he also showed numerically that, even in the absence of epistasis, LD is positive, maximized in the center of the cline, and decaying to zero with increasing distance from the center. If the loci are tightly linked, D may approach its maximum value of $1/4$ at the center. In addition, a decreasing recombination rate steepens the cline in allele frequencies because stronger LD strengthens selection (Barton and Shpak 2000).

Felsenstein (1977), Slatkin (1978), and Barton (1983, 1999) investigated models of stabilizing selection on a quantitative trait by approximating gene flow by diffusion. Since the models of Felsenstein (1977) and Slatkin (1978) occur as limiting or special cases of Barton's models (and are discussed there), we focus on two of Barton's models but ignore mutation. Under the assumptions of a Gaussian distribution of allelic effects at each of L loci and of linkage equilibrium, Barton (1999, eqs. (4) and (5)) obtained the equations (A.38) for the evolution of the mean and the variance of the trait. As discussed there, the assumption of a Gaussian allelic distribution is rather restrictive; however, if it holds and the optimum changes gradually, the assumption of linkage equilibrium is supported by Felsenstein's (1977) analysis. Barton (1999, eq. (10)) also investigated a model in which n diallelic loci of equal effect and in linkage equilibrium contribute to the trait. For two loci, his 'rare-allele model' is specified in (A.39). It is equivalent to (7.4) if $D(y,t) \equiv 0$ is assumed in (7.4).

In Figure 10 and Figure B.11, our results for $\mathcal{S}$ with 12 demes are compared with the diffusion approximation (7.4) and with Barton's models (A.38) and (A.39). To compare the diffusion approximations with our discrete model, we assumed that the habitat is the interval $[1, 12]$. Therefore, the boundary conditions

$$\frac{\partial x_i}{\partial y}(1,t) = \frac{\partial x_i}{\partial y}(12,t) = 0 \quad \text{for every } i \text{ and every } t \geq 0 \tag{7.4b}$$

are imposed. The diffusion rate σ^2, calculated as the variance in dispersal distance, depends on the position of the demes; see (A.41), (A.42), (A.43). Because $\sigma^2 = m$ holds to a close approximation (A.44), we use this as the uniform value. Equations (A.38), (A.39), and (7.4) were solved by using the *Mathematica* routine *NDSolve* and assuming spatially uniform initial conditions.

Figure 10 and Figure B.11 show that the 12-deme and the PDE models yield similar clines in the mean phenotype. In Scenario A, the clines for linked loci are slightly steeper in the center of the cline than for unlinked ones. This was already predicted by Slatkin (1975) for

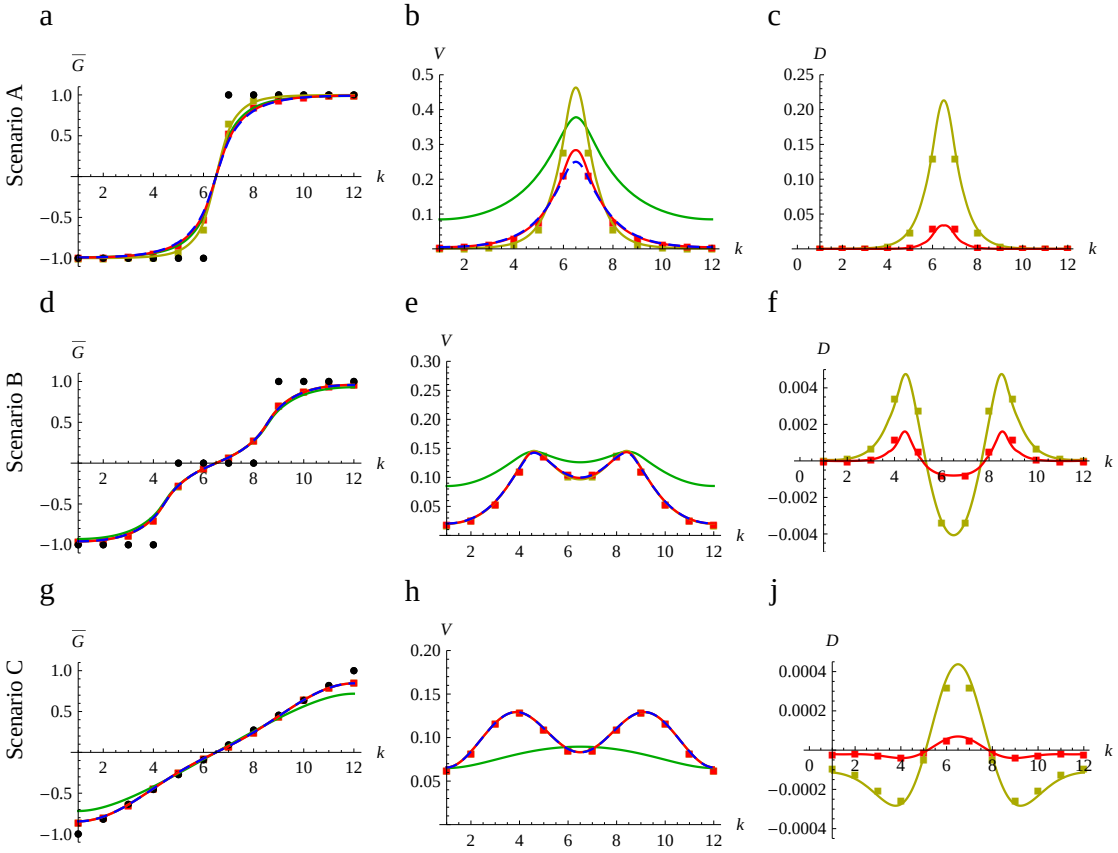

Figure 10: Clines in the mean phenotype (left), the genetic variance (middle), and LD (right) for the Gaussian PDE model (A.38) (green lines), Barton's PDE model (A.39) which assumes linkage equilibrium (blue dashed lines), and our model (7.4). The model (7.4) is shown for $r = 0.01$ (yellow lines) and $r = 0.5$ (red lines). Because (A.38) and (A.39) assume linkage equilibrium, LD is shown only for (7.4). Yellow and red dots show clines from the 12-deme stepping-stone model for $r = 0.01$ and $r = 0.5$, respectively. In panels d, e, g, and h, blue dashed, yellow, and red lines overlap. Other parameters are $s = 0.2$ and $\sigma^2 = m = 0.13$.

a model with linear directional selection. In Scenario C, the Gaussian model (A.38) leads to less adaptation than all other models near the boundaries of the habitat. The Gaussian model also exhibits large deviations from the variance maintained in all other models. This may not be too surprising because a Gaussian distribution of allelic effects is not suitable to approximate the distribution in a diallelic model. This could be different for models with many or a continuum of alleles.

In general, mean, variance, and LD in the 12-deme stepping-stone model are very accurately approximated by the PDE model (7.4), although with stronger dispersal the approximation for LD may become slightly less accurate (Figures B.11f, j). If LD is low, whether recombination is strong or weak, Barton's linkage equilibrium approximation (A.39) for the mean and the variance is essentially indistinguishable from that based on (7.4). If LD is large, which is the case only in Scenario A near the environmental step, it affects the genetic variance to a notable extent. Then it leads to an elevated variance near the environmental step which, in turn, entails a slightly steeper gradient of the cline in the mean.

The clines in the mean, variance, and LD displayed in Figures 10 and B.11 are unique although in Scenarios B and C the underlying genotype-frequency equilibria are not. In fact, there are pairs of stable equilibria that have the same mean, variance, and LD (cf. Figure 7 and Proposition 5.2). If migration is much weaker than selection, the clines in the variance and in LD are no longer uniquely determined as already shown for the stepping-stone model (Figure 9).

7.3 Loci with unequal effects

If unequal locus effects ($\kappa < 1$) and arbitrary linkage are admitted, there is a much larger number of possible equilibrium configurations. Already for $n = 2$, the analysis is much more intricate than that in Section 4 (cf. Geroldinger and Bürger 2014). There are several reasons for these complications.

(i) Single-locus polymorphisms may be stable for $m \geq 0$ and their stability depends in a complicated way on r and κ.

(ii) Four different equilibrium configurations can occur in the limit of strong migration, one with a globally asymptotically stable internal equilibrium, one with two locally stable internal equilibria, one with two locally stable SLPs, and the one with M^2 and M^3 locally stable (see Bürger 2000, p. 207). The latter applies if and only if $1/2 \leq \kappa \leq 1$ and $r \geq r_1$, where $r_1 = (-1 - \kappa^2 + 2\sqrt{1 - \kappa^2 + \kappa^4})/[3(1 + \kappa)^2]$. In this case a numerical linear stability analysis shows that $m_{\mathrm{st}}^{\mathrm{X},\mathcal{M}}(\mathsf{M}^{2,3})$ decreases in κ.

(iii) The definition (A.23) of the equilibria I^1, I^2, I^3, I^4, and I^5 can be extended to $\kappa < 1$. However, the movement of the equilibria in the state space with increasing migration rate is much more complicated. Nevertheless, for a large set in the parameter space either two equilibria (I^4 and I^5) are simultaneously stable or a unique stable equilibrium (I^1) exists. In contrast to $\kappa = 1$, where pairs of equilibria (such as I^2, I^3 or I^4, I^5) have the same mean, variance, and LD, this not so if $\kappa < 1$. A frequently occurring analogue of the patterns in Figure 7 is shown in Figure B.12.

8 Discussion

Here we recapitulate our model and results in a non-technical way and discuss the relation to previous literature. The purpose of this work was to investigate the effects of migration patterns and selection scenarios on the maintenance and the properties of clines in a quantitative trait. We assumed that the trait is determined additively by two diallelic, recombining loci. Fitness decays quadratically from a phenotypic optimum. Because the position of the optimum, which depends on space, may be anywhere within the range of possible phenotypes, the trait may be under stabilizing or directional selection.

The population is subdivided into $n \geq 2$ discrete demes, representing different locations in space (Section 2), or inhabits continuous space, i.e., a bounded one-dimensional interval (Section 7.2). One of the advantages of using discrete demes is that different migration patterns can be modeled easily, whereas diffusion models are based on the assumption that there is mainly short-distance migration and evolutionary forces are weak. In particular, we used the island model (denoted by $\mathcal{I}$), in which there is no distance because every island (deme) is reached with the same probability, the single-step stepping-stone model ($\mathcal{S}$), and a multi-step stepping-stone model ($\mathcal{S}_2$) in which more distant demes can be reached with reduced probability (Section 5.1). Demes are ordered from 1 to n, although this (spatial) order is irrelevant in the island model. If $n = 2$, all three migration patterns coincide. Therefore, the analysis of the two-deme model in Section 4 is of central importance.

In addition, we employed four different selection scenarios. They are illustrated in Figure 4. In Scenario A, the phenotypic optimum is at the left boundary of the phenotypic range in demes $1, \ldots, n/2$ (n even) and at the right boundary in the others. Thus, there is a single, abrupt environmental change in the middle of the spatial domain. In Scenario B, there is directional selection toward the extreme phenotypes (as in Scenario A) in the left and the right third of demes, whereas the trait is under stabilizing selection in the middle third. Thus,

there are two environmental steps and hybrids are favored in the middle of the spatial range. In Scenario C, the phenotypic optimum changes linearly from the left to the right boundary of the phenotypic range, thus reflecting a gradual change of the environment. In Scenario D, there is spatially uniform stabilizing selection toward the middle of the phenotypic range.

In the hybrid zone literature, selection schemes which disfavor hybrids everywhere (Scenario A) are sometimes referred to as 'ecotone zone', whereas selection schemes which favor intermediate genotypes (Scenarios B and C) are also known as 'hybrid superiority zones' (Kawakami and Butlin 2012). Although we assume exogenous selection, selection is not purely exogenous in the sense of Kruuk et al. (1999) because our fitnesses display dominance and epistasis.

Our study complements or extends previous investigations that were based on diffusion models in several ways. For instance, Felsenstein (1977) and Slatkin (1978) assumed a multivariate normal distribution of allelic effects. Felsenstein assumed a linearly changing optimum, as in our Scenario C, whereas Slatkin considered Scenarios A and C. Slatkin (1975) studied a diallelic two-locus diffusion model with a step environment (Scenario A) that can be interpreted as a model of a quantitative trait under linear directional selection. Except for different assumptions about selection, Slatkin's (1975) model is identical to our diffusion model (7.4). Barton (1983) and Barton and Shpak (2000) assumed multiple loci and spatially independent (endogenous) selection against hybrids (without or with epistasis, respectively). Kruuk et al. (1999) compared aspects of models of endogenous selection with a model similar to our Scenario C. Barton (1999) investigated a diffusion-based model that is equivalent to our diffusion model (7.4), except that his ignores LD. He compared his so-called rare-alleles model to several of the above mentioned models (which are stated in Appendix A.11).

Because clines result from polymorphic equilibria, we first summarize the results about equilibrium configurations and bifurcation patterns. The important limiting cases of weak and of strong migration are analyzed in Section 3. They apply to every migration pattern and selection scenario.

If migration is sufficiently weak relative to selection, then in selection scenarios B, C, and D there are multiple, simultaneously stable polymorphic equilibria for every migration pattern. Their number increases (approximately) exponentially in n and, for given n, from B to C to D (Section 5.2). For Scenarios B and C, the critical migration rate below which more than two polymorphic equilibria are simultaneously stable is usually one or two orders of magnitude smaller than the selection parameter s. This range is indicated by the orange bars in Figure 5. Its upper bound is the critical migration rate $m_{\mathrm{un}}^{\mathrm{X},\mathcal{M}}(\mathsf{I}^{2,3})$ (see also Table A.1). For Scenario

A and weak (or moderate) migration, there is always a unique fully polymorphic equilibrium (I^1), i.e., $m_{\mathrm{un}}^{\mathrm{X},\mathcal{M}}(\mathsf{I}^{2,3}) = 0$.

If migration is sufficiently strong relative to selection, then no polymorphism is maintained for any selection scenario or migration pattern because one of the haplotypes with intermediate phenotype (Ab or aB) swamps the whole population. In this case, the monomorphic equilibria M^2 and M^3 are the only stable equilibria. The critical migration rate $m_{\max}$ above which no stable polymorphism can be maintained is given by $m_{\mathrm{st}}^{\mathrm{X},\mathcal{M}}(\mathsf{M}^{2,3})$ for Scenarios $\mathrm{X} = \mathrm{A}, \mathrm{B}, \mathrm{C}$ and by $m_{\mathrm{un}}^{\mathrm{D},\mathcal{M}}(\mathsf{I}^{2,3})$ for Scenario D; see (5.17). The gray regions in Figure 5 show $m \geq m_{\max}$. Notably, for every given migration pattern, $m_{\max}$ decreases from Scenario A to B to C to D (5.18). Hence, in a step environment stable polymorphic equilibria can be maintained for much higher gene flow than in a gradually changing environment.

As the number of demes increases, $m_{\max}$ increases slowly (in proportion to $1-1/n$) for the island model and Scenarios A, B, and D; eqs. (5.9), (5.12), (5.14). In Scenario C, this can be violated for reasons explained in Section 5.3. For the stepping-stone model, $m_{\max}$ increases faster than linear in n for Scenarios A, B, and C (Figure 6). This much faster increase is not surprising because isolation by distance increases with the number of demes. Finally, for any given selection scenario, $m_{\max}$ increases from $\mathcal{I}$ to $\mathcal{S}_2$ to $\mathcal{S}$, again supporting the intuition that increasing isolation by distance facilitates the maintenance of polymorphism.

The range of migration rates between the critical values $m_{\mathrm{un}}^{\mathrm{X},\mathcal{M}}(\mathsf{I}^{2,3})$ and $m_{\max}$ can be partitioned into up to three different intervals in which there is either a unique, globally asymptotically stable internal equilibrium, I^1, or a pair of asymptotically stable internal equilibria, I^4 and I^5 (Section 5.3). For Scenario D, such an intermediate range does not exist because $m_{\max} = m_{\mathrm{un}}^{\mathrm{X},\mathcal{M}}(\mathsf{I}^{2,3})$. The range of migration rates for which there is a unique stable equilibrium decreases from Scenario A to B to C to D, for which it vanishes (Figure 5, Table A.1). Interestingly, every bifurcation pattern that was found for $n > 2$ in any of the selection scenarios occurs in essentially the same form for a certain range of positions of the optima (P and $-P$) in the two-deme model of Section 4. They are displayed in Figure 2. The only qualitative difference is that for two demes and weak migration, at most two internal equilibria are stable instead of many (up to $2^n - 2$ in Scenario D).

Stable polymorphic equilibria give rise to (stable) clines. Because our interest is in quantitative traits and how local adaptation and genetic variation depend on migration patterns and selection scenarios, we studied clines in the mean phenotype and in the (total) genetic variance. In addition, we investigated LD and its spatial dependence. Except for very weak migration ($m < m_{\mathrm{un}}^{\mathrm{X},\mathcal{M}}(\mathsf{I}^{2,3})$), when there are many simultaneously stable equilibria, the clines

in the mean, variance, and LD are unique even if the underlying polymorphic equilibria differ. This is due to the symmetry assumptions of the model (cf. Figure B.11).

In the language of hybrid zones, the results discussed above show that in a hybrid superiority zone clines exist only for lower migration rates than in an ecotone zone and, for very low migration rates, initial conditions play a more important role because of the existence of multiple clines. The reason for the former finding is that in a hybrid superiority zone, the haplotypes Ab and aB swamp the entire population easier than in an ecotone zone.

The shape of the clines is strongly influenced by both the migration pattern and by the selection scenario. This is exemplified by Figure 7 and documented extensively by Figures B.2, B.3, and B.4. In most cases, the degree of local adaptation (as measured by the deviation of the mean from the optimum) increases from migration pattern $\mathcal{I}$ to $\mathcal{S}_2$ to $\mathcal{S}$, i.e., with increasing isolation by distance. This seems to be universally true for Scenario A, but is violated for Scenario B in the demes with stabilizing selection (e.g., Figure 7d). In these demes, the island model provides maximum adaptation, whereas in the demes with directional selection the stepping-stone model ($\mathcal{S}$) maximizes local adaptation. There are also rare exceptions in Scenario C.

For the island model, the genetic variance is spatially uniform in Scenario A and weakly dependent on space in Scenarios B and C. In the latter, it may be maximized or minimized in the center, or it may be bimodal (Figures B.3, B.4). For the stepping-stone models and a step environment (Scenario A), the genetic variance is always maximized in the center of the cline and decreases toward its boundaries. For Scenarios B and C, the variance may be maximized in the center or elsewhere (Figures 7e,h). Distinctive bimodal patterns occur mainly for weak single-step migration (Figures B.3, B.4). The modes occur in demes at the boundary between regions of stabilizing and of directional selection.

An increase in m has a simple effect on local adaptation: it is progressively reduced until the cline collapses at $m_{\max}$. Its effects on the genetic variance are more complex, as is documented by Figures B.2, B.3, and B.4. However, the variance V_T of the total population is rather insensitive to changes of m over a wide range (Figure 8). It may be slowly decreasing in m or be maximized at intermediate values. In Scenario A, tight linkage may substantially increase V_T, whereas it is almost independent of r in Scenario B and C.

Next, we discuss LD and the role of recombination. The examples presented in Figure 7 are representative for a large range of parameters. A much more complete picture is obtained from Figures B.2, B.3, B.4 for $r = 0.5$ and Figures B.5, B.6, B.7 for $r = 0.05$. Although the details are complex, some general conclusions emerge.

(i) The highest linkage disequilibria occur in Scenario A in the demes adjacent to the environmental step. LD is always positive, as is expected under a balance between directional selection and migration (Li and Nei 1974, Christiansen and Feldman 1975, Slatkin 1975, Bürger and Akerman 2011, Akerman and Bürger 2014b), although this is not universally true in the presence of epistasis (Geroldinger and Bürger 2014). Of course, LD increases with tighter linkage.

(ii) In Scenario C, LD is very weak under stepping-stone migration. This is in line with Felsenstein's (1977) result that for normally distributed allelic effects and a linearly changing optimum, LD is absent at equilibrium. For the island model, small positive LD is maintained in the demes under directional selection and small negative LD otherwise.

(iii) The most complex patterns occur for Scenario B because in the central demes there is stabilizing selection which induces negative LD. In general, the absolute magnitude of LD is between those of Scenarios A and C, and stronger recombination obviously reduces LD. The typical spatial patterns are displayed in Figure 7f. Interestingly, for the stepping-stone models, LD is nearly absent for weak or moderately strong migration, but becomes appreciable for strong migration. For the island model, essentially the opposite is true; LD is relatively high for low migration and vanishes for large m (see Figure B.8 for details). The reason for this finding is the different degree of mixing exhibited by the migration patterns.

Because LD is low in Scenario B and almost absent in Scenario C, the clines in the mean and the variance are hardly affected by recombination or LD. In Scenario A, recombination and LD affect the clines as follows. Because lower r induces higher LD, the variance is somewhat inflated if the increase in LD is sufficiently high. For the stepping-stone model, this occurs near the center of the cline, and for the island model it is a spatially universal effect (Figure B.5). As in Slatkin's (1975) model, reduced r leads to a slightly steeper cline and to a slight increase in local adaptation. The reason is that stronger positive LD strengthens selection at each locus (cf. Barton 1983).

The approximations for LD based on the assumptions of neutrality (7.3) or quasi-linkage equilibrium (Barton and Shpak 2000, eq. (14)) perform well in Scenarios B and C if migration is sufficiently weak, so that LD is very small (Figure B.10). In Scenario A, but not otherwise, a variant of (7.3) performs very well over a wide range of migration rates. If migration is not weak, the neutral approximation (7.3) tends to overestimate LD, whereas the quasi-linkage-equilibrium approximation tends to underestimate it.

The majority of our numerical results is based on the assumption of strong selection. The choice $s = 0.2$ in many of the figures implies that in the demes under directional selection, the

fitness of the least fit phenotype is only 20% of that of the optimum phenotype. In Scenario A, this applies to every deme. Nevertheless, comparison of the 12-deme model to the diffusion model (7.4), whose derivation is based on the assumption of weak evolutionary forces (Nagylaki 1975, 1989a), shows excellent concordance (Figure 10, Figure B.11). Therefore, most of our discussion above carries over to the corresponding diffusion models. These figures (as well as the discussion above) also show that Barton's (1999) 'rare-alleles' diffusion model (eq. (A.39) in Appendix A), which ignores LD, provides accurate approximations to the clines in the mean and the variance unless loci are tightly linked. The Gaussian model (eq. (A.38)) yields almost accurate clines in the mean, but distinctively deviant ones in the variance.

Finally, most of our analysis is based on symmetry assumptions. Throughout, we assumed a one-to-one correspondence of demes in which the phenotypic optimum is P or $-P$, and we assumed symmetric migration (3.7). Most of the analysis is also based on the assumption of loci of equal effects. Deviation from any of these assumptions will have multiple consequences. First, most pitchfork bifurcations will be replaced by (pairs of) saddle-node bifurcations. Second, different polymorphic equilibria will give rise to different clines, hence clines in the mean, variance, and LD will no longer be unique, unless there is a unique polymorphic equilibrium (corresponding to I^1). Third, stability of single-locus polymorphisms will be facilitated. Forth, even in the limit of strong migration, a globally stable fully polymorphic equilibrium (hence a cline) can be maintained if locus effects are sufficiently different and linkage is tight (Section 7.3). Therefore, $m_{\max}$ can be infinite. As demonstrated by Geroldinger and Bürger (2014) for a haploid model, even if $m_{\max}$ is finite, a reduction of the ratio κ of locus effects can lead to an increase or a decrease of $m_{\max}$, depending on whether recombination is low or high. Fifth, deviation from the symmetry assumptions about selection or migration will, in general, lead to a reduction of $m_{\max}$ by facilitating fixation of the haplotype with the highest mean fitness, i.e., averaged across demes and weighted by the principal eigenvector of the migration matrix.

Acknowledgments. We are grateful to Professors Eva Kisdi and Thomas Nagylaki for their comments on a previous version. Financial support by the Austrian Science Fund (FWF) through the Vienna Graduate School of Population Genetics (Project W1225) and Project P25188 is gratefully acknowledged.

A Appendix

A.1 The internal equilibrium for $m = 0$

We prove that in a panmictic population a unique internal equilibrium F exists if $0 \leq P < 3/4$. If $P \geq 3/4$, no internal equilibrium exists and M^4 is globally asymptotically stable. The case $P \leq 0$ follows from symmetry. Under the assumption of linkage equilibrium, this result was shown by Hastings and Hom (1990)

The dynamics is given by (2.3a), where we suppress the deme label k. From (2.3a) we deduce easily

$$\frac{x_2'}{x_3'} - \frac{x_2}{x_3} = \frac{rw_{14}(x_3 - x_2)D}{x_3(x_3w_3 + rw_{14}D)}. \tag{A.1}$$

Therefore, equilibria satisfy $x_2 = x_3$ or $D = 0$. From the recursion for D, it is easily verified that an internal equilibrium does not satisfy $D = 0$. Therefore, every internal equilibrium satisfies $x_2 = x_3$ or, equivalently in terms of allele frequencies, $p = q$. We leave the proof that in the simple case of $P = 0$ the unique internal equilibrium is given by $p = q = 1/2$ and $D = (4r - \sqrt{16r^2 + s^2})/(4s)$ to the reader. As in the main text we assume $r > 0$.

From (2.3a), we deduce easily

$$\bar{w}(p' - p) = \frac{s}{4}\left[p(1-p)(3 - 4P - 2p - 4q) + D(1 - 4P - 2q)\right]. \tag{A.2}$$

By solving $p' - p = 0$ we find that every equilibrium with $p = q$ satisfies

$$D = -\frac{p(1-p)(6p + 4P - 3)}{2p + 4P - 1}. \tag{A.3}$$

From the constraints $x_i \geq 0$ and $\sum_{i=1}^4 x_i = 1$, one obtains that D has to fulfill

$$-\min\left\{pq, (1-p)(1-q)\right\} \leq D \leq \min\left\{p(1-q), (1-p)q\right\}. \tag{A.4}$$

If $p = q$, $P > 0$, and $r > 0$, straightforward calculations show that D given by (A.3) satisfies (A.4) if and only if $0 < p < 1/2$ and $1/2 < p + P < 3/4$, which can be rearranged as

$$\pi_1 < p < \pi_2, \tag{A.5}$$

where $\pi_1 = \max\left\{0, \frac{1}{2} - P\right\}$ and $\pi_2 = \min\left\{\frac{1}{2}, \frac{3}{4} - P\right\}$.

Substituting $q = p$ and (A.3) into $D' = D$, we obtain that the coordinate p of an internal equilibrium must be a zero of the quartic polynomial

$$\psi(p) = \phi_1(p) - \phi_2(p), \tag{A.6a}$$

where

$$\phi_1(p) = 4^3 s \left(\frac{1}{2} - p\right)\left(p + P - \frac{1}{2}\right)\left(\frac{3}{4} - p - P\right)\left(p + P - \frac{1}{4}\right), \tag{A.6b}$$

$$\phi_2(p) = 12r(1 - sP^2)\left(p + 2P - \frac{1}{2}\right)\left(p + \frac{2}{3}P - \frac{1}{2}\right). \tag{A.6c}$$

Now we assume $0 < P < 3/4$. By distinguishing the three cases $0 < P \leq 1/4$, $1/4 < P < 1/2$, and $1/2 \leq P < 3/4$, the following can be shown, where we assume (A.5):

(i) $\phi_1(\pi_1) \geq 0 > \phi_2(\pi_1)$ and $0 = \phi_1(\pi_2) < \phi_2(\pi_2)$,

(ii) $\phi_1(p_0) > 0$ if $p_0 \in (\pi_1, \pi_2)$,

(iii) if $p_0 \in (\pi_1, \pi_2)$, then $\frac{d\phi_1}{dp}(p_0) > 0$ implies $\frac{d^2\phi_1}{dp^2}(p_0) < 0$,

(iv) ϕ_1 has no minimum in (π_1, π_2) (follows from (iii)) and at most one (local) maximum,

(v) if ϕ_1 has no maximum in (π_1, π_2), it is strictly monotone decreasing (occurs only if $P \gtrapprox 0.629$),

(v) $\frac{d\phi_2}{dp}(p_0) > 0$ and $\frac{d^2\phi_2}{dp^2}(p_0) > 0$ for every $p_0 \in (\pi_1, \pi_2)$.

Therefore, there exists a unique $\hat{p}$ satisfying (A.5) and $\psi(\hat{p}) = 0$. Because the interval (A.5) contains the admissible solutions, $\hat{p}$ gives rise to the unique internal equilibrium F. In addition, $\phi_2(1/2 - 2P/3) = 0$ implies $\hat{p} > 1/2 - 2P/3$, whence $\hat{D} < 0$. If $P \to 3/4$, then $\hat{p} \to 0$ and $\mathsf{F} \to \mathsf{M}^4$.

Finally, we prove global asymptotic stability of M^4 if $P \geq 3/4$. First, assume $p + q < 1$. Then $pq < (1-p)(1-q)$ and (A.4) shows that $D \geq -pq$. Substituting this into (A.2) and observing that $1 - 4P - 2q < 0$, we deduce that

$$\bar{w}(p' - p) \leq -\frac{s}{4}p(1 - p - q)(4P - 3 + 2p + 2q) < 0 \tag{A.7}$$

if $p > 0$. Similarly, $\bar{w}(p' - p) < 0$ if $p + q > 1$. Therefore, $p(t)$ converges monotonically to 0. By symmetry, the same holds for $q(t)$.

A.2 Proof of Proposition 3.1

If $m = 0$, the equilibrium configuration in deme k is determined by the position of the optimum P_k, which partitions the phenotypic range into five intervals with differing equilibrium configurations (Section 3.1). Accordingly, the sets N_i in Proposition 3.1 partition the set of demes into five groups. It can be verified that M^1_k, G_k, H_k, J_k, and M^4_k are hyperbolic if $k \in N_1$, $k \in N_2$, $k \in N_3$, $k \in N_4$, and $k \in N_5$, respectively. Depending on the values P_k, up to four sets N_i can be empty. From the results in Section 3.1 and the perturbation theory in Karlin and McGregor (1972b) it follows immediately that the equilibria given by (3.5) exist and are

asymptotically stable. The equilibria in (3.6) are admissible because they are perturbations of either the only internal unstable equilibrium (F) or of transversally stable equilibria, whose unstable components (F_k) are internal.

A.3 Proof of Proposition 3.4

The derivation of the first statement follows from the perturbation theory in Bürger (2009a) is analogous to that in Section 5 of Geroldinger and Bürger (2014). It is based on the fact that for sufficiently strong migration the dynamics (2.3) converges to its so called strong-migration limit in which the genotype frequencies become identical among demes (Nagylaki and Lou 2007; Bürger 2009a). The strong-migration limit has the same dynamics as the continuous-time version of the panmictic model in Section 3.1, but with suitably averaged optimum $\bar{P}$. Assumption (3.7) implies that $\bar{P} = 0$ for every n. The uniqueness of the internal equilibrium follows from Appendix A.1 or Bürger (2000), p. 207.

Because $\kappa = 1$, the equilibrium configuration of the panmictic model with $\bar{P} = 0$, and hence the equilibrium configuration of the strong-migration limit, is independent of the recombination rate r (Bürger 2000, p. 208).

Second, we prove that the critical migration rate $m_{\mathrm{st}}^{\mathrm{X},\mathcal{M}}(\mathsf{M}^{2,3})$ at which M^2 and M^3 become asymptotically stable is independent of r. We consider allele frequencies p_k, q_k, and LD D_k instead of gamete frequencies and assume the following ordering of the variables $(p_1, \ldots, p_n, q_1, \ldots, q_n, D_1, \ldots, D_n)$. Then the Jacobian of the discrete dynamics (2.3) at M^2 or M^3 (expressed in terms p_k, q_k, and D_k) is of the form

$$J = \begin{pmatrix} \mathcal{M}J_p & 0 & \mathcal{M}\tilde{J}_p \\ 0 & \mathcal{M}J_q & \mathcal{M}\tilde{J}_q \\ 0 & 0 & \mathcal{M}J_D \end{pmatrix}, \tag{A.8}$$

where each block is an $n \times n$ matrix. The matrices J_p, $\tilde{J}_p$, J_q, $\tilde{J}_q$, and J_D are diagonal matrices resulting from linearization of the dynamics in the absence of migration. Obviously, the set of eigenvalues of J is the union of the sets of eigenvalues of $\mathcal{M}J_p$, $\mathcal{M}J_q$, and $\mathcal{M}J_D$. The first two sets are independent of r because they pertain to the marginal one-locus systems corresponding to M^2 or M^3.

Because $\kappa = 1$, the diagonal entries of J_D are $1 - r$, whence the eigenvalues of $\mathcal{M}J_D$ are $(1 - r)\lambda_k$, where λ_k is the kth eigenvalue of $\mathcal{M}$. Because $|\lambda_k| \leq 1$, the stability conditions of M^2 and M^3 are independent of r.

If $\kappa < 1$, the eigenvalues of $\mathcal{M}J_D$ are $(1-r)(w_{14,k}/w_{22,k})\lambda_k$. Because $w_{14,k}/w_{22,k}$ depends on k and may exceed unity, $m_{\mathrm{st}}^{\mathrm{X},\mathcal{M}}(\mathsf{M}^{2,3})$ depends on r.

A.4 Approximations of equilibria

If all evolutionary forces are weak, the discrete dynamical system (2.3) can be approximated by the following system of differential equations

$$\dot{x}_{i,k} = \frac{d}{dt}x_{i,k} = x_{i,k}(w_{i,k} - \overline{w}_k) - \eta_i r D_k + \sum_{l=1}^{n} \tilde{m}_{kl} x_{i,l}, \tag{A.9}$$

where $\tilde{m}_{kl} = m_{kl} - \delta_{kl}$ and δ_{kl} is the Kronecker-Delta. The systems (A.9) and (2.3) have the same equilibrium configurations if r is redefined. A derivation of (A.9) from (2.3) can be found in Section 5.3 of Bürger (2009a).

In the following we present approximations for the coordinates of the equilibria I^1, I^2, I^3, I^4 and I^5 by assuming (A.9) and $n = 2$. The accuracy of these approximations is demonstrated in Figure B.13. Under the assumption of linkage equilibrium ($D = 0$), I^1 is given by (4.4) and

$$p_1(\mathsf{I}^1) = q_1(\mathsf{I}^1) = \frac{1}{2} + \frac{2P}{9} - \frac{\sqrt{s\,(144m + 27s + 16P^2 s)}}{9s}\ \mathrm{Sin}\left[\frac{1}{3}\ \mathrm{ArcSin}\left[\frac{4Ps\left(216m - 81s + 16P^2 s\right)}{\sqrt{s\,(144m + 27s + 16P^2 s)^3}}\right]\right]. \tag{A.10}$$

If $P = 0$ and assuming linkage equilibrium ($D = 0$), the coordinates of the equilibria I^2 and I^3 are given by (4.4) and

$$p_1(\mathsf{I}^2) = q_1(\mathsf{I}^3) = \frac{1}{2} - \frac{1}{2}\sqrt{1 - \frac{16m}{s}}, \tag{A.11a}$$

$$q_1(\mathsf{I}^2) = p_1(\mathsf{I}^3) = \frac{1}{2} + \frac{1}{2}\sqrt{1 - \frac{16m}{s}}, \tag{A.11b}$$

which leads to

$$m_{\mathrm{na}}(\mathsf{I}^{2,3}) = \frac{s}{16}. \tag{A.12}$$

The coordinates of the equilibria I^4 and I^5 are given by

$$p_1(\mathsf{I}^5) = q_1(\mathsf{I}^4) = P + \frac{1}{2} - \frac{\sqrt{8m + s}}{4\sqrt{s}} - \frac{1}{4}\sqrt{9 + 16P^2 + \frac{40m}{s} - \frac{24P\sqrt{8m + s}}{\sqrt{s}}}, \tag{A.13a}$$

$$q_1(\mathsf{I}^5) = p_1(\mathsf{I}^4) = P + \frac{1}{2} - \frac{\sqrt{8m + s}}{4\sqrt{s}} + \frac{1}{4}\sqrt{9 + 16P^2 + \frac{40m}{s} - \frac{24P\sqrt{8m + s}}{\sqrt{s}}}, \tag{A.13b}$$

$$D_1(\mathsf{I}^4) = D_1(\mathsf{I}^5) = 0, \tag{A.13c}$$

and (5.6), but here $\hat{D}_1(\mathsf{I}^4) = \hat{D}_1(\mathsf{I}^5) = 0$ is a result, not a simplifying assumption. The migration rates $m_{\mathrm{na}}(\mathsf{I}^{4,5}) = m_{\mathrm{st}}(\mathsf{I}^1)$ and $m_{\mathrm{ad}}(\mathsf{I}^{4,5}) = m_{\mathrm{un}}(\mathsf{I}^1)$ can be calculated from (A.13) and are given by

$$m_{\mathrm{na}}(\mathsf{I}^{4,5}) = m_{\mathrm{st}}(\mathsf{I}^1) = s\left(\frac{26}{25}P^2 - \frac{6}{25}P\sqrt{16P^2 - 5} - \frac{9}{40}\right), \tag{A.14a}$$

$$m_{\mathrm{ad}}(\mathsf{I}^{4,5}) = m_{\mathrm{un}}(\mathsf{I}^1) = s\left(\frac{26}{25}P^2 + \frac{6}{25}P\sqrt{16P^2-5} - \frac{9}{40}\right). \tag{A.14b}$$

A.5 The functions F_i

The functions F_1, F_2, F_3, and F_4 used in Figure 2 are given by

$$F_1(p_1,p_2) = G(p_1,p_2,\frac{1}{2},\frac{1}{2},0,1), \tag{A.15a}$$

$$F_2(p_1,p_2,q_2,q_2) = q_1+q_2-(p_1+p_2), \tag{A.15b}$$

$$F_3(p_1,p_2) = G(p_1,p_2,\frac{5}{2},\frac{4}{5},\frac{1}{2},1), \tag{A.15c}$$

$$F_4(p_1,p_2) = G(p_1,p_2,8,\frac{9}{10},\frac{7}{10},1), \tag{A.15d}$$

where

$$\begin{aligned} G(p_1,p_2,k_1,k_2,k_3,k_4) = {} & p_1 + k_1p_2(p_1-k_2)(p_1-k_3) \\ & - (1-k_1p_2)(p_1-k_3)(p_1-k_4) \\ & + k_1p_2(p_1-k_2)(p_1-k_4). \end{aligned} \tag{A.15e}$$

The functions F_2 and G were guessed from the properties of I_1, I_2, I_3, I_4, I_5; see Proposition 5.2. The values k_i for F_1, F_3, and F_4 were obtained by numerical trials.

A.6 Properties of the island model

The following proposition demonstrates the lack of spatial structure in the island model.

Proposition A.1. *The coordinates of the equilibria depend on k only through P_k.*

Proof. Let $\hat{x}$ be an equilibrium. From the recursion relation (2.3c) and the migration rates (5.1) in the island model we obtain for every deme k:

$$\begin{aligned} \hat{x}_{i,k} = \hat{x}'_{i,k} &= m_{kk}\hat{x}^{(s)}_{i,k} + \sum_{l\neq k} m_{kl}\hat{x}^{(s)}_{i,l} \\ &= (1-m)\hat{x}^{(s)}_{i,k} - \frac{m}{n-1}\hat{x}^{(s)}_{i,k} + \frac{m}{n-1}\sum_l \hat{x}^{(s)}_{i,l} \\ &= \left(1-m-\frac{m}{n-1}\right)\hat{x}^{(s)}_{i,k} + \frac{m}{n-1}c_i \quad \text{for every gamete } i, \end{aligned} \tag{A.16}$$

where c_i is independent of k (but depends on the model parameters, including the set of values P_k). By the structure of (2.3a), $\hat{x}^{(s)}_{i,k}$ depends on k only through $\hat{x}_k$ and P_k. Therefore, the solution $\hat{x}_k$ of (A.16) depends on k only through P_k. □

The next proposition demonstrates a close relation of the island model to models that have as many demes as different optima.

Proposition A.2. *1. Let $\hat{x} = (\hat{x}_1, \hat{x}_2)$ be an equilibrium of the two-deme model with optima $P_1 = -P_2 = -P$ and migration rate m. Let n be even and*

$$P_k = \begin{cases} -P & \text{if } 1 \le k \le \frac{n}{2}, \\ P & \text{if } \frac{n}{2} < k \le n. \end{cases} \tag{A.17}$$

Then $(\underbrace{\hat{x}_1, \ldots, \hat{x}_1}_{n/2}, \underbrace{\hat{x}_2, \ldots, \hat{x}_2}_{n/2})$ is an equilibrium of the island model with migration rate $\bar{m} = 2\left(1 - \frac{1}{n}\right) m$.

2. Let $\hat{x} = (\hat{x}_1, \hat{x}_2, \hat{x}_3)$ be an equilibrium of a three-deme model with optima $P_1 = -P_3 = -P$, $P_2 = 0$, and migration rate m. Let n be a multiple of three and

$$P_k = \begin{cases} -P & \text{if } 1 \le k \le \frac{n}{3}, \\ 0 & \text{if } \frac{n}{3} < k \le \frac{2n}{3}, \\ P & \text{if } \frac{2n}{3} < k \le n. \end{cases} \tag{A.18}$$

Then $(\underbrace{\hat{x}_1, \ldots, \hat{x}_1}_{n/3}, \underbrace{\hat{x}_2, \ldots, \hat{x}_2}_{n/3}, \underbrace{\hat{x}_3, \ldots, \hat{x}_3}_{n/3})$ is an equilibrium of the island model with migration rate $\bar{m} = \frac{3}{2}\left(1 - \frac{1}{n}\right) m$.

Proof. 1. The assumption implies that in the two-deme model $\hat{x}'_{i,2} = \hat{x}_{i,2} = m\hat{x}^{(s)}_{i,1} + (1-m)\hat{x}^{(s)}_{i,2}$. Because islands with the same position of the optimum are exchangeable, it is sufficient to show that $\hat{x}'_{i,n} - \hat{x}_{i,n} = 0$ for $\bar{m}$ in the island model. Since $\hat{x}_{i,h} = \hat{x}_{i,1}$ for every $h \le n/2$, we also have $\hat{x}^{(s)}_{i,h} = \hat{x}^{(s)}_{i,1}$ for every $h \le n/2$. Analogously, $\hat{x}^{(s)}_{i,h} = \hat{x}^{(s)}_{i,2}$ for every $h > n/2$. Therefore, (2.3) and (5.1) yield

$$\begin{aligned} \hat{x}'_{i,n} - \hat{x}_{i,n} &= \frac{\bar{m}}{n-1} \sum_{h \ne n} \hat{x}^{(s)}_{i,h} + (1-\bar{m})\hat{x}^{(s)}_{i,n} - \hat{x}_{i,2} \\ &= \frac{2m}{n}\left(\frac{n}{2}\hat{x}^{(s)}_{i,1} + \left(\frac{n}{2} - 1\right)\hat{x}^{(s)}_{i,2}\right) + \left(1 - 2m\left(1 - \frac{1}{n}\right)\right)\hat{x}^{(s)}_{i,2} - \hat{x}_{i,2} \\ &= m\hat{x}^{(s)}_{i,1} + m\left(1 - \frac{2}{n}\right)\hat{x}^{(s)}_{i,2} + \left(1 - 2m\left(1 - \frac{1}{n}\right)\right)\hat{x}^{(s)}_{i,2} - \left(m\hat{x}^{(s)}_{i,1} + (1-m)\hat{x}^{(s)}_{i,2}\right) \\ &= \left[m\left(1 - \frac{2}{n}\right) + \left(1 - 2m\left(1 - \frac{1}{n}\right)\right) - (1-m)\right]\hat{x}^{(s)}_{i,2} = 0. \end{aligned}$$

The proof of 2. is analogous. □

The following proposition shows that in the island model with Scenario B and weak migration, LD is non-positive in the demes under stabilizing selection and positive in the demes under directional selection.

Proposition A.3. *In the island model with Scenario B, first-order weak-migration approximations yield that at all stable equilibria*

$$\hat{D}_l \leq 0 \quad \text{if } P_l = 0, \text{ i.e., } n/3 < l \leq 2n/3, \text{ (stabilizing selection)}, \tag{A.19}$$

$$\hat{D}_l > 0 \quad \text{if } |P_l| = 1, \text{ i.e., } l \leq n/3 \text{ or } l > 2n/3, \text{ (directional selection)}. \tag{A.20}$$

Proof. Let $\mathsf{E} = \prod_{k=1}^{n} \mathsf{E}_k$ be a stable equilibrium for $m = 0$ and $\hat{x}_{i,l}$ the frequency of gamete i in deme l at E. If $|P_l| = 1$, then $\mathsf{E}_l \in \{\mathsf{M}_{1,l}, \mathsf{M}_{4,l}\}$, whereas $\mathsf{E}_l \in \{\mathsf{M}_{2,l}, \mathsf{M}_{3,l}\}$ if $P_l = 0$. The proportions of gametes i immigrating into deme l are given by $\phi_{i,l} = \sum_{k \neq l} m_{lk} \hat{x}_{i,k} = \frac{m}{n-1} \sum_{k \neq l} \hat{x}_{i,k}$. The $\phi_{i,l}$ are independent of P_k, since the E_k are monomorphic equilibria. Therefore, the vector $\phi_l = (\phi_{1,l}, \phi_{2,l}, \phi_{3,l}, \phi_{4,l})$ is of the form:

$$\phi_l = \frac{m}{n-1}\left(\frac{n}{3} - 1, u, \frac{n}{3} - u, \frac{n}{3}\right), \qquad 0 \leq u \leq \frac{n}{3}, \quad \text{if } \mathsf{E}_l = \mathsf{M}_{1,l}, \tag{A.21a}$$

$$\phi_l = \frac{m}{n-1}\left(\frac{n}{3}, u, \frac{n}{3} - u, \frac{n}{3}\right), \qquad 1 \leq u \leq \frac{n}{3}, \quad \text{if } \mathsf{E}_l = \mathsf{M}_{2,l}, \tag{A.21b}$$

$$\phi_l = \frac{m}{n-1}\left(\frac{n}{3}, u, \frac{n}{3} - u, \frac{n}{3}\right), \qquad 0 \leq u \leq \frac{n}{3} - 1, \quad \text{if } \mathsf{E}_l = \mathsf{M}_{3,l}, \tag{A.21c}$$

$$\phi_l = \frac{m}{n-1}\left(\frac{n}{3}, u, \frac{n}{3} - u, \frac{n}{3} - 1\right), \qquad 0 \leq u \leq \frac{n}{3}, \quad \text{if } \mathsf{E}_l = \mathsf{M}_{4,l}. \tag{A.21d}$$

The coordinates of the weak-migration perturbation of E in deme l are obtained from a four deme island-model with optima $P_1 = -1$, $P_2 = P_3 = 0$, $P_4 = 1$, migration matrix $((1-m)\delta_{kl} + \phi_{k,l})_{kl}$ and some appropriate u (δ_{kl} denotes the Kronecker-Delta). Calculating $\hat{D}_l$ for weak migration in the four-deme model shows that $\hat{D}_l \leq 0$ if $P_l = 0$ and $\hat{D}_l > 0$ if $|P_l| = 1$ for all u. □

Remark A.4. If (A.20) is relaxed to $\hat{D}_l \geq 0$, the statement of Proposition (A.3) also holds for the stepping-stone model. Since only neighboring demes influence first-order weak-migration approximations in the stepping-stone model, it is sufficient to consider three demes $l-1$, l, $l+1$ with suitable positions of the optima. With a case distinction depending on the stable equilibria in the demes $l-1$ and $l+1$ one can show the assertion with *Mathematica* by calculating $\hat{D}_l$ for weak migration.

A.7 Migration matrices of the generalized stepping-stone model

We use the following matrices of $\mathcal{S}_2$ for $n = 6$ and $n = 12$:

$$\begin{pmatrix} 1-m & \frac{2m}{3} & \frac{m}{3} & 0 & 0 & 0 \\ \frac{m}{2} & 1-m & \frac{m}{3} & \frac{m}{6} & 0 & 0 \\ \frac{m}{6} & \frac{m}{3} & 1-m & \frac{m}{3} & \frac{m}{6} & 0 \\ 0 & \frac{m}{6} & \frac{m}{3} & 1-m & \frac{m}{3} & \frac{m}{6} \\ 0 & 0 & \frac{m}{6} & \frac{m}{3} & 1-m & \frac{m}{2} \\ 0 & 0 & 0 & \frac{m}{3} & \frac{2m}{3} & 1-m \end{pmatrix} \tag{A.22a}$$

$$\begin{pmatrix}
1-m & \frac{m}{2} & \frac{m}{4} & \frac{m}{8} & \frac{m}{8} & 0 & 0 & 0 & 0 & 0 & 0 & 0 \\
\frac{m}{2} & 1-m & \frac{m}{4} & \frac{m}{8} & \frac{m}{16} & \frac{m}{16} & 0 & 0 & 0 & 0 & 0 & 0 \\
\frac{m}{4} & \frac{m}{4} & 1-m & \frac{m}{4} & \frac{m}{8} & \frac{m}{16} & \frac{m}{16} & 0 & 0 & 0 & 0 & 0 \\
\frac{m}{8} & \frac{m}{8} & \frac{m}{4} & 1-m & \frac{m}{4} & \frac{m}{8} & \frac{m}{16} & \frac{m}{16} & 0 & 0 & 0 & 0 \\
\frac{m}{16} & \frac{m}{16} & \frac{m}{8} & \frac{m}{4} & 1-m & \frac{m}{4} & \frac{m}{8} & \frac{m}{16} & \frac{m}{16} & 0 & 0 & 0 \\
0 & \frac{m}{16} & \frac{m}{16} & \frac{m}{8} & \frac{m}{4} & 1-m & \frac{m}{4} & \frac{m}{8} & \frac{m}{16} & \frac{m}{16} & 0 & 0 \\
0 & 0 & \frac{m}{16} & \frac{m}{16} & \frac{m}{8} & \frac{m}{4} & 1-m & \frac{m}{4} & \frac{m}{8} & \frac{m}{16} & \frac{m}{16} & 0 \\
0 & 0 & 0 & \frac{m}{16} & \frac{m}{16} & \frac{m}{8} & \frac{m}{4} & 1-m & \frac{m}{4} & \frac{m}{8} & \frac{m}{16} & \frac{m}{16} \\
0 & 0 & 0 & 0 & \frac{m}{16} & \frac{m}{16} & \frac{m}{8} & \frac{m}{4} & 1-m & \frac{m}{4} & \frac{m}{8} & \frac{m}{8} \\
0 & 0 & 0 & 0 & 0 & \frac{m}{16} & \frac{m}{16} & \frac{m}{8} & \frac{m}{4} & 1-m & \frac{m}{4} & \frac{m}{4} \\
0 & 0 & 0 & 0 & 0 & 0 & \frac{m}{16} & \frac{m}{16} & \frac{m}{8} & \frac{m}{4} & 1-m & \frac{m}{2} \\
0 & 0 & 0 & 0 & 0 & 0 & 0 & \frac{m}{8} & \frac{m}{8} & \frac{m}{4} & \frac{m}{2} & 1-m
\end{pmatrix} \tag{A.22b}$$

A.8 The equilibria I_j for weak migration

The following equilibria play a central role in our analysis. Let n be even and migration weak. We recall Proposition 3.1 and define

$$\mathsf{I}^1 = I_m\left(\prod_{k\in N_1}\mathsf{M}_k^1 \times \prod_{k\in N_2\cup N_3\cup N_4}\mathsf{F}_k \times \prod_{k\in N_5}\mathsf{M}_k^4\right), \tag{A.23a}$$

$$\mathsf{I}^2 = I_m\left(\prod_{k\in N_1}\mathsf{M}_k^1 \times \prod_{k\in N_2}\mathsf{E}_k^{\mathcal{B},1} \times \prod_{k=v}^{\frac{n}{2}}\mathsf{M}_k^2 \times \prod_{k=\frac{n}{2}+1}^{w}\mathsf{M}_k^3 \times \prod_{k\in N_4}\mathsf{E}_k^{\mathcal{B},0} \times \prod_{k\in N_5}\mathsf{M}_k^4\right), \tag{A.23b}$$

$$\mathsf{I}^3 = I_m\left(\prod_{k\in N_1}\mathsf{M}_k^1 \times \prod_{k\in N_2}\mathsf{E}_k^{\mathcal{A},1} \times \prod_{k=v}^{\frac{n}{2}}\mathsf{M}_k^3 \times \prod_{k=\frac{n}{2}+1}^{w}\mathsf{M}_k^2 \times \prod_{k\in N_4}\mathsf{E}_k^{\mathcal{A},0} \times \prod_{k\in N_5}\mathsf{M}_k^4\right), \tag{A.23c}$$

where $v = |N_1| + |N_2| + 1$, $w = n - |N_4| - |N_5| - 1$, and

$$\mathsf{I}^4 = I_m\left(\prod_{k\in N_1}\mathsf{M}_k^1 \times \prod_{k\in N_2}\mathsf{E}_k^{\mathcal{B},1} \times \prod_{k\in N_3}\mathsf{M}_k^2 \times \prod_{k\in N_4}\mathsf{E}_k^{\mathcal{A},0} \times \prod_{k\in N_5}\mathsf{M}_k^4\right), \tag{A.23d}$$

$$\mathsf{I}^5 = I_m\left(\prod_{k\in N_1}\mathsf{M}_k^1 \times \prod_{k\in N_2}\mathsf{E}_k^{\mathcal{A},1} \times \prod_{k\in N_3}\mathsf{M}_k^3 \times \prod_{k\in N_4}\mathsf{E}_k^{\mathcal{B},0} \times \prod_{k\in N_5}\mathsf{M}_k^4\right). \tag{A.23e}$$

In the following we specify the stable equilibria for each of the selection scenarios (5.4).

In Scenario A, we obtain that I^1 is the unique stable equilibrium for weak migration by observing that $N_2 = N_3 = N_4 = \emptyset$.

In Scenario B we have $N_2 = N_4 = \emptyset$. Therefore, for weak migration the stable internal equilibria are given by

$$I_m\left(\prod_{k=1}^{n/3}\mathsf{M}_k^1 \times \prod_{k=n/3+1}^{2n/3}\mathsf{G}_k \times \prod_{k=2n/3+1}^{n}\mathsf{M}_k^4\right), \tag{A.24a}$$

$$\mathsf{G}_k \in \{\mathsf{M}_k^2, \mathsf{M}_k^3\}. \tag{A.24b}$$

In Scenario C the stable internal equilibria for weak migration are given by

$$I_m\left(\prod_{1\le k\le n_1}\mathsf{M}_k^1 \times \prod_{n_1<k\le n_2}\mathsf{G}_k \times \prod_{n_2<k\le n_3}\mathsf{H}_k \times \prod_{n_3<k\le n_4}\mathsf{J}_k \times \prod_{n_4<k\le n}\mathsf{M}_k^4\right), \tag{A.25a}$$

where

$$\mathsf{G}_k \in \{\mathsf{E}_k^{\mathcal{A},1}, \mathsf{E}_k^{\mathcal{B},1}\},\ \mathsf{H}_k \in \{\mathsf{M}_k^2, \mathsf{M}_k^3\}, \mathsf{J}_k \in \{\mathsf{E}_k^{\mathcal{A},0}, \mathsf{E}_k^{\mathcal{B},0}\}, \tag{A.25b}$$

and

$$n_1 = \lfloor\frac{7+n}{8}\rfloor, n_2 = \lfloor\frac{1}{8}(5+3n)\rfloor, n_3 = \lfloor\frac{1}{8}(3+5n)\rfloor, n_4 = \lfloor\frac{1}{8}(1+7n)\rfloor. \tag{A.25c}$$

Hence, the number of stable internal equilibria is

$$2^{n_4-n_1}, \tag{A.26}$$

which simplifies to $2^{3(n-1)/4}$ if $n = 8q+1$ for some q.

In Scenario D we have $N_1 = N_2 = N_4 = N_5 = \emptyset$. Therefore, for weak migration the stable equilibria are given by

$$I_m\left(\prod_{k=1}^{n}\mathsf{G}_k\right), \quad \text{where } \mathsf{G}_k \in \{\mathsf{M}_k^2, \mathsf{M}_k^3\}. \tag{A.27}$$

Except when $\mathsf{G}_k = \mathsf{M}_k^2$ for every k or $\mathsf{G}_k = \mathsf{M}_k^3$ for every k, these equilibria are internal.

A.9 Critical migration rates

		Island				Generalized stepping-stone				Stepping-stone			
$s = 0.1, r = 0.5$	n=6	A	B	C	D	A	B	C	D	A	B	C	D
	$m_{\text{un}}^{\text{X},\mathcal{M}}(\mathsf{I}^{2,3})$	0	0.009	0.008	0.008	0	0.008	0.007	0.008	0	0.007	0.007	0.035
	$m_{\text{st}}^{\text{X},\mathcal{M}}(\mathsf{I}^{1})$	0	0.021	0.029	-	0	0.029	0.058	-	0	0.047	-	-
	$m_{\text{un}}^{\text{X},\mathcal{M}}(\mathsf{I}^{1})$	0.220	0.138	0.063	-	*	0.396	0.159	-	*	*	-	-
	$m_{\text{st}}^{\text{X},\mathcal{M}}(\mathsf{M}^{2,3})$	0.245	0.187	0.140	0	*	*	0.378	0	*	*	*	0
	n=12												
	$m_{\text{un}}^{\text{X},\mathcal{M}}(\mathsf{I}^{2,3})$	0	0.010	0.005	0.008	0	0.010	0.010	0.042	0	0.014	0.015	0.203
	$m_{\text{st}}^{\text{X},\mathcal{M}}(\mathsf{I}^{1})$	0	0.023	-	-	0	0.044	0.117	-	0	0.163	-	-
	$m_{\text{un}}^{\text{X},\mathcal{M}}(\mathsf{I}^{1})$	0.242	0.152	-	-	*	*	0.303	-	*	*	-	-
	$m_{\text{st}}^{\text{X},\mathcal{M}}(\mathsf{M}^{2,3})$	0.269	0.206	0.133	0	*	*	*	0	*	*	*	0
$s = 0.2, r = 0.5$	n=6	A	B	C	D	A	B	C	D	A	B	C	D
	$m_{\text{un}}^{\text{X},\mathcal{M}}(\mathsf{I}^{2,3})$	0	0.018	0.015	0.014	0	0.016	0.014	0.035	0	0.013	0.014	0.067
	$m_{\text{st}}^{\text{X},\mathcal{M}}(\mathsf{I}^{1})$	0	0.041	0.056	-	0	0.058	0.111	-	0	0.095	0.269	-
	$m_{\text{un}}^{\text{X},\mathcal{M}}(\mathsf{I}^{1})$	0.372	0.262	0.131	-	*	*	0.337	-	*	*	0.382	-
	$m_{\text{st}}^{\text{X},\mathcal{M}}(\mathsf{M}^{2,3})$	0.403	0.335	0.265	0	*	*	*	0	*	*	*	0
	n=12												
	$m_{\text{un}}^{\text{X},\mathcal{M}}(\mathsf{I}^{2,3})$	0	0.020	0.013	0.015	0	0.019	0.018	0.08	0	0.027	0.028	0.393
	$m_{\text{st}}^{\text{X},\mathcal{M}}(\mathsf{I}^{1})$	0	0.045	-	-	0	0.087	0.225	-	0	0.332	-	-
	$m_{\text{un}}^{\text{X},\mathcal{M}}(\mathsf{I}^{1})$	0.409	0.289	-	-	*	*	*	-	*	*	-	-
	$m_{\text{st}}^{\text{X},\mathcal{M}}(\mathsf{M}^{2,3})$	0.444	0.369	0.254	0	*	*	*	0	*	*	*	0
$s = 0.2, r = 0.01$	$n = 6$	A	B	C	D	A	B	C	D	A	B	C	D
	$m_{\text{un}}^{\text{X},\mathcal{M}}(\mathsf{I}^{2,3})$	0	0.007	0.005	0.003	0	0.005	0.004	0.006	0	0.003	0.003	0.009
	$m_{\text{st}}^{\text{X},\mathcal{M}}(\mathsf{I}^{1})$	0	0.039	0.050	-	0	0.058	0.111	-	0	0.095	0.288	-
	$m_{\text{un}}^{\text{X},\mathcal{M}}(\mathsf{I}^{1})$	0.372	0.264	0.138	-	*	*	0.332	-	*	*	0.352	-
	$m_{\text{st}}^{\text{X},\mathcal{M}}(\mathsf{M}^{2,3})$	0.403	0.335	0.265	0	*	*	*	0	*	*	*	0
	$n = 12$												
	$m_{\text{un}}^{\text{X},\mathcal{M}}(\mathsf{I}^{2,3})$	0	0.007	0.003	0.003	0	0.005	0.003	0.008	0	0.006	0.006	0.04
	$m_{\text{st}}^{\text{X},\mathcal{M}}(\mathsf{I}^{1})$	0	0.042	-	-	0	0.087	0.226	-	0	0.333	-	-
	$m_{\text{un}}^{\text{X},\mathcal{M}}(\mathsf{I}^{1})$	0.409	0.290	-	-	*	*	*	-	*	*	-	-
	$m_{\text{st}}^{\text{X},\mathcal{M}}(\mathsf{M}^{2,3})$	0.444	0.369	0.254	0	*	*	*	0	*	*	*	0

Table A.1: Critical migration rates for different selection scenarios and migration patterns. The symbol '-' indicates that the critical migration rate does not exist. The symbol '*' indicates that the migration rate would exist for smaller selection intensities s. Equilibrium configurations were calculated in steps of $\Delta m = 10^{-3}$. The values indicate the lowest migration rate for which a different equilibrium configuration was observed. The data for $s = 0.2$ and $r = 0.5$ are visualized in Figure 5.

A.10 Weak-migration approximations for the island model

Here, we give simple approximations of LD, the deviation of the genotypic mean from the optimum and the genetic variance at stable equilibria for weak migration in the island model with Scenario A and Scenario B. In Scenario A, I_1 is the unique stable equilibrium for weak migration. LD, the deviation of the genotypic mean from the optimum and the genetic variance at I_1 in deme k are given by

$$D_k(\mathsf{I}^1) = \frac{n}{2(n-1)} \frac{m}{r+s-rs} + O(m^2), \tag{A.28}$$

$$|\bar{G}_k(\mathsf{I}^1) - P_k| = \frac{n}{2(n-1)} \frac{m}{s} \frac{8r(1-s)+2s}{r+s-rs} + O(m^2), \tag{A.29}$$

$$V_k(\mathsf{I}^1) = \frac{n}{2(n-1)} \frac{m}{s} \frac{4r(1-s)+2s}{r+s-rs} + O(m^2). \tag{A.30}$$

The fractions different from $n/[2(n-1)]$ are obtained by a weak-migration approximation of I_1 for $n = 2$, whereas the factor $n/[2(n-1)]$ is inferred from Remark 5.1. We note that in accordance with Proposition A.1, the expressions (A.28), (A.29), and (A.30) are independent of k.

In Scenario B, I^2, I^3, I^4 and I^5 are stable for weak migration. The corresponding approximations at I^4 and I^5 are given by

$$D_k(\mathsf{I}^{4,5}) = \frac{2n}{3(n-1)} \frac{m}{2(r+s-rs)} + O(m^2) \quad \text{if } k \le n/3, k > 2n/3, \tag{A.31a}$$

$$D_k(\mathsf{I}^{4,5}) = O(m^2) \quad \text{if } n/3 < k \le 2n/3, \tag{A.31b}$$

$$|\bar{G}_k(\mathsf{I}^{4,5}) - P_k| = \frac{2n}{3(n-1)} \frac{m}{s} \frac{6r(1-s)+3s}{r+s-rs} + O(m^2) \quad \text{if } k \le n/3, k > 2n/3, \tag{A.32a}$$

$$|\bar{G}_k(\mathsf{I}^{4,5}) - P_k| = O(m^2) \quad \text{if } n/3 < k \le 2n/3, \tag{A.32b}$$

$$V_k(\mathsf{I}^{4,5}) = \frac{2n}{3(n-1)} \frac{m}{s} \frac{3r(1-s)+2s}{r+s-rs} + O(m^2) \quad \text{if } k \le n/3, k > 2n/3, \tag{A.33a}$$

$$V_k(\mathsf{I}^{4,5}) = \frac{2n}{3(n-1)} \frac{2m}{s} + O(m^2) \quad \text{if } n/3 < k \le 2n/3. \tag{A.33b}$$

The terms different from $2n/[3(n-1)]$ are obtained from a weak-migration perturbation for $n = 3$ ($P_1 = -1, P_2 = 0, P_3 = 1$), whereas the factor $2n/[3(n-1)]$ is obtained using an argument analogous to that in Remark 5.1; see Proposition A.2.2. We note that in contrast to the two-deme model, $D(\mathsf{I}^{4,5}) \neq 0$. From (A.31) it is also apparent that the inequality in (A.19) can not be strict.

At I^2 and I^3 we obtain the following approximations

$$D_k(\mathsf{I}^{2,3}) = \frac{5n}{6(n-1)} \frac{2m}{5(r+s-rs)} + O(m^2) \quad \text{if } k \leq n/3, k > 2n/3, \tag{A.34a}$$

$$D_k(\mathsf{I}^{2,3}) = \frac{5n}{6(n-1)} \left(-\frac{m}{5r}\right) + O(m^2) \quad \text{if } n/3 < k \leq 2n/3, \tag{A.34b}$$

$$|\bar{G}_k(\mathsf{I}^{2,3}) - P_k| = \frac{5n}{6(n-1)} \frac{12m}{5s} \frac{2r(1-s)+s}{r+s-rs} + O(m^2) \quad \text{if } k \leq n/3, k > 2n/3, \tag{A.35a}$$

$$|\bar{G}_k(\mathsf{I}^{2,3}) - P_k| = O(m^2) \quad \text{if } n/3 < k \leq 2n/3, \tag{A.35b}$$

$$V_k(\mathsf{I}^{2,3}) = \frac{5n}{6(n-1)} \frac{4m}{5s} \frac{3r(1-s)+2s}{r+s-rs} + O(m^2) \quad \text{if } k \leq n/3, k > 2n/3, \tag{A.36a}$$

$$V_k(\mathsf{I}^{2,3}) = \frac{5n}{6(n-1)} \frac{12m}{5\ s} + O(m^2) \quad \text{if } n/3 < k \leq 2n/3. \tag{A.36b}$$

The terms different from $5n/[6(n-1)]$ are obtained from a weak-migration perturbation for $n = 6$. (The equilibria I^2 and I^3 do not exist for $n = 3$). In analogy to Remark 5.1 and Proposition A.2.2 one obtains the factor $5n/[6(n-1)]$.

A.11 Diffusion models

We assume that gamete frequencies $x_i(y,t)$ are continuous functions in space and time, where $y \in (-y_0, y_0)$ and $t \in (0, \infty)$. Then, also allele frequencies $p(y,t)$, $q(y,t)$, LD $D(y,t)$, genotypic mean $\bar{G}(y,t)$ and genetic variance $V(y,t)$ are continuous functions in space and time. Further, we assume that the position of the trait optimum $P(y)$ is a (non-necessarily) continuous function in space. Then, the analogue of the fitness function (2.1) is given by

$$w(G,y) = 1 - s(G - P(y))^2 \tag{A.37}$$

and w_i and $\bar{w}$ are (non-necessarily) continuous functions in space. We denote the variance of dispersal in the domain by σ^2.

Assuming that allelic effects are approximately Gaussian distributed, the model in Slatkin (1978) and Barton (1999) describes the evolution of mean $\bar{G}(y,t)$ and variance $V(y,t)$ according to

$$\frac{\partial \bar{G}}{\partial t} = \frac{\sigma^2}{2} \frac{\partial^2 \bar{G}}{\partial y^2} - 2sV(\bar{G} - P) \quad \text{in } (-y_0, y_0) \times (0, \infty), \tag{A.38a}$$

$$\frac{\partial V}{\partial t} = \frac{\sigma^2}{2} \frac{\partial^2 V}{\partial y^2} + \frac{\sigma^2}{4} \left(\frac{\partial \bar{G}}{\partial x}\right)^2 - \frac{sV^2}{2} \quad \text{in } (-y_0, y_0) \times (0, \infty), \tag{A.38b}$$

$$\frac{\partial \bar{G}}{\partial y} = \frac{\partial V}{\partial y} = 0 \quad \text{on } \{-y_0, y_0\} \times (0, \infty). \tag{A.38c}$$

The rare-alleles model of Barton (1999) is given by

$$\frac{\partial p}{\partial t} = \frac{\sigma^2}{2}\frac{\partial^2 p}{\partial y^2} - sc^2 p(1-p)(1-2p+2\delta) \qquad \text{in } (-y_0, y_0)\times(0,\infty), \tag{A.39a}$$

$$\frac{\partial q}{\partial t} = \frac{\sigma^2}{2}\frac{\partial^2 q}{\partial y^2} - sc^2 q(1-q)(1-2q+2\delta) \qquad \text{in } (-y_0, y_0)\times(0,\infty), \tag{A.39b}$$

$$\frac{\partial p}{\partial y} = \frac{\partial q}{\partial y} = 0 \qquad \text{on } \{-y_0, y_0\}\times(0,\infty), \tag{A.39c}$$

where $\delta = (\bar{G} - P)/c$ and $c = c_1 = c_2 = 1/2$ is the genotypic effect per locus. Since the selection intensity in Barton (1999) is half the selection intensity of our model, (A.38) and (A.39) were adapted accordingly. In (A.38) a typo of eq. (5) in Barton (1999) was corrected.

In continuous space we define the selection scenarios in close analogy to (5.4):

$$\text{Scenario A} : P(y) = \begin{cases} -1 & \text{if } -y_0 < y \le 0, \\ 1 & \text{if } 0 < y < y_0, \end{cases} \tag{A.40a}$$

$$\text{Scenario B} : P(y) = \begin{cases} -1 & \text{if } -y_0 < y < -y_0/3, \\ 0 & \text{if } -y_0/3 \le y \le y_0/3, \\ 1 & \text{if } y_0/3 < y < y_0, \end{cases} \tag{A.40b}$$

$$\text{Scenario C} : P(y) = y/y_0. \tag{A.40c}$$

To compare these models with the n-deme model, we set $y_0 = (n-1)/2$. Then $(-y_0, y_0)$ has length $n-1$ and can be shifted to $(1, n)$. The dispersal variance at position $y_k = -y_0 - 1 + k = -(n+1)/2 + k$ $(1 \le k \le n)$ is

$$\sigma^2(y_k) = \sum_{l=1}^{n} l^2 m_{kl} - \left(\sum_{l=1}^{n} l m_{kl}\right)^2. \tag{A.41}$$

Since in (A.38), (A.39), and (7.4) it is assumed that dispersal is independent of position y, we average (A.41) over all positions y_k, which produces

$$\sigma^2 = \frac{1}{n}\sum_{k=1}^{n} \sigma^2(y_k). \tag{A.42}$$

Assuming the stepping-stone migration pattern (5.3), (A.41) and (A.42) yield that

$$\sigma^2(y_k) = \begin{cases} m & \text{if } 1 < k < n, \\ m(1-m) & \text{if } k = 1, n, \end{cases} \tag{A.43}$$

and

$$\sigma^2 = m - 2\frac{m^2}{n} = m + O(m^2). \tag{A.44}$$

B Appendix

Figure B.1

Region of stability (dotted) of I^1 for the two-deme model with $P = 0.6$. The solid lines show the analytical approximations given by (A.14) in the main text. The recombination rate is $r = 0.5$.

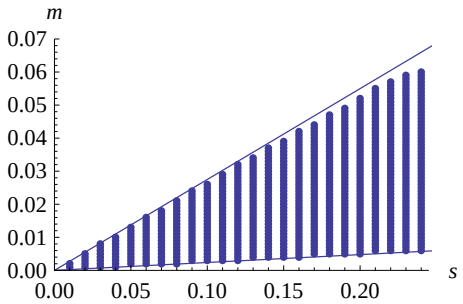

Regions of stability (dotted) of I^1 for various migration patterns and selection scenarios and $n = 6, 12$. The figure supports equations (5.10), (5.13), and (5.16) from the main text. The recombination rate is $r = 0.5$.

$n=6$

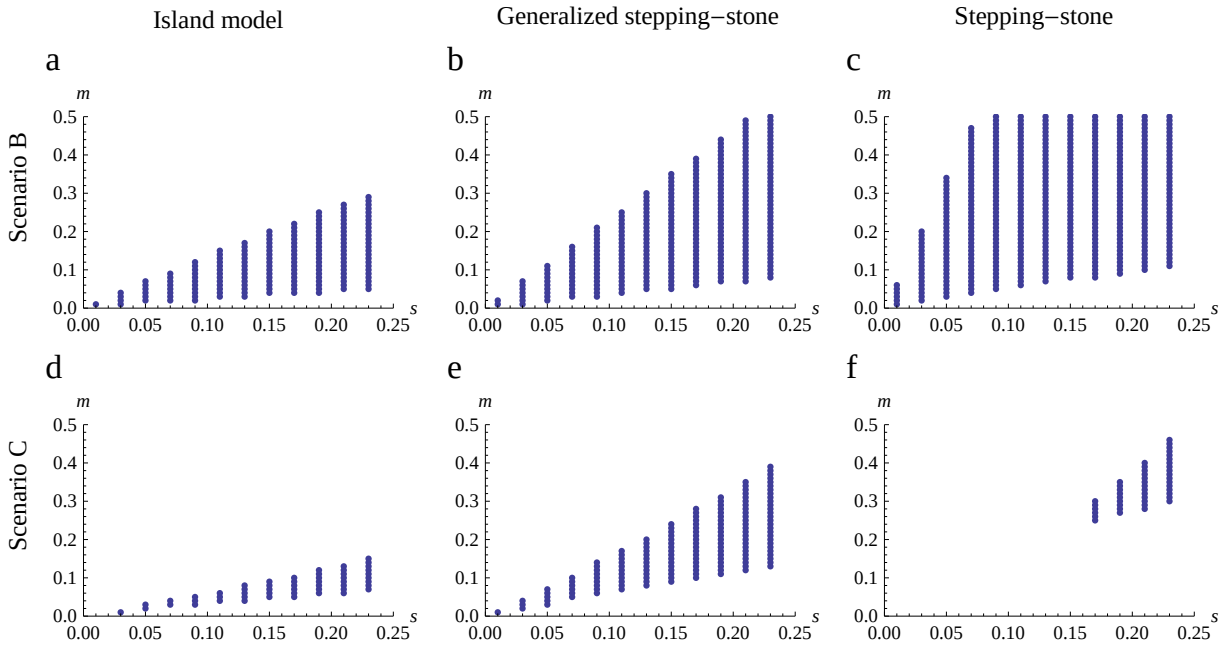
Island model
Generalized stepping−stone
Stepping−stone
a
b
c
d
e
f
Scenario B
Scenario C
m
s
0.0
0.1
0.2
0.3
0.4
0.5
0.00
0.05
0.10
0.15
0.20
0.25

$n=12$

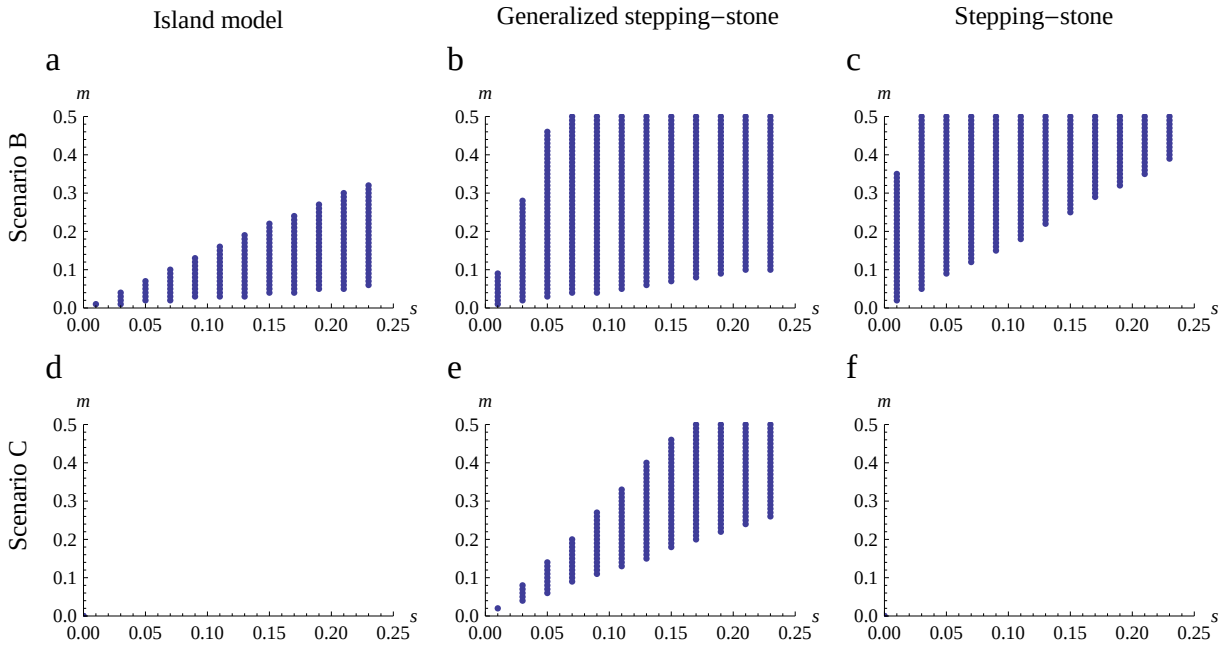
Island model
Generalized stepping−stone
Stepping−stone
a
b
c
d
e
f
Scenario B
Scenario C
m
s
0.0
0.1
0.2
0.3
0.4
0.5
0.00
0.05
0.10
0.15
0.20
0.25

Figure B.2

Clines in the mean phenotype, the genetic variance, and LD for Scenario A and a grid of migration rates. Blue lines indicate the island model, red lines the stepping-stone model, and green lines the generalized stepping-stone model. Magenta lines show the stepping-stone model with selection intensity $\tilde{s}$. Solid lines indicate that I^1 is the unique stable equilibrium, whereas dashed lines indicate that I^4 and I^5 are simultaneously stable (they exhibit the same mean, variance, and LD). In the left column, the dots mark the positions of the phenotypic optimum. The figure complements Figures 6a,b,c. Parameters are $s = 0.2$, $r = 1/2$, and $n = 12$.

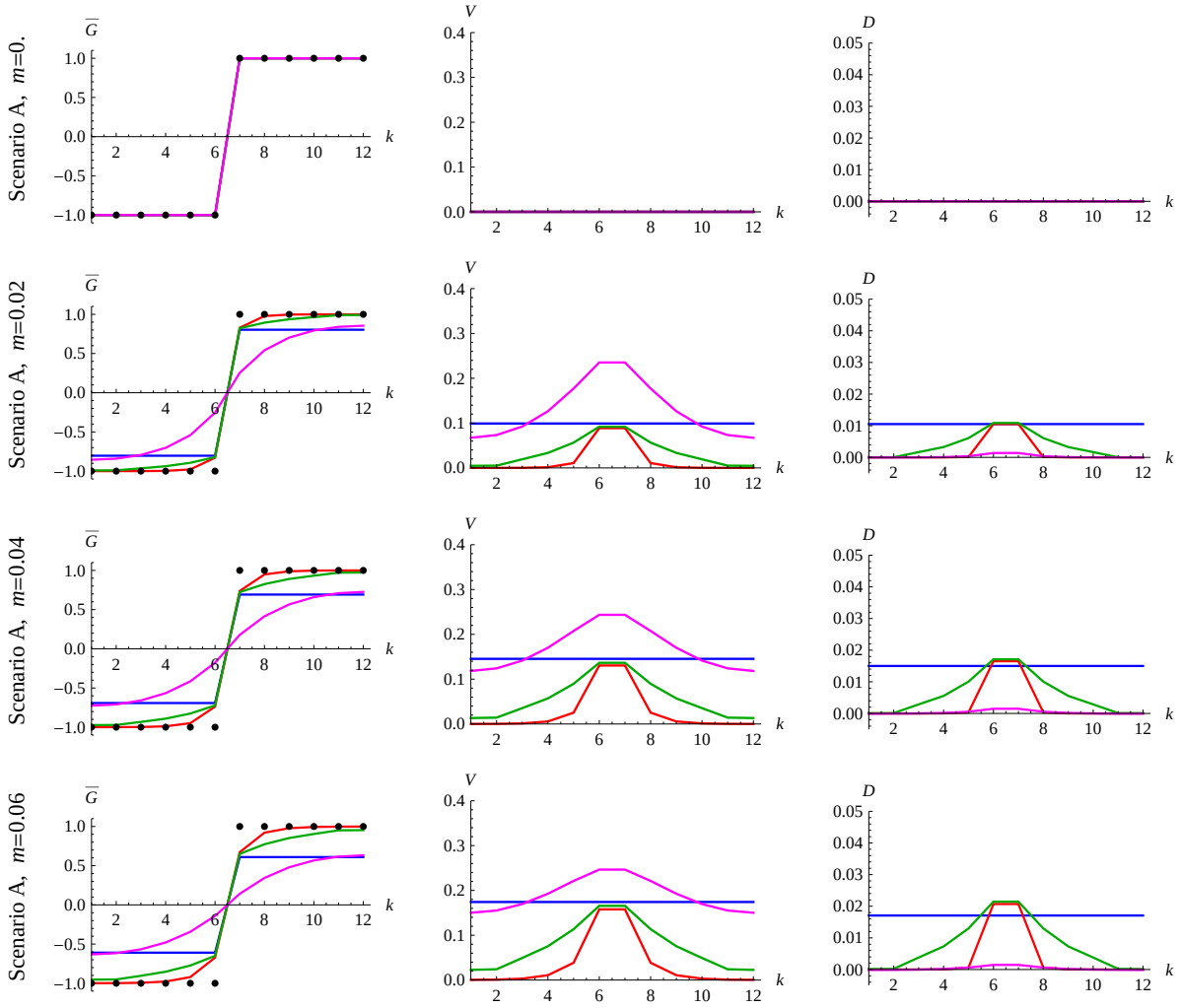

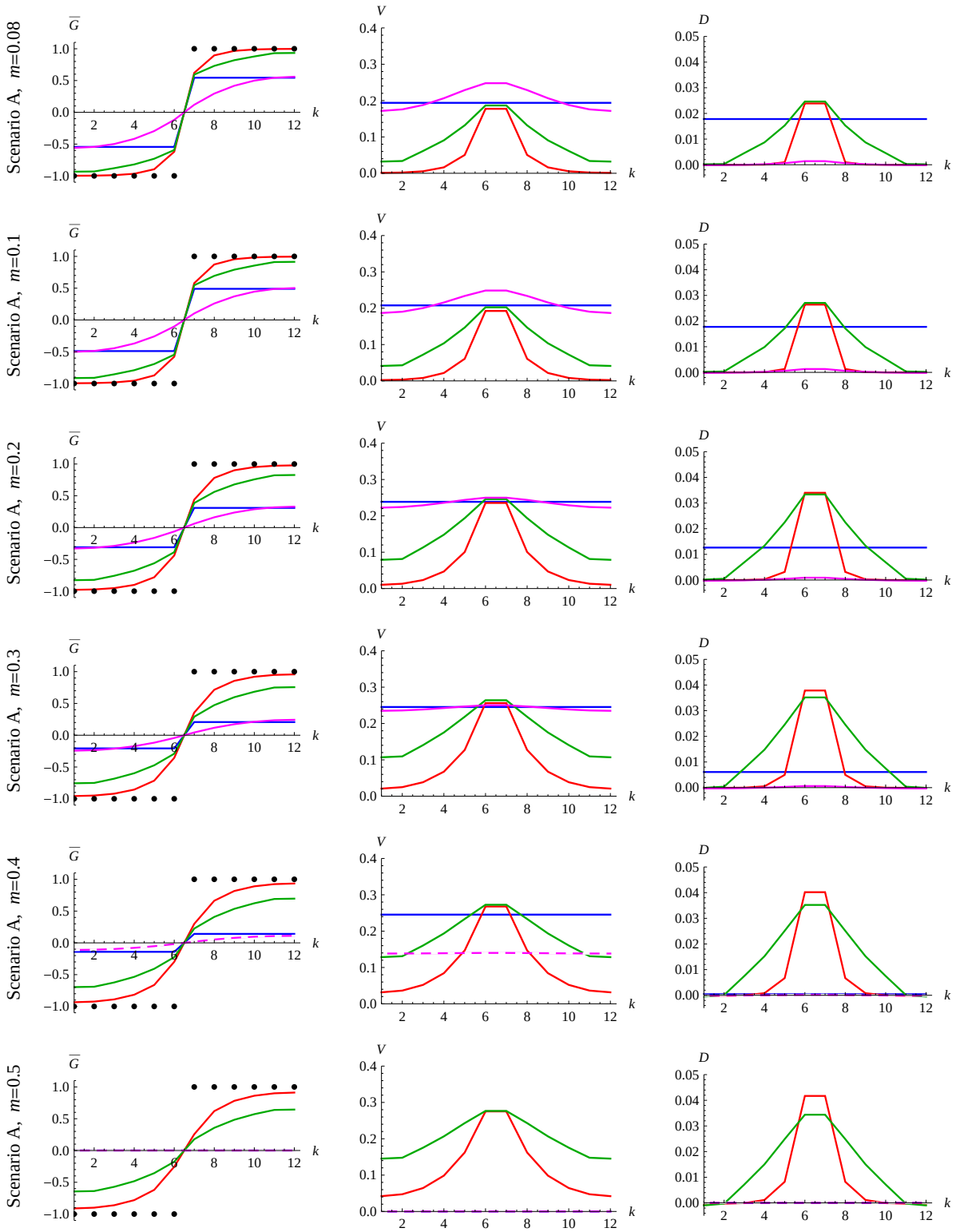
Scenario A, m=0.08
Scenario A, m=0.1
Scenario A, m=0.2
Scenario A, m=0.3
Scenario A, m=0.4
Scenario A, m=0.5
G
V
D
k

Figure B.3

Clines for Scenario B, analogously to Figure B.2 and Figure 6 in the main text. Line colors and parameters are as in Figure B.2 and Figure 6.

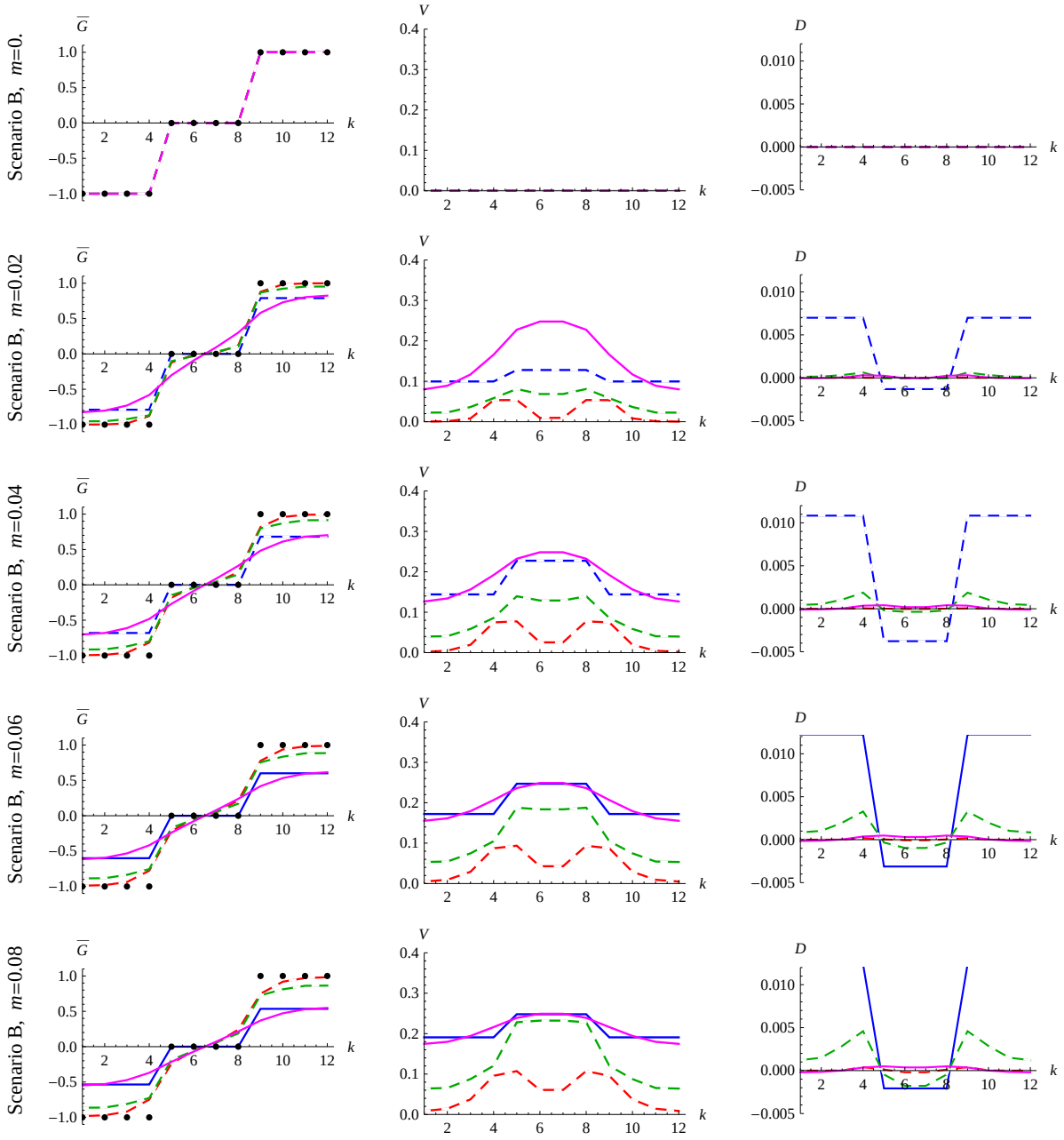

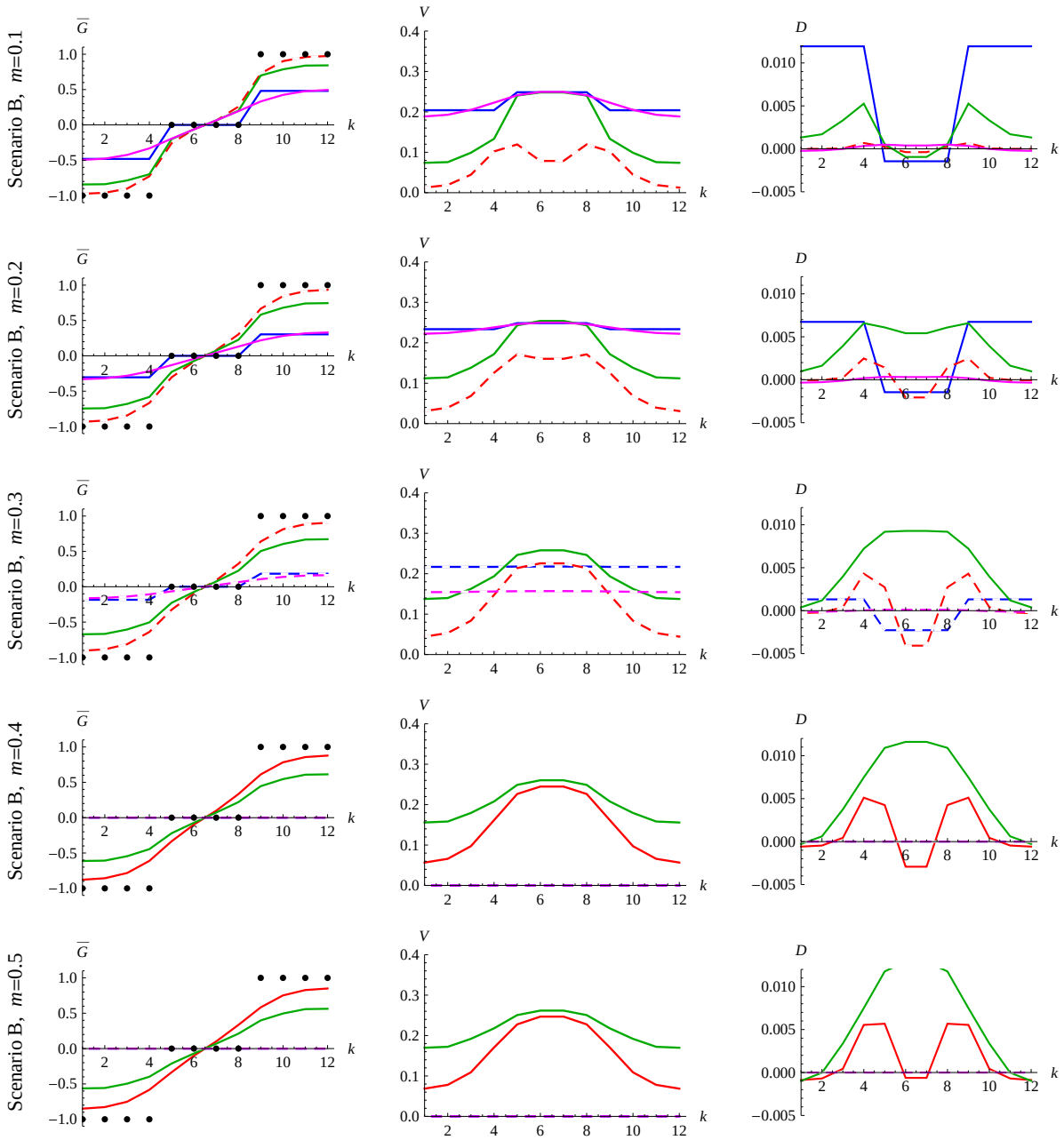
Scenario B, m=0.1
Scenario B, m=0.2
Scenario B, m=0.3
Scenario B, m=0.4
Scenario B, m=0.5
G
V
D
k

Figure B.4

Clines for Scenario C, analogously to Figures B.2, B.3, and Figure 6 in the main text. Line colors and parameters are as in Figure B.3 and Figure 6.

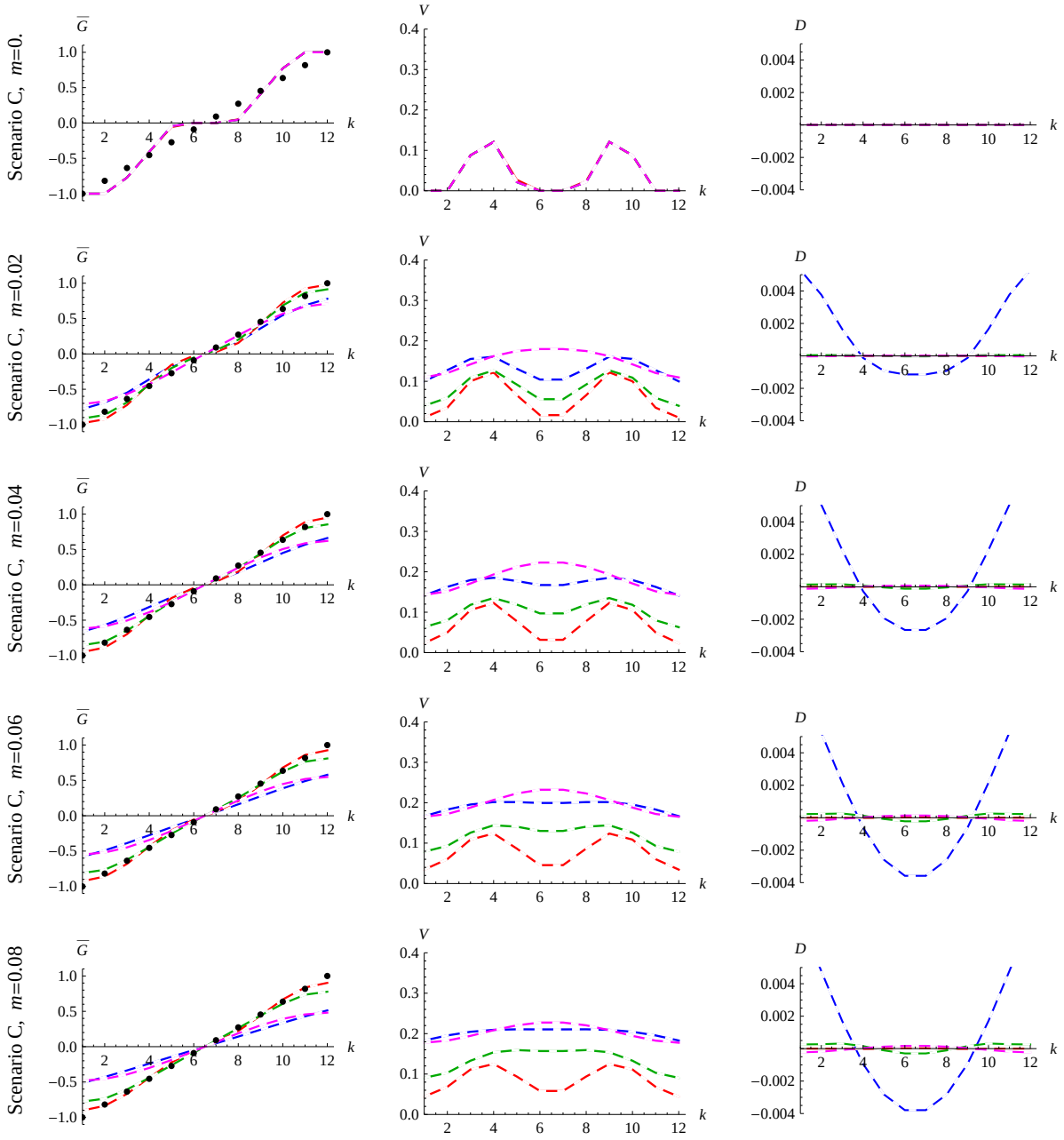

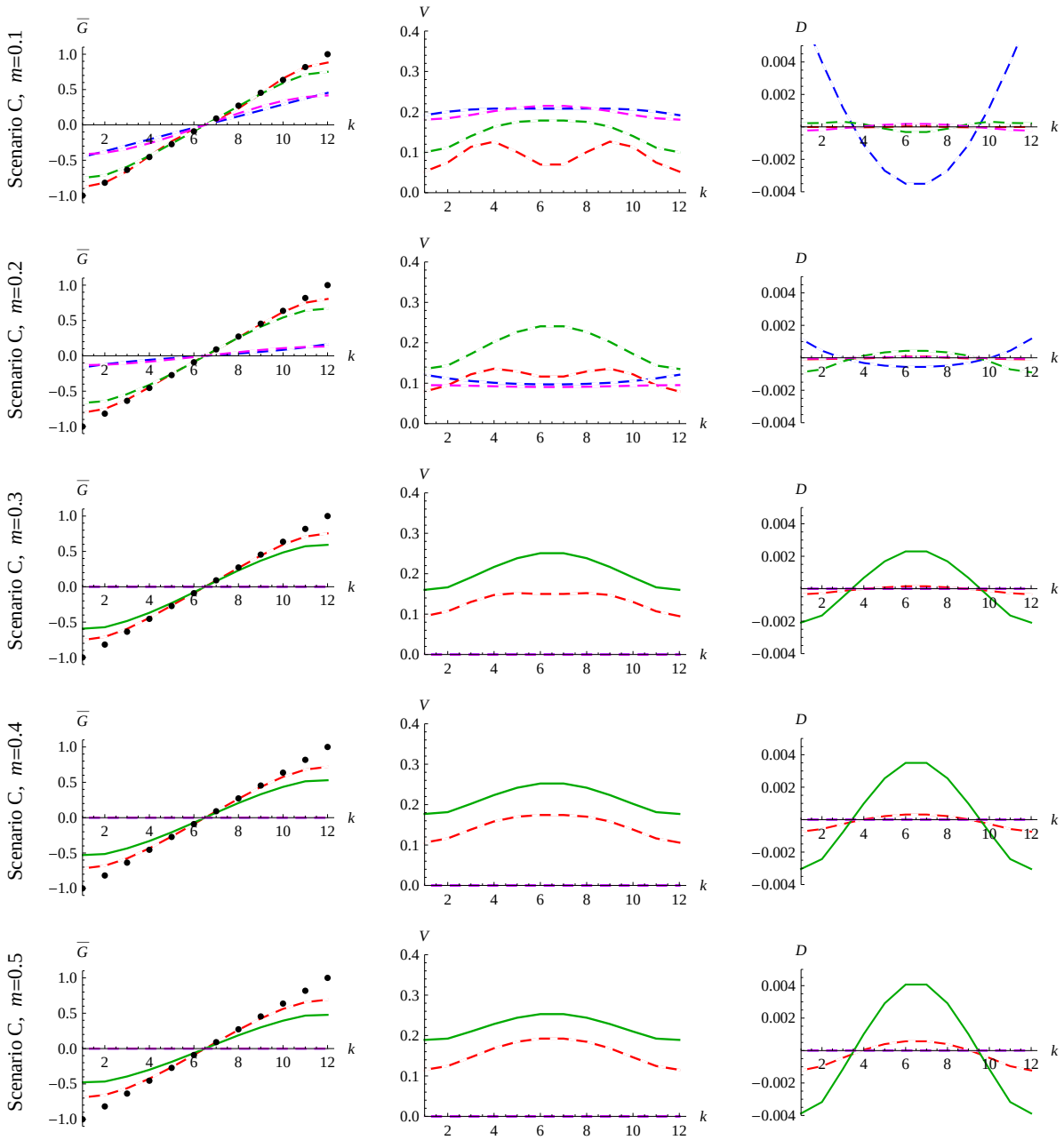
Scenario C, m=0.1
Scenario C, m=0.2
Scenario C, m=0.3
Scenario C, m=0.4
Scenario C, m=0.5
G
V
D
k

Figure B.5

Clines in mean phenotype, genetic variance, and LD for Scenario A and different recombination rates. The island model (blue) is shown for $r = 0.5$ (dark) and $r = 0.05$ (light). Red and orange lines show the stepping-stone model for $r = 0.5$ and $r = 0.05$, respectively. As in Figures B.2, B.3, B.4 and Figure 6, solid lines indicate that I^1 is the unique stable equilibrium, whereas dashed lines indicate that I^4 and I^5 are simultaneously stable (they exhibit the same mean, variance, and LD). In the left column, the dots mark the positions of the phenotypic optimum. Parameters are $s = 0.2$ and $n = 12$.

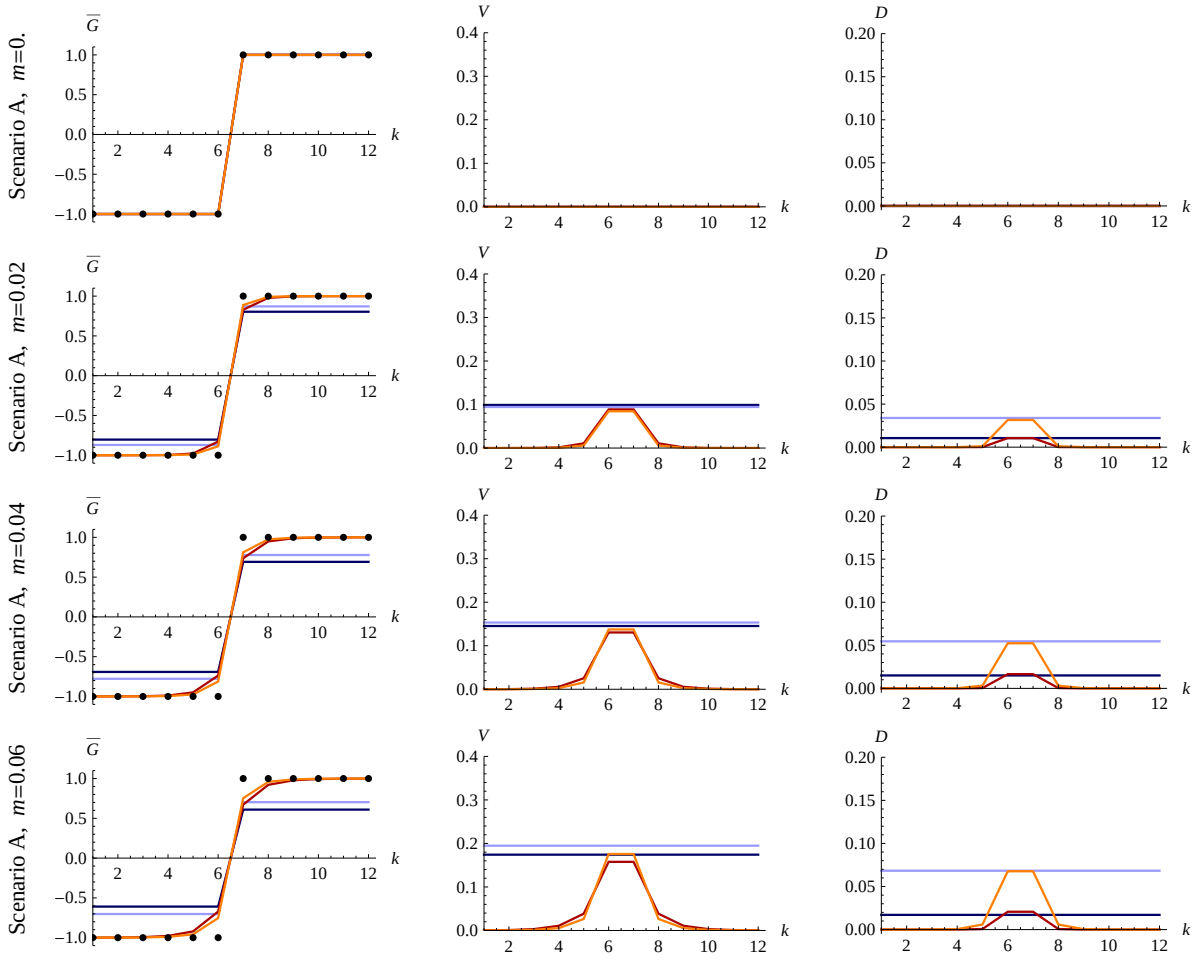

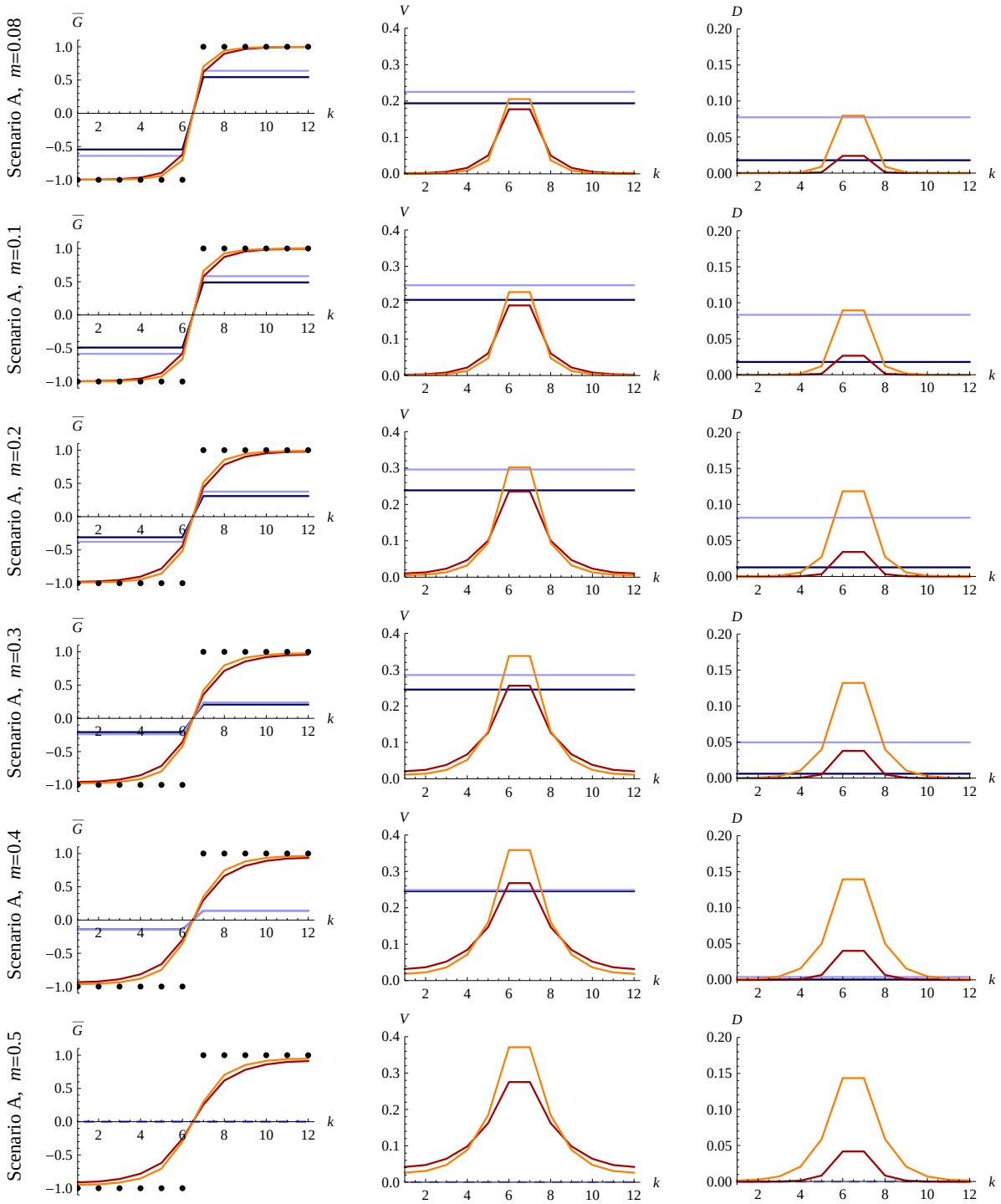
Scenario A, m=0.08
Scenario A, m=0.1
Scenario A, m=0.2
Scenario A, m=0.3
Scenario A, m=0.4
Scenario A, m=0.5
G
V
D
k

Figure B.6

Clines for Scenario B and different recombination rates. Line colors and parameters are as in Figure B.5.

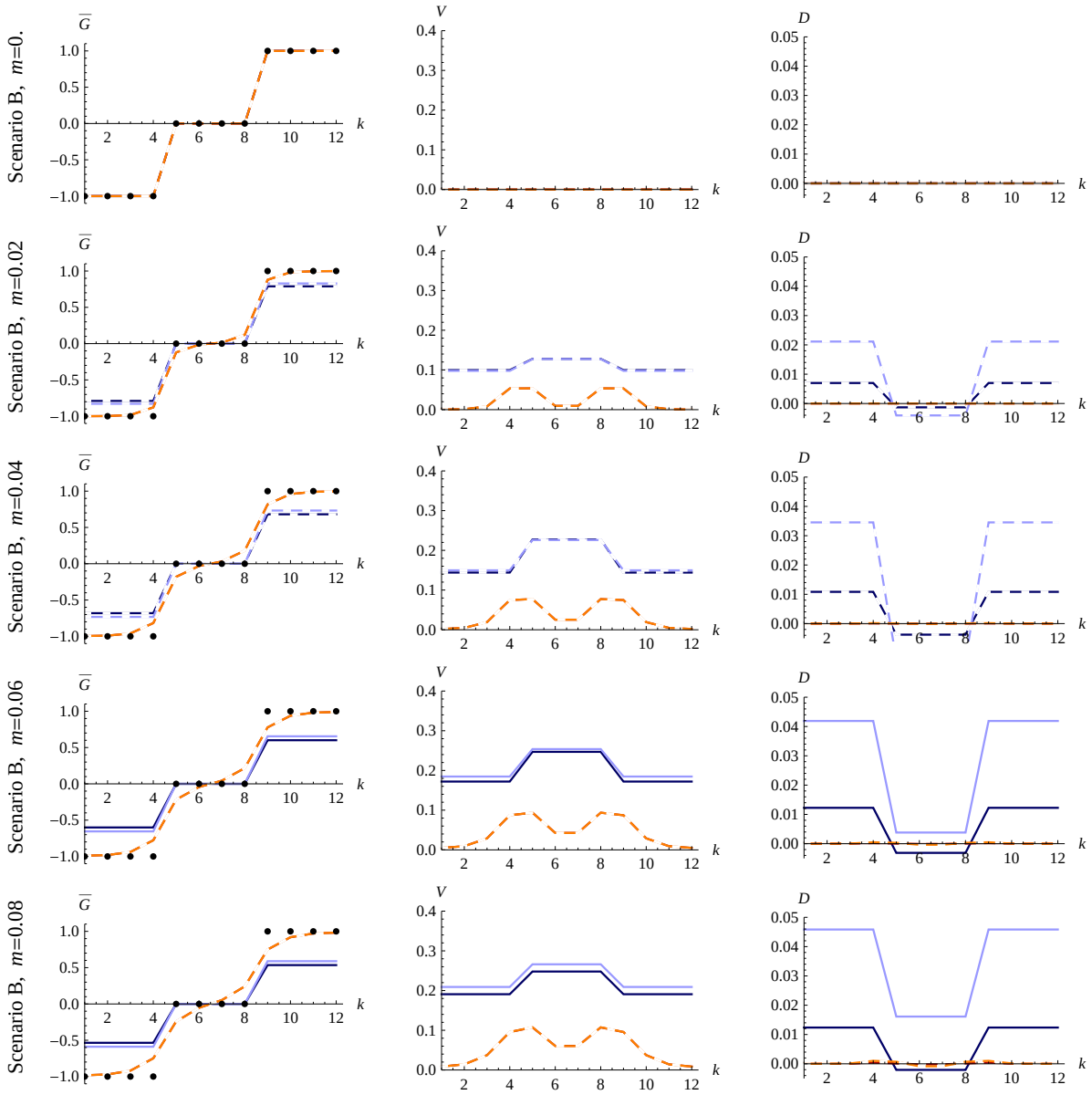

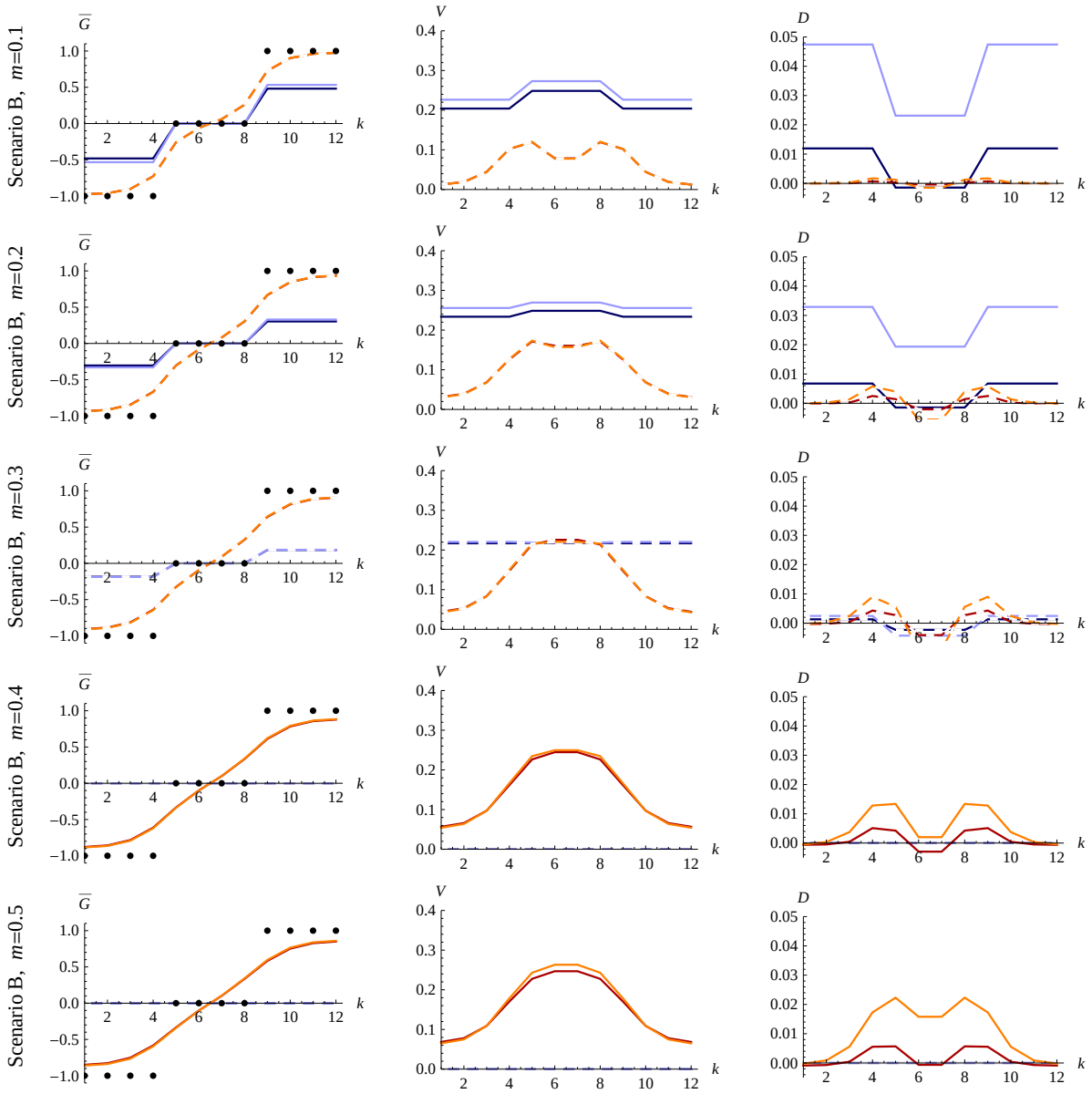
Scenario B, m=0.1
Scenario B, m=0.2
Scenario B, m=0.3
Scenario B, m=0.4
Scenario B, m=0.5
G
V
D
k

Figure B.7

Clines for Scenario C and different recombination rates. Line colors and parameters are as in Figures B.5 and B.6.

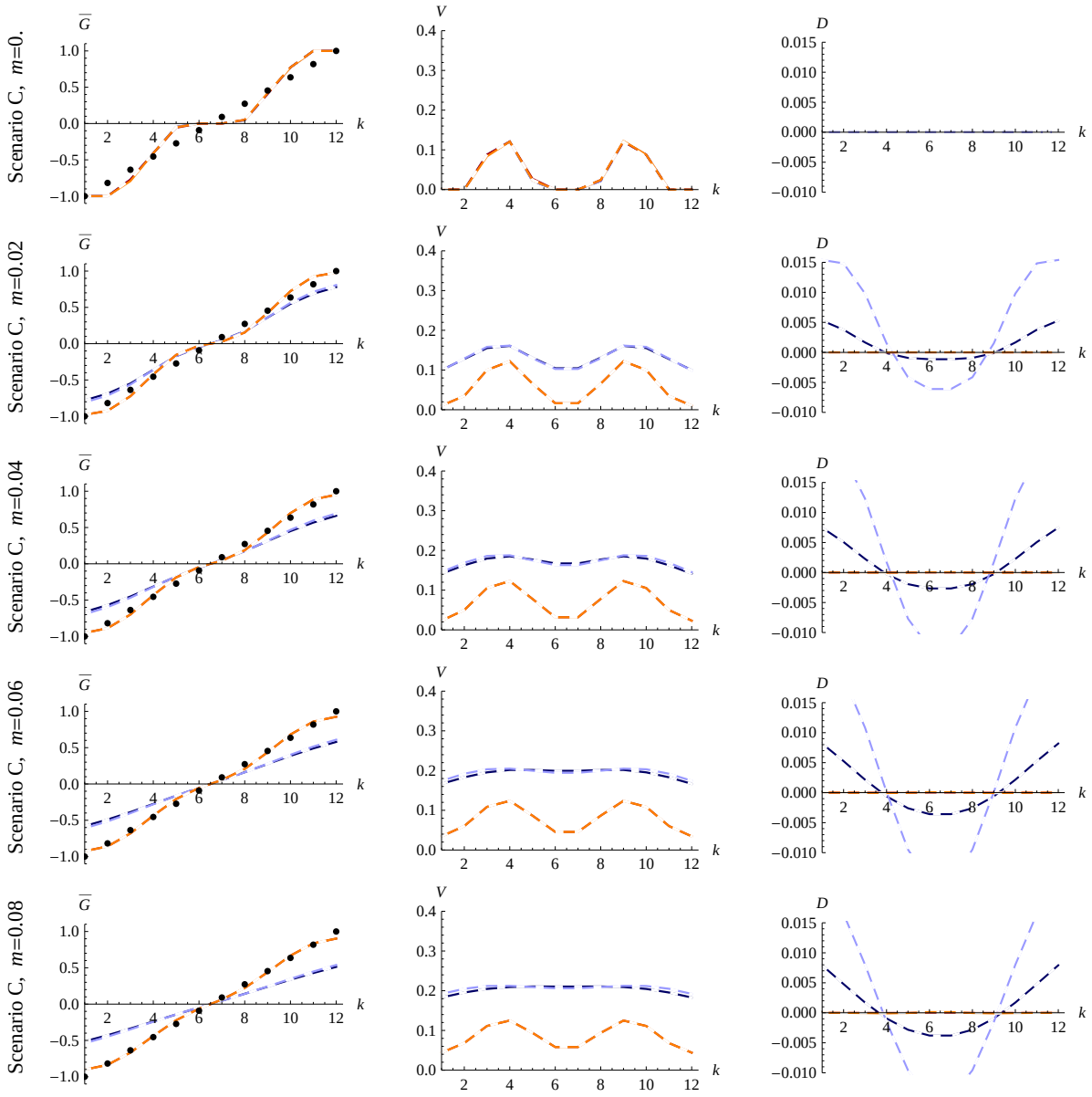

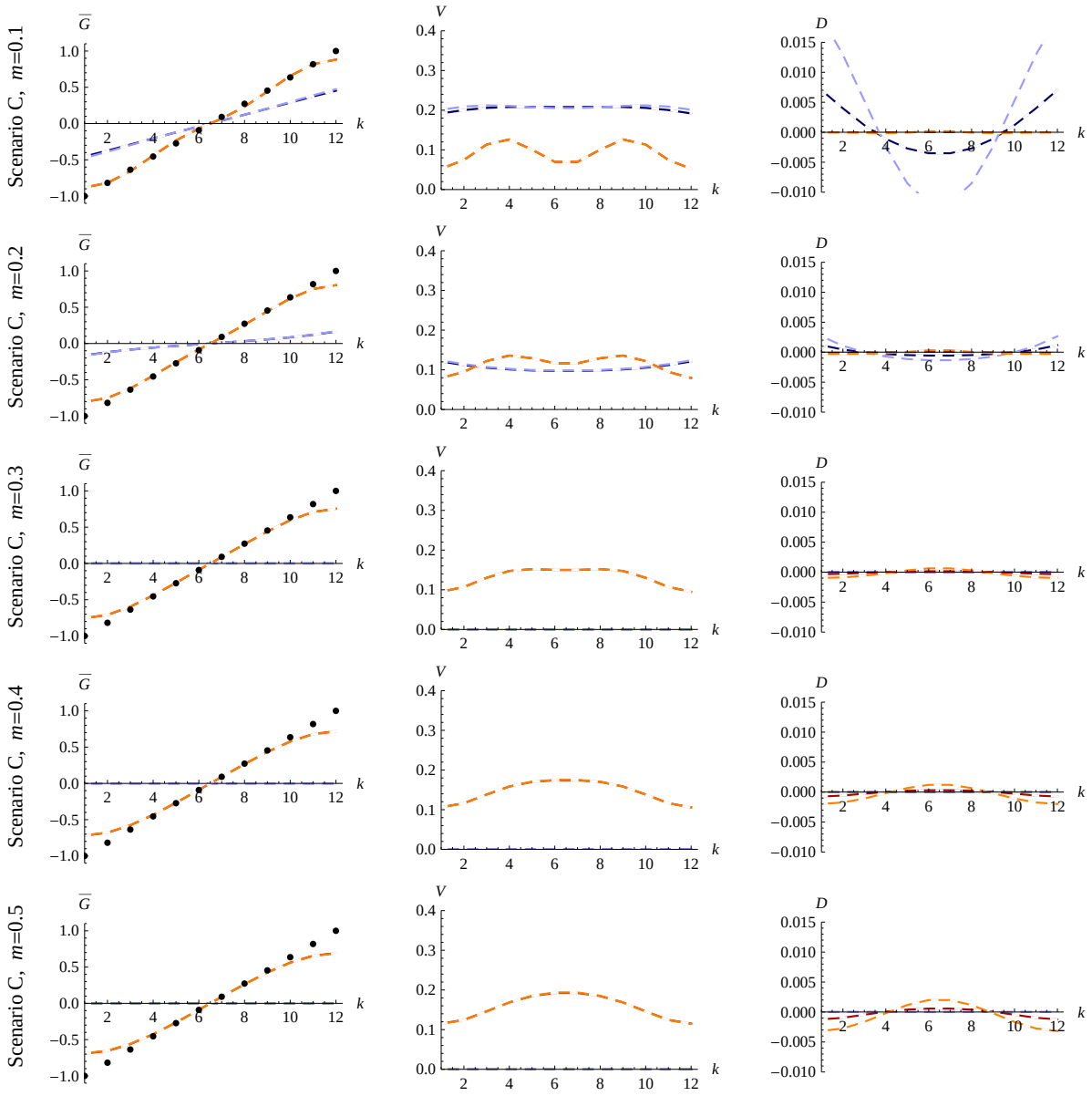
Scenario C, m=0.1
Scenario C, m=0.2
Scenario C, m=0.3
Scenario C, m=0.4
Scenario C, m=0.5
G
V
D
k

Figure B.8

Linkage disequilibrium in deme 1 and deme 6 as a function of the migration rate. The island model (blue) is shown for $r = 0.5$ (dark) and $r = 0.05$ (light). Red and orange lines show the stepping-stone model for $r = 0.5$ and $r = 0.05$, respectively. At dashed lines, equilibria are simultaneously stable (M^2 and M^3 if $m > m_{\mathrm{st}}^{\mathrm{X},\mathcal{M}}(\mathsf{M}^{2,3})$; I^4 and I^5 otherwise). For reasons of visibility only $D_k(\mathsf{I}^{4,5})$ is shown for $m < m_{\mathrm{st}}^{\mathrm{X},\mathcal{M}}(\mathsf{I}^{2,3}) \leq 0.028$, whereas D_k at the other stable equilibria is not displayed. Parameters are $s = 0.2$ and $n = 12$.

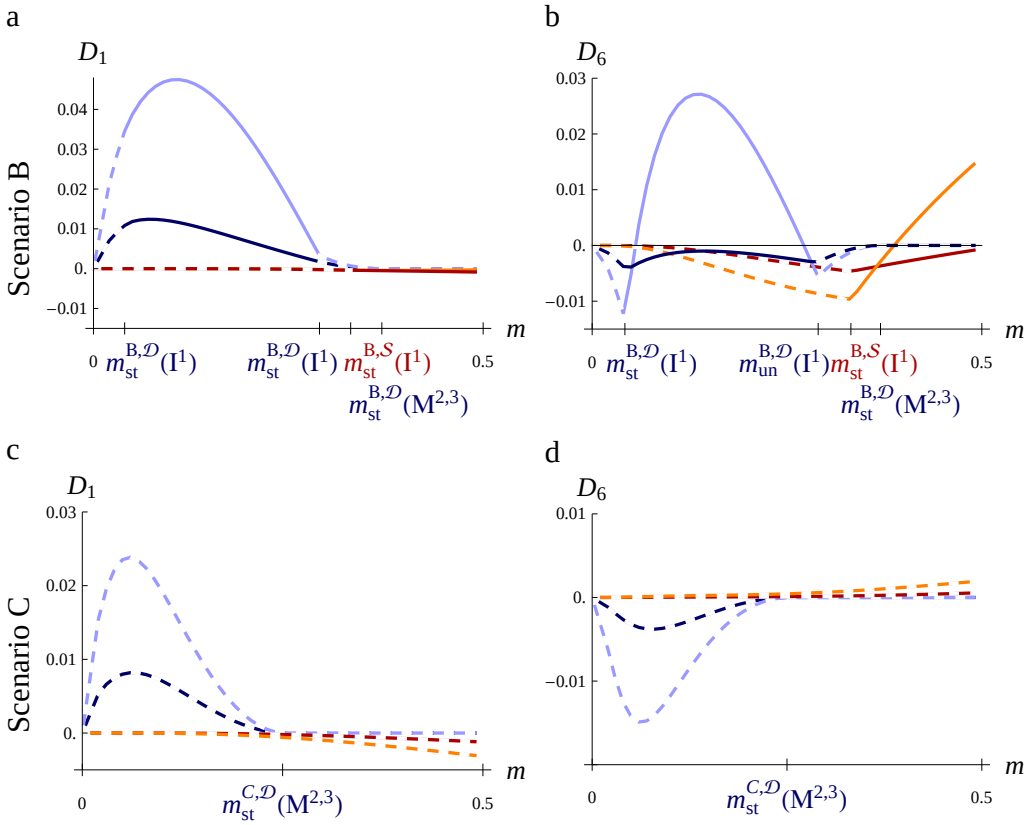

The figure confirms that for weak migration LD is non-negative in demes under directional selection (deme 1) and non-positive in demes under stabilizing selection (deme 6). As the migration rate increases, the fraction of gametes AB and ab immigrating into the central deme grows, which contributes positively to LD. This effect dominates above $m_{\mathrm{st}}^{\mathrm{X},\mathcal{M}}(\mathsf{I}^1)$ (over local selection which induces negative LD). Then it depends on the recombination rate whether LD becomes positive for $m > m_{\mathrm{st}}^{\mathrm{X},\mathcal{M}}(\mathsf{I}^1)$ (panel b). If I^1 remains unstable, as is usually the case in Scenario C, LD remains negative in the center of the cline (panel c).

Figure B.9

Clines in mean phenotype (a), genetic variance (b), and LD (c) in the neutral stepping-stone model of Feldman and Christiansen (1975). The red dot in panel c shows the approximation for D in the center of the cline; see equation (7.1) in the main text. The parameters $r = 0.5$, $m = 0.13$, and $n = 12$ are used (deme 1 and 12 denote the continents).

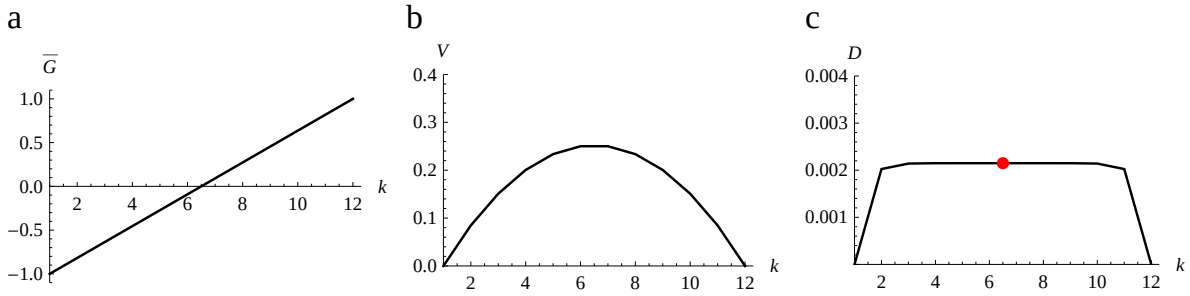

Figure B.10

Accuracy of approximations for LD in the stepping-stone model assuming neutrality or quasi-linkage equilibrium. Red lines show D_6 ($n = 12$), whereas the black and blue lines show various approximations for D_6. Black solid lines show

$$D_k \approx \frac{m}{r}(p_k - p_{k+1})(q_k - q_{k+1}),$$

given by equation (7.2) in the main text. Since equation (7.2) assumes $p_{k-1} - p_k = p_k - p_{k+1}$ and $q_{k-1} - q_k = q_k - q_{k+1}$, which is poorly satisfied in Scenario A (panels a, b), we also show

$$D_k \approx \frac{m}{r}\frac{p_{k-1} - p_{k+1}}{2}\frac{q_{k-1} - q_{k+1}}{2}$$

(black dashed), which performs much better. Because in panels c, d, e, f, $p_{k-1} - p_k \approx p_k - p_{k+1}$ and $q_{k-1} - q_k \approx q_k - q_{k+1}$ hold approximately, the black solid lines and black dashed lines overlap.

Barton and Shpak (2000, eq. (14)) derived the quasi-linkage equilibrium approximation

$$D_k \approx \frac{1}{r}\left(m\frac{\partial p_k}{\partial y}\frac{\partial q_k}{\partial y} + \frac{\partial \log(\bar{w}_k)}{\partial D_k}p_k(1-p_k)q_k(1-q_k)\right)$$

for continuous time and space (y denotes the spatial variable). Adapting this approximation to discrete time and space and our fitness function, we obtain

$$D_k \approx \frac{1}{r}\left(m\frac{p_{k-1} - p_{k+1}}{2}\frac{q_{k-1} - q_{k+1}}{2} - sp_k(1-p_k)q_k(1-q_k)\right)$$

which is shown by blue solid lines. Barton and Shpak (2000) neglected $\frac{\partial^2 D}{\partial y^2}$ in the derivation of their eq. (14) from eq. (13) because their fitness does not depend on space. Including the term $\frac{\partial^2 D}{\partial y^2}(y=k) \approx \frac{D_{k-1}-2D_k+D_{k+1}}{2}$, leads to

$$D_k \approx \frac{1}{r+m}\left(m\frac{D_{k-1}+D_{k+1}}{2} + m\frac{p_{k-1}-p_{k+1}}{2}\frac{q_{k-1}-q_{k+1}}{2} - sp_k(1-p_k)q_k(1-q_k)\right)$$

which is shown by blue dashed lines. The recombination rate is r=1/2.

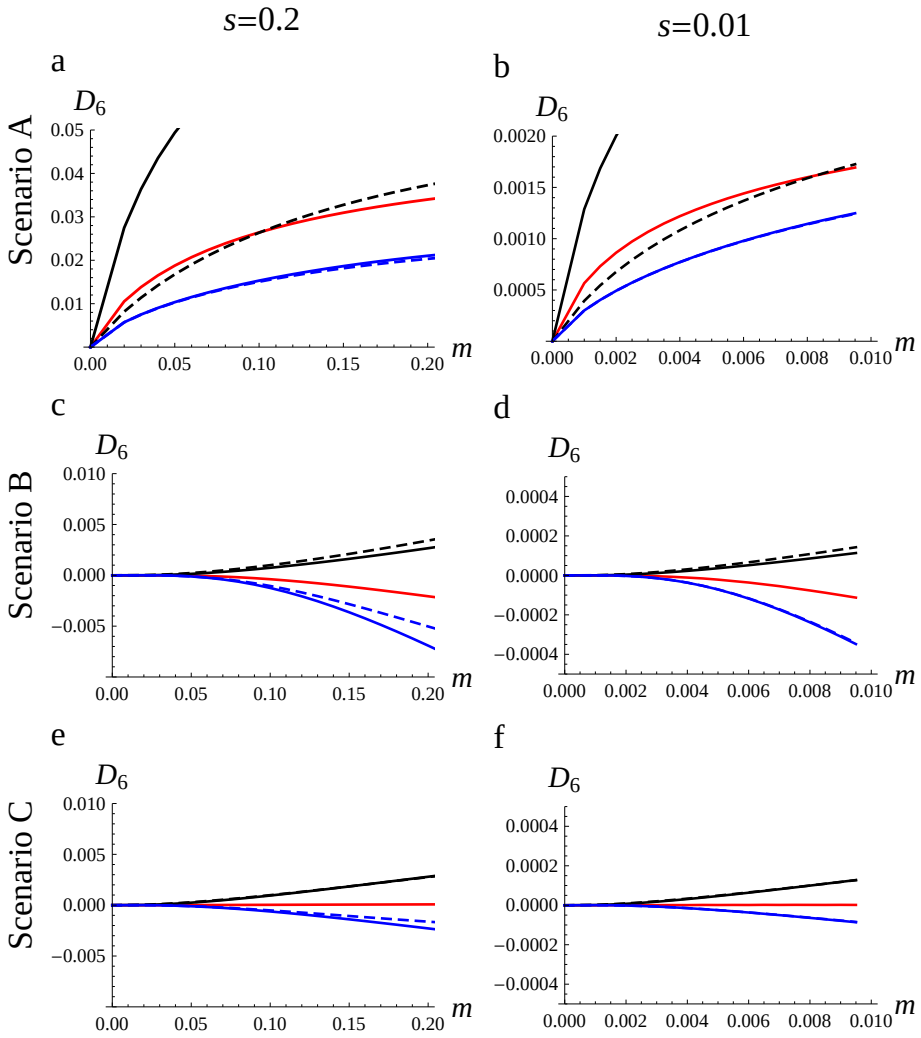

Figure B.11

Clines for models in continuous space, analogously to Figure 10 in the main text. Line colors and parameters are as in Figure 10, except that here we use $m = \sigma^2 = 0.5$.

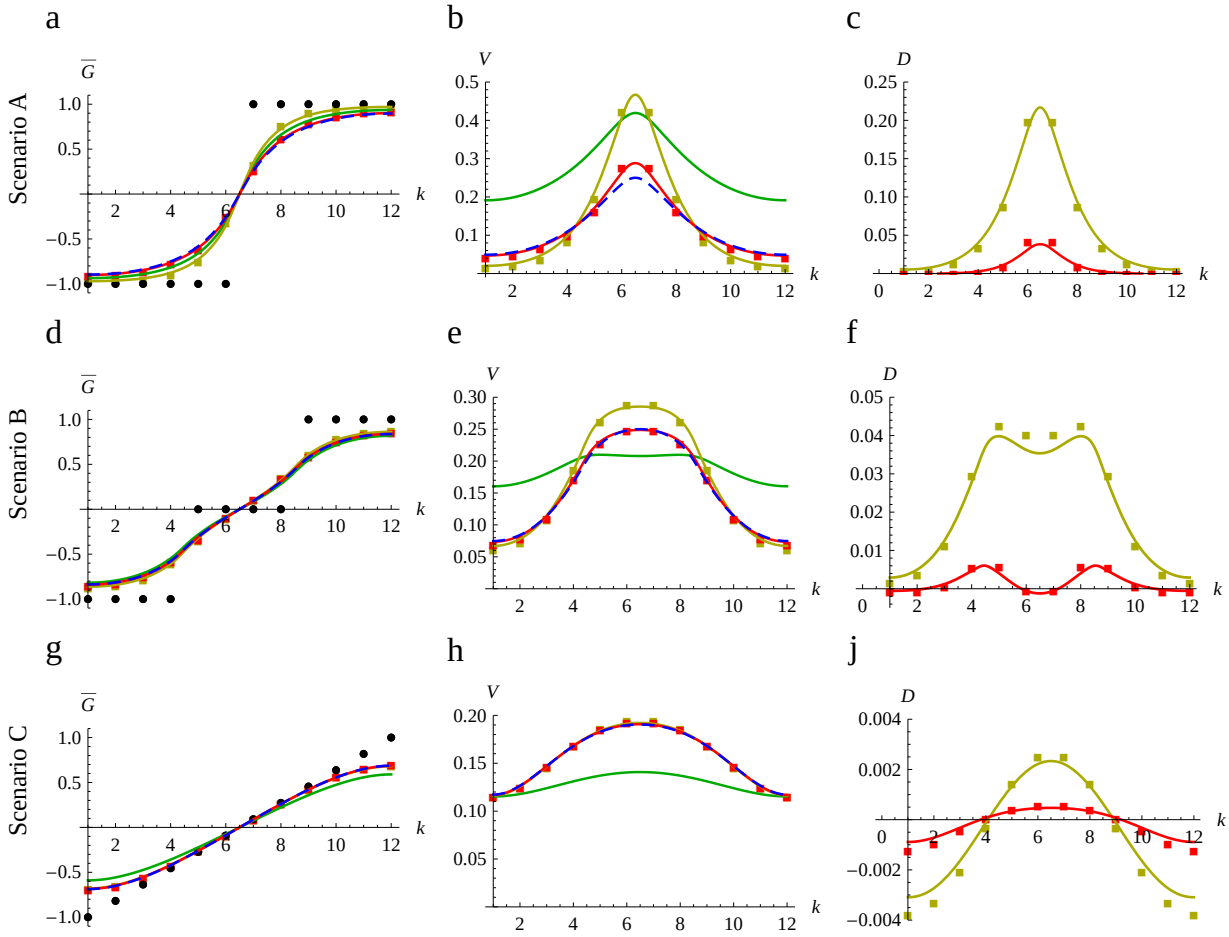

Figure B.12

Clines for unequal locus effects with the stepping-stone model and Scenario B. The red solid lines show $m = 0.325 > m_{\mathrm{st}}^{\mathrm{B},\mathcal{S}}(\mathsf{I}^1) \approx 0.3$, where the equilibrium I^1 is stable. The dashed brown and magenta lines represent I^4 and I^5 at $m = 0.1 < m_{\mathrm{st}}^{\mathrm{B},\mathcal{S}}(\mathsf{I}^1)$. For $\kappa = 1$ the dashed lines would coincide. The parameters $r = 1/2$, $\kappa = 0.75$, $s = 0.2$, and $n = 12$ are used.

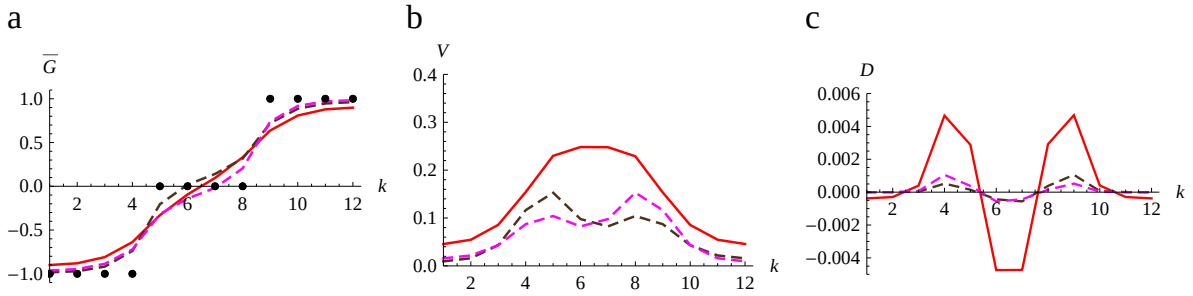

Figure B.13

The accuracy of the approximations given in Appendix A.4 of the main text is demonstrated. Black dots show numerically evaluated allele frequencies p_1 of the discrete dynamical system (2.3). The green lines show the approximation for I^1 (A.10). The approximation (A.11) for I^2 and I^3 is shown in orange. Red lines show (A.13) which approximates I^4 and I^5.

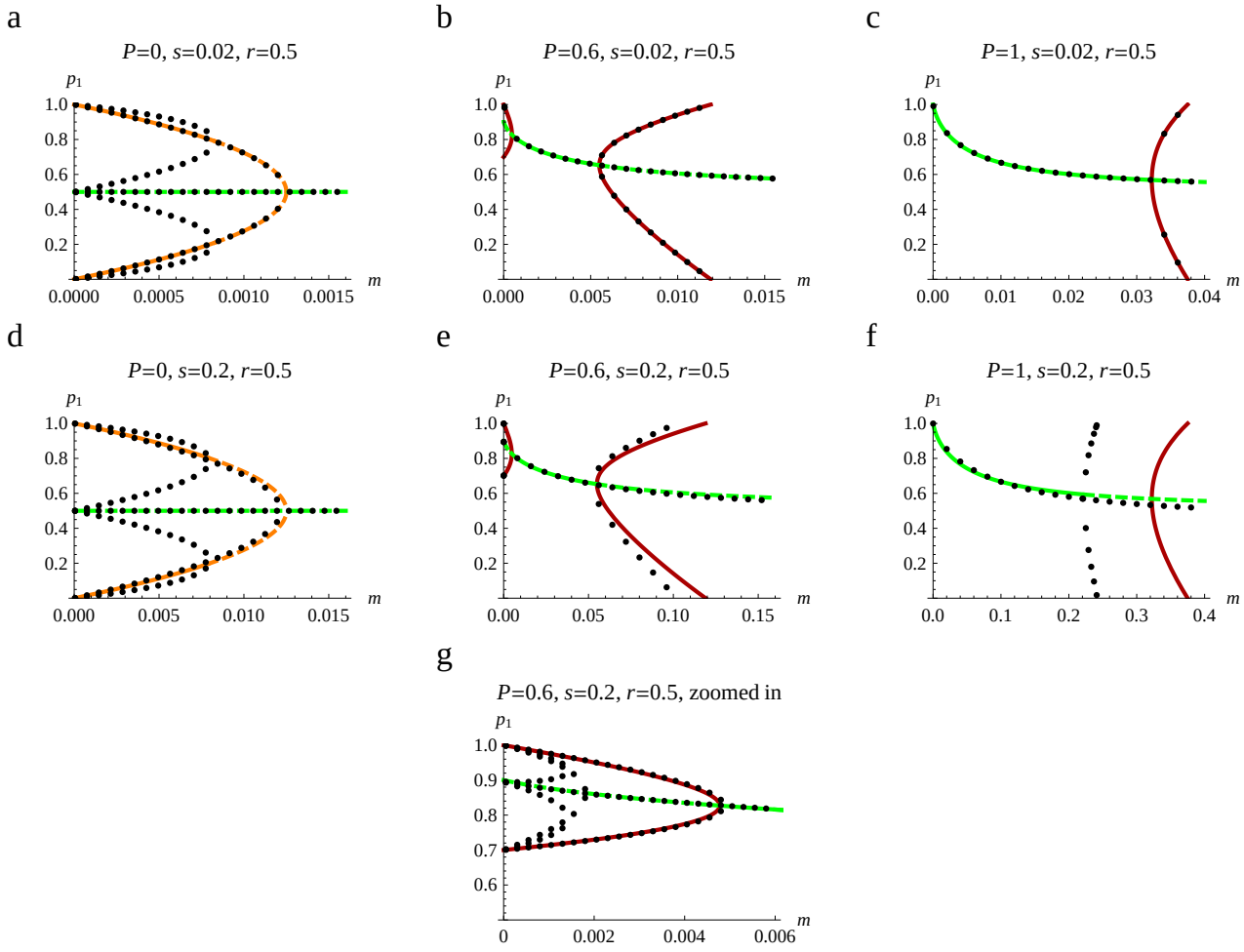

Bibliography

Akerman, A., Bürger, R., 2014a. The consequences of dominance and gene flow for local adaptation and differentiation at two linked loci. Theoretical Population Biology 94, 42–62.

Akerman, A., Bürger, R., 2014b. The consequences of gene flow for local adaptation and differentiation: a two-locus two-deme model. Journal of Mathematical Biology 68, 1135–1198.

Akin, E., 1993. The general topology of dynamical systems. American Mathematical Society, Providence, RI.

Bank, C., Bürger, R., Hermisson, J., 2012. The limits to parapatric speciation: Dobzhansky-Muller incompatibilities in a continent-island model. Genetics 191, 845–863.

Barton, N., Shpak, M., 2000. The effect of epistasis on the structure of hybrid zones. Genetical Research 75, 179–198.

Barton, N. H., 1983. Multilocus clines. Evolution 37, 454–471.

Barton, N. H., 1986. The maintenance of polygenic variation through a balance between mutation and stabilizing selection. Genetical Research 57, 209–216.

Barton, N. H., 1999. Clines in polygenic traits. Genetical Research 74, 223–236.

Barton, N. H., Bengston, B. O., 1986. The barrier to genetic exchange between hybridising populations. Heredity 56, 357–376.

Barton, N. H., Keightley, P. D., 2002. Understanding quantitative genetic variation. Nature Reviews Genetics 3, 11–21.

Bazykin, A. D., 1973. Population-genetic analysis of the ideas of disruptive and stabilizing selection. Communication II. Systems of adjacent populations and populations with a continuous area. Genetika 9, 156–166, (Translated in Soviet Genetics 9:253-261).

Bulmer, M., 1972. The genetic variability of polygenic characters under optimizing selection, mutation and drift. Genetical Research 19, 17–25.

Bürger, R., 2000. The Mathematical Theory of Selection, Recombination, and Mutation. Wiley, Chichester.

Bürger, R., 2002. On a genetic model of intraspecific competition and stabilizing selection. The American Naturalist 160, 661–682.

Bürger, R., 2009a. Multilocus selection in subdivided populations. I: Convergence properties for weak or strong migration. Journal of Mathematical Biology 58, 939–978.

Bürger, R., 2009b. Multilocus selection in subdivided populations II. Maintenance of polymorphism under weak or strong migration. Journal of Mathematical Biology 58, 979–997.

Bürger, R., 2010. Evolution and polymorphism in the multilocus Levene model with no or weak epistasis. Theoretical Population Biology 78, 123–138.

Bürger, R., 2014. A survey of migration-selection models in population genetics. Discrete and Continuous Dynamical Systems B 19, 883–959.

Bürger, R., Akerman, A., 2011. The effects of linkage and gene flow on local adaption: A two-locus continent-island model. Theoretical Population Biology 80, 272–288.

Bürger, R., Gimelfarb, A., 1999. Genetic variation maintained in multilocus models of additive quantitative traits under stabilizing selection. Genetics 152, 807–820.

Bürger, R., Hofbauer, J., 1994. Mutation load and mutation-selection-balance in quantitative genetic traits. Journal of Mathematical Biology 32, 193–218.

Christiansen, B. F., 1986. The deviation from linkage equilibrium with multiple loci varying in a stepping-stone cline. Journal of Genetics 66, 45–67.

Christiansen, F. B., Feldman, M. W., 1975. Subdivided populations: A review of the one- and two-locus deterministic theory. Theoretical Population Biology 7, 13–38.

Cruickshank, T. E., Hahn, M. W., 2014. Reanalysis suggests that genomic islands of speciation are due to reduced diversity, not reduced gene flow. Molecular Ecology 23, 3133–3157.

Dewar, R. C., Sherwin, W. B., Thomas, E., Holleley, C. E., Nichols, R. A., 2011. Predictions of single-nucleotide polymorphism differentiation between two populations in terms of mutual information. Molecular Ecology 20, 3156–3166.

Feder, J. L., Egan, S. P., Nosil, P., 2012. The genomics of speciation-with-gene-flow. Trends in Genetics 28, 342–350.

Feder, J. L., Nosil, P., 2010. The efficacy of divergence hitchhiking in generating genomic islands during ecological speciation. Evolution 64, 1729–1747.

Feldman, M. W., Christiansen, F. B., 1975. The effect of population subdivision on two loci without selection. Genetical Research 24, 151–162.

Felsenstein, J., 1976. The theoretical population genetics of variable selection and migration. Annual Review of Genetics 10, 253–280.

Felsenstein, J., 1977. Multivariate normal genetic models with a finite number of loci. In: Proceedings of the international conference of quantitative genetics (Ed. Pollak, E., Kempthorne, O., Bailey, T. B., Jr.). Iowa State University Press, Ames, IA, pp. 227–246.

Fu, R., E Gelfand, A., Holsinger, K. E., 2003. Exact moment calculations for genetic models with migration, mutation, and drift. Theoretical Population Biology 63, 231–243.

Gale, J., Kearsey, M., 1968. Stable equilibria under stabilising selection in the absence of dominance. Heredity 23, 553–561.

Gavrilets, S., Hastings, A., 1993. Maintenance of genetic variability under strong stabilizing selection: A two-locus model. Genetics 134, 377–386.

Geroldinger, L., Bürger, R., 2014. A two-locus model of spatially varying stabilizing or directional selection on a quantitative trait. Theoretical Population Biology 94, 10–41.

Guillaume, F., Rougemont, J., 2006. Nemo: an evolutionary and population genetics programming framework. Bioinformatics 22, 2556–2557.

Haldane, J., 1948. The theory of a cline. Journal of Genetics 48, 277–284.

Hastings, A., Hom, C. L., 1990. Multiple equilibria and maintenance of additive genetic variance in a model of pleiotropy. Evolution, 1153–1163.

Hill, W. G., 2010. Understanding and using quantitative genetic variation. Philosophical Transactions of the Royal Society B 365, 73–85.

Hofbauer, J., 1990. An index theorem for dissipative semiflows. Rocky Mountain Journal 20, 1017–1031.

Hu, X.-S., 2005. Tension versus ecological zones in a two-locus system. Theoretical Population Biology 68, 119–131.

Huisman, J., Tufto, J., 2012. Comparison of non-Gaussian quantitative genetic models for migration and stabilizing selection. Evolution 66, 3444–3461.

Johnson, T., Barton, N., 2005. Theoretical models of selection and mutation on quantitative traits. Philosophical Transactions of the Royal Society B 360, 1411–1425.

Karlin, S., 1982. Classification of selection-migration structures and conditions for protected polymorphism. Evolutionary Biology 14, 61–204.

Karlin, S., Campbell, R., 1980. Selection-migration regimes characterized by a globally stable equilibrium. Genetics 94, 1065–1084.

Karlin, S., McGregor, J., 1972a. Application of method of small parameters to multi-niche population genetic models. Theoretical Population Biology 3, 186–209.

Karlin, S., McGregor, J., 1972b. Polymorphisms for genetic and ecological systems with weak coupling. Theoretical Population Biology 3, 210–238.

Kawakami, T., Butlin, R. K., 2012. Hybrid Zones. eLS. Wiley, Chichester.

Kermany, A. R., Zhou, X., Hickey, D. A., 2008. Joint stationary moments of a two-island diffusion model of population subdivision. Theoretical Population Biology 74, 226–232.

Kimura, M., 1965. A stochastic model concerning the maintenance of genetic variability in quantitative characters. Proceedings of the National Academy of Sciences of the United States of America 54, 731–736.

Kobayashi, Y., Hammerstein, P., Telschow, A., 2008. The neutral effective migration rate in a mainland-island context. Theoretical Population Biology 74, 84–92.

Kruuk, L., Baird, S., Gale, K., Barton, N., 1999. A comparison of multilocus clines maintained by environmental adaptation or by selection against hybrids. Genetics 153, 1959–1971.

Kuznetsov, Y. A., 1998. Elements of applied bifurcation theory. Springer, New York.

Lande, R., 1975. The maintenance of genetic variability by mutation in a polygenic character with linked loci. Genetical Research 26, 221–235.

Latter, B., 1960. Natural selection for an intermediate optimum. Australian Journal of Biological Sciences 13, 30–35.

Lenormand, T., 2002. Gene flow and the limits to natural selection. Trends in Ecology & Evolution 17, 183–189.

Li, W.-H., Nei, M., 1974. Stable linkage disequilibrium without epistasis in subdivided populations. Theoretical Population Biology 6, 173–183.

Lou, Y., Nagylaki, T., Ni, W.-M., 2013. An introduction to migration-selection PDE models. Discrete and Continuous Dynamical Systems A 33, 4349–4373.

Lythgoe, K. A., 1997. Consequences of gene flow in spatially structured populations. Genetical Research 69, 49–60.

Nagylaki, T., 1975. Conditions for the existence of clines. Genetics 80, 595–615.

Nagylaki, T., 1989a. The diffusion model for migration and selection. In: Some Mathematical Questions in Biology. Lecture Notes on Mathematics in the Life Sciences, vol. 20. (Ed. Hastings, A.). American Mathematical Society, Providence, RI., pp. 55–75.

Nagylaki, T., 1989b. The maintenance of genetic variability in two-locus models of stabilizing selection. Genetics 122, 235–248.

Nagylaki, T., 2012. Clines with partial panmixia in an unbounded unidimensional habitat. Theoretical Population Biology 82, 22–28.

Nagylaki, T., Lou, Y., 2007. Evolution under multiallelic migration–selection models. Theoretical Population Biology 72, 21–40.

Nagylaki, T., Lou, Y., 2008. The dynamics of migration-selection models. In: Tutorials in Mathematical Biosciences. IV. Springer, Berlin, pp. 119–172.

Phillips, P. C., 1996. Maintenance of polygenic variation via a migration-selection balance under uniform selection. Evolution 50, 1334–1339.

Rutschman, D. H., 1994. Dynamics of the two-locus haploid model. Theoretical Population Biology 45, 167–176.

Slatkin, M., 1975. Gene flow and selection in a two-locus system. Genetics 81, 787–802.

Slatkin, M., 1978. Spatial patterns in the distributions of polygenic characters. Journal of Theoretical Biology 70, 213–228.

Spichtig, M., Kawecki, T., 2004. The maintenance (or not) of polygenic variation by soft selection in heterogeneous environments. The American Naturalist 164, 70–84.

Su, L., Nagylaki, T., 2014. Clines with directional selection and partial panmixia in an unbounded unidimensional habitat. Discrete and Continuous Dynamical Systems A, in press.

Tufto, J., 2000. Quantitative genetic models for the balance between migration and stabilzing selection. Genetical Research 76, 285–293.

Turelli, M., 1984. Heritable genetic variation via mutation-selection balance: Lerch's zeta meets the abdominal bristle. Theoretical Population Biology 25, 138–193.

Via, S., 2009. Natural selection in action during speciation. Proceedings of the National Academy of Sciences 106, 9939–9946.

Whitlock, M. C., 2008. Evolutionary inference from Q_{ST}. Molecular Ecology 17, 1885–1896.

Willensdorfer, M., Bürger, R., 2003. The two-locus model of Gaussian stabilizing selection. Theoretical Population Biology 64, 101–117.

Wolfram Research, Inc., 2010. Mathematica Version 8.0. Wolfram Research, Inc.

Wright, S., 1935. Evolution in populations in approximate equilibrium. Journal of Genetics 30, 257–266.

Yeaman, S., 2013. Genomic rearrangements and the evolution of clusters of locally adaptive loci. Proceedings of the National Academy of Sciences 110, E1743–E1751.

Yeaman, S., Guillaume, F., 2009. Predicting adaption under migration load: The role of genetic skew. Evolution 63, 2926–2938.

Yeaman, S., Whitlock, M. C., 2011. The genetic architecture of adaption under migration-selection balance. Evolution 65, 1897–1911.

Curriculum Vitae

Personal Data

Name: Ludwig Geroldinger

Date of birth: 27.9.1987

e-mail: ludwig_geroldinger@gmx.at

Education

1997–2005: BRG Carnerigasse, Graz

2005-2010 Study of Mathematics and Physics (Diplom) at the University of Vienna

Feb. 2007: First section in physics (1. Studienabschnitt) with distinction

Jan. 2010: Master degree in mathematics with distinction

Sep. 2010 - Dec.2014: PhD Student at the University of Vienna in Biomathematics, employed by the FWF and member of the Vienna Graduate School of Population Genetics

Experience

Talk at the Congress of the ESEB [1] in Ottawa in 2011

Academic guest at the ETH Zürich (April-June 2013)

Talk at the Congress of the ESEB in Lisbon in 2013

Talk and organization of a Mini-Symposium at the ECMTB [2] in Gothenburg in 2014

Teaching of 'Exercises in Mathematical Ecology' in the summer term 2014

[1] European Society for Evolutionary Biology

[2] European Conference of Mathematical and Theoretical Biology

List of Publications

1 Geroldinger L. and Bürger R., 2014. A two-locus model of spatially varying stabilizing or directional selection on a quantitative trait. Theoretical Population Biology 94, 10-41

Contribution of Geroldinger L.: Model design, performance of mathematical and numerical analysis, interpretation of results, drafting and revising of the manuscript

Contribution of Bürger R.: Project conception and guidance concerning analyses, performance of mathematical analysis, writing and revising of the manuscript

2 Geroldinger L. and Bürger R., 2014. Clines in quantitative traits: The role of migration patterns and selection scenarios. Theoretical Population Biology, in press

Contribution of Geroldinger L.: Model design, performance of mathematical and numerical analysis, interpretation of results, drafting and revising of the manuscript

Contribution of Bürger R.: Project conception and guidance concerning analyses, performance of mathematical analysis, writing and revising of the manuscript